Analysis of piles and piled raft foundation under horizontal load

Dissertation

submitted to and approved by the

Department of Architecture, Civil Engineering and Environmental Sciences
University of Braunschweig – Institute of Technology

and the

Department of Civil and Environmental Engineering
University of Florence

in candidacy for the degree of a
Doktor-Ingenieur (Dr.-Ing.) /
Dottore di Ricerca in Civil and Environmental Engineering

by
Stefano Stacul
born 10/10/1986
from Lucca (LU), Italy

Submitted on	25th August 2017
Oral examination on	8th November 2017
Professorial advisors	Prof. Joachim Stahlmann Prof. Nunziante Squeglia

2018

Abstract

Doctor of Philosophy

Analysis of piles and piled raft foundation under horizontal load

by Stefano STACUL

It is well known that there are only few experimental evidences and analysis methods for piled raft foundations subjected to lateral loads. On the contrary, a lot of studies are focused on piled rafts under vertical loads and it was seen how more rational design methods can led to great benefits in terms of performance and in saving of construction materials.
Piled raft foundations have a response to lateral loading that makes use of different mobilization mechanisms (in this work, only the lateral resistance of the piles and the friction resistance at the raft-soil interface are considered) and experimental evidences show how the contribution offered by the raft can be significant and how in serviceability conditions can help to reduce the pile bending moments.
The evaluation of horizontal displacements and load sharing requires numerical analyses and, even today, the most used analysis methods for pile foundations are Winkler-based approaches, while FEM (Finite Element Method) analyses, despite the big potential, have strong disadvantages and require high computational costs.
In this work, some FEM analyses were carried out on a piled raft model (considering different pile group layouts) in order to understand better the mechanism of the response under lateral loading and it was found that not always the piled raft performance is better compared to the raft alone.
It is then presented the development and the validation of a 'Hybrid BEM - p-y curves' method for the analysis of single piles and of a BEM-based method (BEM: Boundary Element Method) for the analysis of pile groups and piled rafts under static horizontal loads.
The latter can consider the contribution offered by the raft-soil contact, the interactions between all the foundation system elements using the Mindlin's and Cerutti's solutions and includes: a) the non-linear behaviour of the soil; b) the non-linear response of reinforced concrete pile sections, taking into account of the influence of tension stiffening; c) the influence of suction, using the so-called 'Modified Kovaks Model'; d) the modelling of the shadowing effect, using a similar approach as presented in the so-called 'Strain Wedge Model'.
Some parametric studies were realized and the results are compared with those obtained using methods developed by other authors.
The proposed analysis methods result in saving computational costs compared to more sophisticated FEM codes and can provide reliable results using as input, data that come from a standard site investigation.
The reliability of these simplified methods, for the analysis of single piles, pile groups and piled rafts, was verified by comparing the results with data from well documented full-scale, 1-g and centrifuge tests. These analyses were carried out not as back-analyses but as direct predictions using the actual pile and soil properties.

Acknowledgements

Firstly, I would like to express my sincere gratitude to my tutors Prof. Joachim Stahlmann and Prof. Nunziante Squeglia and to my co-tutor Prof. Alessandro Mandolini for the continuous support of my Ph.D study and related research, for their patience, motivation, and immense knowledge. Their guidance helped me in all the time of research and writing of this thesis.

Besides my tutors, I would like to thank Prof. Diego Lo Presti, Dr. Lorenzo Leoni, Dr. Martino Leoni, Prof. Gianpiero Russo, Prof. Arnoldas Norkus and Dr. Sarunas Skuodis for their insightful comments and encouragement.

I thank my fellow of doctorate for the stimulating discussions, and for all the experiences we have had in the last three years. Also I thank a special person Antonia ('la ragazza di mare aperto') for all her support despite the distance and my 'historical' friends Tommaso and Alberto for all the free-time and nights we have spent together during this period talking about our future.

Last but not the least, I would like to thank my family: my parents and my sister for supporting me spiritually through the writing this thesis.

Contents

List of Symbols

A	cross sectional area	m^2
A, A_c, A_s	coefficients of non-linear spring for sand	(-)
A_c	area of the concrete element	m^2
A_{ct}, $A_{c,eff}$	area of the concrete cross section effectively influenced by cracks	m^2
A_{raft}	area in plan of the raft	m^2
$\overline{A_s}$	coefficient of non-linear spring for stiff clay	(-)
A_s, A_{st}	area of the tension bars	m^2
a	equivalent radius of a square raft element	m
a	position of the point of rotation of the raft	m
a_{ij}	soil flexibility coefficient (PRAB)	$\mathrm{m\,N}^{-1}$
a_{ij}	pile flexibility coefficient	$\mathrm{m\,N}^{-1}$
B, b	pile section width	m
B_s	coefficient of non-linear spring for stiff clay	(-)
BC	total length of the passive wedge face	m
b	pile width or diameter	m
b	width of a rectangular raft	m
b_{ij}	soil flexibility coefficient	$\mathrm{m\,N}^{-1}$
$\overline{C}$	coefficient of non-linear spring for sand	(-)
C_N	overburden correction factor	(-)
C_U	coefficient of uniformity	(-)
c	concrete cover	m
c	distance between the surface of the half-space and the load point	m
c, c'	effective cohesion	$\mathrm{N/m}^2$
c_a	average undrained shear strength	$\mathrm{N/m}^2$
c_{ii}	soil 'near-field' flexibility coefficient	$\mathrm{m\,N}^{-1}$
c_{ij}	coefficient of the matrix $[F_{RS}]$	$\mathrm{m\,N}^{-1}$
c_u	undrained shear strength	$\mathrm{N/m}^2$
D, d	diameter of pile section	m
$[D]$	matrix of finite-difference coefficients	
D_{10}	diameter corresponding to 10% passing on the grain-size distribution curve	m
D_{50}	median grain size	m
D_{60}	diameter corresponding to 60% passing on the grain-size distribution curve	m
D_R, D_r	relative density	%
D_x, D_y, D_z	rigid body translations (APRAF)	m
d	diameter of the raft foundation	m
d	diameter steel bars	m
d_{eq}	equivalent diameter	m
d_{ij}	coefficient of the matrix $[F_{SR}]$	$\mathrm{m\,N}^{-1}$

E	Young's modulus	$\mathrm{N/m^2}$
E_0, E_{s0}, E_{s1}	soil elastic modulus at depth $z = 0$	$\mathrm{N/m^2}$
E_{50}, E_{50}^{ref}	soil secant stiffness and reference secant stiffness (HS model)	$\mathrm{N/m^2}$
E_c	concrete elastic modulus	$\mathrm{N/m^2}$
E_{ct}	fictitious tangent elasticity modulus of the concrete in tension representative of the tension stiffening	$\mathrm{N/m^2}$
$E_{ct,lim}$	limit value of E_{ct}	$\mathrm{N/m^2}$
E_{fdn}	elastic modulus of foundation material	$\mathrm{N/m^2}$
E_i	soil elastic modulus at point i	$\mathrm{N/m^2}$
E_j	soil elastic modulus at point j	$\mathrm{N/m^2}$
E_{max}	soil elastic modulus at small strain level	$\mathrm{N/m^2}$
E_{oed}, E_{oed}^{ref}	soil one-dimensional stiffness and reference one-dimensional stiffness (HS model)	$\mathrm{N/m^2}$
E_p	modulus of elasticity of pile material	$\mathrm{N/m^2}$
E_{py}	soil reaction modulus	$\mathrm{N/m^2}$
E_s	horizontal subgrade modulus	$\mathrm{N/m^2}$
E_s	soil elastic modulus	$\mathrm{N/m^2}$
E_s	steel elastic modulus	$\mathrm{N/m^2}$
E_{sAV}	soil elastic modulus at depth $z = 0.5D$	$\mathrm{N/m^2}$
E_{sb}	soil elastic modulus at pile base	$\mathrm{N/m^2}$
E_u	undrained soil elastic modulus	$\mathrm{N/m^2}$
E_{ur}, E_{ur}^{ref}	soil unloading/reloading stiffness and reference unloading/reloading stiffness (HS model)	$\mathrm{N/m^2}$
EA	axial stiffness or cross sectional rigidity	N
$(EA)_{beam}$	axial stiffness of the beam element	N
$(EA)_{solid}$	axial stiffness of the solid elements	N
EI, E_pI_p	flexural rigidity of a pile section	$\mathrm{Nm^2}$
$(EI)_{beam}$	flexural rigidity of the beam element	$\mathrm{Nm^2}$
$(EI)_{solid}$	flexural rigidity of the solid elements	$\mathrm{Nm^2}$
$(E_cI)_{intact}$	intact flexural rigidity	$\mathrm{Nm^2}$
$(E_cI)_{sec,u}$	secant flexural rigidity at M_{ult}	$\mathrm{Nm^2}$
$(E_cI)_{sec,y}$	secant flexural rigidity at M_y	$\mathrm{Nm^2}$
E_pI_k	flexural rigidity of k-th pile section	$\mathrm{Nm^2}$
e	horizontal load eccentricity	m
e	void ratio	(-)
e_{ij}	coefficient of the matrix $[F_{RR}]$	$\mathrm{m\,N^{-1}}$
e_{max}	maximum void ratio	(-)
e_{min}	minimum void ratio	(-)
F	soil resistance factor. $F(s/D) = \frac{s/D-1}{5}$	(-)
$[F]$	flexibility matrix	
$F(e)$	function of the void ratio. $F(e) = 1/e^{1.3}$	(-)
$[F_P]$	pile flexibility matrix	
$[F_{RR}]$	flexibility matrix containing the coefficients e_{ij}	
$[F_{RS}]$	flexibility matrix containing the coefficients c_{ij}	
$[F_S]$	soil flexibility matrix	
$[F_{SFF}]$	soil 'far-field' flexibility matrix	
$[F_{SNF}]$	soil 'near-field' flexibility matrix	

$[F_{SR}]$	flexibility matrix containing the coefficients d_{ij}	
F_x, F_y, F_z	force along x, y and z direction	N
f	horizontal load eccentricity	m
f, f_m	p-multiplier coefficient	(-)
f_1	coefficient of Stroud relationship	(-)
f_c	the concrete's compressive strength	$\mathrm{N/m^2}$
f_{ct}	the concrete's tensile strength	$\mathrm{N/m^2}$
f_u	ultimate stress of the steel bars	$\mathrm{N/m^2}$
f_y	yielding stress of the steel bars	$\mathrm{N/m^2}$
G	shear modulus	$\mathrm{N/m^2}$
G	average soil shear modulus	$\mathrm{N/m^2}$
G^*	corrected shear modulus	$\mathrm{N/m^2}$
G_0	initial shear modulus	$\mathrm{N/m^2}$
G_e	group efficiency under vertical load	%
G_{max}	soil shear modulus at small strain level	$\mathrm{N/m^2}$
G_{ref}	shear modulus at $p = p_{ref}$	$\mathrm{N/m^2}$
G_s	specific gravity of soil particle	(-)
G_{sec}	soil secant shear modulus	$\mathrm{N/m^2}$
G_{tan}	soil tangent shear modulus	$\mathrm{N/m^2}$
g	gravity	
g	parameter of the Fahey and Carter modulus reduction curve	(-)
H	horizontal load	N
H_0	exposed pile length	m
H_1, H_m	horizontal loads at the pile-heads	N
H_g, H_{group}	horizontal load acting on the pile group	N
H_i	length of i-th block between two cracks	m
H_i	thickness of sublayer i	m
H_j	horizontal load acting on j-th pile	N
H_{max}	maximum lateral load during a test	N
H_{PR}	horizontal load carried by a piled raft	N
H_R, H_{raft}	horizontal load carried by the raft	N
H_s, H_{single}	horizontal load acting on the single pile	N
h	passive wedge depth	m
h	height of the concrete cross section	m
h_c	rise of water in a capillary tube	m
h_{c0}	equivalent capillary rise in the porous medium	m
$h_{c,eff}$	effective height of the concrete cross section	m
h_k	generic lateral load increment	N
h_k^{new}	updated lateral load increment	N
I	area moment of inertia	$\mathrm{m^4}$
$[I]$, $[I_i]$, $[I_1]$ $[I_2]$, $[I_3]$, $[I_4]$	matrices of soil-displacement-influence factors	
I_F	influence factor to consider foundation flexibility	(-)
I_G	influence factor for a Gibson soil profile	(-)
I_{ij}, $I_{i,ij}$, I_{1ij} I_{2ij}, I_{3ij}, I_{4ij}	terms of $[I]$, $[I_i]$, $[I_1]$, $[I_2]$, $[I_3]$, $[I_4]$ matrices	
I_M	normalised bending moment	(-)
I_p	area moment of inertia of pile section	$\mathrm{m^4}$
$[I_r]$	influence matrix of the pinned raft (APRAF)	
$[I_{sp}]$	influence matrix of the pile-enhanced	

	soil continuum (APRAF)	
$I_{u,x}$, $I_{u,xx}$	normalised horizontal displacement	(-)
I_{yH}, I_{yM}, $I_{\theta H}$ $I_{\theta M}$, I_{yF}	influence factors in a homogeneous soil	(-)
I_{yH}', I_{yM}', $I_{\theta H}'$ $I_{\theta M}'$, I_{yF}'	influence factors in a Gibson soil profile	(-)
I_{yY}, I_{MY}	non linear dimensionless factors for a fixed-head pile	(-)
I_{yY}^{free}, $I_{\theta Y}^{free}$, I_{MY}^{free}	non linear dimensionless factors for a free-head pile	(-)
J	coefficient of non-linear spring for soft clay	(-)
J	coefficient of non-linear spring for stiff clay	(-)
K, K_R	pile-soil relative stiffness	(-)
K_0	at-rest earth pressure coefficient	(-)
K_0	initial pile-soil relative stiffness	(-)
K_1	bond reinforcement coefficient	(-)
K_2	strain distribution coefficient	(-)
K_a, k_a	active earth pressure coefficient	(-)
K_F	foundation flexibility factor	(-)
K_G	pile-group stiffness under vertical load	$\mathrm{N\,m^{-1}}$
$K_{M\theta}$	pile-cap rotational stiffness	$\mathrm{N\,m\,rad^{-1}}$
K_p, k_p	passive earth pressure coefficient	(-)
K_R	raft stiffness under vertical load	$\mathrm{N\,m^{-1}}$
K_x^P, K_y^P	horiz. shaft soil spring constants at pile nodes	$\mathrm{N\,m^{-1}}$
K_x^R, K_y^R	horiz. soil spring constant at raft nodes	$\mathrm{N\,m^{-1}}$
K_z^P	vertical shaft soil spring constant at pile nodes	$\mathrm{N\,m^{-1}}$
K_z^R	vertical soil spring constant at raft nodes	$\mathrm{N\,m^{-1}}$
$K_{\Delta c}$	pile axial stiffness in compression	$\mathrm{N\,m^{-1}}$
$K_{\Delta t}$	pile axial stiffness in tension	$\mathrm{N\,m^{-1}}$
k	overconsolidation ratio exponent	(-)
k	soil reaction modulus	$\mathrm{N/m^2}$
k_p	lateral stiffness of the pile-group alone	$\mathrm{N\,m^{-1}}$
k_p	lateral stiffness of the piled-raft	$\mathrm{N\,m^{-1}}$
k_{py}	initial coefficient of subgrade reaction of non-linear spring for sand	$\mathrm{N/m^3}$
k_{pys}, k_s	coefficient of subgrade reaction of non-linear spring for stiff clay	$\mathrm{N/m^3}$
k_r	lateral stiffness of the raft alone	$\mathrm{N\,m^{-1}}$
L	length, pile length	m
L_c	critical pile length	m
L_e	effective pile length	m
L_{em}	embedded pile length	m
L/D	pile slenderness	(-)
$LCNV$	lateral capacity under pure lateral load	N
$LCWV$	lateral capacity with vertical load	N
l	length of a pile segment	m
l	length of a rectangular raft	m
l_k	distance between pile-head and lower part of k-th block	m
M, M_z	bending moment	$\mathrm{N\,m}$

M	mass	kg
M_{adim}	dimensionless bending moment	(-)
$M_{max,E}$, M_L	maximum bending moment in a linear elastic analysis	$\mathrm{N\,m}$
$M_{max,Y}$, M_{NL}	maximum bending moment in a non-linear analysis	$\mathrm{N\,m}$
M_y	yielding bending moment of a section	$\mathrm{N\,m}$
M_{ult}	ultimate bending moment of a section	$\mathrm{N\,m}$
m	number of piles in a group	(-)
m	power for stress level dependency of stiffness	(-)
m	slope of the line between points k and m of non-linear spring for sand	(-)
m	slope of soil modulus increase	$\mathrm{N/m^3}$
m^*	corrected slope of soil modulus increase	$\mathrm{N/m^3}$
N	axial force	N
N	number of element blocks	(-)
N_k	bearing capacity factor	
N_{SPT}	standard penetration test (SPT) blow counts	(-)
N_u	ultimate axial resistance of a section	N
n	number of pile blocks	(-)
n	number of piles in a group	(-)
n	porosity	(-)
n	power of the parabolic section of non-linear spring for sand	(-)
n	steel-concrete relative stiffness	(-)
n	stress exponent	(-)
OCR	overconsolidation ratio	(-)
$[P]$	known-term vector	
P	soil reaction force	N
$P_{average}$	mean lateral load on a pile in a pile-group	N
P_j	load acting on point j	N
P_j	load acting on j-th pile-block	N
P_p	lateral load carried by the pile-group in the piled-raft	N
P_{pile}	horizontal load acting on a pile	N
P_r	interfaces forces acting on the raft (APRAF)	N
P_r	lateral load carried by the raft in the piled-raft	N
P_{sp}	interfaces forces acting on the pile-group (APRAF)	N
PIC	percentage of improvement in lateral capacity	$\%$
p	order of accuracy of a numerical method	(-)
p	soil reaction	$\mathrm{N\,m^{-1}}$
p, p_i, p_k	soil pressure (in BEM approaches)	$\mathrm{N/m^2}$
p_0	confining pressure	$\mathrm{N/m^2}$
p_a	active soil pressure	$\mathrm{N\,m^{-1}}$
p_a	atmospheric pressure	$\mathrm{N/m^2}$
p_{cd}	ultimate soil reaction for stiff clay	$\mathrm{N\,m^{-1}}$
p_{ct}	ultimate soil reaction for stiff clay	$\mathrm{N\,m^{-1}}$
p_m	soil reaction of non-linear spring for sand. $p_m = B_s p_s$	$\mathrm{N\,m^{-1}}$
p_p	passive soil resistance	$\mathrm{N\,m^{-1}}$

p^p	pile-soil interface pressure	$\mathrm{N/m^2}$
p_r	resulting soil resistance. $p_r = p_p - p_a$	$\mathrm{N\,m^{-1}}$
p^r	raft-soil interface pressure	$\mathrm{N/m^2}$
p_{ref}	reference confining pressure (HS model)	$\mathrm{N/m^2}$
p_s	minimum ultimate soil reaction for sand	$\mathrm{N\,m^{-1}}$
p_{sd}	ultimate soil reaction for sand	$\mathrm{N\,m^{-1}}$
p_{sp}	soil reaction (single pile)	$\mathrm{N\,m^{-1}}$
p_{st}	ultimate soil reaction for sand	$\mathrm{N\,m^{-1}}$
p_u, p_{ui}, p_{ult}	ultimate soil resistance (in BEM approaches)	$\mathrm{N/m^2}$
p_u, p_{ult}	ultimate soil reaction	$\mathrm{N\,m^{-1}}$
$p_{ult,def}$	final soil resistance	$\mathrm{N\,m^{-1}}$
Q	horizontal load acting on the piled-raft	N
Q_i, Q_j	vertical load acting on a generic pile	N
Q_P	horizontal load carried by the piles	N
$Q_{P,lim}$	single pile vertical bearing capacity	N
Q_R	horizontal load carried by the raft	N
$Q_{R,lim}$	raft vertical bearing capacity	N
q	deviatoric stress	$\mathrm{N/m^2}$
q	uniform vertical load acting on a rectangular area	$\mathrm{N/m^2}$
q	vertical stress applied to the raft	$\mathrm{N/m^2}$
q_t	cone tip resistance	$\mathrm{N/m^2}$
R	distance in Cerutti's solution scheme	m
R, R_j	overlapping ratio (strain wedge model)	(-)
R_1, R_2, R_3	distances in the elastic solution for a vertical loading on a rectangular area	m
R_1, R_{1ij}, R_2, R_{2ij}	distances in Mindlin's solution scheme	m
R_f	non linear factor (HS model)	(-)
R_f	parameter of the Fahey and Carter modulus reduction curve	(-)
R_{inter}	strength reduction factor (HS model)	(-)
r	number of pile sub-blocks in the y-direction	(-)
r_0, r_p	pile radius	m
r_{ij}	distance in Mindlin's solution scheme	m
r_m	'magic' radius as defined by Randolph and Wroth (1978)	m
S_a	degree of saturation due to adhesion	%
S_a^*	truncated value of S_a	%
S_c	degree of saturation due to capillary	%
S_r	degree of saturation	%
SF	safety factor	(-)
SL	stress level	(-)
SL_g	stress level due to passive wedge interference	(-)
s	number of pile sub-blocks in the z-direction	(-)
s	pile spacing	m
s	steel bars spacing	m
s_{ij}	displacement induced at a point i by a load at point j	m
s_{rm}	mean value of cracking interaxis	m
s/D, s/d	pile spacing ratio	(-)
t	foundation thickness or wall thickness	m

tol	tolerance	(-)
U_C	coefficient of uniformity	(-)
u	horizontal displacement	m
u/D	normalised horizontal displacement	(-)
V	vertical load	N
V_s	shear wave velocity	$\mathrm{m\,s^{-1}}$
V_{ult}	ultimate vertical load	N
w, w_i	vertical displacement	m
$w_{1,i}$	vertical settlement of the single pile subjected to a unit load	$\mathrm{m\,N^{-1}}$
w_i	overall deformation (PRAB)	
w_L	liquit limit	%
w_p	average displacement of the pile-group in the piled-raft	m
w_{pr}	average displacement of the piled-raft	m
w_r	average displacement of the raft in the piled-raft	m
w_{raft}	raft vertical displacement	m
$[X]$	unknowns vector	
x	coordinate along x axis	
x	depth	m
x	distance from the cracked section	m
x	neutral axis depth	m
x_i	distance from last row of trailing piles to center of pile i	m
x_y	abscissa where the stress in the steel begins to be less to the yield stress	m
Y_0	pile-head deflection (strain wedge model)	m
y	coordinate along y axis	
y	lateral displacement	m
y_0	lateral displacement at the pile-head	m
y_{50}	lateral displacement at one-half of p_{ult}	m
y_E, y_L	pile-head deflection in a linear elastic analysis	m
$\overline{y_H}$	displacement of a single pile under an unitary load	$\mathrm{m\,N^{-1}}$
y_i	lateral displacement of i-th pile-block	m
y_k	lateral displacement of k-th pile	m
y_m	lateral displacement of non-linear spring for sand. $y_m = b/60$	m
y_p	vector of pile displacements	
y_{pair}	horizontal displacement of a pair of piles	m
y_s	vector of soil displacements	
$y_{sing,pile}$	horizontal displacement of a single pile	m
y_u	lateral displacement of non-linear spring for sand. $y_u = 3b/80$	m
y_Y, y_{NL}	pile-head deflection in a non-linear analysis	m
y/D	norm. lateral displacement (displacement level)	(-)
z	coordinate along z axis	
z	depth	m
z^*	conventional depth at which evaluate soil E_s	m
z_i	depth of i-th pile-block, depth of point i	m

z_j	depth of j-th pile-block, depth of point j	m
α, α_1, α_2, α_3, $\alpha_{k,j}$	interaction factors	(-)
α	mean value of curvature	m^{-1}
α_1	curvature in the uncracked section	m^{-1}
α_2	curvature in the fully cracked section	m^{-1}
$\alpha_{H,CPRF}$	proportion of horizontal load carried by piles	(-)
α_{ii}	coefficient on the main diagonal of the global flexibility matrix	
α_{ij}	interaction coefficient	(-)
α_{pr}	interaction factor of the raft on the pile-group	(-)
α_r	raft coefficient on the main diagonal of the global flexibility matrix	(-)
α_{rp}	interaction factor of the pile-group on the raft	(-)
α_y, α_{yH}, α_{yM}, α_{yF}	interaction factors for pile-head displacement	(-)
α_θ, $\alpha_{\theta H}$, $\alpha_{\theta M}$	interaction factors for pile-head rotation	(-)
β	departure angle	rad
β	long term effects factor	(-)
β_m	wedge angle (strain wedge model)	rad
γ	shear strain	(-)
γ	unit weight	$\mathrm{N/m}^3$
γ'	buoyant unit weight or submerged unit weight	$\mathrm{N/m}^3$
γ_{ref}	reference shear strain. $\gamma_{ref} = \frac{\tau_{max}}{G_{max}}$	(-)
Δ, Δ_i, Δ_k	pile block thickness	m
Δ, Δ_i, δ	length of a pile segment (or block)	m
Δ_r	raft element width	m
Δ_{tot}	relative displacement between two sections	m
ΔL	pile element length (PRAB)	m
ΔP_{base}	variation of the axial load carried by the pile base	N
ΔP_c	variation of the axial load for the pile in compression	N
ΔP_{shaft}	variation of the axial load carried by the pile shaft	N
ΔP_t	variation of the axial load for the pile in tension	N
Δu	excess pore water pressure	$\mathrm{N/m}^2$
Δu_1	incremental displacement at the pile-head using one load step	m
Δu_2	incremental displacement at the pile-head using two load steps	m
Δy, Δy_i	vertical displacement of the pile	m
$\Delta\theta$	rotation of the raft	rad
$\Delta\sigma_h$	horizontal stress change	$\mathrm{N/m}^2$
$\Delta\sigma_{hf}$	horizontal stress change at failure	$\mathrm{N/m}^2$
$\Delta\sigma_z$	induced vertical stress	$\mathrm{N/m}^2$
δ	angle of friction at the raft-soil interface	rad
δ, δ_i	linearized deflection angle	
δ_i	displacement of i-th block between two sections	m
δ_r, δ_{r0}	displacement at the centre of a raft element (APRAF)	m

δ_{sp}	vector of interface displacement (APRAF)	
ε	horizontal strain	(-)
ε	incremental ratio. $\varepsilon = \frac{\Delta u_2 - \Delta u_1}{\Delta u_1}$	(-)
ε_{50}	strain corresponding to one-half of maximum principal stress difference	(-)
ε_g	horizontal strain due to passive wedge interference	(-)
ε_{ph}	horizontal strain perpendicular to pile movement	(-)
ε_u	ultimate strain of the steel bars	(-)
ε_v	vertical strain	(-)
ε_y	yielding strain of the steel bars	(-)
ζ	distribution coefficient	(-)
η	group efficiency under lateral load	%
Θ	volumetric water content	(-)
Θ_m	base angle (strain wedge model)	rad
θ_{A-B}	rotation between two consecutive cracked sections	rad
θ_0	rotation at the pile-head	rad
θ_1, θ_m	rotations at the pile-heads	rad
θ_E	pile-head rotation in a linear elastic analysis	rad
θ_i, θ_j	relative rotation between the two faces of the i-th or j-th block	rad
θ_x, θ_y, θ_z	rigid body rotations (APRAF)	rad
θ_Y	pile-head rotation in a non-linear analysis	rad
λ	distance between two adjacent cracks	m
λ	geometrical scaling factor (prototype/model size)	(-)
λ_{min}	minimum distance between two adjacent cracks	m
ν	Poisson's ratio	(-)
ν_s	Poisson's ratio of soil	(-)
ρ	lateral displacement at each pile node using Mindlin's solution (PRAB)	m
ρ, ρ_s	steel reinforcement ratio	(-)
$\rho_{d,max}$	maximum dry density	$\mathrm{kg/m^3}$
$\rho_{d,min}$	minimum dry density	$\mathrm{kg/m^3}$
$\rho_{p,eff}$	effective reinforcement ratio	(-)
ρ_s	soil grain density	$\mathrm{kg/m^3}$
ρ_x, ρ_{ij}	horizontal displacement evaluated with Cerutti's solution	m
σ_1'	major principal effective stress	$\mathrm{N/m^2}$
σ_3'	minor principal effective stress	$\mathrm{N/m^2}$
σ_3, σ_c	confining pressure	$\mathrm{N/m^2}$
σ_h	horizontal stress	$\mathrm{N/m^2}$
σ_m'	mean effective stress. σ_m'=(σ_1'+2σ_3')/3	$\mathrm{N/m^2}$
σ_n	normal stress	$\mathrm{N/m^2}$
σ_s	stress in the reinforcement in tension calculated in a cracked section	$\mathrm{N/m^2}$
σ_{scr}	stress in the steel upon first cracking	$\mathrm{N/m^2}$
σ_{SF}	stress in the reinforcement in tension causing first cracking	$\mathrm{N/m^2}$

$\sigma_{s,max}$	maximum stress in the steel bar at the cross sections where the crack forms	$\mathrm{N/m^2}$
$\sigma_{s,min}$	minimum stress in the steel bar at the midline section	$\mathrm{N/m^2}$
σ_{v0}	geostatic vertical stress	$\mathrm{N/m^2}$
$\sigma_{v0}{}'$	effective vertical stress	$\mathrm{N/m^2}$
σ_{zz}	vertical stress	$\mathrm{N/m^2}$
τ	shear stress	$\mathrm{N/m^2}$
τ	side shear (strain wedge model)	$\mathrm{N/m^2}$
τ_{b1}	bond stress when the reinforcing bar is in the elastic phase	$\mathrm{N/m^2}$
τ_{b2}	bond stress when the reinforcing bar is in the plastic phase	$\mathrm{N/m^2}$
τ_f	shear stress at failure	$\mathrm{N/m^2}$
τ_{max}	maximum shear resistance	$\mathrm{N/m^2}$
τ_{rel}	relative shear stress	(-)
Φ_s	mean value of reinforcing bars diameter	m
ϕ, ϕ'	angle of internal friction	rad
ϕ	reinforcing bar diameter	m
ϕ_m	mobilized friction angle	rad
ϕ_x, ϕ_y, ϕ_z	rotations	rad
ϕ_s	diameter of the bar in tension	m
φ	friction angle	rad
φ_m	mobilized friction angle	rad
χ	curvature	$\mathrm{m^{-1}}$
χ_A	curvature at the cracked section A	$\mathrm{m^{-1}}$
$\chi_{\frac{\lambda}{4}A}$	curvature at $\frac{\lambda}{4}$ from the cracked section A	$\mathrm{m^{-1}}$
$\chi_{\frac{\lambda}{2}A}$	curvature at $\frac{\lambda}{2}$ from the cracked section A	$\mathrm{m^{-1}}$
$\chi_{\frac{\lambda}{4}B}$	curvature at $\frac{\lambda}{4}$ from the cracked section B	$\mathrm{m^{-1}}$
Ψ	dilatancy angle	rad
ψ	matrix suction	$\mathrm{N/m^2}$

To my parents (Ai miei genitori)

Chapter 1

Introduction

This PhD research project is about the analysis of piled-raft foundation subjected to horizontal load. A piled-raft foundation is a foundation system composed by a pile-group and a raft. In a pile-group the raft is not in contact with the ground (so the interaction between the raft and the soil is neglected in the analysis), in a piled-raft the raft is in contact with the ground, thus the collaboration among raft and piles and the raft-soil interaction are not neglected. The main aim of this PhD thesis is to develop a BEM based analysis method to study the single pile, the pile-group and the piled raft response under this loading condition. In order to validate the proposed method some comparisons with available lateral load tests, found in the literature, are realized, and in the final part of the thesis are shown the results of parametric studies using the developed method. Moreover, some FEM analyses (with Plaxis 3D AE) are carried out to investigate the main features of the piled-raft behaviour.

In much of the available literature, emphasis has been placed on the bearing capacity and settlement under vertical loads. While this is a critical aspect, even other issues must also be addressed. In some cases, the pile requirements may be governed by the bending moments applied by wind loading, rather than the vertical dead and live loads. Normally, piles will be necessary under relatively heavy column loadings when the raft thickness is not sufficient to provide the necessary shear and moment resistance, or when the localized settlement is excessive. In addition, the presence of high lateral loadings, for example, due to wind or earthquakes, may require that piles be placed near the edges of the raft, even though under normal serviceability loadings, the settlements near the edges may not be large. The design philosophy should be based on both ultimate load capacity and settlement/horizontal displacement criteria, with the key question to be answered being: 'what is the minimum number of piles

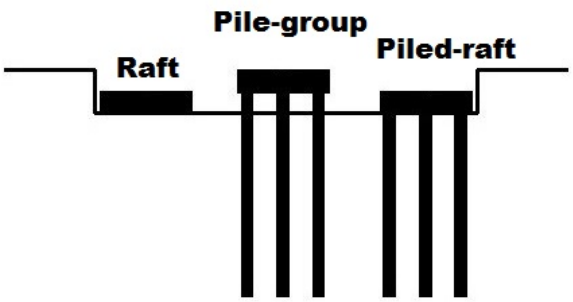

Figure 1.1: Types of foundations: raft, pile-group and piled-raft

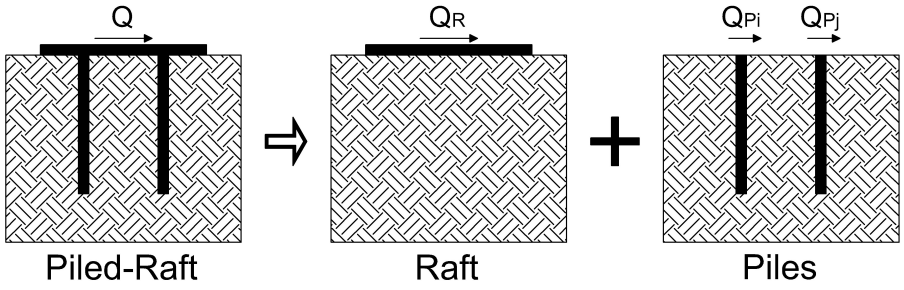

Figure 1.2: Piled-raft foundation and its components

required to be added to the raft such that the ultimate load, settlement, differential settlement and horizontal displacement criteria are satisfied?'. According to Hartmann and Jahn (2001), positive effects of the piled raft foundation are the following:

- reduction of heave caused by the excavation of the pit;
- reduction of settlement, differential settlement and tilt;
- centralization of actions and resistances if there are large load eccentricities;
- reduction of the bending moments of the raft.

Many authors emphasize the importance of improving the knowledge about the behaviour of piled-raft under horizontal loads, with experimental tests and numerical analysis, in order to define more specific design criteria.

Some quotes are listed below in order to underline the importance of further studies on piled-raft foundations:

- 'Concerning the load bearing behaviour of vertically loaded Combined Pile-Raft Foundations many studies and publications are available whereas for Combined Pile-Raft Foundations subjected to lateral loads scientific results or case histories are very rare. But also for horizontal loading it is possible to obtain a very economic foundation design and to reduce displacements by using a Combined Pile-Raft Foundation (CPRF)' (Katzenbach and Turek, 2005);
- 'Although pile caps have considerable ability to resist lateral loads, this resistance is often neglected in design. Published cases involving a variety of pile and cap sizes, soil conditions, and loading conditions indicate that the lateral-load resistance of pile caps can be significant, but it is difficult to generalize on the basis of these results because of the variations in conditions involved in the tests.' (Mokwa and Duncan, 2001);
- 'In many cases the criterion for the design of piles to resist lateral loads is not the ultimate lateral capacity but the deflection of the piles. Despite the intensive experimental and numerical research on the subject the last two decades, many questions regarding the interaction between soil, piles and superstructures remain for the scientific community to resolve. It is however commonly accepted that for the same mean load, the piles of a pile group exhibit significantly greater deflection than an identical single pile' (Papadopoulou and Comodromos, 2010).

Chapter 2

Piles and piled-raft response to lateral loads

2.1 Typical aspects of the single pile response under horizontal loading

Consider a pile with a vertical axis, a circular section and embedded in a homogeneous soil. At first, the normal stresses acting on the lateral surface of the pile have an axisymmetric distribution whose resultant is zero (Figure 2.1b).

When the pile-head is subject to a horizontal force and/or an applied moment it induces a translation, y, in the soil (Figure 2.1a). The soil stress diagram, consequently, changes; normal stresses in front of the pile increase and the soil tends to move away from the pile in the radial direction. The normal stresses placed on the back side of the pile, conversely, decrease while the soil tends to move towards the pile still along the radial direction. Along the pile edges the horizontal stresses have normal and tangential components. The resultant, p [Force/Length], of these actions is along the pile movement direction but opposed to it (Figure 2.1).

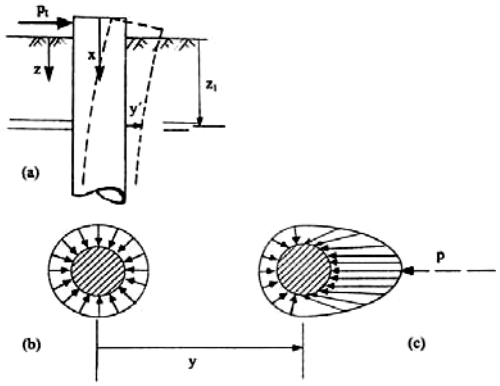

Figure 2.1: Pile-Soil Interaction (Reese and Van Impe, 2001)

At a certain load level the soil placed in the back of the pile and close to the ground surface tends to separate from its shaft; the soil placed in front of the pile, instead, tends to reach an ultimate condition. At greater depths the soil tends to flow along the pile edge without a separation on the opposite side. Therefore, because of these considerations it is evident that the soil reaction, p, depends both on the pile displacement (y) and on the depth (z). Consequently, the pile response to an increasing horizontal load, in terms of 'load-displacement' curve, or in terms of 'load–maximum bending

moment' curve, is non-linear. An example of a 'load-displacement' curve at the pile-head and of a 'load-maximum bending moment' curve is shown in Figure 2.2.

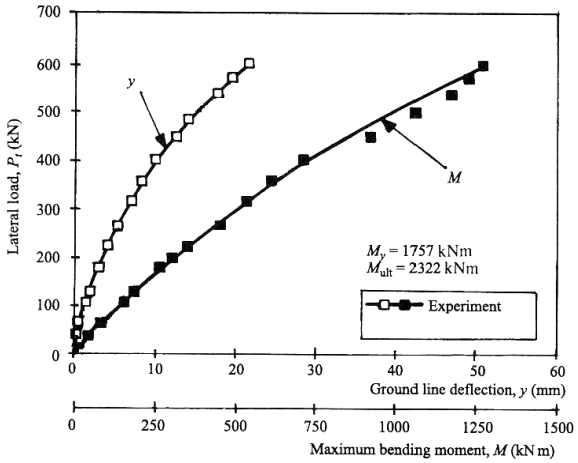

Figure 2.2: Experimental Load-Displacement and Load-Maximum bending moment curves (Reese, Cox, and Koop, 1975)

The displacements of a pile subjected to horizontal forces are generally confined in its upper part. Rarely, can be observed relevant movements at depths greater than 10 diameters below the ground surface (Fleming et al., 2008). The depth at which the pile movements become negligible is identified as the critical pile length (Randolph, 1981). The total pile length is, practically always, greater than the critical one; a pile for which this event occurs is defined flexible. For this reason, the total pile length seems to be a not significant parameter to describe the overall response of the pile-soil system to horizontal loading.

The value of the critical pile length depends of course by some system parameters, and the most important one is the pile-soil relative stiffness. Several authors (Davies and Budhu, 1986; Kuhlemeyer, 1979; Randolph, 1981) have attempted to determine the value of that length. Because of the pile movements are confined in the first diameters in depth, it is clear that the pile-soil response to horizontal loading depends essentially on the mechanical properties of the soil close to the ground level. It is therefore particularly important to realize a proper characterization of the soil mechanical properties at the first few meters in depth.

Moreover, it's possible to say that the pile maximum bending moment can be found at the pile-head in case of fixed-head restraint conditions, or along its shaft in case of free-to-rotate restraint conditions. The depth at which the maximum bending moment occurs, in the latter case, is about few pile-diameters and depends primarily on the pile-soil relative stiffness. Both the critical pile length value and the depth of the maximum bending moment section depend on the load level. As the load increases there is an increase of both the critical pile length and of the depth at which the maximum bending moment occurs (Figure 2.3).

During the design of a pile subjected to horizontal loads the most critical aspect is the proper prediction of the bending moments acting on the pile.

The single-pile response to horizontal loading depends, first of all, by the soil properties and by the way in which the resultant p varies with the increase of the pile displacement (y) and of the depth (z). The response depends, however, by many other factors, among which can be mentioned:

- the way the load is applied;
- the pile-head restraint conditions;
- the pile execution technique;
- the geometrical and mechanical properties of the structural section of the pile.

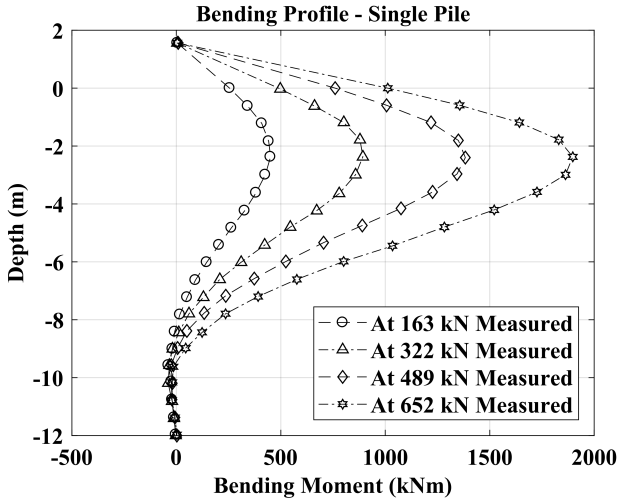

Figure 2.3: Increase of the depth of the maximum bending moment section with the horizontal load (FH) increase (Remaud, Garnier, and Frank, 1998)

2.1.1 Influence of the load mode

The load can be applied in a static, cyclic, or dynamic way. The different test modes have the aim to reproduce the loading conditions at which it is believed that the actual pile foundation will be subjected.

In the static test it is assumed that the load is applied in a monotonic form, with step-by-step increments, and short (short-term loading) or prolonged time intervals (sustained or maintained loading). In fine-grained soils a test like the first one refers to undrained conditions, the second type refers to drained conditions. An example of the relationship between the soil reaction (p) and the displacement, in a static test, is shown in Figure 2.4. Typically, can be easily recognized an initial linear trend, at which follows a highly non-linear trend (a-b, Fig. 2.4) and at the end the attainment of an asymptotic value, p_{ult}. The soil reaction modulus E_{py} (defined as $E_{py} = p/y$) is, consequently, constant for a first short segment and then starts to decrease.

The soil reaction, p, varies as a function of the displacement and as a function of the reference depth z. Figure 2.5 shows, at different depths, some experimental p-y curves obtained by Reese, Cox, and Koop (1975) during static load tests performed on cylindrical piles (diameter = 641 mm, length = 15.2 m) in overconsolidated clays. It is noted that the initial stiffness of the soil behaviour grows with depth, as well as the ultimate resistance value.

The response obtained in static tests, with loads applied for short time intervals or with loads kept constant for prolonged time intervals, does not vary significantly if the soil on which the test is realized is mainly composed by granular materials or overconsolidated clays. The effects, on the pile-soil system response, of a sustained load, however, may be not negligible in case of soft clays. Rarely a static test reproduces the

load mode at which the foundation will be actually subjected. However, for this test mode there is a clear correlation between the results obtained and the soil mechanical properties. Anyway, the results of static tests are important in order to compare them with those obtained using different load modes.

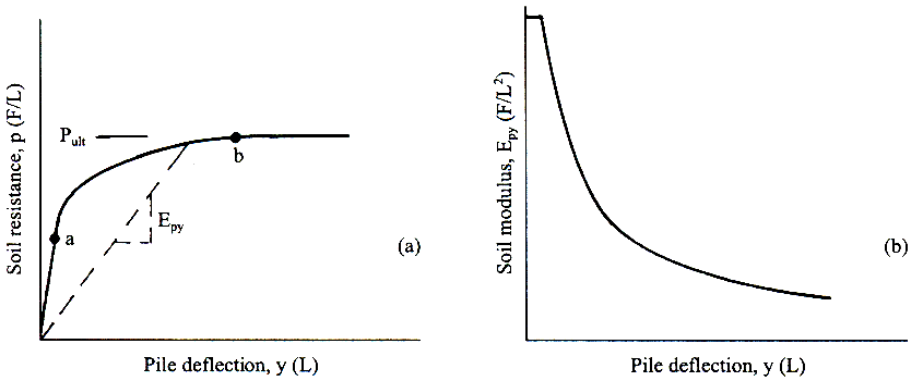

Figure 2.4: Reaction p and soil reaction modulus variations during a static load test (Reese and Van Impe, 2001)

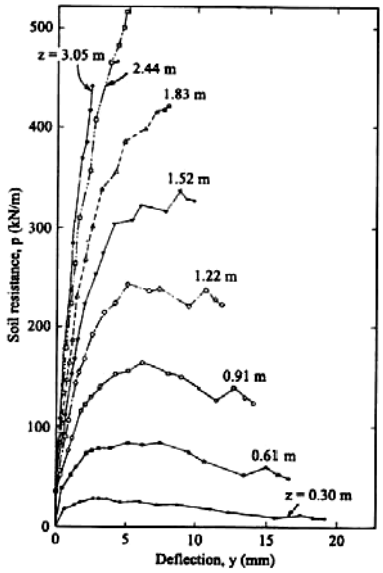

Figure 2.5: Experimental 'p-y' curves for different depth values (Reese, Cox, and Koop, 1975)

A cyclic load test provides that reached a certain load level, the same is made vary for a predetermined number of times nearby of the reached value. The effect of cycles is to decrease the overall stiffness of the pile-soil system and the ultimate resistance value p_{ult} (Figure 2.6). Usually, once reached a certain number of cycles, the soil response becomes independent from them.

Dynamic tests, instead, are performed to simulate the forces generated on structures by traffic, industrial machinery, by the waves and the earthquakes. Specific studies in this field have been conducted in relation to the effects generated by rotating

machinery or by earthquakes (for example, Gazetas and Mylonakis (1998)). Tests performed in different ways from the static mode are, even today, scanty. It is, therefore, still difficult to draw general trends.

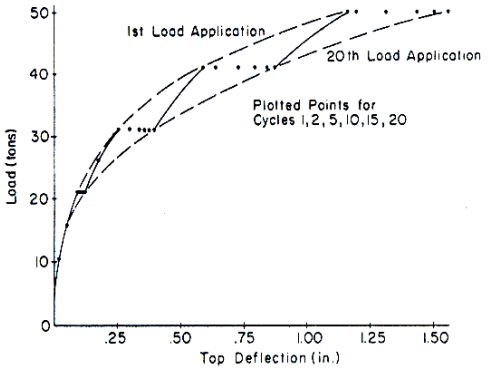

Figure 2.6: Influence of loading cyclic numbers on a 'p-y' curve (Reese and Welch, 1975)

2.1.2 Influence of the pile-head restraint conditions

The pile response to horizontal loads in the two extreme conditions of fixed or hinged head is significantly different. The displacements in fixed-head piles (i.e. without head rotation) are considerably smaller – about the half (Randolph, 1981) – than those in free-to-rotate condition, for a given load level. This is a consequence of the fact that a pure fixed-head pile interacts with the soil up to greater depths compared to the free-to-rotate pile. The distribution of the load on a greater soil volume results in a reduction in the pile displacement.

The restraint conditions affect also the internal forces distribution along the pile shaft. In the case of a free-to-rotate pile the maximum bending moment is located along the shaft of the pile, at depths generally fairly shallow (a few pile diameters). In the case of a pure fixed-head pile the maximum bending moment is placed at the rigid-connection itself. The bending moment acting on a fixed-head pile is significantly greater than the maximum bending moment acting on a free to rotate pile, the first can be also 4 times greater than the second (Dente and Gullà, 1983).

Assuming a pure-fixed head condition requires the assessment of the pile-connecting structure (pile-cap) capability to handle the expected bending moment.

2.1.3 Effect of the pile execution technique

The pile execution technique affects in a significant way the pile response to axial loads. The installation method (i.e., full displacement or non-displacement), in fact, significantly changes the stress state of the soil in contact with the pile.

In the case of a driven pile, because of the displacement induced in the soil, the horizontal stresses along the shaft grow compared to the value in geostatic conditions until reaching, as a limit, the passive resistance. Conversely, for a bored pile (realized removing the soil) the horizontal stresses decrease until reaching, as a limit, the active pressure. The changes in the stress state concern a reduced soil thickness but in correspondence of this thin layer, however, starts to develop the tangential stresses responsible for the pile shaft resistance to the axial loading.

The effects of the soil stress state changes, induced by the pile installation technique, on the response of a laterally loaded pile are much lower. This is because the

soil volume which affects the pile behaviour under horizontal loads is much greater than that for vertical loads. Figure 2.7 shows, in a qualitative way, a typical representation of the soil-wedge responsible for the response of a pile under lateral loads.

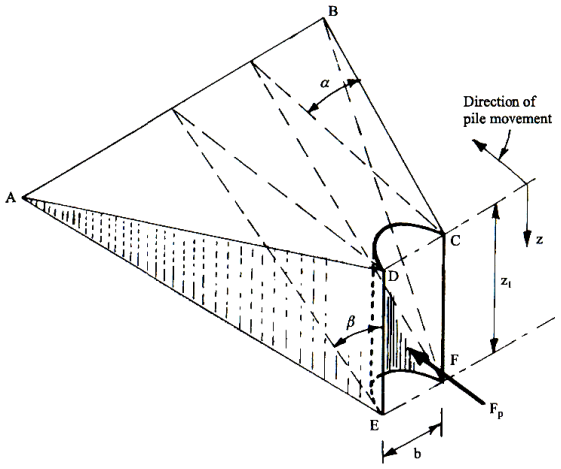

Figure 2.7: Soil-wedge responsible for the horizontal loading response (Reese and Van Impe, 2001)

Some authors (Huang and Hsueh, 2001; O'Neill, 1984) have tested piles realized in different ways, without, however, obtain definitive information on the influence of technology. Other tests indicate that the variability of the response due to the soil heterogeneity is an influence factor significantly more relevant than the installation technology.

In order to determine the pile response to horizontal loads in serviceability conditions, the most common analysis method is the 'p-y curves' method. To properly select the 'p-y curve' to use in the analysis, various authors (Matlock, 1970; Reese, Cox, and Koop, 1975; Terzaghi, 1955) have taken into account many factors, but not the pile execution technique.

2.1.4 Pile geometrical characteristics and mechanical properties

The geometry of the pile section affects the pile-soil response to horizontal loads. The horizontal stress distribution along the pile edge, in fact, varies according to the section shape (circular, square, or rectangular, H, etc..). Consequently, the soil reaction p value is variable, both in serviceability conditions and in ultimate conditions.

A possible way to take into account the effects of the pile shape, for geometries different from the circular one, is to identify an equivalent diameter value d_{eq}. Considerations on the pile shape influence are explained, for example, in Rowe (1956) and in Reese and Van Impe (2001).

The soil reaction p is also affected by the pile material. Considering again, a square pile orthogonally loaded, the values of the shear stresses that are induced on the faces parallel to the force direction are reasonably different depending on the pile material (concrete, steel, or wood). The interface roughness is a function of the material used for the pile and of the execution technique.

The pile mechanical characteristics in terms of flexural rigidity, E_pI_p (E_p elasticity modulus; I_p moment of inertia of the pile section), affect, obviously, the response. For the same geometrical characteristics and soil type, a pile with a greater flexural

rigidity, E_pI_p, induces stresses in the subsoil to a greater depth compared to a more flexible pile. The external force is transferred on a larger soil volume, consequently, the response of a more rigid pile is better in terms of displacement.

In the light of what can be found in literature, it can be assumed that the influence of the load mode and the restraint condition at the pile-head are the most important factors to consider for the description of the pile response.

2.1.5 Influence of vertical loadings on single piles

Piles are in general subjected to both vertical and horizontal loads, however, in the current design practice it is assumed that the effect of these two loads is independent of each other and thus it is accepted that the design/analysis process can be done considering these loads separately. Analysis methods based on Winkler approach (p-y curves methods) also do not consider the interaction between the vertical and horizontal loads. On this topic, unfortunately there are only few numerical and analytical studies and the experimental results are even more scanty and in some way contradictory.

For example, analytical investigations show that for a given horizontal load, the presence of vertical load can increase the horizontal displacement. Instead, laboratory (Anagnostopoulos and Georgiadis, 1993; Jain, Ranjan, and Ramasamy, 1987) and field investigations (Karasev, Talanov, and Benda, 1977; Sorochan and Bykov, 1976; Zhukov and Balov, 1978) suggest a decrease in lateral deflection when the horizontal load is applied after the application of a vertical load.

Anagnostopoulos and Georgiadis (1993) for example, suggested that the change in soil stresses and local plastic volume variations in the soil continuum under combined loads cannot be modelled in using standard subgrade-reaction or elastic half-space analysis methods, therefore, it's necessary to introduce some assumptions and some rational modifications in these models in order to consider the effect of combined loads. Therefore, they suggested to use a nonlinear 3-dimensional finite element technique to study this kind of problem.

Karthigeyan, Ramakrishna, and Rajagopal (2006) tried to understand the influence of vertical loads on the lateral response of single piles installed in sandy soils and Karthigeyan, Ramakrishna, and Rajagopal (2007) in sandy and in clayey soils, through 3-dimensional finite element analyses. In the numerical model, the pile was modelled in a linear elastic manner (square pile-section: 1200 mm x 1200 mm) and the soil constitutive model used was a Drucker–Prager model with a non-associated flow rule.

The authors tried to evaluate in particular the influence of the sequence of load application, of the shear strength (angle of internal friction and dilation angle) of soil, of the pile head constraint conditions and the pile slenderness ratio (L/B = Length/Pile section width).

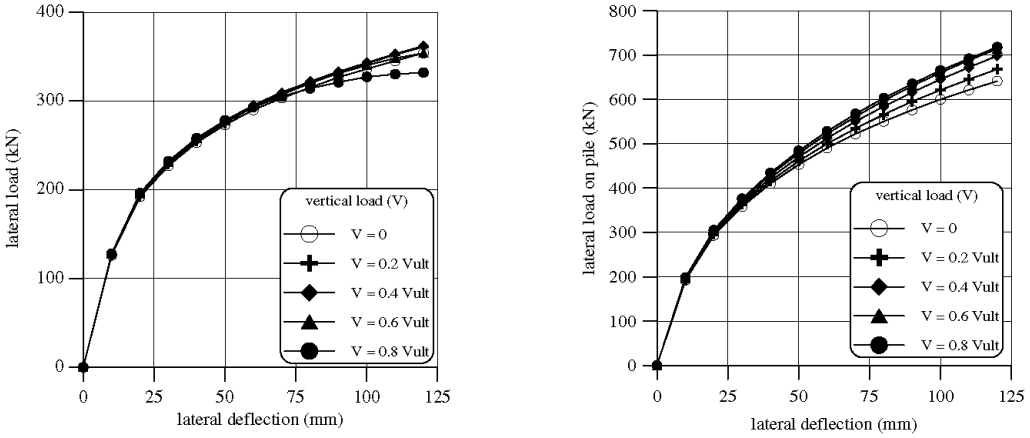

Figure 2.8: Lateral load–deflection behaviour of a pile in loose sand (left-plot) and in dense sand (right plot) for the $SAVL$ case (Karthigeyan, Ramakrishna, and Rajagopal, 2006)

The main results obtained in this work were:

- the load sequence has an important role in single piles in sandy soils; it can be seen in Figure 2.8 that when the vertical load is applied in the same moment of the horizontal one ($SAVL$ = simultaneous application of vertical and lateral loads) the effect of the vertical load on the lateral response of the single pile in a loose sand (ϕ=30 °; $\gamma = 18kN/m^3$; $E_s = 20MPa$) and in a dense sand (ϕ= 36 °; $\gamma = 20kN/m^3$; $E_s = 50MPa$) is negligible even for high vertical loads (80% of the single pile bearing capacity) and high displacement level (maximum horizontal displacement in the analysis = 120 mm = 10% of B); in Figure 2.9 instead, only in the case of a single pile in dense sand the influence of the vertical load, applied before the application of the lateral one (VPL = vertical prior lateral load), can be significant and leads to an increase of the lateral resistance as the vertical load increases.

- in order to quantify the improvement in lateral response the authors defined the quantity called PIC (= Percentage Improvement in lateral Capacity) that can be obtained with the expression:

$$PIC = \frac{(LCWV - LCNV)}{LCNV} 100 \tag{2.1}$$

  where: $LCWV$= Lateral capacity with vertical load; $LCNV$= Lateral capacity under pure lateral load (no vertical load). According to the authors, the improvements can be attributed to the development of additional lateral soil stresses in front of the pile and additional frictional resistance developed along its length.

- performing the same analyses on fixed-head piles, however, the authors found that in this head-constraint conditions the vertical load influence is less in comparison to free head piles especially at larger deformation levels.

- another important result is that the influence of vertical loads is less significant in the case of long flexible piles as can be seen in Figure 2.10. The influence of vertical loads is negligible beyond an L/B ratio higher than 16 in sandy soils.

- the maximum bending moment increases by as much as 30 to 35% in sandy soils.

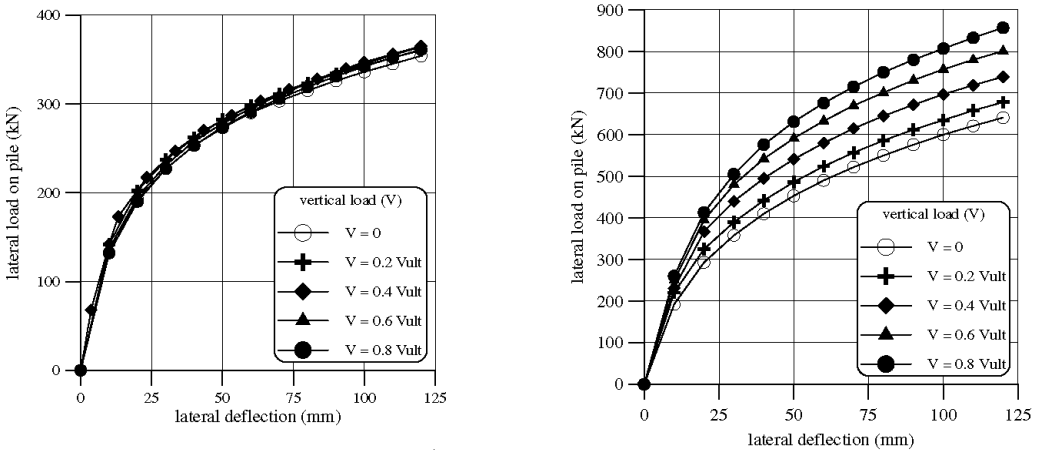

Figure 2.9: Lateral load–deflection behaviour of a pile in loose sand (left-plot) and in dense sand (right plot) for the VPL case (Karthigeyan, Ramakrishna, and Rajagopal, 2006)

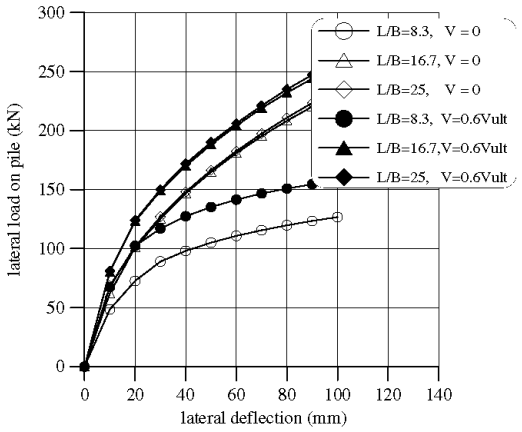

Figure 2.10: Influence of vertical load on the lateral response of piles with respect to different L/B ratios (Karthigeyan, Ramakrishna, and Rajagopal, 2006)

In Karthigeyan et al. (2007) moreover the influence of the vertical load on the response of a single pile in clayey soil under horizontal loading was also investigated, and the main findings were:

- the presence of a vertical load marginally reduces the lateral capacity of piles in clayey soils for vertical load levels up to $0.6V_{ult}$;
- the influence of vertical loads remains constant beyond an L/B ratio of 16 in clayey soils;
- in the case of clayey soils, the maximum bending moment increases by about 10 to 15% for L/B values less than 15 and about 30% for longer piles.

2.2 Pile group response to lateral loading

In the previous section has been described the typical response of a single pile subjected to horizontal loads. In real cases, however, the piles arranged below a foundation structure are not in isolated conditions, but are part of a group, linked together by

a suitable connecting structure (plates, footings, foundation beams). The behaviour of a pile within a group subject to horizontal actions differs from that of a single isolated pile. In this section are described the typical response aspects of pile groups subjected to horizontal loading. The main factors that influence the response of a pile group, and of each single pile within the group, are:

- 'pile-soil-pile' interaction;
- 'connecting structure-soil' interaction;
- stiffness of the connecting structure.

In the case of a pile group subjected to horizontal loads the stiffness of the connecting structure, loaded in its plane, is significantly higher than that of the piles (shear and bending stiffness). Therefore, with good approximation the connecting structure can be considered infinitely rigid and assume that the pile-heads displacements are all equal. Heterogeneous, vice versa, is the load distribution between the piles within the group. The load tests conducted on pile groups (published in literature) confirm the validity of this assumption.

What is mentioned is based on the collection of the results obtained through the realization of static horizontal load tests on pile groups, in full-scale or in centrifuge. Given the difficulties, for economic and technological issues, to perform load tests on pile foundations having a considerable size, the series of experiments on pile groups do not include cases in which there are a large number of piles.

2.2.1 Efficiency

Pile-soil-pile interaction causes a decrease of the stiffness of the overall system. In general, for an equal average load at each pile, the displacement of a pile group is greater than the displacement of a single isolated pile; in the same way, for a given displacement (at the pile-head), the load supported by an isolated pile is higher than the average load supported by a pile within the group (Figure 2.11).

Quantitatively, the interaction intensity is represented defining the efficiency η of a group composed by m piles; this parameter indicates the ratio, for a given pile-head displacement, between the average load H_g/m acting on a pile within the group (H_g is the total load acting on the group) and the load acting on a single isolated pile H_s:

$$\eta = \frac{H_g}{mH_s} \tag{2.2}$$

The interaction phenomena become more relevant as the distance between the piles in the group is reduced. Conversely, the interaction tends to disappear increasing the distance between the piles. Experimental evidences showed how the interaction effects decrease considerably for distances of 5D (McVay, Casper, and Shang, 1995) and can null for distances exceeding 6D (Cox, Dixon, and Murphy, 1984) (D=pile diameter). In this case, each pile within the group behaves like a single isolated pile.

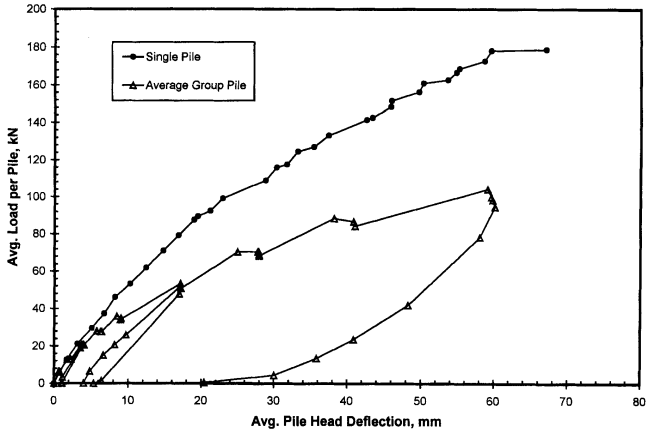

Figure 2.11: Load-displacement relationship for a single pile and a 3x3 pile group (Rollins, Peterson, and Weaver, 1998)

As a result of these reciprocal interactions in a group (where the piles are connected by a connecting structure infinitely rigid not in contact with the ground) each pile behaves in a different manner from the others. The response of each pile is essentially a function of the position that it occupies within the group. In particular, the response of the single pile within the group is influenced by:

- the belonging row within the group (shadow effect or shadowing);
- the position within a single row (edge effect).

The first of the two phenomena has a greater importance. Mainly, it was observed a significant difference in the response mode of the first row, which is more rigid, compared to the subsequent (that are more flexible). The first row (or front-row) is the first in the group advancement direction and it is the row that pushes into an undisturbed soil. The second of the two phenomena induces, within a same row, a load concentration on the outer piles, which carry a bigger rate of load compared to the piles located in the inner part of the row.

The value of the efficiency is, for pile-groups having a small spacing, lower than the unity. As the distance between the piles increases the efficiency tends to unity, to become exactly equal to one when the relative distances between the piles are such as to delete every interaction phenomenon.

The efficiency of a pile group is not constant, but varies with the increase of the load acting on the group. The initial stiffness of a group and that of a single pile are almost equal (Brown, Reese, and O'Neill, 1987) (Figure 2.12); it follows that for low displacement values, the efficiency can be assumed equal to one. As the load increases, the interaction phenomena increase and the efficiency exhibits a decreasing trend until reaching an asymptotic value in correspondence of displacements sufficiently large. The trend assumed by η in laterally loaded piles is opposite to that seen in case of pile groups subjected to vertical forces (Figure 2.13, where G_e is equal to η). These different trends demonstrate the presence of different interaction mechanisms (Mandolini, Russo, and Viggiani, 2005).

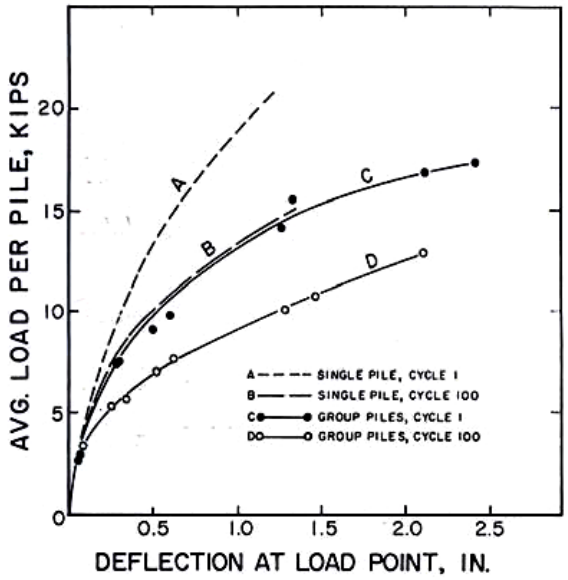

Figure 2.12: Average load – displacement for a single pile and a 3x3 pile-group: they have the same initial stiffness (Brown, Reese, and O'Neill, 1987)

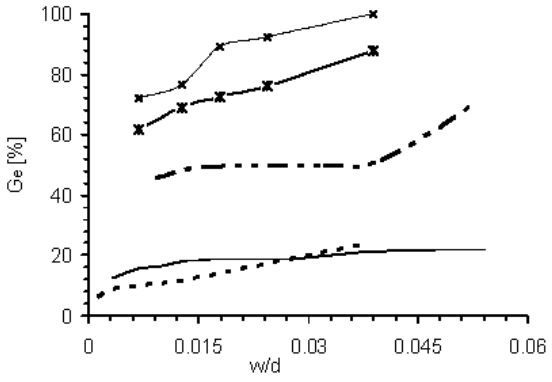

Figure 2.13: Efficiency G_e trend for pile-groups (from 4 to 144 piles) under vertical loads, to vary the relative group displacement w/d (Mandolini, Russo, and Viggiani, 2005)

The observation of experimental data suggests that the pile group efficiency depends on all of the following aspects:

- soil properties;
- pile-soil relative stiffness;
- relative distance between the piles;
- number of piles within the group and geometry;
- displacement level.

The centrifuge has allowed to realize load tests on groups progressively increasing in size. The observation of experimental data obtained in these tests suggests that the

influence of the number of rows on the efficiency values gradually stops. Reached a certain number of rows (five, (McVay et al., 1998)) or a specific number of piles, the efficiency becomes independent to the group size. Although the experimental results available right now seem to confirm these statements, it is appropriate to observe that the pile groups sizes on which the tests were carried out are substantially modest (up to 16 piles in full-scale tests, a maximum of 21 piles in centrifuge tests and up to 4 piles per row). There are no experimental evidences available that guarantee the extensibility of these considerations to larger groups.

The experimental data available allow a further consideration. The group efficiency is not constant and tends to reach an asymptotic value for sufficiently high displacements. McVay et al. (1998) identify, on the basis of their results, in 0.06D the displacement value needed to reach the asymptotic value.

2.2.2 Pile group load distribution: Shadowing Effect and Edge Effect

The total load acting on a pile group with a spacing sufficiently reduced ($s/D < 6$) and subjected to a static horizontal load is divided in an inhomogeneous way among the single piles.

The loading rate taken by each pile is conditioned mainly by the pile belonging row within the group. The available tests show that the row carrying the higher loading rate is the front one, that encounters the resistance of a soil not disturbed by the presence of the other rows. The subsequent rows, instead, carry lower loading rates. The uneven load distribution due to the belonging row within the group is commonly known as shadowing effect (Brown, Morrison, and Reese, 1988).

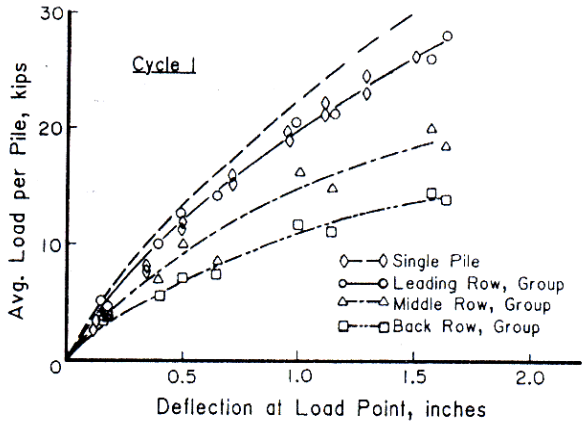

Figure 2.14: Average load – displacement curves for a single pile and the rows of a 3x3 pile group (Brown et al., 1988)

The piles belonging to the first row of the group tend to show a behaviour similar to that of the single pile. If it is compared the load-displacement curve of the piles in the first row (Figure 2.14) with that of the single pile, no particular differences can be observed. The stiffness of the first row of a pile group is therefore comparable to that of a single pile.

The load-displacement curves related to subsequent rows, instead, are significantly more flexible. In fact, the movements of the front piles induce a reduction in the stress state of the soil between the two rows of piles. The following rows, therefore, are in contact with a soil conditioned by the presence of the other piles (Figure 2.15).

The stiffness reduction concerns essentially the most superficial soil layers. Experimentally it was observed as, on average, the second row is more flexible than the first, the third than the second (but, for example, Rollins et al., 1998 is an exception), the fourth than the third. From the fourth row onwards, however, there is not a further loss of resistance. This statement is supported by data obtained by both centrifuge tests (McVay et al., 1998) and in situ tests (Rollins et al., 2005).

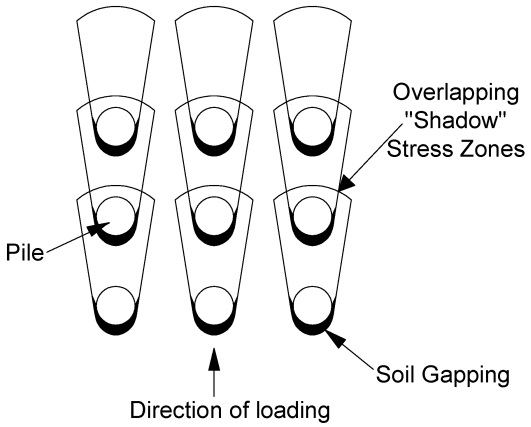

Figure 2.15: Overlapping of soil shear strength areas in a horizontally loaded pile-group (Rollins et al., 1998)

The arise of an inhomogeneous load distribution between the piles belonging to the same row is identified as edge effect. From a physical point of view, this phenomenon is generated by the progressive overlapping of passive wedges of soil. The soil resists to the piles action by means of the arise of resistance wedges in front of the piles. As the external loads increase, the volume grows and the wedge overlaps with those of the adjacent piles (Figure 2.16). This effect is more evident for the inner piles compared to the outer piles in the same row. For this reason, the inner piles are more flexible and carry a smaller loading rate; the outer piles instead are more rigid, and carry a higher loading rate. The edge effect, even if is less significant compared to the shadowing effect, represents a peculiar aspect of the pile groups behaviour.

Many authors, who have realized tests on pile groups, assume reasonable that the load distribution between the piles belonging to the same row is basically homogeneous (Brown, Morrison, and Reese, 1988; Rollins, Lane, and Gerber, 2005). In the case studies where the load distribution between the piles belonging to the same row is shown, however (Ilyas et al., 2004; Rollins, Lane, and Gerber, 2005), not always the difference between the loading rate carried by the outer piles and by the inner piles is negligible (Figure 2.17).

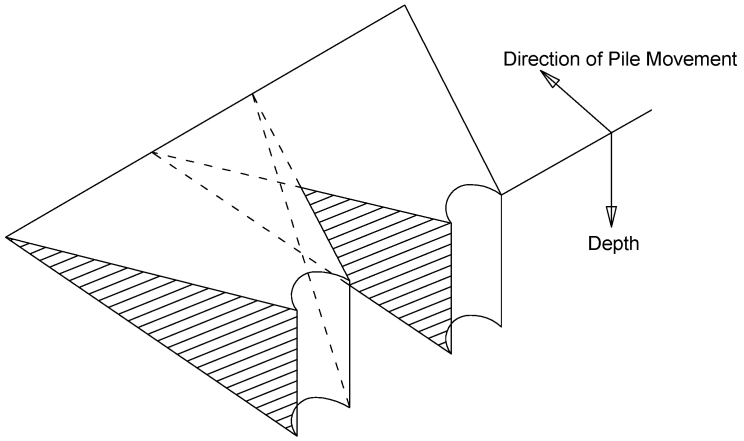

Figure 2.16: Overlapping soil shear strength zones in a same row of piles (Brown et al., 1988)

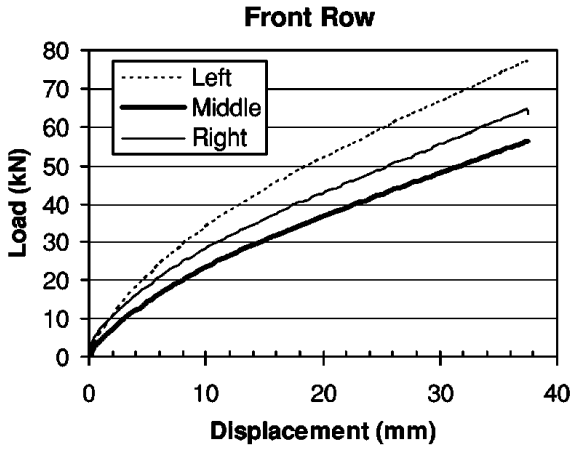

Figure 2.17: Load – displacement curves for three piles in the first row of a 3x3 pile-group (Rollins, Lane, and Gerber, 2005)

2.2.3 Bending moments

The different load distribution in a pile-group, and the different soil ability to provide resistance to the piles horizontal movements due to their belonging row, in turn, generate a different trend of the bending moment profiles in the piles of the group.

The piles located in the rows behind the first one are subjected to lower loads. In absolute terms, therefore, they are subjected to bending moments lower than those in the front piles (Figure 2.18).

The piles in the front row carry loads similar to those of a single pile. They interact, substantially, with an undisturbed soil. As a consequence, the bending moment profile of a pile in the front row is analogous to that of a single pile (Brown et al., 1988; Figure 2.19b).

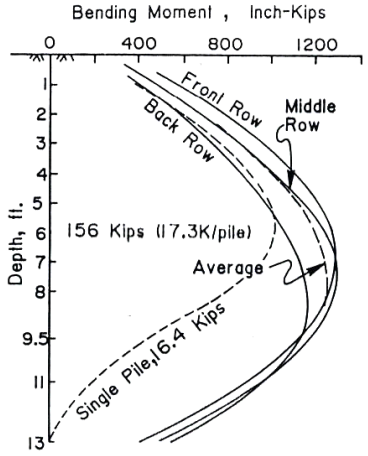

Figure 2.18: Average bending moment distributions for the three rows of 3x3 pile-group (Brown, Reese, and O'Neill, 1987)

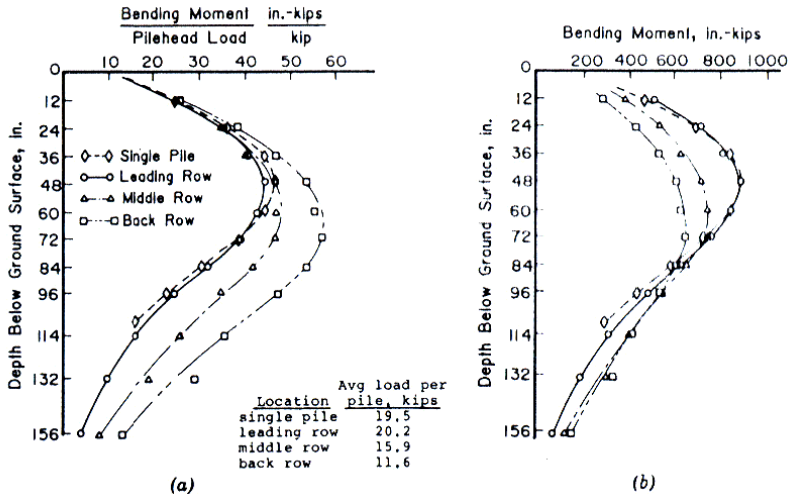

Figure 2.19: Bending moment distribution for a single pile and for the piles in the rows of a 3x3 pile-group, normalized to the shear-load acting (a) and in absolute values (b) (Brown et al., 1988)

If the value of the bending moment acting on the pile is normalized over the load acting on its head it can be observed as the bigger normalized moments occur in the piles in the back rows (Brown, Morrison, and Reese, 1988; Rollins, Lane, and Gerber, 2005) (Figure 2.19a). This is a consequence of the fact that these piles interact with a soil conditioned by the presence of the other piles of the group. Since the most influenced soil volumes are those close to the ground surface, for the rows subsequent to the first one the maximum bending moment values occur gradually deeper (Brown, Reese, and O'Neill, 1987) (Figure 2.20).

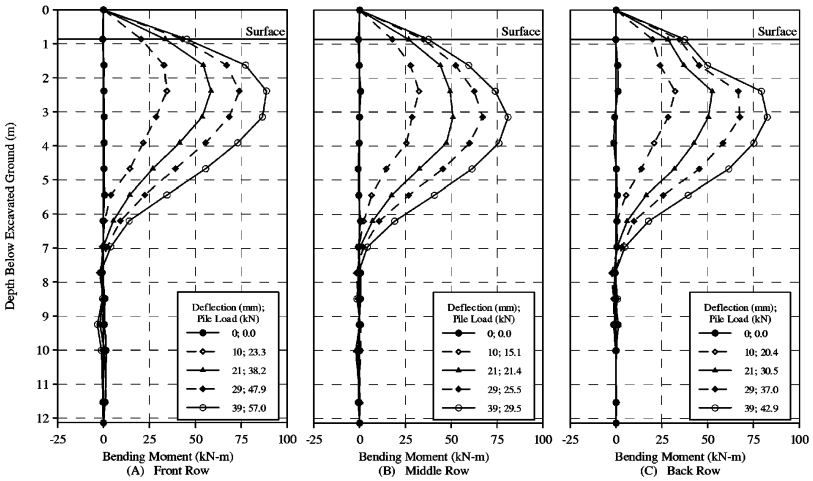

Figure 2.20: Bending moment distributions for the piles of the three rows in a 3x3 pile-group at different load levels (Rollins, Lane, and Gerber, 2005)

2.2.4 Influence of the execution technique

In the description of the single pile behaviour under horizontal loads, it has been explained that the pile installation technique is one of the factors that can influence the response. However, compared to the other factors, this aspect is less important.

When the problem is about the pile groups this consideration may not be true again. If the spacing between the piles of the group is reduced, in fact, the mechanical properties of the soil located near the installation area can be modified in a non-negligible way by the realization of the piling. In particular, if the execution technology involves the installation of the piles with soil displacement procedures (driven piles), it can lead to an improvement of the soil mechanical properties. The piles that would benefit this improvement are mainly those belonging to the inner rows of the group, because they lie in an area more conditioned by these changes. The piles of the outer rows, and in particular those of the front row, instead, continue to act in a soil with properties similar to those undisturbed.

To quantify the soil properties changes induced by the pile group installation technology, would be desirable to perform in situ tests before and after the piles realization, within the area of the piling. In some cases, these information are available (Ochoa and O'Neill, 1989; Brown, Morrison, and Reese, 1988; Rollins, Lane, and Gerber, 2005).

Huang and Hsueh (2001) carried out full-scale lateral load tests on a group of bored and on a group of driven precast piles as part of a research project for the high-speed rail system in Taiwan. Standard penetration tests, cone penetration tests (CPT), and Marchetti Dilatometer tests (DMT) were performed before the pile installation and also after pile installation.

The authors observed that the pile group installation, bored or driven, tended to disrupt a crustlike material near the ground surface and lower the in situ lateral stress. Bored pile group construction appeared to loosen the soil surrounding the piles, whereas the driven pile group construction apparently caused a densifying effect. The construction effects were limited to the top 15 m from ground surface, where soil conditions have the greatest effect on the behaviour of laterally loaded piles.

This study outlines that the lateral soil resistance against piles in a group can be highly dependent on the type of pile installation (driven or bored) and preconstruction

soil conditions. It is not simply a matter of geometry as typically assumed in current practice. Separation of mechanical effects from installation effects is likely to result more consistent.

Numerical analyses of the laterally loaded piles were conducted using p-y curves derived from preconstruction and postconstruction DMT and by applying the concept of p multipliers. Comparisons between preconstruction and postconstruction CPT and DMT data and evaluation of the results of computations show that the installation of bored piles softened the surrounding soil, whereas the driven piles caused a densifying effect.

2.2.5 Influence of vertical loading on pile groups

As explained in the section about the influence of vertical loads on the lateral response of a single pile, the numerical analysis realized by Karthigeyan et al. (2006, 2007) showed substantially that the effects can be really important only in the case of single piles having a slenderness ratio less than 16 (short piles) with free-head constraint condition, in dense sand where the vertical load is applied prior to the application of the horizontal load and for vertical load values higher than the 40% of the pile bearing capacity. In these conditions the single pile exhibits an improvement of its own lateral capacity due to the development of additional lateral soil stresses in front of the pile and additional frictional resistance developed along its length. While in case of clayey soil instead the influence of the vertical load leads to some marginal reduction of the lateral response.

However, the literature is even more scanty of findings regarding the simultaneous application of both vertical and lateral loading on pile groups.

The work presented by Abbasa, Chik, and Taha (2015) is practically the only one that tried to understand and to quantify the effect of simultaneous load combinations on the lateral pile response within group. In order to evaluate these effects, 3-dimensional finite element analyses were conducted using the software Plaxis 3D-Foundation, where the piles (elastic beams with a diameter = 1.0 m and a length = 15.0 m) and the pile-cap were modelled using a linear elastic constitutive model, and the soil (cohesioneless (E_s = 13 MPa; ϕ=30 °; c'=0 kPa) and cohesive soils (E_s = 10 MPa; ϕ=25 °; c'=5 kPa)) was modelled using the Mohr-Coulomb constitutive model and using 16-nodes interface elements. Three pile groups layout were investigated (i.e., 2x1, 2x2 and 3x2) with four pile spacings (i.e., s = 2D, 4D, 6D and 8D). Laterally applied loads were 50, 250 and 450 kN. In addition, forces of 2H, 4H, 6H, 8H and 10H represent the axial loads.

It was observed that the lateral pile displacement changes and the lateral soil pressure redistributed when the level of axial load was increases. This was also observed by Karthigeyan et al. (2006, 2007) for the single isolated pile case.

The main finding of this works is that the group interaction effect led to reduced lateral resistance for the pile in the group compared to the single pile case under a pure lateral load, while, in case of simultaneous combined loads, with large axial load intensities (i.e., more than 6H, where H is lateral load values), have been noted an increase of the group piles capacities.

However, in my opinion all these results were obtained using a very simplified 3D-model, in fact:

- the piles were simple elastic-beams, thus the influence of the volume occupied by the piles was neglected;

- the software used (Plaxis 3D-Foundation) suffers of some lacks to properly study this really difficult soil-structure interaction problem compared to the newest version of Plaxis 3D;
- moreover the constitutive model used herein for the soil is an elastic-perfectly plastic model that can't consider properly the stress-dependency of the soil stiffness (this kind of dependency can be captured using more advanced constitutive models like the Hardening Soil Model or the Hardening Soil model with Small Strain Stiffness that can consider even of the strain dependency of the soil stiffness).

Finally, in order to provide some suggestion on the response of a pile-group under combined loads (vertical and lateral loads), some experimental results (in particular from full-scale tests) are absolutely necessary in order to verify the appropriateness of the predictions obtained using 3-D finite element software.

2.3 Piled raft response to lateral loading

Horizontal loads on a piled-raft foundation are resisted by (Viggiani, Mandolini, and Russo, 2011):

1. the piles;
2. the passive resistance of the soil on the front of the embedded structure;
3. the frictional resistance along the embedded sides;
4. the frictional resistance along the base of the raft.

Generally, in the conventional design approach only the resistance offered by the piles is considered by the methods usually used to study pile groups. But even more in this loading condition compared to the vertical loads, such a design approach may be overly conservative since it neglects all the additional resistances provided by the raft-soil system, previously indicated at the points (2), (3) and (4) (2.21).

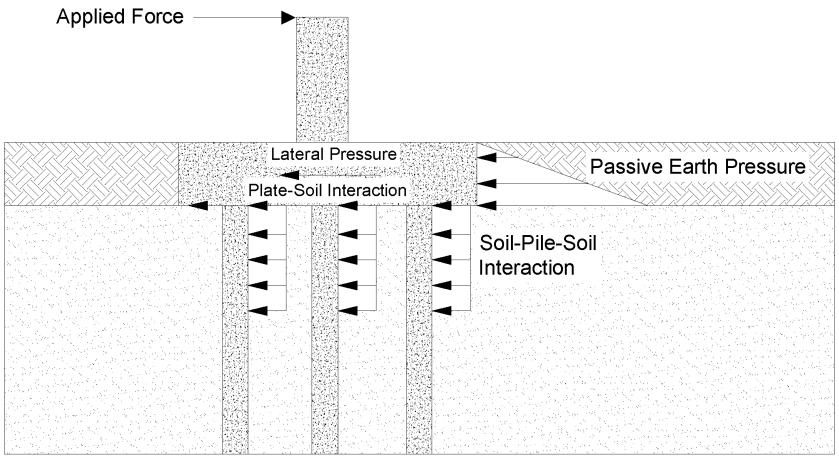

Figure 2.21: Piled raft response to horizontal loads

Nevertheless, the above resistances start to develop at different displacement level so that progressive failure starting from the stiffer component could occur, and it's

clear that if the piles are the stiffer component of the foundation, the situation could be dangerous.

2.3.1 Lateral resistance of embedded pile-cap (full scale tests)

Only four publications were found about tests performed to investigate the lateral-load resistance of pile caps considering the resistance offered by the soil in front, along the sides and along the base of an embedded raft. The results of these studies, summarized in Table 2.1 and in Figure 2.22 , show that the lateral-load resistance provided by the pile caps is significant and cap resistance can exceed the resistance provided by the piles themselves.

Table 2.1: Summary of previous load tests performed to evaluate the lateral resistance of pile caps

Ref.	Pile type	Cap size	Foundation soils	Cap Load rate (%)
Beatty (1970)	2x3 group of step-tapered mandrel-driven concrete piles 0.38 m diameter at top	4.1 m long 4.0 m wide 2.7 m thick	Miscellaneous fill over soft silty clay and clay	>50
Rollins et al (1997)	3x3 group of 0.3 m diameter steel pipe piles	2.7 m long 2.7 m wide 1.2 m thick	Compacted sandy gravel fill over silt and clay	about 50
Zafir et al (1998)	2x2 group of 0.6 m diameter drilled shafts	3.4 m diam 3.0 m thick	Silty sand clayey sand and sandy clay with caliche layers	>50
Mokwa (1999)	3 - 2x2 group of 0.25 m diameter driven steel H piles	1.5 m wide 0.46 m thick (1) 0.91 m thick (2)	Silty sand Sandy clay	>40

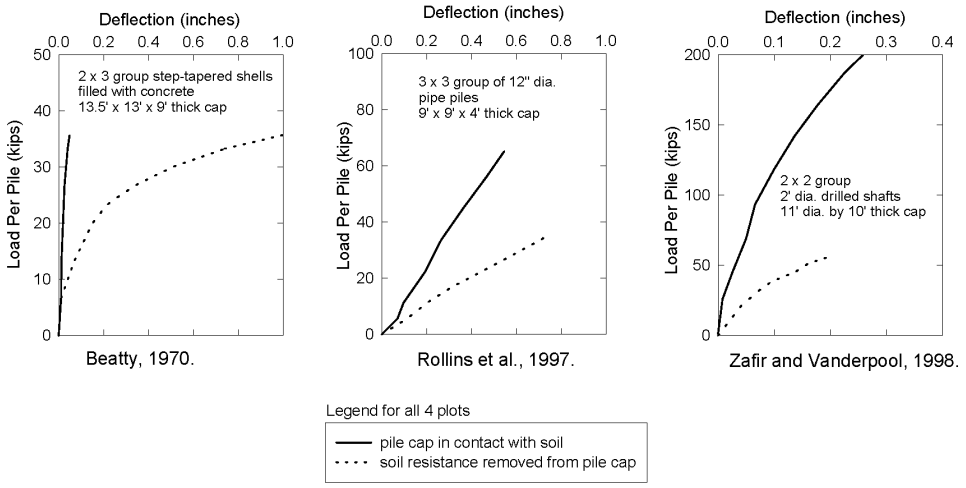

Figure 2.22: Comparison of published Load versus Deflection Curves, Mokwa (1999)

The tests realized by Beatty (1970) considered only the passive resistance at the front of the cap. In this work, Beatty tested two 6-pile groups of step-tapered piles and found that approximately 50% of the applied lateral load was resisted by the pile cap.

Rollins et al. (1997) instead investigated the response of a group of nine piles under statnamic lateral loading tests founding that the pile cap resistance was approximately

equal to the lateral resistance of the pile group. As in the work of Beatty (1970), Rollins et al. (1997) investigated just the passive resistance of the soil in front of the cap in dynamic loading condition. Zafir and Vanderpool (1998) tested a group of four drilled shafts, 0.6 m in diameter, with a 3.4 m diameter, 3 m thick cap, and estimated that the horizontal resistance of the cap was greater than the lateral resistance provided by the drilled shafts. These tests involved a variety of pile and cap sizes, soil conditions, and loading conditions.

In the work of Mokwa (1999) were realized tests on three groups of four HP 10x42 piles (one with a cap 0.46-m thick and two with caps 0.91-m thick, the caps were 1.5 x 1.5 m in plan) with a spacing of 4D (D = 250 mm), a buried concrete wall (or bulkhead) with no piles, and two single HP 10x42 piles, as shown in Figure 2.23 and the pile lengths varied from 3 to 6 m. Thirty-one lateral-load tests were conducted at the field test. In particular, were investigated the effects of cap side resistance, cap depth, pile length, and backfill type.

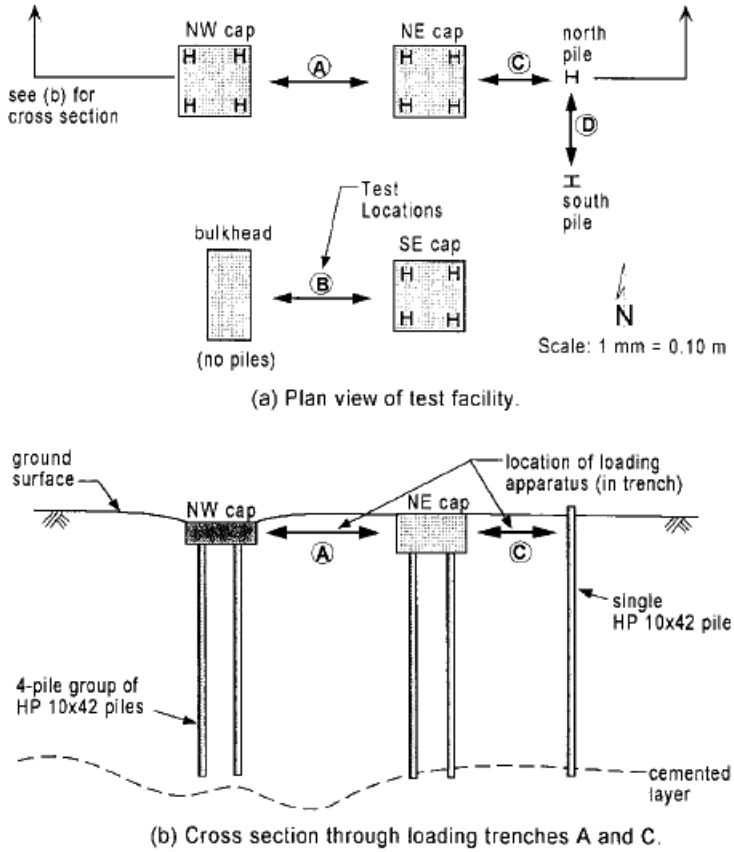

Figure 2.23: Field test facility - Mokwa (1999)

Two different type of soil were used as backfill in these tests: New Castle sand and crusher run gravel. These materials were selected because they are representative of the types of materials often used for backfill.

During the tests were observed pile-cap deflections relatively small, often <5 mm at the maximum load of 620 kN (the capacity of the loading system). This corresponds to a lateral load per pile of 155 kN, which exceeds typical design loads for HP 10x42 piles. These results are significant, considering that many foundations are designed for maximum deflections of 12–25 mm, with no consideration of the resistance provided by the pile cap.

In the first series of tests, the pile groups were tested with the caps embedded in the natural soil. The results from these tests are shown in Figure 2.24. The percentages of overall lateral resistance provided by the pile caps are as follows:

- Northeast cap—40% at 2.3-mm deflection
- Northwest cap—50% at 1.3-mm deflection
- Southeast cap—50% at 3.2-mm deflection

The resistance provided by the pile caps can also be seen in terms of the increase in deflection at the same load after excavating soil from around the caps. The percentages by which the deflections increased were:

- Northeast cap—150% at 620-kN load
- Northwest cap—400% at 620-kN load
- Southeast cap—500% at 400-kN load

Additional lateral load tests were performed after backfilling around the caps with gravel. The comparison between the lateral-deflection curves for the tests in natural soil and gravel backfill are presented in Figure 2.25.

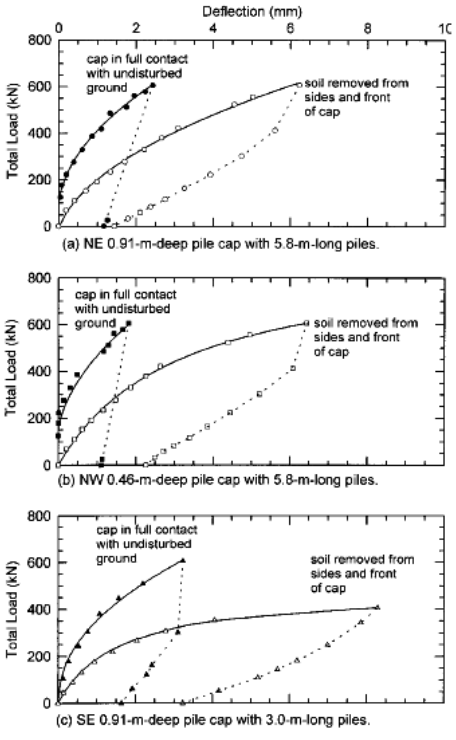

Figure 2.24: Load-Deflection response with and without Pile-Cap embedment in Natural-Soil - Mokwa (1999)

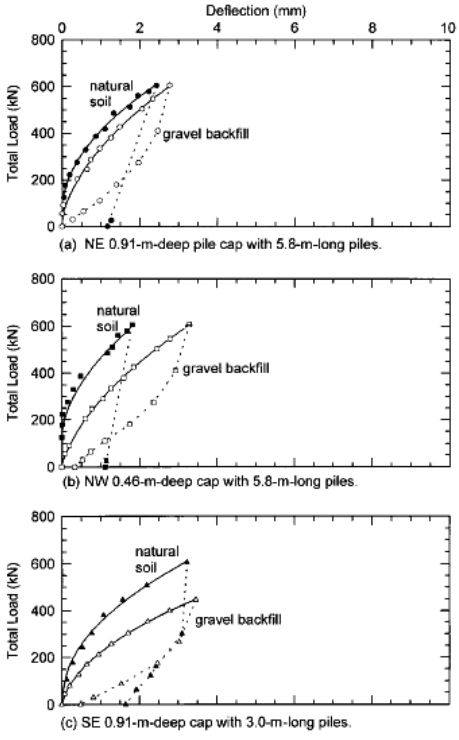

Figure 2.25: Comparison between Natural Soil and Compacted Gravel Backfill - Mokwa (1999)

It was observed that caps embedded in the stiff natural soils exhibited stiffer responses compare to the caps backfilled with compacted gravel. Other tests were performed using four different backfill conditions, to study the effect of backfill strength.

Smaller deflections were observed in the stiffer soils and deflections increased noticeably as soil strength and stiffness decreased.

Finally, it was found that the stiffest and strongest soil was the natural undisturbed soil, followed in order of decreasing stiffness by dense gravel, dense sand, loose sand, and no soil. For these reason the author remarked that not only the cap can provide a significant resistance rate, but also the magnitude of this resistance can be increased by increasing the strength and stiffness of soil around the cap.

2.3.2 Lateral resistance of non-embedded pile-cap (experimental results)

Only few publications were found about tests performed to investigate the lateral-load resistance of pile caps considering only the resistance offered by the soil along the base of the raft. Here are reported the main findings obtained with centrifuge tests (Horikoshi et al., 2003), small scale laboratory tests (Katzenbach and Turek, 2005; Matsumoto et al., 2010; Unsever, Matsumoto, and Ozkan, 2015; Hamada et al., 2015), full-scale field tests (Kim, Brungraber, and Singh, 1979). Some attempts have been done to capture the phenomenon under generalized loading by numerical analyses (e.g. (Cunha and Zhang, 2006)), but further investigations on the effect of a raft in contact with soil are needed.

Kim et al. (1974) performed lateral load tests on two identical pile groups, one free standing and another one with the raft in contact with the ground. In the early stages of the test the maximum bending moments observed in the piles were very similar in these experiments; this finding has been explained with a negligible mobilization of the friction between the raft and the soil. At higher load level, however, the observed moments in the piles of the raft in contact were less than half those in the free standing group, due to the contribution of the friction between the raft and the soil resulting in a decrease of the loads transmitted to the pile head.

Horikoshi et al. (2003) performed a series of horizontal loading tests on piled raft models and their components (single piles and rafts alone) on sand in centrifuge (50g). The main aim of the work was to clarify the effects of the rigidity at the pile head connection on the piled raft behaviour. In these tests the authors, observed that the raft-soil friction is fully mobilized at a displacement much lower than that needed to mobilize the lateral bearing capacity of the piles. In this study the vertical load was applied by increasing the initial raft mass to 2298 N at 50g and about 40% of the vertical loads were carried by the 4 piles before performing the horizontal test in both cases (rigid and hinged connection between piles and raft). The main findings of the authors were:

- the stiffness and the resistance of the single pile in piled raft and those in a single isolated pile are different because of the difference in the confining stress condition (Figure 2.26). Piles in hinged piled-raft have a smaller horizontal stiffness compared to the isolated single pile. This fact indicates that the interaction between the piles and the raft base probably reduced the stiffness per pile in the piled raft model. In the rigid pile head model, higher pile head rigidity and confining stress prevailed over the interaction effects between the piles and the raft base;
- the initial stiffness of a piled raft is not always higher than that of a raft alone (because the piles reduce a lot the contact pressure between raft and soil);
- higher horizontal load is transferred to the piles in the piled raft with rigid pile head connection (Figure 2.27), which leads to higher initial horizontal stiffness compared with that in the piled raft with hinged pile head connection;

- according to Figure 2.27 the total horizontal resistance of the rigid connection piled raft is higher than that of the raft alone, whereas the total resistance is lower in the hinged connection model. This fact is related to the higher horizontal resistance of the piles in rigid connection condition;
- the maximum bending moments (Figure 2.28) in the hinged connection model were smaller than those in the rigid connection model. The proportion of the horizontal load transferred to each component is also shown (Figure 2.29). The proportion of the raft load rapidly decreased as the piled raft displacement increased. The reduction in the proportion of the raft load was more significant in the rigid connection model, which was related to a higher horizontal stiffness of the piles;
- in the rigid model the soil beneath the raft was constrained by the existence of the piles, which reduced the shear deformation of the upper soils, and thus the mobilized shear stress at the raft-soil interface was less than the estimation conducted by the authors. In the hinged connection model, the shear deformation of the upper soils may not be highly constrained compared with that for the rigid connection model.

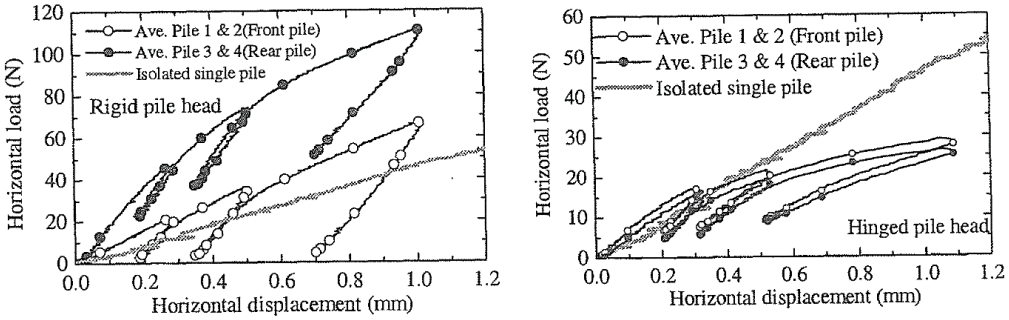

Figure 2.26: Horizontal load-displacement relationships of piles in rigid and hinged pile head model - Horikoshi et al. (2003)

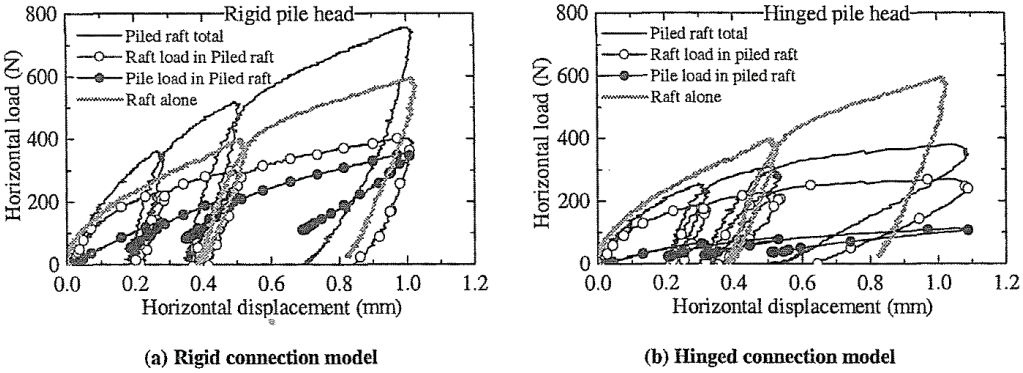

(a) Rigid connection model **(b) Hinged connection model**

Figure 2.27: Horizontal load-displacement relationships of piled-rafts (rigid and hinged) - Horikoshi et al. (2003)

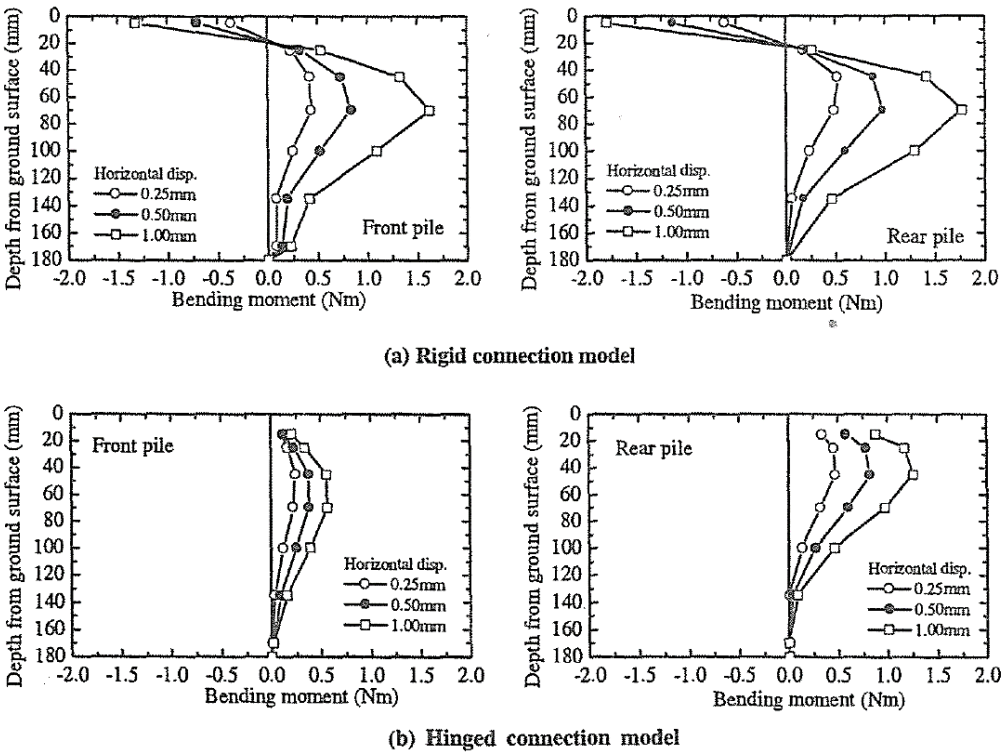

Figure 2.28: Distributions of bending moments along pile shaft - Horikoshi et al. (2003)

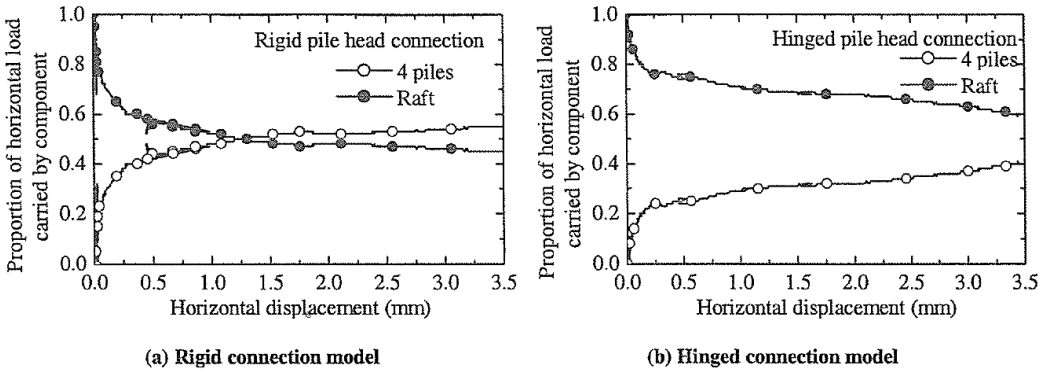

Figure 2.29: Proportion of horizontal load carried by each component - Horikoshi et al. (2003)

Katzenbach and Turek (2005) performed 1g horizontal loading tests with a model of a CPRF (Figure 2.30). In addition, tests with a pile group (no raft-soil contact, same pile geometry and pile positions as the CPRF) and with a raft foundation (same raft geometry as the CPRF) were carried out.

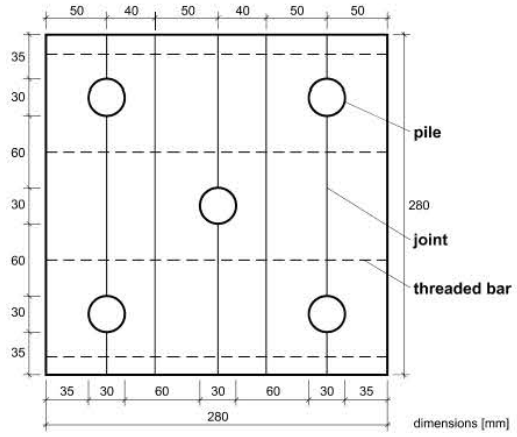

Figure 2.30: Plan view of the model (Katzenbach and Turek, 2005)

The geometry of the model components was determined based on typical dimensions of Combined Pile-Raft Foundations in Frankfurt am Main and a model scale of length of $\lambda = 1/50$. The tests were performed with a group of 5 piles. The piles were connected to the raft with a 'fixed-head' restraint. Half of the tests were carried out with loose sand and half of the tests with dense sand. For each foundation type except the pile group, horizontal load tests (with a maximum value of 1200 N) in loose and dense sand with vertical loads of 1000 N, 3000 N and 5000 N were carried out. The horizontal load was applied, after the vertical one (the vertical load remained constant). The relationship between horizontal displacement and load of CPRF and pile group (PG) for the different vertical load levels obtained from the tests in dense sand are summarized in Figure 2.31.

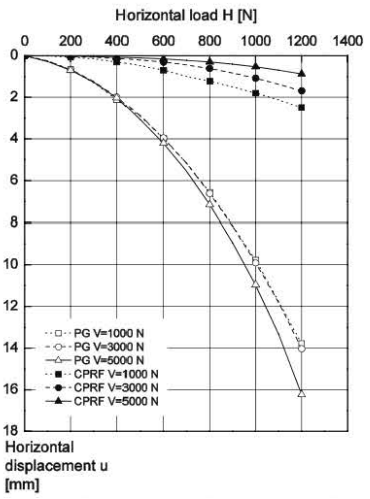

Figure 2.31: Horizontal displacement of CPRF and pile group (PG) in dense sand (Katzenbach and Turek, 2005)

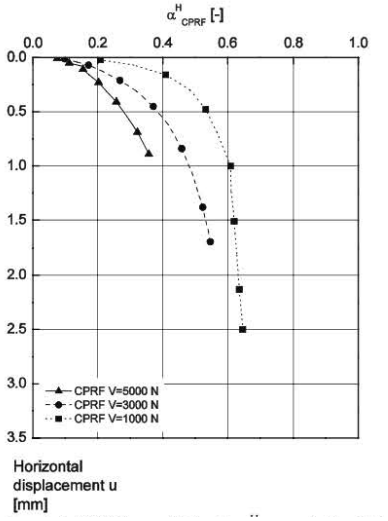

Figure 2.32: Horizontal CPRF coefficient $\alpha_{H,CPRF}$ derived from tests in dense sand (Katzenbach and Turek, 2005)

It can be seen from that the horizontal displacements u of the CPRF are depending on the vertical load level. The displacements decrease with increasing vertical load. For a vertical load level of 1000 N the horizontal resistance of the CPRF is about 2.5 times higher than the horizontal resistance of the pile group. For vertical load levels of

3000 N and 5000 N the horizontal resistance of the CPRF is even 4 respectively 6 times higher due to the resistance provided by the raft. The parameter $\alpha_{H,CPRF}$ describes the proportion of horizontal load carried by the piles. Thus the value of $\alpha_{H,CPRF}$ can range from 0 for a raft foundation to 1 for a pile group. The values of $\alpha_{H,CPRF}$ are plotted versus horizontal displacement in Figure 2.32. With increasing horizontal displacements $\alpha_{H,CPRF}$ increases to values of 0.4 - 0.6. Higher vertical load levels are leading to a decrease of $\alpha_{H,CPRF}$. Especially for small horizontal displacements and high vertical load levels the major part of the horizontal load was carried by the raft.

The measurements of the bending moments of the piles indicated, that the maximum bending moment of the pile group is more than 4 times higher than the maximum bending moment of the CPRF. The relationship between the lateral resistance of the piles and the horizontal displacement of the CPRF for the tests with vertical loads of 1000 N and 5000 N are shown in Figure 2.33.

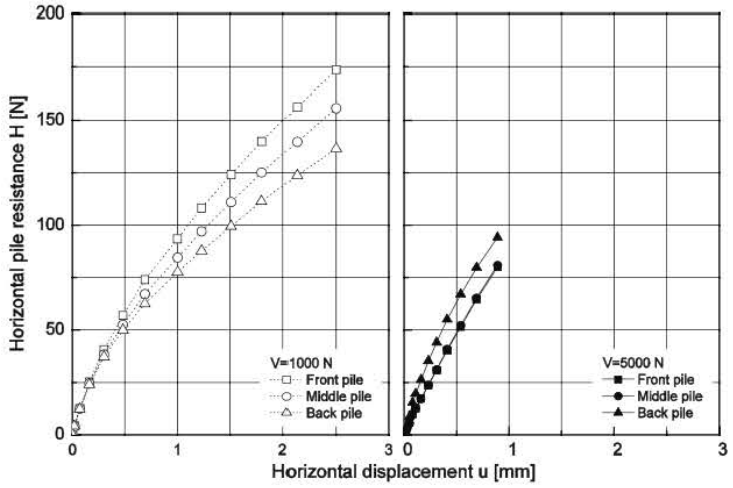

Figure 2.33: Horizontal resistance of piles of CPRF versus horizontal displacement in dense sand (Katzenbach and Turek, 2005)

Even if the relationship between horizontal pile resistance and horizontal displacement seems to be practically the same for both vertical load levels, it was observed some differences in the load sharing between the piles. For a vertical load of 1000 N the pile load distribution was as expected dominated by the shadowing effect. The highest pile load was measured in the front piles while the soil resistance of the trailing rows (middle pile and back piles) was reduced because of the presence of the front piles. In opposite to this behaviour the results of the tests with a vertical load of 5000 N shown that the resistance of the back piles is higher than the resistance of the middle and front piles. The authors justified this effect with the increase of stresses and stiffness in the soil beneath the raft, which was caused by the high vertical load transferred by the raft. The highest increase of stresses and stiffness occurred in the soil beneath the center of the raft while no increase occurred beneath the edges of the raft.

Matsumoto et al. (2010) realized a series of 1g tests in order to investigate what is the influence of different pile head connection conditions between raft and piles on the behaviour of piled-raft foundation systems in dry sand subjected to vertical and static cyclic horizontal loading.

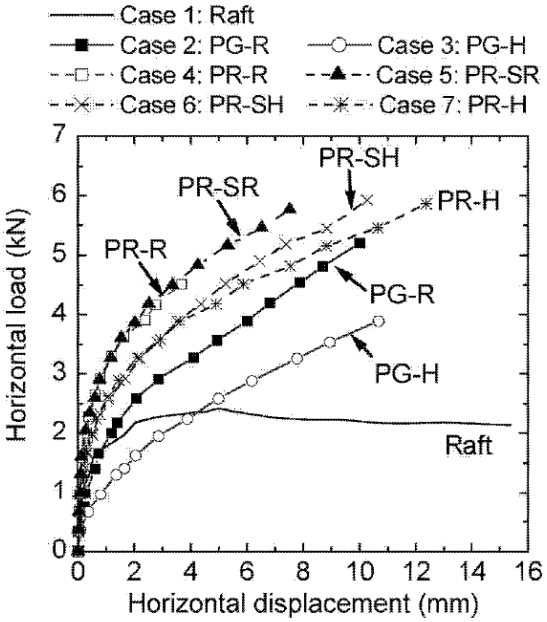

Figure 2.34: Horizontal load vs horizontal displacement at maximum load in each cycle for all the test cases (Matsumoto et al. 2010)

The main findings of this work were:

- the horizontal stiffness of the piled rafts is larger than that of a pile group with the same configuration as the piled raft, because the raft acts as a 'horizontal displacement reducers' (Figure 2.34). In the figure PG = pile group; PR = piled raft; R = rigid, SR = semi-rigid, SH = semi-hinged, H = hinged pile head connection;
- the bending moments of the piles in the piled raft are reduced, compared with those in the pile group (Figure 2.36);
- in the case of the piled rafts, rotation of the raft decreases as the pile-head connection rigidity becomes lower, although the horizontal stiffness also becomes lower;
- the horizontal loads carried by the piles in the piled raft are not influenced by the pile head connection rigidity, whereas the horizontal load proportion carried by the raft becomes lower as the pile head becomes less rigid (Figure 2.35).

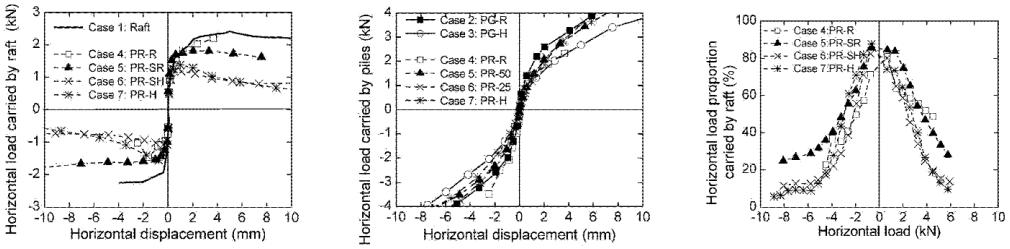

Figure 2.35: Load carried by 1) raft, 2) piles versus horizontal displacement and 3) Load proportion carried by raft (Matsumoto et al. 2010)

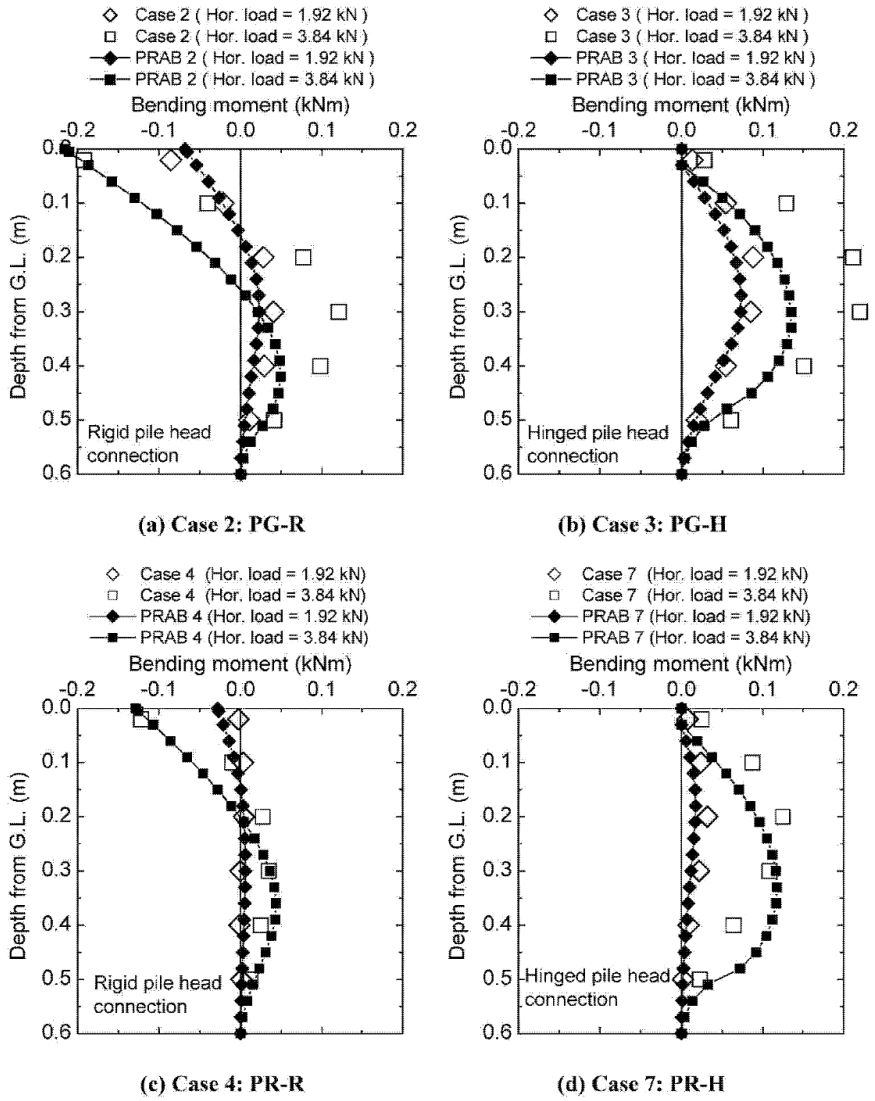

Figure 2.36: Comparison of calculated and measured distributions of bending moments in pile (Matsumoto et al., 2010)

Unsever et al. (2015) in order to understand the behaviour of piled raft foundations under vertical and horizontal loading realized a series of 1g vertical load test and horizontal load test (static and cyclic) on a 3-pile piled raft model in dry sand. Load test of the components of the piled raft model, such as raft alone and single pile, were also performed. Before the application of the cyclic horizontal load of the piled raft model, a vertical load of 497 N was applied on the raft. The measured and calculated relationship of the horizontal load, H, and normalised horizontal displacement u/D are presented in Figure 2.37.

The horizontal load carried by the 3 piles continues to increase with increasing u/D, while the raft resistance tends to remain constant after the normalised displacement exceeds the 0.05 value. At the beginning of the test, the raft carried about the 85% of the total horizontal load, but this percentage decreases with increasing u/D and at the end became practically constant around 25%. After starting of the horizontal test the vertical load on the front pile (P3) starts to increase, while the vertical load on the rear one (P1) starts to decrease. This fact reflects that contact pressure at the raft base increases around P3. The maximum negative bending moment occurs at the pile

heads, while the maximum positive occurs at depths of 0.55-0.6 of the pile length. The bending moments in the front pile are larger than that of the centre pile (Figure 2.38).

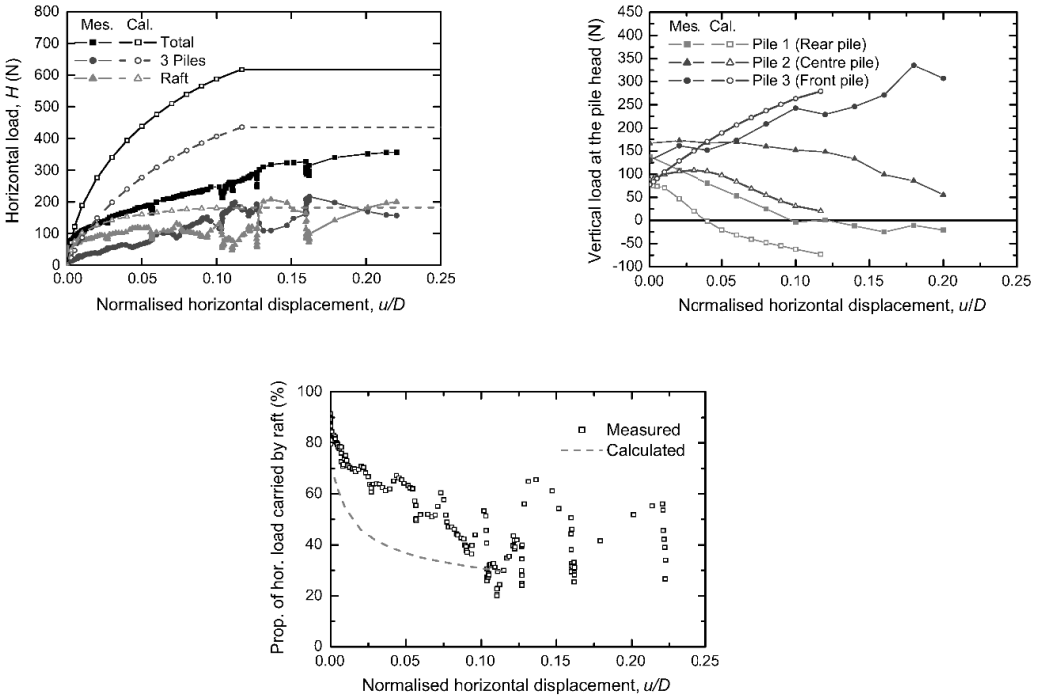

Figure 2.37: Test results – Horizontal load vs Normalised displacement - Unsever et al. (2015)

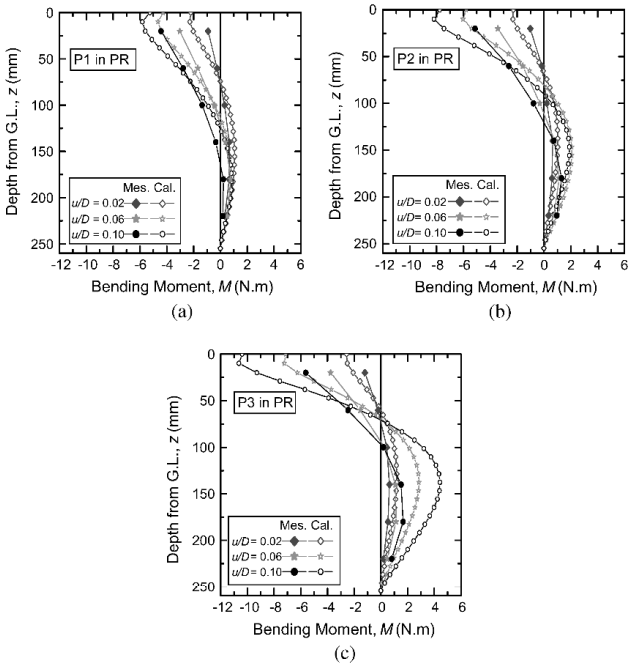

Figure 2.38: Bending moment distribution along each pile shaft (P1, P2 and P3) – Unsever et al. (2015)

The authors moreover tried to simulate the horizontal load test with the commercial code Plaxis 3D. As can be noted in Figure 2.37 and Figure 2.38, this software seems to overestimate the experimental results (piles loads, raft load and pile bending moments), nevertheless reproducing well the trends of the load distribution between piles and raft.

Hamada et al. (2015) carried out 1g static cyclic lateral loading tests on piled-raft foundations in order to investigate the influence of vertical load and pile spacing ratios during extreme events like earthquakes. The test models were pile groups and piled rafts with a concrete footing supported by a 4x4 pile group. The tests were conducted on pile groups (a steel plate was used to restrict vertical displacement), piled rafts (no vertical displacement restrictions) and raft alone (where the vertical load was varied).

In the case 2-1 (vertical load = 32.2 kN) a piled raft with small pile diameter (s/D = 13) was tested (Figure 2.39) and was observed that the friction resistance at the raft-soil interface was much higher than the pile's shear forces. The pile's shear forces were proportional to the lateral displacement, while the total lateral load behaviour was non-linear. The rear and the intermediate piles carried much more lateral load than the front piles, particularly at large lateral displacements. During loading, the sum of the axial forces of the piles changed considerably at large displacements. The piles experienced pulling forces and the contact pressure beneath the raft became larger (the initial value was 22.0 kPa). Therefore, it's possible that the soil modulus in front of the rear and intermediate piles probably increased.

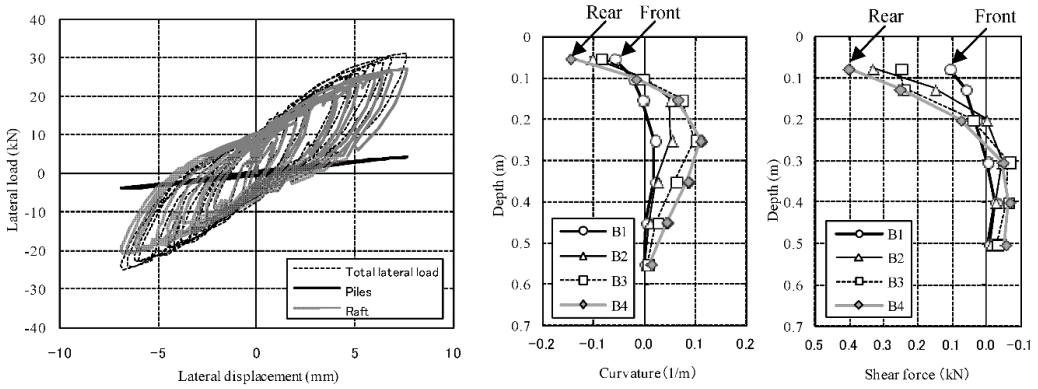

Figure 2.39: Case 2-1 results – Hamada et al. (2015)

In the case 3-1 (vertical load = 32.2 kN) a piled raft with a large pile diameter (s/D = 3.3) was tested (Figure 2.40) and was observed that the friction resistance at the raft-soil interface was higher than the pile's shear forces like in the case 2-1. However, here, the difference between the forces carried by the front and rear piles was negligible because two opposing phenomena offset each other. The soil modulus in front of the rear piles was larger than that of the front piles, whereas the front piles carry much more lateral load that the rear piles due to well-known group effects related to the small spacing ratio (here s/d was equal to 3.3). Based on these tests, the authors remarked that the sharing ratio for vertical load was one of the key factors that conditioned the lateral resistance of piled-rafts.

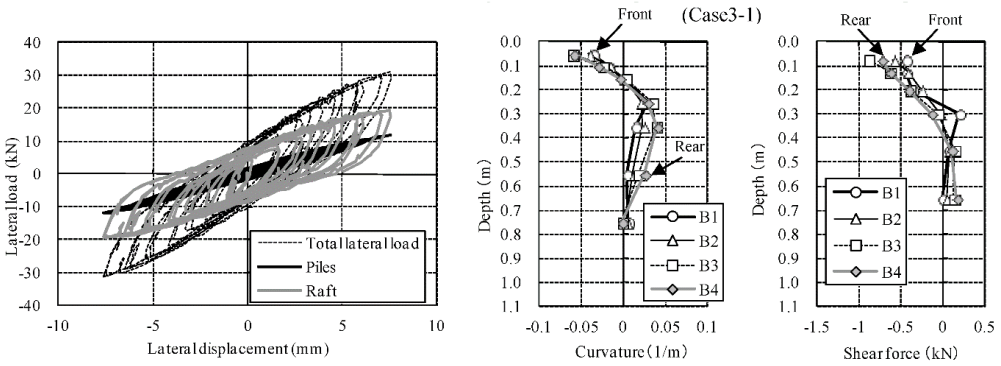

Figure 2.40: Case 3-1 results – Hamada et al. (2015)

Moreover, Hamada et al. (2015) with the Figure 2.41 compared the 'lateral displacement vs lateral loads' of a piled raft (Case 2-1), the analogous simple pile group (raft not in contact with soil) and the raft alone. Filled circles denote the experimental results at different loading levels, solid lines show approximate curves and the dashed line indicates the sum of the approximate resistance curves of pile groups and raft foundations. The results for the raft foundation, in which the contact pressure was 22.4 kPa, were adjusted to a contact pressure of 21 kPa because the lateral resistance of the raft foundations depends on the contact pressure as in Case 2-1 which modelled piled rafts.

The authors observed that when the lateral displacement was less than about 1.5 mm, the lateral resistance of the piled-raft was similar to the sum of the separate lateral loads of the piles and raft. However, at higher displacements, the resistance of the piled rafts was larger than the sum of the separate lateral loads of the raft and pile groups, which means that the friction resistance increased as the contact pressure increased at large displacements. The pressure might have undergone an incremental change due to a possible positive dilatancy of the soil deposit and/or piles that behaved like anchors.

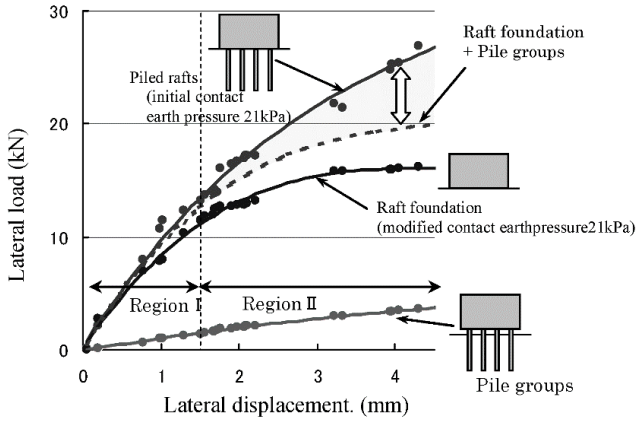

Figure 2.41: Comparison of lateral resistance between pile rafts, rafts, pile groups – Hamada et al. (2015)

2.3.3 Influence of vertical loadings on piled-rafts

In the work presented by Hussien et al. in 2014 the effect of vertical loads on the lateral response of a 3x5 pile-groups installed in sandy soil having free-head condition (simple pile group, no cap in contact with the ground) and connected together by a concrete cap in contact with the ground (piled-raft system) was investigated through a series of 2D FE analyses (using the software called FLIP).

The 2D analyses focus on the five piles in the middle row of the group. The piles are steel-pipe piles with an outer diameter of 0.324 m (a wall thickness of 9.5 mm), an embedded length of 11.6 m and the spacing was selected to be equal to 3.92 diameters. The concrete-cap in the piled-raft systems analyses has a thickness of 0.495 m. The interactions between the pile and the surrounding soil in 3D type was modelled in these 2D analyses by means of soil–pile interaction springs with hysteretic non-linear load displacement relationship. The sandy soil was characterized with a G_{max} = 127 MPa, a soil unit weight of 1.83 ton/m^3 and an angle of internal friction chosen to be equal to 33 °. Joint elements were used at the soil–pile and soil–cap interfaces to represent sliding mechanism between them. Sliding will initiate when the shear stress at the interface exceeds a certain value of τ_f according to a simple frictional relationship (a Mohr-Coulomb law-type). Free-head single piles, free-head pile-groups and piled-rafts were analyzed for comparisons for a total of 8 cases. Pure lateral loads were considered in half of these cases while a combination of vertical and lateral loads was considered in the others.

When combined loads condition was considered the analyses were performed in two stages. In the first stage, a vertical working load that causes a vertical displacement equal to 0.02D was applied on the pile head or through the pile cap. In the second stage, a horizontal load was applied until a target lateral displacement corresponding to 80 mm was achieved. It's important to underline that, however, the vertical applied displacement at the pile head or through the pile cap was kept constant during all the second stage of the analysis. The findings of this work were:

- For pile-groups and piled-rafts (called in this work, capped pile-group): the same vertical loads applied to the free-head piled-group and the piled-raft increased the overall lateral resistance by 32% and 39% for the free-head and capped pile groups, respectively. It was observed that the effect on individual piles in the pile group or in the piled-raft was different and related mainly on the pile position (Figure 2.42). In the free-head pile-group, for example, the vertical load leads to 14%, 30%, 24%, 25%, and 50% increases in the lateral resistances of piles 1–5 (pile 1 is the front pile, pile 5 is the rear pile), respectively (Figure 2.42). In the piled raft system, instead, the vertical load leads to 23%, 36%, 64%, and 82% increase in the lateral resistance of piles 2–5, respectively, while the lateral resistance of the leading pile (pile 1) seems to be unaffected by the influence of the vertical load (Figure 2.42). Therefore, in the work of Hussien et al. (2014), the effect of vertical loads on the lateral response of piles is more significant when a cap in contact with the ground is added above the pile-heads.

- The distribution of lateral loads between the piles in a piled-raft tends to be more uniform when vertical loads were considered.

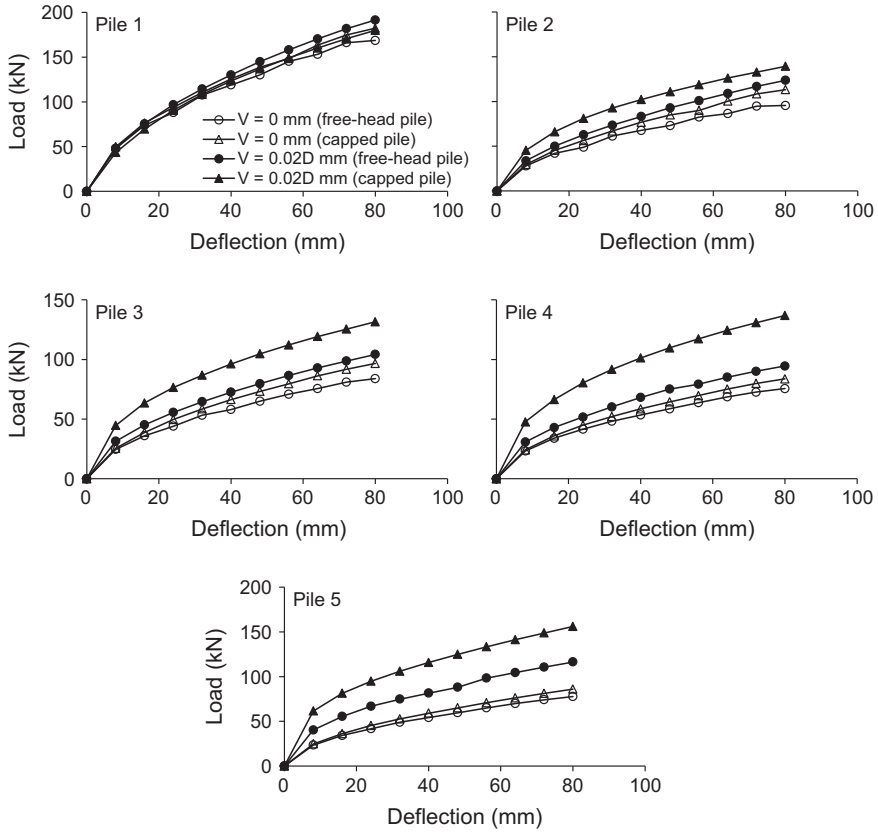

Figure 2.42: Load–deflection curve of each pile in free-head pile group and in a piled-raft (Hussien et al., 2014)

However, in a similar way, like I explained in the section of the thesis about the influence of vertical loads on simple pile groups, it should be noted that even these results were obtained using a simplified modelling of the problem (2D-FEM analyses), in fact: a) the piles were one-dimensional beam elements, thus the influence of the volume occupied by the piles was neglected; b) the 2D-FEM software used (FLIP) suffers of some lacks to properly study this really difficult soil-structure interaction problem. And again, as for the simple pile group case, in order to provide more appropriate and experimentally based suggestion on the response of a pile-group and a piled-raft under combined loads (vertical and lateral loads), some new experimental results (in particular from full-scale tests) are absolutely necessary in order to verify the appropriateness of the predictions obtained using 2-D, 3-D finite element software, BEM-based software or simplified approaches.

Chapter 3

Available analysis methods

3.1 Introduction

Estimation of the deformations and load distributions in a group of piles subjected to general loading conditions normally requires the use of computer-based methods of analysis. Numerical techniques for pile group and piled-raft analysis may be classified into the following two categories:

- continuum-based approaches;
- load-transfer (or subgrade reaction) approaches.

The latter category, based on Winkler spring idealization of the soil, employs load-transfer functions to represent the relationship between the load at any point along the pile and the associated soil deformation at that point. Such a semi-empirical method is widely adopted for the analysis and design of single piles, especially where non-linear soil behaviour has to be considered and/or soil stratification is complicated (e.g. the $t-z$ or $p-y$ curve methods of analysis). The computer programs PILGP1 (O'Neill, Ghazzaly, and Ha, 1977), FLPIER (Hoit et al., 1996) and GROUP (Reese et al., 2000) are included in this category. The main limitations associated with this approach are as follows:

- The modulus of subgrade reaction is not an intrinsic soil property but instead gives the overall effect of the soil continuum as seen by the pile at a specific depth, and hence its value will depend not only on the soil properties but also on the pile properties and loading conditions;
- The load-deformation relationship along the pile is modelled using discrete independent springs and no information is available from the analysis regarding the deformation pattern around the pile. Disregarding continuity through the soil makes it impossible to find a rational way to quantify the interaction effects between piles in a group.
- It is uncertain how the p-y curves are influenced by pile-head fixity.

The above shortcomings may be removed by means of soil continuum based solutions which are generally based on the finite element method (FEM) (Ottaviani, 1975) or the boundary element method (BEM) (Butterfield and Banerjee, 1971). These solutions provide an efficient means of retaining the essential aspects of pile interaction through the soil continuum and hence a more realistic representation of the problem. Further, the mechanical characteristics to be introduced into the model now have a clear physical meaning and they can be measured directly. Finite element analyses are

valuable for clarifying the mechanism of load transfer from the pile to the surrounding soil but, especially for pile groups, are not readily applicable to practical problems. The considerable effort of data preparation and the high computational cost (particularly if non-linear soil behaviour is to be considered) preclude the routine use of such techniques in design.

By contrast, BEM provides a complete problem solution in terms of boundary values only, specifically at the pile-soil interface. This leads to a drastic reduction in unknowns to be solved for, thereby resulting in substantial savings in computing time and data preparation effort. This feature is particularly important for three-dimensional problems such as pile groups and piled rafts.

DEFPIG (Poulos, 1990), based on a simplified BEM analysis and the use of interaction factors, models soil non-linearity in an approximate manner by means of an elastic- plastic interface model. Two main shortcomings are associated with this model:

- the non-linear features of stress-strain behaviour are not captured until the load corresponding to the yield of the first interface element is reached;
- deformations are often seriously underestimated at high loads levels. An alternative approach is offered by the widely used computer program MPILE, originally developed by Randolph (1980) under the name of PIGLET. The analysis is based on a semi-empirical method which makes use of approximate analytical solutions for single pile response and for interaction between two piles, in which linear elastic soil behaviour is assumed.

It is important to note that the interaction factor approach (such as is employed in DEFPIG and MPILE) solves the group problem by calculating the influence coefficients for each pair of piles and by merely superimposing the effects.

A fundamental limitation of the linear elastic methods is that they result in a considerable overestimation of the load concentration at the outer piles of the group, and this may lead to an over-conservative design. Indeed, it has long been recognized that consideration of soil non-linearity results in a reduction of the load carried by the corner piles. This results in a redistribution of the loads in the individual piles, leading to a more uniform distribution than that predicted by linear models.

3.2 Winkler-based approaches

3.2.1 Introduction

The approaches based on the Winkler schematization model the soil as a series of independent springs; consequently, deformations occur only at the points where the forces are not zero. Methods based on Winkler model, also called $p-y$ curves methods, are the most widespread and used. These allow, in fact, to characterize in a rather simple way the non-linearity of the response, the variation of soil stiffness with depth, the stratification (Poulos and Davis, 1980). The parameters that characterize the soil response (soil reaction modulus k, representing spring stiffness) are determined on the basis of a large number of experimental tests. The inability to model the soil continuity is the major limitation of this approach.

With this approach, it is customary to divide the pile into $n - blocks$ and assume that on each of them, at a given depth z, is acting a reaction P [Force] (Figure 3.1). This reaction represents the resistance that the soil provides to pile displacements in

the horizontal direction. In general, it is usual to consider the reaction per unit length p [Force/Length].

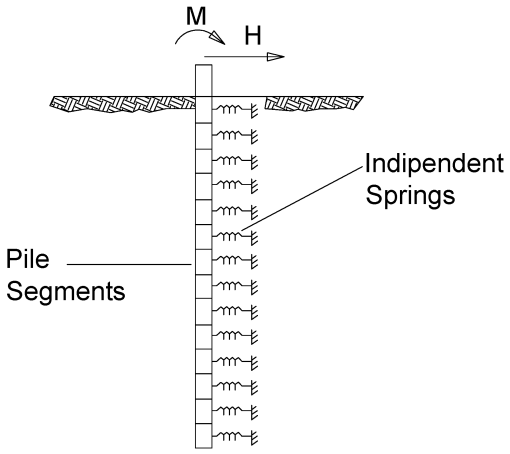

Figure 3.1: Winkler soil modelling

The key parameter that characterizes this type of modelling is the reaction modulus k of the spring. The parameter k defines the relationship between the resistance per unit length p of the soil and the displacement y of the pile at that point. The value of the reaction modulus k depends on the reference depth z and on the displacement value y.

3.2.2 Load transfer 'p-y curves' - determination

The main burden of a model in which the soil is represented by a series of springs consists in determining the reaction modulus k value, variable as a function of the reference depth z and of the displacement y. Since k is a function of the displacement y, it is usual to represent the reaction modulus by the representation of the corresponding $p - y$ curve. The sources through which many authors have come to the identification of the k-trend for different soil types are the results of experimental tests on real piles. The determination of a p-y curve related to a given test in a specific soil can occur in two ways:

- directly, by measuring the soil pressure;
- indirectly, by measuring the bending moments acting along the pile.

In the first case, measuring the pressure which the soil exerts on the pile in some points placed along its lateral surface, with load-cells. At the same time measuring the shaft displacement y at different depths.

In the second case, the p-y curves determination is obtained by measuring, at some points, the bending moments acting along the pile shaft. This measure is usually obtained using strain transducers suitably arranged inside the pile or along its lateral surface. These bending moment values can be interpolated by analytical functions that provide the continuity of the moment along the shaft.

It is important to emphasize how, in each case, the reaction modulus of the soil, k, represents a Winkler soil model parameter and doesn't represent a real soil property.

Several authors have tried to define these curves varying the type and characteristics of the reference soil (for example: Figure 3.2). In their book Reese and Van Impe

(2001) reported the suggested p-y curves to adopt for the analysis of a pile (or a pile-group) under horizontal loads.

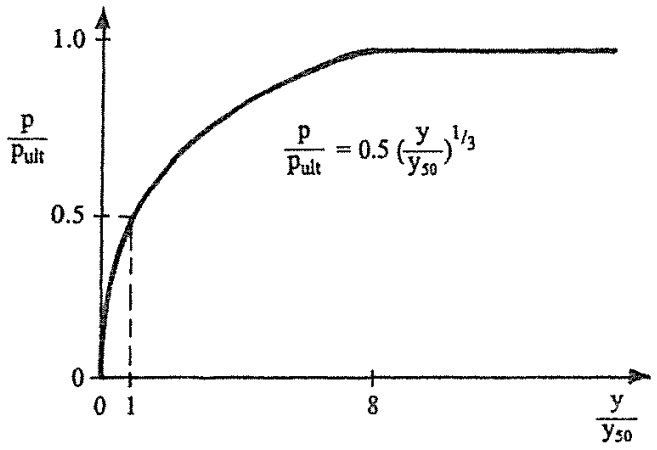

Figure 3.2: Characteristic 'p-y curve' for soft clay below the water table (Matlock, 1970)

3.2.3 Pile-group effects in p-y curves methods

Modelling the soil according to the Winkler approach, the springs exert reactions on the pile in an independent way to each other. The Winkler model inability to represent the soil continuity becomes a serious limitation when the analysis, starting from the study of the single pile behaviour, extends to the analysis of a pile group. The pile group response to horizontal loading, in fact, is strongly influenced by the interactions between the piles in the group. These interactions affect the response changing the behaviour of the piles in the group due to their belonging row and their position within the same row. These phenomena can't be modelled with the Winkler model. It becomes necessary to introduce variations, in an empirical way, to permit the use of the p-y curves even for the pile-group case.

The first solutions to this problem were introduced by Focht and Koch (1973) and by Leung and Chow (1987).

To model the pile group response to horizontal loads with p-y curves is necessary to introduce some changes to the shape of the curves obtained for the single pile case. These changes, however, can't be deduced by an assessment of the interaction between the piles obtained using an elastic analysis. The p-y curve defined for a single pile can be changed by means of a pair of multiplier coefficients, which can appropriately provide a correction to the p and y values. The criterion to evaluate these coefficients is totally empirical. Brown et al. (1988) (Figure 3.3), despite the original idea to use a pair of coefficients, preferred to use a single coefficient f, with the aim to modify only the p value in the p-y curve.

The full-scale tests carried out in the last years had as main purpose to collect enough data to determine the value to assign to the coefficient f. The values of this coefficient, always smaller than one, are assigned to each pile according to the position within the group. This multiplier takes into account of the interaction effects with the other piles in the group in an overall way.

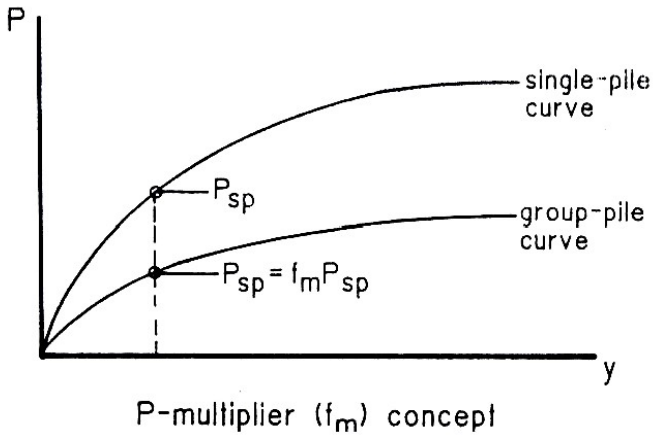

Figure 3.3: p-multiplier concept for pile groups (Brown et al, 1988)

From the data available in literature it's possible to state that the coefficient f value changes mainly as a function of the pile belonging row, and not as a function of the position within the row. With this approach, therefore, the edge effect is neglected: the loads taken by the piles in the same row are considered equal.

Rollins et al. (1998, 2005) using the available collection of experimental data, proposed 'project curves' useful for the determination of the multiplier coefficients f as a function of the pile belonging row and of the pile relative spacing s/D.

Similar attempts to identify the trends of the p-y curves multipliers were realized by Mokwa (1999). In Figure 3.4 are shown the multipliers suggested by Mokwa (1999), distinguished for the first, the second, the third and the fourth (and subsequent) row. The effects of the interactions dissolve for a relative spacing s/D equal or bigger than 6.

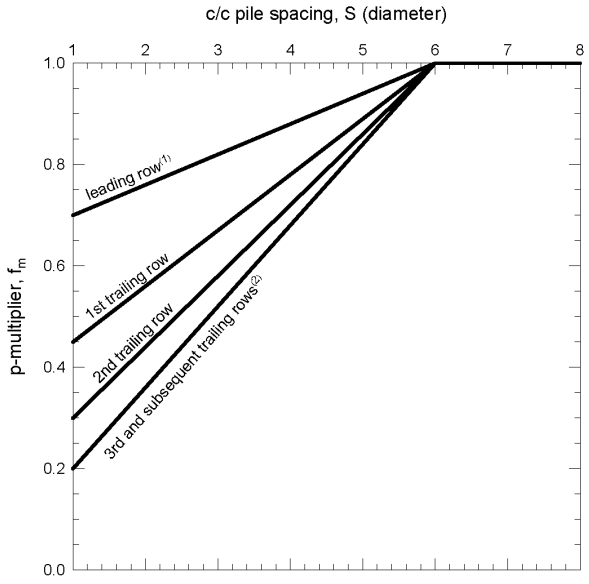

Figure 3.4: p-multiplier values as a function of pile spacing and the pile belonging row (Mokwa, 1999)

It is evident that the main research effort, in the multipliers determination, is directed to the definition of the behaviour of each row in the group, and to the evaluation

of the spacing influence. The coefficients f, as they are defined, are not affected by the pile-head restraint conditions, the technology used to realize the piles, the shape of their section, nor, especially, the soil properties.

Some data in literature (Rollins and Sparks, 2002) showed that the values of the coefficients f are not significantly influenced by the pile-head restraint conditions.

The interaction coefficients f, moreover, are assumed to be independent of the pile-head displacement level. Consequently, the increase of the external load results in a constant efficiency of the pile-group. These assumptions reflect the behaviour observed experimentally only starting from a certain displacement level. The load distribution rates between the rows and the efficiency of the group are not constant, however, for small displacement values. It follows that the use of the p-y curve multiplier method permits to determine the behaviour of a pile-group only starting from a certain displacement level (McVay et al., 1998). In order to model more rigorously the pile-group efficiency evolution would be necessary to provide a decreasing trend for the coefficients f as a function of the displacement y (Rollins et al., 2005).

3.3 Strain Wedge Model

3.3.1 Single pile

The strain wedge model (SW) (Ashour, Norris, and Pilling, 1998) correlates traditional one-dimensional beam on elastic foundation response to envisioned three-dimensional soil-pile interaction. In particular, the Young's elastic modulus of the soil (E) is related to the corresponding horizontal subgrade modulus (E_s); the deflection pattern of the pile (y versus depth x) is related to the strain (ε) that exists in the developing passive wedge in front of the pile; and the beam on elastic foundation line load (p) for a given deflection is related to the horizontal stress change ($\Delta\sigma_h$) acting along the face of the developing passive wedge.

One of the main assumptions associated with the SW mode is that the deflection pattern of the pile is taken to be linear over the controlling depth of the soil near the pile top, resulting in a linearised deflection angle δ. This assumption allows uniform horizontal and vertical strains to be assessed (Figure 3.5).

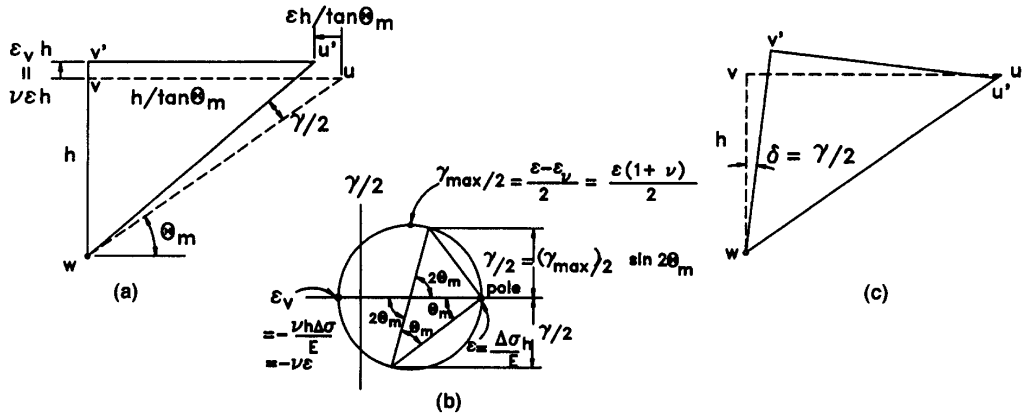

Figure 3.5: (a) Distortion of the wedge; (b) Associated Mohr circle of strain; (c) Relationship between pile deflection and wedge distortion (Ashour and Norris, 1998)

The SW model represents the mobilized passive wedge in front of the pile, which is characterized by base angles, Θ_m and β_m; the current passive wedge depth h; and

the spread of the wedge fan angle, φ_m (the mobilized friction angle). The horizontal stress change at the passive wedge face, $\Delta\sigma_h$, and the side shear, τ, act as shown in Figure 3.6.

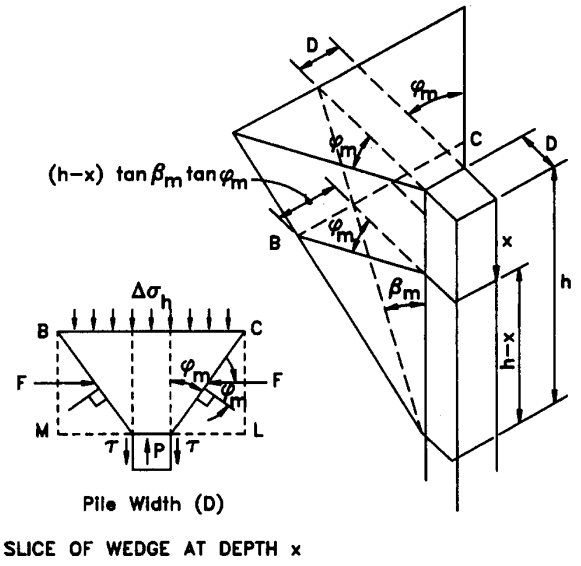

Figure 3.6: Basic strain wedge in uniform soil (Ashour and Norris, 1998)

Changes in the shape and depth of the passive wedge, along with changes in the state of loading and pile deflection, occur with change in the uniform strain in the developing passive wedge. The configuration of the wedge at any instant of load and mobilized friction angle, φ_m, and wedge depth, h, is given by the following expression:

$$\Theta_m = 45^\circ - \frac{\varphi_m}{2} \tag{3.1}$$

or its complement

$$\beta_m = 45^\circ + \frac{\varphi_m}{2} \tag{3.2}$$

The width, $\bar{BC}$ of the wedge face at any depth is:

$$\bar{BC} = D + (h - x)2tan\beta_m tan\varphi_m \tag{3.3}$$

where:

- x = the depth below the top of the studied passive wedge;
- D = the width of the pile cross-section;
- h = the entire mobilized depth of the passive wedge in front of the pile (related to the current depth of zero deflection of the pile).

It should be noted that the SW model is based upon an effective stress analysis of both sand and clay soils. As a results, the mobilized fanning angle, φ_m, is not zero in clay as assumed by several authors. For this reason, the SW model requires the involvement of the evaluation of the excess pore water pressure Δu (this procedure is not presented here, but it is described in Ashour and Norris, 1998).

The SW model can handle the problem of multiple soil layer of different types. The multi-sublayer technique is based upon dividing the soil profile and the loaded pile into sublayers and segments of constant thickness. Each sublayer of soil is considered to behave as a uniform soil and have its own properties according to the sublayer location and soil type.

As shown in Figure 3.7, there may be different soil layers and a transition in wedge shape from one layer to the next, with all components of the compound wedge having in common the same depth h.

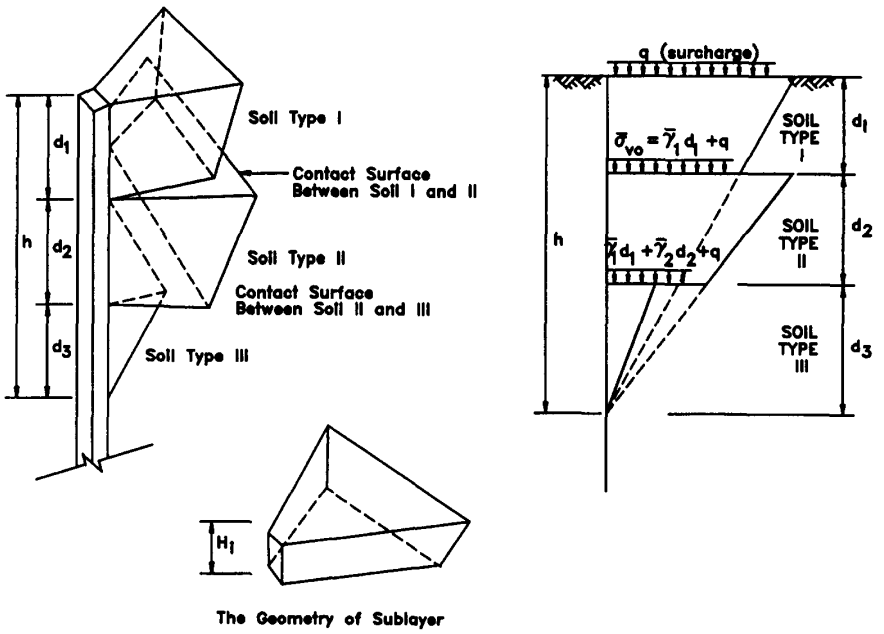

Figure 3.7: Proposed geometry of compound passive wedge (Ashour and Norris, 1998)

In fact, there may be a continuous change over a given sublayer, but the values of stress level (SL) and mobilized friction angle (φ_m) at the middle of each sublayer of height, H_i, are treated as the values for the entire sublayer.

The effects of the soil and pile properties are associated with the soil reaction along the pile by the Young's modulus of the soil, the stress level in the soil, the pile deflection and the beam on elastic foundation modulus of subgrade reaction between the pile segment and each soil sublayer. To account for the interaction between the soil and the pile, the deflected part of the pile is considered to respond as a continuous beam loaded with different short segments of uniform load and supported by non-linear elastic supports along soil sublayers as shown in Figure 3.8. An iterative process is performed to satisfy the equilibrium between the mobilized geometry of the passive wedge of the layered soil and the deflected pattern of the pile for any level of loading.

The SW model in layered soil provides a means for distinguishing layers of different soil types as well as sublayers within each layer where conditions (ε_{50}, SL, φ_m) vary even though the soil and its properties (γ, e or D_R, φ, etc.) remain the same. The horizontal strain (ε) in the soil in the passive wedge in front of the pile is the predominant parameter in the SW model. Consequently, the horizontal stress change ($\Delta\sigma_h$) is constant across the face width ($\overline{BC}$) of the passive wedge at a specific depth.

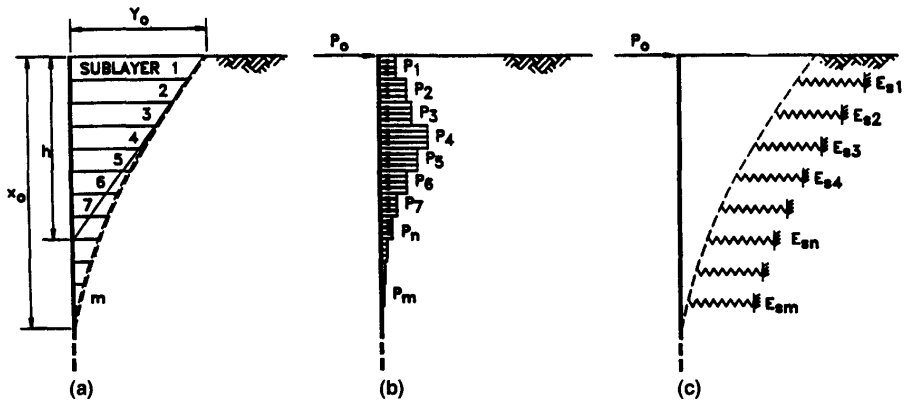

Figure 3.8: Soil-Pile interaction in multi-sublayer technique: (a) Pile deflection pattern; (b) Soil reaction distribution along the pile; (c) Soil-pile modelling (Ashour and Norris, 1998)

The stress-strain relationship is defined based on the results of the isotropically consolidated drained (sand) or undrained (clay) triaxial test. These properties are summarized as follows:

- the major principle stress change ($\Delta\sigma_h$) in the wedge is in the direction of pile movement, and it is equivalent to the deviatoric stress change in the triaxial test as shown in Figure 3.9;
- the horizontal stress change ($\Delta\sigma_h$) in the direction of pile movement at depth x is related to the current level of horizontal strain (ε) and the associated Young's modulus in the soil as are the deviatoric stress and the deviatoric stress and the axial strain to the secant Young's modulus ($E = \Delta\sigma_h/\varepsilon$) in the triaxial test;
- both the vertical strain (ε_v) and the horizontal strain perpendicular to pile movement (ε_{ph}) are equal and are given as $\varepsilon_v = \varepsilon_{ph} - \nu\varepsilon$.

The corresponding stress level (SL) and mobilized friction angle (φ_m) are given as:

$$SL = \frac{\Delta\sigma_h}{\Delta\sigma_{hf}} = \frac{tan^2(45^\circ + \varphi_m/2) - 1}{tan^2(45^\circ + \varphi/2) - 1} \tag{3.4}$$

Where the horizontal stress change at failure ($\Delta\sigma_{hf}$) (or the deviatoric stress at failure in the triaxial test) is:

$$\Delta\sigma_{hf} = \sigma_{v0}[tan^2(45^\circ + \varphi/2) - 1] \tag{3.5}$$

The relationship above clearly shows that the passive wedge response and configuration change with the change in φ_m or SL in the soil.

The Young's modulus of soil in both the shear loading phase of the triaxial test and the strain wedge model is:

$$E_i = \frac{(\Delta\sigma_h)_i}{\varepsilon} = \frac{SL_i(\Delta\sigma_{hf})_i}{\varepsilon} \tag{3.6}$$

where SL and φ_m are evaluated at any value of soil strain (ε). The SW model relies on calculating the instantaneous variation, with depth, in the subgrade modulus E_s, which reflects the soil-pile interaction at any level of pile loading or soil strain. E_s also represents the secant slope at any point on the p-y curve:

$$E_s = \frac{p}{y} \tag{3.7}$$

Note that p = force unit length of the pile, or the beam on elastic foundation soil-pile reaction; and y symbolizes the pile deflection at that soil depth.

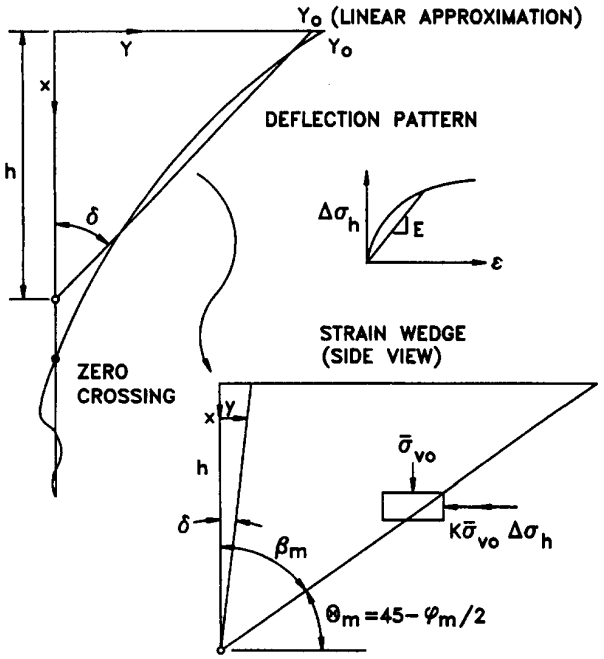

Figure 3.9: Deflection pattern of laterally loaded long pile and associated strain wedge (Ashour and Norris, 1998)

By assuming the multi-sublayer technique, the deflection (y) of the pile can be calculated starting with the base of the mobilized passive wedge and moving upward along the pile, accumulating the deflection values at each sublayer as given in the following relationships (see Figure 3.10):

$$Y_0 = \sum_{i=1}^{n} y_i \tag{3.8}$$

with:

$$y_i = H_i \delta_i \tag{3.9}$$

where H_i indicates the thickness of sublayer i; and n symbolizes the current number of sublayers in the mobilized passive wedge. Finally, the pile head deflection, Y_0, from the SW model analysis is compared to that calculated from the beam on elastic foundation analysis based on the given profile of E_s until the targeted convergence is achieved.

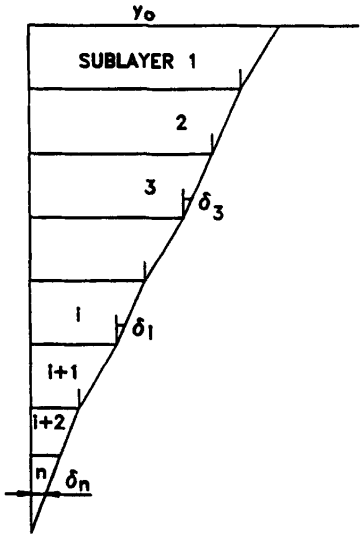

Figure 3.10: Assembling of pile head deflection using multi-sublayer technique (Ashour and Norris, 1998)

3.3.2 Pile group

In the work of Ashour and Norris (2004) the interaction among the piles in a group is determined based on the envisioned geometry of the developing passive wedge of soil in front of the pile in addition to the pile spacing. The assumed overlap of shear zones among the piles in a group varies along the length of the pile as shown in Figure 3.11.

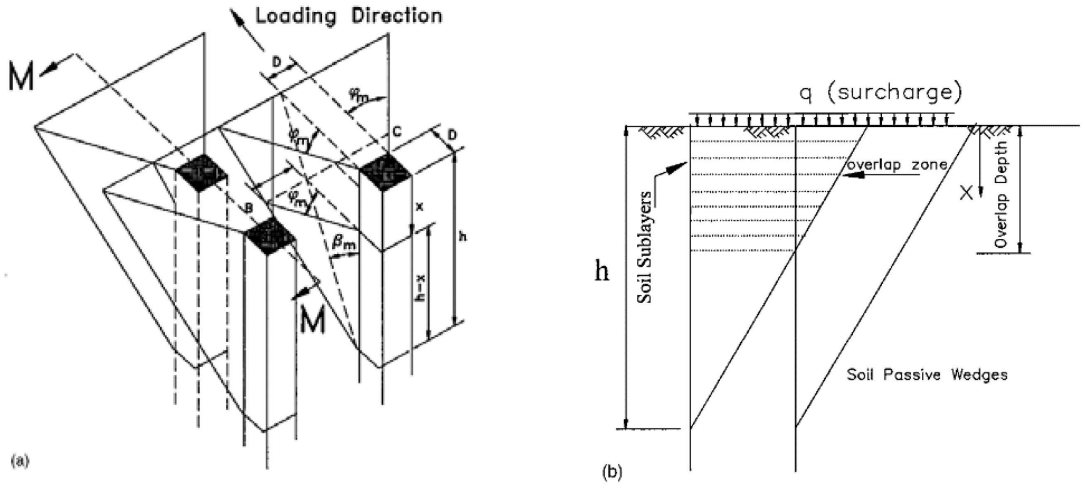

Figure 3.11: a) Mobilized passive wedges and associated pile group interaction and b) front overlap among soil sublayers in two adjacent passive wedges (Section M-M) (Ashour, Pilling, and Norris, 2004)

Also, the interaction among the piles grows with the increase in lateral load. E_s, which is determined based on the SW model approach, will account for the additional strains (and so stresses) in the adjacent soil due to pile interaction within the group (Figure 3.12). Thus E_s of an individual pile in a group will be reduced in a mobilized

fashion according to pile and soil properties, pile spacing and position, the level of loading, and depth.

As seen in Figure 3.11, the soil passive wedge in front of a pile in the group overlaps horizontally with those of adjacent piles by an amount that varies with depth. The overlap of the wedges of neighbouring piles at depth x in different sublayers over the depth of the interaction is characterized as shown in Figure 3.12.

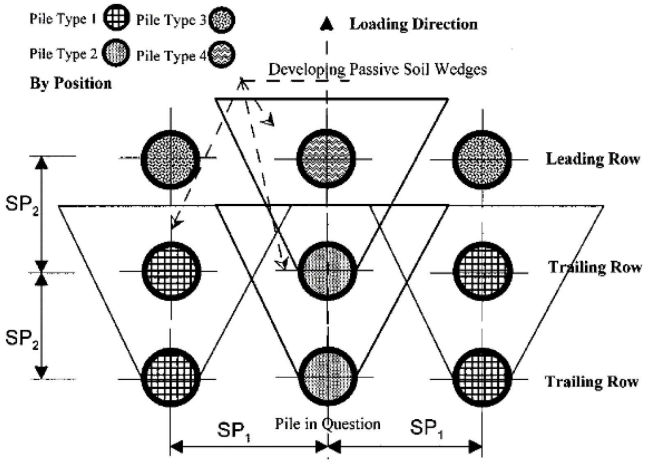

Figure 3.12: Horizontal (lateral and frontal) interaction for particular pile in pile group at given depth (Ashour and Norris, 2004)

The main objective in the calculation of the area of overlap among the piles is to determine the increase in soil strain within the passive wedge of the pile in question.

According to classification of the piles in a group shown in Figure 3.12, the load carried by inner piles is less than the load carried by the outer piles in a given row. Such behaviour was observed in a number of field tests (Brown, Reese, and O'Neill, 1987; Brown, Morrison, and Reese, 1988; Rollins, Lane, and Gerber, 2005; Rollins et al., 2006; Ruesta and Townsend, 1997).

Wedges will overlap and interfere with neighbouring ones, as seen in Figure 3.11 and Figure 3.12. At a given depth (see Figure 3.12) zones of overlap will exhibit larger values of soil strains and stresses as compared to the isolated pile. The increase in average soil stress attributable to the passive wedge of a given pile will depend upon the number and area of interfering wedges overlying the wedge of the pile in question (Figure 3.13-a). The overlap of a uniform stress change is considered at the face of the passive wedge of the pile in question (Figure 3.13-b).

Such overlap depends on the position of the pile in the group. The type of pile by position is based on the location of the pile by row (leading/trailing row) and the location of the pile in its row (side/interior pile) as seen in Figure 3.12.

The average value of deviatoric stress accumulated at the face of the passive wedge at a particular soil sublayer (i) is:

$$(\Delta\sigma_h)_g = SL_g \Delta\sigma_{hf} \tag{3.10}$$

Similar to the p-multiplier technique, the average stress level in a soil layer (SL_g) due to passive wedge interference is evaluated based on the following empirical relationship that provides good agreement with field test results. However, the values of SL_g vary with depth and level of loading:

$$SL_g = SL_i(1 + \sum R_j)^{1.5} \leq 1 \tag{3.11}$$

where j = number of neighbouring passive wedges in soil layer i that overlap the wedge of the pile in question; R = ratio between the length of the overlapped portion of the face of the passive wedge (L) and the total length of the face of the passive wedge (BC); and R_j is determined from all the neighbouring piles (sides and front piles) of the pile in question (Figure 3.12).

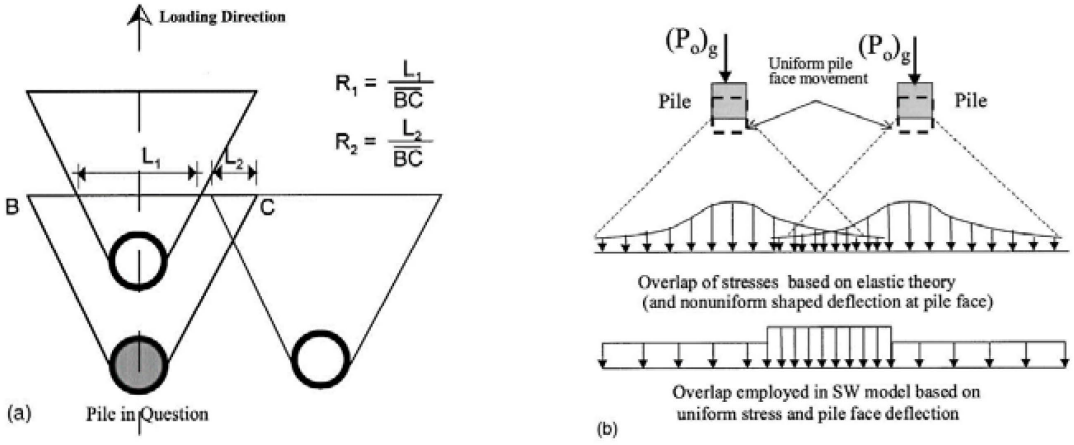

Figure 3.13: a) Overlapping ratios among piles in pile group and b) stress overlapping among piles in pile group (Ashour and Norris, 2004)

The SL_i value on the right side of the previous equation, is equal to $(SL)_i$ of the single pile to get $(SL_g)_i$ (i.e. $(\varepsilon_g)_i$) caused by the passive wedge interference via an iterative process until $\sum R_j$ (i.e. $(\varepsilon_g)_i$) converges. As a result, the passive wedge of the pile in question would reach its final geometry for this particular step of loading.

The angles and dimensions of the passive wedge (φ_m, β_m, and $\bar{BC}$) obtained will be modified for group effect according to the calculated value of SL_g and ε_g. For instance, for a pile in the group, φ_m in a soil sublayer i that is associated with the current SL_g is obtained from the following equation:

$$(SL_g)_i = (\frac{(\Delta\sigma_h)_g}{\Delta\sigma_{hf}})_i = \frac{tan^2(45^\circ + (\varphi_m)_i/2) - 1}{tan^2(45^\circ + (\varphi)_i)/2) - 1} \tag{3.12}$$

where $(\Delta\sigma_h)_g$ = current horizontal stress change (due to pile-head lateral load and pile group interaction); and $\Delta\sigma_{hf}$ = unchanged value of the deviatoric stress at failure for the full friction angle φ. The mobilized friction angle φ_m calculated with the equation above reflects the stresses in the soil around the pile in question at depth x for the corresponding pile head deflection with consideration of the stresses from neighbouring piles.

Based on the modified value of soil strain assessed at depth x at the current level of loading, the value of Young's modulus $(E_g)_i$, of the soil sublayer i is obtained:

$$(E_g)_i = \frac{(SL_g)_i(\Delta\sigma_{hf})_i}{(\varepsilon_g)_i} \tag{3.13}$$

where $(E_g)_i$ calculated with the expression above results from the original strain in the passive wedge (ε) as an isolated pile and the additional soil strain ($\Delta\varepsilon$) which

develops due to overlap zones between the pile in question and the neighbouring piles. Based on the concepts of the SW model the modulus of subgrade reaction for a pile in a group $(E_{sg})_i$ for a soil sublayer can be then evaluated.

However, with SW model is not possible to study all the piles in the pile-group in the same analysis, but each pile in the group needs to be analysed alone.

The Strain Weddge Model hasn't been extended to the piled raft case.

3.4 BEM - Models

3.4.1 Introduction

Continuous elastic approaches model the soil as an elastic half-space, identified by E (Young's modulus) and ν (Poisson's ratio). The analysis methods based on the elastic theory have the quality, despite Winkler model approach, to represent the soil as a continuum.

This property is particularly useful when the study is extended to the pile-groups; in this case, the use of a continuous medium can represent the effects of pile-soil-pile mutual interaction. In contrast, the need to model layered soils or soils with not homogeneous stiffness requires the introduction of numerical approximations.

Appropriate modifications to the elastic half-space model are also used to represent the non-linear soil response. The elastic continuous models presented in this section are solved with the boundary element method (BEM). Adopting this method to study the pile-soil system is sufficient to discretize the interfaces of all the elements. In this way the BEM method represents a method for easier application and less computational cost than the finite element method (FEM), for which it is necessary to discretize the overall volume domain of the problem.

The methodological approach that distinguishes the application of the boundary element method is the following: the element object of study (in this case, the pile-foundation embedded within the soil and subjected to an external action) is divided into a certain number of elements, considered appropriate to describe the problem with an acceptable approximation; the solution equation system is obtained imposing the compatibility between the pile-elements displacements and the soil-movements and imposing the equilibrium and the boundary conditions. To evaluate the soil movements is necessary to define a Green's function, the validity of which is defined within the considered domain.

The function often used, in the study of pile-soil interaction problems, is the Mindlin equation (Appendix). This function, that defines the displacement at a point of an elastic half-space caused by a point-load acting within the same half-space, has to be integrated in an appropriate way on the pile surface. Because of this procedure, BEM methods applied to continuous elastic models are also called 'integral equation methods'.

The development of this type of modelling, as an alternative to the 'p-y curves' approach based on a Winkler soil modelling, is motivated, once again, by the possibility to consider the soil as a continuous medium. The basic features of the analysis procedure are similar to those used for vertically loaded piles. The first analyses in which the soil was modelled as an elastic medium belong to Douglas and Davis (1964) and Spillers and Stoll (1964).

In the first case, the study wasn't oriented to the behaviour of pile foundation, but to thin plates embedded in an elastic half-space and loaded by a horizontal force or a moment. In the second case was provided a first proposal for the study of a pile embedded in an elastic half-space.

Also the ability to model the non-linearity of the system response was introduced, allowing relative movements between the pile and the soil when the values of the soil-pressure reached or exceeded the ultimate values. On the basis of these works, in 70s and 80s some elastic continuous models were realized with which comprehensive parametric studies were conducted with the aim to investigate the effects of the different factors involved in the pile-soil system response, like: the pile-size, the pile slenderness, the pile-soil relative stiffness, the restraint conditions at the pile-base and at the pile-head, the assumption of homogeneity or non-homogeneity of the soil, the linearity or non-linearity of the response, the effects of the load-eccentricity, and more.

The most significant parametric studies related to the behaviour of the single pile and the pair of piles, were carried out by the following authors: (Poulos, 1971a; Poulos, 1972; Poulos, 1973a; Poulos and Davis, 1980; Banerjee and Davies, 1978; Dente and Gullà, 1983; El Sharnouby and Novak, 1985; El Sharnouby and Novak, 1986; Davies and Budhu, 1986; Budhu and Davies, 1987; Budhu and Davies, 1988).

3.4.2 Poulos method (Poulos, 1971, 1971a, 1972, 1973, Poulos and Davis 1980)

The continuous elastic model, used for the analysis of a vertical floating pile subjected to horizontal or bending loads at the pile-head, has its roots in a similar model used to study the behaviour of piles subjected to vertical loading (Poulos, 1968). The pile was embedded in an elastic, homogeneous and isotropic medium, characterized by the elastic parameters E and ν.

The first elastic formulation was related to the study of the single pile (Poulos, 1971a) and of the pile group (Poulos, 1971b), then the analysis was extended to an 'elastic-perfectly plastic' model (Poulos, 1973b). Specifically, this was an elastic model working with a 'cut-off' procedure, where the hypothesis of displacements compatibility at the pile-soil interface is removed once achieved some ultimate soil resistance values. In this way, it was accepted that relative movements might occur between the pile-blocks and the soil.

A further work dealt with the problem of rock socketed piles (Poulos, 1972). However, the constraint condition at the pile-base, doesn't influence the pile lateral response in the most common cases (Poulos, 1973b). The summary of the results obtained in these different works was presented in Poulos and Davis (1980).

Pile modelling

The pile was modelled as a thin vertical strip, with a width, D, a length, L, and a constant flexural rigidity E_pI_p. The flexural rigidity, E_pI_p, of the strip was equal to the flexural rigidity of the actual pile. The width, D, of the strip was the pile diameter in the case of a circular cross section, or, the dimension orthogonal to the load direction in the case of a rectangular cross section.

The pile was divided into $n+1$ elements, where $n-1$ had a length equal to $\delta = L/n$; the first and the last elements had a length equal to $\delta/2$ (Figure 3.14). On each block acted a uniform horizontal pressure, p_i, (due to the soil reaction) that was assumed to be constant across the pile width D. A comparison with the results obtained by Douglas and Davis (1964), who consider a non-uniform distribution of the soil reaction along the pile width, D, showed that this assumption led to an underestimation of the displacements and rotations at the pile-head in case of very short piles ($L/D = 2$); instead the error became negligible for $L/D > 15$.

The shear stresses which arise between the soil and the pile along its edges were not modelled. The accuracy of the solution was significantly dependent on the number of blocks in which the pile was divided. The solution adopted by the author, that best fit both the computational requirements (for computers of the 70s) and the solution accuracy, was to use 21 blocks.

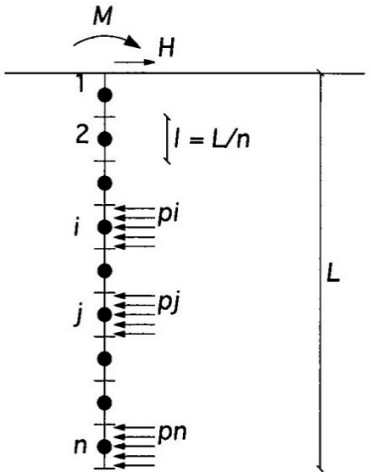

Figure 3.14: Subdivision of pile in blocks and soil pressures (Poulos, 1971)

Soil modelling

The soil was modelled as an ideal elastic, homogeneous and isotropic half-space, characterized by a Young's modulus, E_s, and a Poisson's ratio ν. These values were not affected by the pile presence. E_s was constant with depth (Poulos, 1971b). This is an ideal assumption that often differs from the actual soil properties (such as in normally consolidated sands or clays), for which it is reasonable to assume E_s variable with depth (z). The possibility to consider E_s variable with depth ($E_s = f(z)$) was covered later (Poulos, 1973b), but was necessary the introduction of an approximation in the use of the Mindlin's equation, that is strictly valid only in the case of a homogeneous half-space.

The displacement of a point for the effect of a load-point acting in a non homogeneous half-space can be obtained using again the Mindlin's equation (Appendix), but proceeding with an arbitrary choice of the E_s value to be used in the formula. Poulos (1973a) recommended the use of the E_s value at the point where the displacement is estimated. Later, as a result of considerations about the pile-behaviour under axial loads, the same author suggested to consider the average between the E_s value at the point where the load is applied and the E_s value where the displacement is evaluated (Poulos, 1979).

Solution system (Poulos and Davis, 1980)

Soil and pile displacements, in purely elastic conditions, were equalized at the center of each pile-blocks, except for the first and the last block. The compatibility equations implied:

$$y_p = y_s \tag{3.14}$$

with y_p the vector of the pile displacements and y_s the vector of the soil displacements. The pile displacements were evaluated using the differential equation of beam deflection:

$$E_p I_p \frac{d^4 y_p}{dz^4} = pD \tag{3.15}$$

This equation was expressed in terms of finite differences for the pile elements from 2 to n, using the appropriate boundary conditions at the first pile-block and at the $n+1$ pile-block. In this way $n-1$ equations were obtained, in which the displacements were expressed as a function of the soil pressures, in the form:

$$-p = \frac{E_p I_p n^4}{DL^4}[D]y_p + \frac{E_p I_p}{DL^4}A \tag{3.16}$$

The matrix $[D]$, of size ($n-1$ x $n+1$), depended on the boundary conditions imposed on the nodes 1 and n, and on the vector A relative to the loads acting on the pile. The displacements of the pile points, at the gravity centers of each pile-block, were expressed according to the equation:

$$y_s = \frac{D}{E_s}[I]p \tag{3.17}$$

in which the terms I_{ij} of the matrix $[I]$ defined the effects, in terms of displacement at the point i-th, of a force acting on a point j-th. The soil reactions were represented, rather than by load-points, by uniform pressures acting on a rectangular area, thus for this reason, it could be used the integration of the Mindlin's equation by means of the formulation proposed by Douglas and Davis (1964).

In the case of rock socketed piles or piles penetrating a very rigid layer (Poulos, 1972) it was proposed to take into account the influence of such a layer on the matrix $[I]$, using a calculation procedure based on the 'image-method'. Randolph (1981), however, showed how, in common cases, the horizontally loaded piles behave as infinitely long elements and their response is not affected by the boundary and soil conditions at the base. The $n-1$ compatibility equations obtained by equating the pile and soil displacements at the nodes were complemented by the global rotational and translational equilibrium equations of the pile.

It was obtained in this way, the $n+1$ equation system used to calculate the $n+1$ unknown soil pressures. Once found these unknowns, it was possible to evaluate the displacements, the rotations, the shears and the bending moments on the pile.

Non-linear analysis

The load-displacement relationship for an actual pile subjected to horizontal loads is markedly non-linear. Furthermore, the elastic analysis shows how, close to the pile-head, the pressures induced on the soil are very high, in particular for flexible piles, even for relatively small values of the load. Therefore, is reasonable assume, that at the pile-soil interface some relative-displacements can occur when certain pressure values are reached.

It was then formulated (Poulos, 1971) and studied in detail (Poulos, 1973a) an analysis type which allowed to model this phenomenon, according to a procedure similar to that proposed by Poulos (1968) for axially loaded piles and by Spillers and Stoll (1964) for horizontally loaded piles. The purely elastic conditions remained such until the stress state induced in the soil, in correspondence of each i-th block, didn't exceed an ultimate value p_{ui}. Once reached this value, it was admitted that in that point

relative-displacements might occur; in other words, it was removed the compatibility hypothesis in correspondence of the block in exam. From the mathematical point of view, this hypothesis involved the elimination, from the global equation system, of the compatibility equation corresponding to the plasticized block. The soil reaction at that block became a known term, equal to p_{ui}.

Subsequent increases of the external loads, acting on the pile, were taken only by the blocks in elastic conditions; these increases were evaluated again according to the elastic theory. In this way, the overall model was forced (on the basis of a purely elastic scheme) to perform an elastic-perfectly plastic analysis. Repeating this procedure and reaching the gradual yielding of all the blocks allowed to obtain the complete load-displacement curve. This procedure didn't involve remarkable errors if the number of plasticized blocks was limited, but might be inadequate when getting close to the ultimate load condition (Poulos and Davis, 1980).

Analysis of pair of piles

The soil was modelled as an elastic, homogeneous and isotropic half-space, characterized by the elastic modulus E_s and the Poisson ratio ν (Poulos, 1971a). Differently from what seen for the single pile case, the effects of the relative-displacements were not considered here: the analyses were carried out exclusively in the elastic field. Moreover, it was investigated only the homogeneous half-space case, having a stiffness constant with depth.

The most important aspects, about the modelling, were similar to those seen for the single pile (Poulos, 1971): the piles were modelled as vertical strips with a length L, a width D and a flexural rigidity, E_pI_p; the flexural rigidity E_pI_p assigned to the strip was, again, the flexural rigidity of the actual pile.

The piles were divided into $n+1$ blocks, where $n-1$ long $\delta = L/n$; the first and the last were long $\delta/2$. In the analysis, n was set equal to 20 (21 blocks). On each block acted a uniform pressure p_i, representing the soil reaction (Figure 3.15). The axes of the two piles were placed at a distance equal to s, while the angle, defined by the line that identifies the direction along which the horizontal force acts and the segment joining the piles axes, was the 'departure angle β'. The piles were identical and identically loaded. The scheme was therefore symmetrical.

The resolving equation system was that obtained considering the compatibility of the horizontal displacements at the $n+1$ points (at the pile-soil interface), and the rotational and translational equilibrium equations, in complete analogy with the single pile case. The main difference lay in the fact that the soil displacements, measured at the gravity centers of each block, were provided by Poulos and Davis (1980), as:

$$y_s = \frac{D}{E_s}[I_1 + I_2]p \tag{3.18}$$

where I_{1ij} and I_{2ij} were the components of the matrices $[I_1]$ and $[I_2]$ that defined, the influence of the element j-th of the pile 1 on the element i-th of the pile 1, and the influence of the element j-th of the pile 2 on the element i-th of the pile 1, respectively. The elements of the matrix $[I_1]$ were evaluated according to the same procedure used for the single pile (integration of the Mindlin's equation according to the formulation of Douglas and Davis, 1964 (Appendix)).

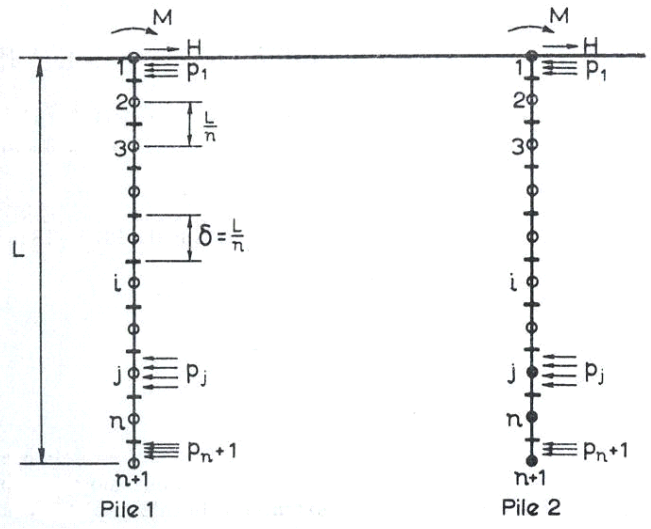

Figure 3.15: Subdivision of the pair of piles in blocks and soil pressures (Poulos, 1971a)

In order to create the matrix $[I_2]$, however, the uniform pressure acting on each block was replaced by a load-point acting on the gravity-center of the considered block. The elements of this matrix were obtained, as a result, directly applying the Mindlin's equation, without performing its integration. This simplification was considered acceptable because, increasing the distance between the load application point and the point at which the displacement was estimated, the replacement of the uniformly distributed pressure with an equivalent force induced negligible approximations.

The solution equation system allowed the evaluation of the influence of the second pile on the first one varying the spacing s and the departure angle β. In particular, the effects induced on displacements and rotations were measured using the parameters α_y and α_θ, defined 'interaction coefficients' for the displacement and rotation, respectively (Poulos, 1971):

$$\alpha_y = \frac{\text{additional displacement due to the adjacent pile}}{\text{pile displacement due to the load acting on itself}} \tag{3.19}$$

$$\alpha_\theta = \frac{\text{additional rotation due to the adjacent pile}}{\text{pile rotation due to the load acting on itself}} \tag{3.20}$$

The displacement (or the rotation) of a pair of piles can, therefore, be expressed by:

$$\frac{y_{pair}}{y_{sing,pile}} = 1 + \alpha \tag{3.21}$$

Interaction coefficients method and pile group analysis

The interaction coefficients method was developed by Poulos (1968) for the study of pile-groups subjected to vertical loads. The study of the pair of piles response with the integral elastic continuum model was extended by the author to a group of 4 identical piles, identically loaded (Figure 3.16). Because of the symmetry of the problem, the displacement of each pile is still evaluable using the equation system used to solve the pair of piles problem.

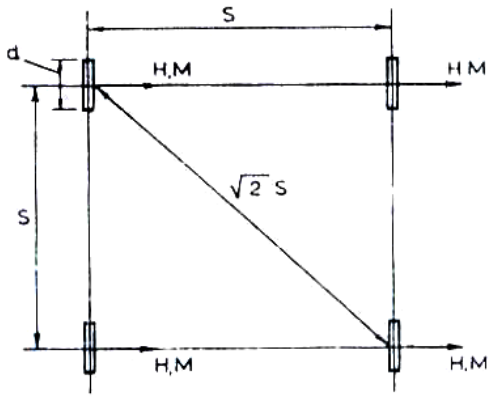

Figure 3.16: Pile-Group (2x2) Scheme (Poulos, 1971a)

In this case, however, it should be considered that the displacement of the soil points, at the pile-soil interface, is provided by:

$$y_s = \frac{D}{E_s}[I_1 + I_2 + I_3 + I_4]p \tag{3.22}$$

where the components $I_{i,ij}$ of the matrices $[I_i]$ defined the influence of the loads acting on the j-th elements of the generic pile on the displacements of the elements i-th of the pile i-th. The displacement of the pile-group (having 4 piles) obtained by a complete analysis was compared with the displacement of the group obtained by considering applicable the 'principle of superposition'. In the latter case, the displacement of the group was obtained starting from the displacement of a single pile, to which the displacement increments induced by the other adjacent piles were added, according to the expression:

$$\frac{y_{group}}{y_{sing,pile}} = 1 + \alpha \tag{3.23}$$

Where:

$$\alpha = \alpha_1 + \alpha_2 + \alpha_3 \tag{3.24}$$

where α_i were the interaction coefficients obtained considering the interactions between each pair of piles. The comparison between the movements of the group obtained using a complete analysis and those obtained by the principle of superposition, varying the geometrical and mechanical parameters, showed small differences, in a range of $\pm 2\%$. This consideration permitted to extend the applicability of the principle of superposition to a generic group of m-piles, and to define an analysis method based on the group interaction coefficients α_i. If it is considered a group of m piles subjected to horizontal loads, the displacement of each k-th pile can be defined as:

$$y_k = \bar{y_H} \sum_{j=1}^{m} \alpha_{kj} H_j \tag{3.25}$$

with α_{ki} equal to 1 for $k = i$, less than 1 otherwise. $\bar{y_H}$ defines the reference unit displacement, i.e. the displacement of an isolated pile subject to a unitary load. H_j are the loads acting on each of the m piles. The total load H_G acting on the group is expressed by:

$$H_G = \sum_{j=1}^{m} H_j \tag{3.26}$$

In the case of equal displacements (connecting structure infinitely rigid, the more realistic hypothesis in case of piles under horizontal loads) the system of $m+1$ equations, just obtained, can be solved in the m-unknowns loads H_j and in the group-displacement u_G (the same for all the piles). In the hypothesis, however, that the loads acting on the piles are all equal (infinitely flexible connecting structure), the load acting on each pile is known:

$$H_j = \frac{H_G}{m} \tag{3.27}$$

and the individual piles displacements can be calculated from the related equations.

3.4.3 Landi and Abagnara Methods (Landi, 2006; Abagnara, 2009)

Landi (2006) and Abagnara (2009) BEM-methods are based on that originally developed by (Poulos, 1971). The pile-soil interface is discretized into n rectangular areas of width D and length l variable with depth; the distribution of stress acting at the interfaces is approximated by n values of horizontal normal stress p uniformly distributed on each area.

The program STHOP (Abagnara, 2009), representing an evolution of the program NAPHOL (Landi, 2006), relies upon the following assumption:

- horizontally layered elastic soil;
- pile with constant or stepwise variable section;
- limiting pressure at the pile-soil interface.

The limiting pressure in the program STHOP is an input datum and different values for each pile segment corresponding to different soil layers may be selected. The authors carried out an extensive validation of the computer code against available experimental evidence and reached the following conclusion:

- the best option for piles in clay is to evaluate the limiting soil reaction as $p = 9c_u d$ (Broms, 1964) starting from a depth $z = 2d$ downwards; from ground level to $z = 2d$ the limiting soil reaction can be linearly interpolated between $p = 0$ at ground level and $p = 9c_u d$ at $z = 2d$;
- for piles in sand the limiting soil reaction may be set to $p = k_p^2 \gamma dz$ (Barton, 1985); a slight improvement may be obtained reducing the limiting soil reaction from ground level to $z = d$ to $p = k_p \gamma dz$.

The elastic modulus in the model, which has a large influence only on the very initial part of the load-displacement relationship, is fixed according to the following suggestion:

- for piles in clay: $E_u = 1000 - 1200 c_u$
- for piles in sand: $E/(\gamma d) = 150\varphi^\circ - 2300$

In the analysis of pile groups, the program STHOP adopts the following further assumptions:

- non-symmetrical extinction distance for the interaction between a couple of segments belonging to different piles in the group; this distance is defined according to the suggestion by Reese and Van Impe (2001);
- check of block failure for small spacings; the program requires a limiting pressure profile as defined for the single pile but when the spacing between the piles is so small as not to allow the full development of soil strength a reduced profile is adopted according to the mechanism of the block failure. The so-called shadowing effect, described before, is thus implemented in the software.

Neverthless the BEM methods developed by Poulos and more recently by other authors (for example: Landi (2006), Abagnara (2009), Basile (1999), Basile2013) are limited to the single pile or to the pile group case. These methods neglects the contact between the soil and the raft.

3.5 Other methods

3.5.1 Kitiyodom and Matsumoto method (Kitiyodom and Matsumoto, 2002; Kitiyodom, Matsumoto, and Horikoshi, 2005)

The method proposed by Kitiyodom and Matsumoto is based on an analytical model that can be described by the scheme in Figure 3.17. This approach has been developed in order to analyse and estimate the deformation and load distribution of piled-raft foundations subjected to vertical, lateral, and moment loads.

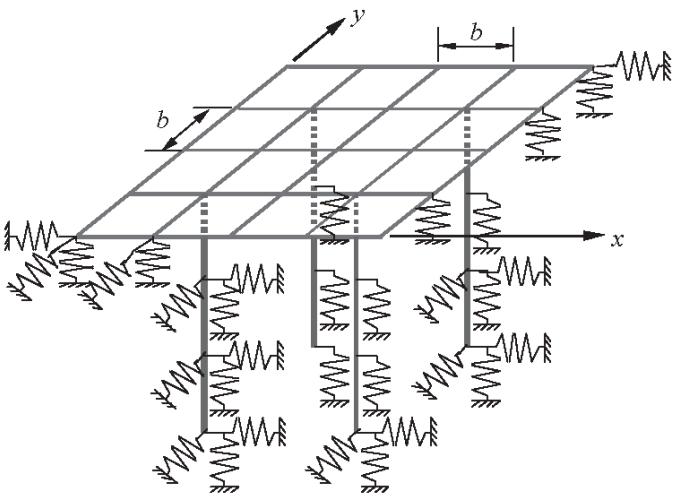

Figure 3.17: Plate-beam-spring modelling of a piled raft foundation (Kitiyodom and Matsumoto (2002, 2005))

This method has been implemented by the authors on the computer program PRAB (Piled Raft Analysis with Batter piles) and is based on a model similar to those developed by O'Neill et al., Chow and Clancy and Randolph, but in this case has been introduced two additional soil springs in the horizontal plane at each node of the piles and the raft to account for the bending moments of the piles, the horizontal soil resistance to the piles, and the shear resistance between the raft and the soil surface.

Analysis method description

Kitiyodom and Matsumoto model the flexible raft as thin plate elements and piles as elastic beam elements, while the soil is treated as springs, thus this approach is a hybrid kind of solution. To model the pile-soil-pile, pile-soil-raft, raft-soil-raft or in general all the 'structural element-soil-structural element' interactions this model uses the Mindlin's solutions both for vertical and lateral forces. The vertical soil spring constant at raft nodes, K_z^R, are expressed with:

$$K_z^R = \frac{4Ga}{1-\nu_s} \tag{3.28}$$

The horizontal soil spring constants at raft nodes, K_x^R and K_y^R are expressed with:

$$K_x^R = K_y^R = \frac{32(1-\nu_s)Ga}{7-8\nu_s} \tag{3.29}$$

where G is the shear modulus of the soil, ν_s is the Poisson's ratio of the soil, a is the equivalent radius of the raft element ($a = b/\sqrt{\pi}$, b = the width of the square raft element). The vertical shaft soil spring constants at the pile shaft nodes, K_z^P, are expressed with:

$$K_z^P = \frac{2\pi G\Delta L}{ln(r_m/r_0)} \tag{3.30}$$

where r_0 is the pile radius, ΔL is the pile element length, $r_m = 2.5L(1-\nu_s)$ and in case of slender piles the length L is replaced by an effective length ($L_e = 1.5D\sqrt{2(1+\nu_s)E_p/E_s}$). The horizontal shaft soil spring constants at each pile node, K_x^P and K_y^P are estimated by means of Mindlin's solution:

$$K_x^P = K_y^P = \frac{pD}{\rho E_s}E_s\Delta L \tag{3.31}$$

where p is the lateral and uniformly distributed force acting on the pile element and ρ is the respective lateral displacement at each pile node calculated using Mindlin's solutions.

Obviously the deformations of individual structural members occur because of the loading, so, since the soil is a continuous material, this deformation will produce additional deformations of the other structural members. Therefore, all the 'structural element-soil-structural element' interactions are studied like shown in the Figure 3.18, and the overall deformation w_i at all nodes are written in this way:

$$w_i = \sum_{j=1}^{n} a_{ij}P_j \tag{3.32}$$

where a_{ij} is defined as soil flexibility coefficient.

The authors used PRAB to realize some interesting parametric studies for piled-raft subjected to lateral loading.

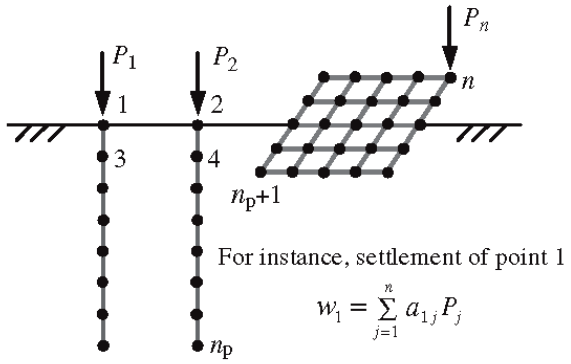

Figure 3.18: Structural member - soil - structural member interaction (Kitiyodom and Matsumoto (2002, 2005))

3.5.2 Small and Zhang method (Small and Zhang, 2006)

This method is able to analyze piled-raft foundations under general loadings even in the case in which the pile-cap or raft is in contact with the ground. The soil is divided into multiple horizontal layers, the raft is modelled as a thin plate and the piles as elastic beams. The approach used by Small and Zhang is based on the finite layer theory, a theory developed by Small and Booker (1986) that permits the analysis of horizontally layered materials. The raft is sustained by both the soil and the piles and it can be subjected to horizontal, vertical loads and bending moments. The movements of the piled raft in the three directions (x, y, z) and rotations in two directions (x, y) can be computed with the software APRAF.

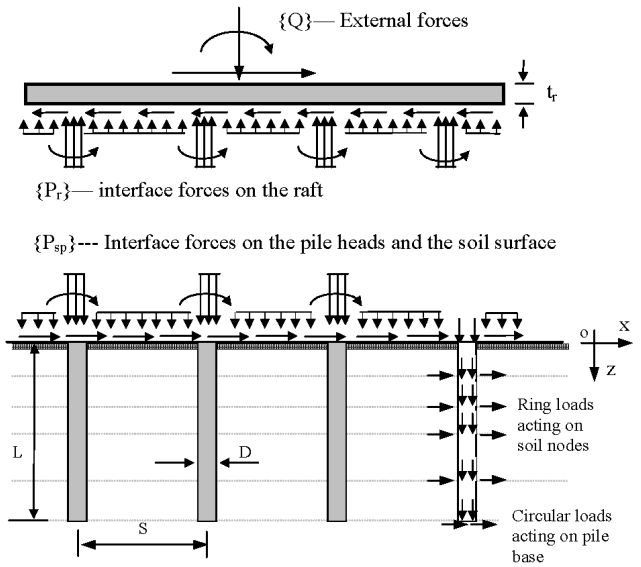

Figure 3.19: Free body diagram of piled raft with external forces and interface forces in all directions (Small and Zhang, 2006)

Analysis method description

As it's possible to see in Figure 3.19, the foundation system can be separated in two sub-systems:

- an isolated raft subjected to external loading Q and interfaces forces P_r;
- a pile group, embedded in a layered soil, subjected to interfaces forces P_{sp} (where the forces between pile and soil can be considered as series of ring loads applied to the nodes located along the pile shaft).

The raft is then divided in a series of rectangular elements where each pile-head assumed to fit within one of the raft elements and where the interface forces are applied to each elements considering them like uniform loads.

Instead, the forces acting on the pile heads are considered to be concentrated loads while the forces applied to the soil surface are assumed to be a series of rectangular uniform pressures. To make the analysis some nodes of the raft must be restrained, thus two corner nodes are restrained, one completely fixed in all kind of directions and the other node is fixed only in the y direction, so in this way, the rigid body translations and rotations about the first raft node are assumed to be D_x, D_y, D_z, θ_x, θ_y and θ_z. The displacement δ_r at the centre of each raft element is expressed by:

$$\delta_r = [I_r]P_r + aD_x + bD_y + cD_z + d\theta_x + e\theta_y + f\theta_z + \delta_{r0} \tag{3.33}$$

where:

- $[I_r]$ = influence matrix of the pinned raft;
- P_r = the vector of interface loads and moments on the raft elements;
- δ_{r0} = displacements at the centres of the raft elements due to applied loads on the pinned raft;
- from a to f = auxiliary vectors related to the raft geometry.

For the analysis of the second sub-system (the pile group) it's necessary to consider all kind of interactions: soil-soil, soil-pile, pile-pile, and pile-soil. The interaction between soil and soil may be evaluated by means of the finite layer theory of Small and Booker (1986), while the other interactions with the procedure indicated in the method presented by Zhang and Small (1999). With this procedure it's possible to express the displacement of each pile-head (at the centre) and of each soil surface element subjected to the interfaces loads transferred by the raft, with the following form:

$$\delta_{sp} = [I_{sp}]P_{sp} \tag{3.34}$$

where:

- $[I_{sp}]$ = influence matrix of the pile-enhanced soil continuum;
- P_{sp} = interface load vector between the raft and the pile-enhanced soil;
- δ_{sp} = vector of interface displacement between the raft and the pile-enhanced soil.

To solve the complete system composed by the two sub-systems (the raft and the pile group) it's then necessary imposing the compatibility (for displacements) and the equilibrium (for the interaction forces):

$$\delta_r = \delta_{sp} \tag{3.35}$$

$$P_r = -P_{sp} \tag{3.36}$$

Finally, it's possible to determine the interface pressures on the pile-enhanced soil and solutions for the displacements in the raft.

3.6 Lesson learned

In Chapter 2 the main parameters and factors that affect the response of a single pile, a pile group and a piled raft under this loading condition have been described, on the basis of the most important research works found in literature. Basically, it has been shown that:

- for a single pile the response is mostly affected by: a) the restraint conditions at the pile-head, b) the pile-soil relative stiffness and c) the way in which the load is applied (statically, cyclically or dynamically), while the actual pile length is not a significant parameter to be considered (with the only exception for short/rigid piles);
- for a pile group the response is mostly affected by: a) the pile-soil relative stiffness, b) the relative spacing between the piles, c) the stiffness properties of the connecting structure and d) the presence of group effects like the shadowing and the edge effect, that are responsible for the load distribution between the piles in the group and for the common decrease of the stiffness of the overall foundation system. In general, for an equal average load at each pile, the displacement of the pile group is greater than the displacement of a single isolated pile; in the same way, for a given displacement at the pile-head, the load supported by an isolated pile is higher than the average load supported by a pile within the group.
- single piles and pile groups subjected to cyclic or dynamic lateral loads show a worse performance compared to the same piles under static loading. However, this PhD thesis has as its main purpose the intent to develop a calculation code that can deal with the analysis of piled-rafts systems, that represents a really more complex soil-structure interaction problem compared to the single pile case. For this reason, the attention has been focused on static loads. It's important to underline that, even nowadays, it's really hard to properly model and study not only a piled-raft but even a single pile with FEM codes considering cyclic or dynamic loading, due to the high computational cost required.

In a piled-raft foundation the horizontal loads are resisted by: 1) the piles; 2) the passive resistance of the soil on the front of the embedded structure; 3) the frictional resistance along the embedded sides and 4) the frictional resistance along the base of the raft. However, in the context of this work only the piles and the resistance offered by the base of the raft will be considered. Only few publications were found that described tests performed to investigate the lateral-load resistance of pile caps considering only the resistance offered by the soil along the base of the raft.

In Chapter 2 the main findings obtained with centrifuge tests (Horikoshi and Matsumoto, 2003), small scale laboratory tests (Katzenbach and Turek, 2005; Matsumoto et al., 2010; Unsever et al., 2015; Hamada et al. ,2015), full-scale field tests (Kim et al. 1974) were reported. The main findings of the authors were:

- the initial stiffness of a piled raft is not always higher than that of a raft alone (because the piles reduce a lot the contact pressure between raft and soil);
- the horizontal stiffness of the piled rafts is larger than that of a pile group with the same configuration as the piled raft, because the raft acts as a 'horizontal displacement reducers';
- the bending moments of the piles in the piled raft are reduced, compared with those in the pile group;
- rotation of the raft decreases as the pile-head connection rigidity becomes lower, although the horizontal stiffness also becomes lower;
- higher horizontal load is transferred to the piles in the piled raft with rigid pile head connection, which leads to higher initial horizontal stiffness compared with that in the piled raft with hinged pile head connection;
- the total horizontal resistance in a rigid connection piled raft is higher than in a hinged connection model;
- the proportion of the raft load rapidly decreased as the piled raft displacement increased. The reduction in the proportion of the raft load was more significant in the rigid connection model, which was related to a higher horizontal stiffness of the piles;
- for small horizontal displacements and high vertical load levels the major part of the horizontal load was carried by the raft.

Moreover, until now, the available literature about the influence of the vertical loads on single piles, pile groups and piled-rafts response to horizontal loads provides scanty and contradictory results.

In Chapter 3 some of the available analysis methods for single piles, pile groups and piled raft were presented. In detail have been described:

- Winkler-based approaches (i.e., '$p - y$ curves');
- BEM-based methods;
- the Strain-Wedge-Model (Ashour and Norris (1998, 2004));
- the 'plate-beam-spring' model proposed by Kitiyodom and Matsumoto (2002, 2005);
- the method proposed by Small and Zhang (2006).

The last two simplified methods are able to study even piled-raft with the raft in contact with the soil.

The first one was implemented by Kitiyodom and Matsumoto (2002, 2005) on the computer program PRAB (Piled Raft Analysis with Batter piles). The authors model the flexible raft as a thin plate element and piles as elastic beam elements, while the soil is treated as springs. To model all the 'structural element-soil-structural element' interactions this model uses the Mindlin's solutions both for vertical and lateral forces. However, all the springs can have only a linear elastic or a linear elastic-perfectly plastic behaviour (because of a limiting soil resistance profile), thus it is strictly necessary,

to choose properly the soil elastic modulus. Usually for laterally loaded piles application, typical values for the elastic modulus range between the 10 and 30% of the elastic modulus at small strain level.

The last one, proposed by Small and Zhang (2006), is able to analyse piled-raft foundations under general loadings even in the case in which the pile-cap or raft is in contact with the ground. The soil is divided into multiple horizontal layers, the raft is modelled as a thin plate and the piles as elastic beams. The approach used by Small and Zhang is based on the finite layer theory, a theory developed by Small and Booker (1986) that permits the analysis of horizontally layered materials. Even in this case the soil can have or a linear elastic or a linear elastic-perfectly plastic behaviour. In both the last two methods is not considered the non-linear behaviour for reinforced concrete pile sections.

Moreover, even if the authors highlighted the ability of their computer program to study piled-raft under general loading conditions, no significant results were presented about the influence of the vertical loads on the response of the foundation under horizontal forces.

It's important to consider that soil-structure interaction problem, as piled raft foundation under horizontal load, represents an interdisciplinary subject characterized by material non-linearities affecting both the soil and the structural elements. The possibility to capture the variation of the soil-structural elements relative stiffness during the application of lateral loads is a key aspect for the assessment of the overall response and of the load distribution between all the components.

Even today, in fact, most of the computational platforms are specialized either for structural or for geotechnical applications. Whereas the formers are able to accurately capture the non-linear response of the structural elements, they are usually poor in modeling soil non-linear behaviour. On the other hand, the latter are capable in advanced modeling of the soil response but typically rough about reproducing the non-linear behaviour of the structural elements.

For these reasons, it is crucial to develop an analysis method for piled raft under lateral load that can consider properly the soil non-linear behaviour, the pile material non-linearity and typical aspects observed experimentally in pile groups and piled rafts as the presence of the shadowing effect.

Finally, it is well known that the response of pile foundation subjected to later load are mainly affected by the shallower soil layers. It is, therefore, an important aspect a proper evaluation of suction in case of partially saturated conditions. Suction can be responsible for a bigger initial stiffness of a pile foundation under lateral load and for a bigger lateral resistance that should be taken into account.

Chapter 4

Numerical Experiments

4.1 Introduction

Piled-Raft behaviour under horizontal loading is still now a geotechnical issue to be clarified at all. This is because a lot of factors affect the response, in terms of load-displacement curve, raft-pile group load sharing, piles and raft bending moments.

These factors are mainly: pile-soil, pile-pile, raft-soil and raft-pile interactions, the constraint condition at the pile heads (ranging from a perfect hinge to a rigid connection and that depends on the raft thickness and stiffness), the pile group layout. For instance, the number of piles in a group and their spacing are important aspects to be considered because are responsible, in a foundation system that has to support also vertical loads, for the magnitude of the contact pressure acting at the raft-soil interface and so in the stress state of the soil under the raft.

The aim of the following FEM-analyses was to better understand the responses and the interaction mechanisms, under horizontal loads, of single piles, pair of piles (having different spacing), pile groups and finally piled-rafts (with a vertical load acting on the raft). The analyses have been performed using Plaxis3D AE (Plaxis BV, 2015).

4.2 Model description

The complete model (Figure 4.1) is composed of a concrete raft having a base and a width of 7.0 m and a thickness of 0.7 m, 25 concrete piles with a diameter of 0.5 m, a spacing of 3 diameters. Two pile lengths have been considered ($L = 20$ m and $L = 10$ m).

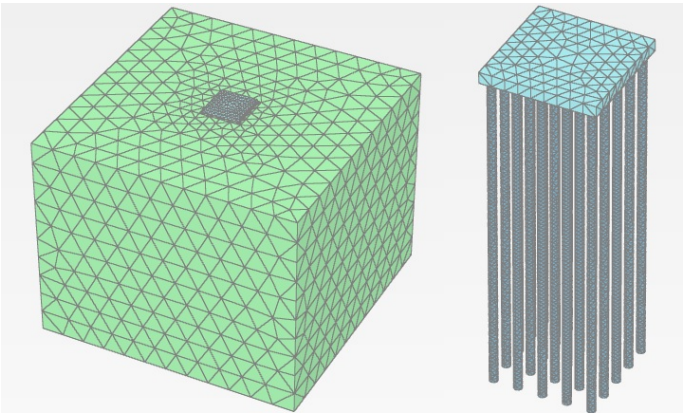

Figure 4.1: Plaxis 3D Model

With the same model and mesh is possible to study different layouts, because each structural component (piles and raft) of the piled-raft system can be activated and deactivated. The overall model has a base and a width of 50.0 m and a thickness of 40.0 m (twice the maximum pile length considered in this work), to minimize boundary effects. A medium size mesh has been generated (with a box refinement of the mesh inside the volume where the piles have been positioned) with 374849 soil elements (10-noded elements) and 552274 numbers of nodes having average element size of 0.521 m.

In many previous works (using finite element codes), the piles were modelled in a traditional manner, using a simple beam element that is a non-volume element. However, it is well known that to properly realize a finite element analysis of a pile group, the pile-volume influence cannot be ignored. Neglecting the area and the volume of piles, makes impossible to properly simulate the interaction between the piles and the soil, that is clearly and highly dependent on the piles geometry.

At the beginning of this work, the FEM analyses were performed using solid elements (volume elements) to model the piles, because Plaxis3D AE is able, with a specific tool, to provide the profile of the internal forces (bending and shear) along the pile shafts even if modelled as a cluster of elements. Instead, to easily read the pile deflection profile, a beam element with a negligible stiffness was positioned along each pile axis.

However, despite the huge number of elements (374849) in this model, the mesh didn't allow to the Plaxis tool, described before, to perform good readings of the bending moment and shear, especially at the pile heads. Because of this remarkable problem, it was impossible or very difficult, in pile group and piled raft analyses, the reading of the load carried by the piles and so the evaluation of the load distribution between all the structural elements of the foundation system.

For this reason, it was decided later to model the piles as hybrid elements composed by a beam element and solid elements that surround the beam, following the procedure described by Kimura and Zhang (2000) (Figure 4.2).

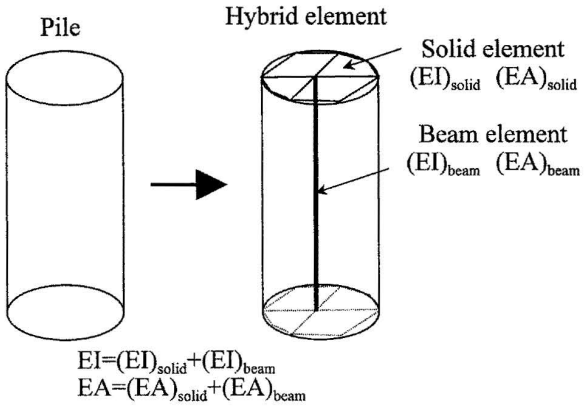

Figure 4.2: Hybrid element (Kimura and Zhang, 2000)

In this approach, the overall pile stiffness (axial stiffness, EA and flexural rigidity, EI) needs to be shared by the beam and the solid elements in a way that the pile flexural rigidity EI is equal to the sum of the flexural rigidity of the beam element $(EI)_{beam}$ and of the solid elements $(EI)_{solid}$. The big advantage of the hybrid modelling of pile is that axial forces, bending moments and shear forces of the pile can be estimated easily from the factored values of those of the beam elements.

To define the proper sharing ratio between the stiffness of the beam and the solid elements some preliminary analyses were performed on fixed-head single piles and pile groups. These analyses were carried out in load control, firstly modelling the piles as solid elements and then as hybrid elements. At each step of the analysis, each pile-head was loaded with the same load, in this way, the resulting load-displacement curve of each pile, using these two different pile-modelling approaches, could be easily obtained and compared.

These analyses were carried out varying the sharing ratio between the stiffness of the beam and the solid elements, keeping well in mind that these solid elements within the hybrid element should be 'hard' enough to represent the pile-size influence. Therefore, it is important to keep large enough the stiffness of solid pile elements compared to the stiffness of the surrounding soil. For this reason, the stiffness of the solid elements should be kept to a certain level.

Finally, the sharing ratio between the stiffness of the beam element and the solid elements was selected as 9 to 1. Considering that the stiffness of concrete is about equal to $30 * 10^3$ MPa and the stiffness of the soil is in the order of 10-30 MPa, the stiffness of the solid elements within the hybrid element is stiff enough to represent the pile-size influence.

The soil used in the analyses is a sand, modelled with the hardening soil model (Schanz, Vermeer, and Bonnier, 1999), while the raft and the piles are modelled using a linear elastic model. The interfaces between structural and soil elements are modelled as joint elements. The material properties of the interfaces are those of the adjacent soil and the roughness of interaction is modelled by choosing a suitable value for the strength reduction factor (R_{inter}). Here it was assumed a R_{inter} value equal to 0.67. The default value of the virtual interface thickness was used. All the input parameters used in the analyses are summarized in Table 4.1.

Table 4.1: Model Parameters

	Sand HS model	Raft	Hybrid Pile Beam element	Solid elements
Young's modulus (MPa)	-	31500	28350	3150
Poisson's ratio (-)	0.3	0.3	0.3	0.3
Angle of friction (°)	33	-	-	-
Interface R_{inter}	0.67	-	-	-
Unit weight (kN/m^3)	18	25	0	25
Confining stress dependent stiffness modulus (MPa)	Hard. Soil Eq.	-	-	-
Reference stiffness modulus E_{50}^{ref} (MPa)	30	-	-	-
Reference stiffness modulus E_{oed}^{ref} (MPa)	30	-	-	-
Reference stiffness modulus E_{ur}^{ref} (MPa)	90	-	-	-
Power for stress-level dependency of stiffness	0.5	-	-	-

Using the hardening soil model is possible to describe better the soil behaviour because it's able to take into account for the stress (confining pressure) dependency of the stiffness with the relationship:

$$E_{50} = E_{50}^{ref}(\frac{ccos\phi - \sigma_3 sin\phi}{ccos\phi + p_{ref} sin\phi})^m \tag{4.1}$$

where E_{50}^{ref} is a reference stiffness modulus corresponding to a reference confining pressure (p_{ref}) chosen to be equal to 100 kPa. In this way it's evident that the actual stiffness is related directly to the value of the minor principle stress, σ_3.

In this work the FEM analyses were performed:

- on fixed-head single piles to study the developing of the active and passive wedge of soil, respectively behind and in front of the pile shaft, responsible for the interactions between the piles in a group;
- on fixed-head pair of piles to investigate about the load distribution and the maximum bending moments varying the pile spacing ratio s/D and considering two departure angles, $\beta = 0°$ (the pair of piles are parallel to the load direction) and $\beta = 90°$ (the pair of piles are orthogonal to the load direction);
- on fixed-head pile groups to better understand group effects (and so interaction mechanisms) considering 4 different group layout (2x2 (s/D=6), 3x3 (s/D=3), 3x3 (s/D=6) and 5x5 (s/D=3));
- on piled-rafts (subjected to the same vertical load, chosen to be 1/3 of the bearing capacity of the raft alone) varying the layout of the pile-group below the raft (the same 4 layouts studied for the simple pile-group analyses were used), and considering two different values for the pile length (L=20 m and L=10 m), in order to study the performance of different piled-raft systems supporting the same vertical load, but having different contact pressures at the interface between the soil and the raft, because of the different number and position of the piles.

4.3 Single pile analyses

Lateral load analyses on fixed-head single piles were carried out to investigate the development of both the active and passive soil wedge, positioned respectively behind and in front of the pile. The load was applied using a rigid surface at the pile-head section, located at the ground surface level (horizontal load with no eccentricity). The conditions imposed at the rigid surface were the following:

- Translation along x-direction = free (F_x = 0);
- Translation along y-direction = imposed load F_y;
- Translation along z-direction = free (F_z = 0);
- Rotation ϕ_x = fixed = 0 (no rotation);
- Rotation ϕ_y = fixed = 0 (no rotation);
- Rotation ϕ_z = fixed = 0 (no rotation).

At each load step, it was pointed out the geometry of the developing active and passive wedges, using vertical sections and horizontal sections at 2 diameters in depth (Figure 4.3 and Figure 4.4). The soil volumes bordered in the pictures are those that have reached a value of the τ_{rel} ranging between 0.9 and 1.0, thus the volumes where the fully mobilization of the shear resistance was attained. τ_{rel} is defined as the ratio among the mobilized shear resistance and the current maximum shear resistance of the soil. When the τ_{rel} is equal to the unity value the soil has mobilized all the available shear resistance.

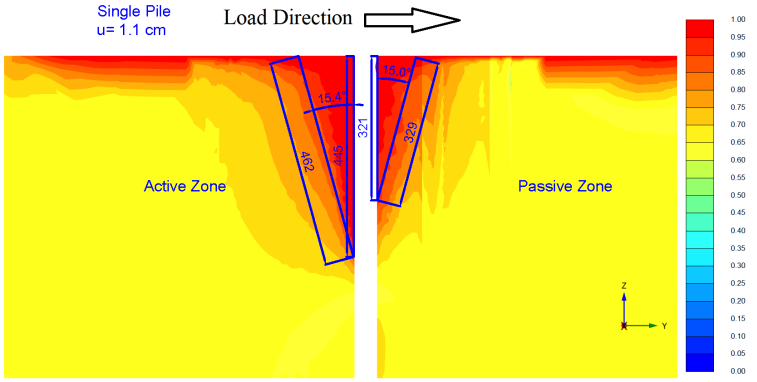

Figure 4.3: Single Pile Analysis – Vertical section – τ_{rel} (Horizontal Displacement = 1.1 cm - ϕ = 33°)

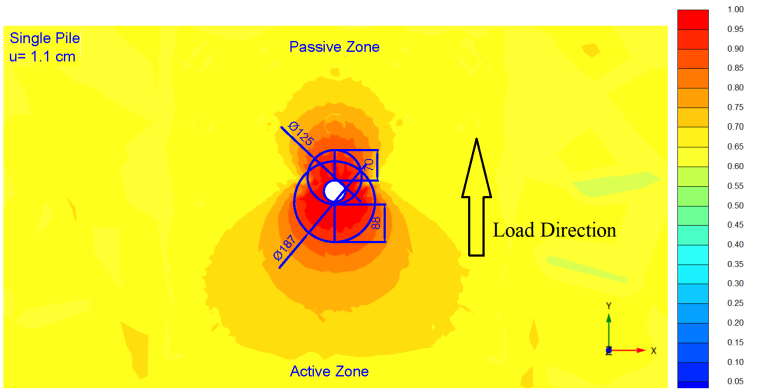

Figure 4.4: Single Pile Analysis – Horizontal section (at 2D depth) - τ_{rel} (Horizontal Displacement = 1.1 cm - ϕ = 33°)

4.4 Pair of piles analyses

The simplest pile group layout to be analysed is composed by a pair of piles. A lot of information can be captured studying the interaction mechanism involved in such simple group configuration. The analyses were performed on pair of piles in which the piles were positioned facing each other along the load direction, using the following spacing values: 3D, 6D, 9D. In these analyses it was used an angle of friction value of 33 degrees. The displacement (analysis in displacement control) was applied using two rigid surfaces at the pile-head sections located at the ground surface level. The conditions imposed at the rigid surfaces were the following:

- Translation along x-direction = free (F_x = 0);
- Translation along y-direction = imposed displacement (u_y = 0, 5, 10, 20, 30, 50 mm);
- Translation along z-direction = free (F_z = 0);
- Rotation ϕ_x = fixed = 0 (no rotation);
- Rotation ϕ_y = fixed = 0 (no rotation);

- Rotation ϕ_z = fixed = 0 (no rotation).

The aim was to better understand and identify the mechanism that rules the response.

Here are presented the responses, under horizontal load, of the pair of piles with a relative spacing s/D = 3 (fixed-head) in terms of 'load - deflection' curve (Figure 4.5), 'maximum bending - load' curve (Figure 4.6) and 'load distribution' (Figure 4.7) between the front and the rear pile, at each displacement level investigated during the analyses. Finally, a vertical section and a horizontal section (at the depth of 2D) representing the relative shear stress (τ_{rel}) color map, in correspondence of a displacement level equal to y/D = 2% (1 cm), is shown (Figure 4.8).

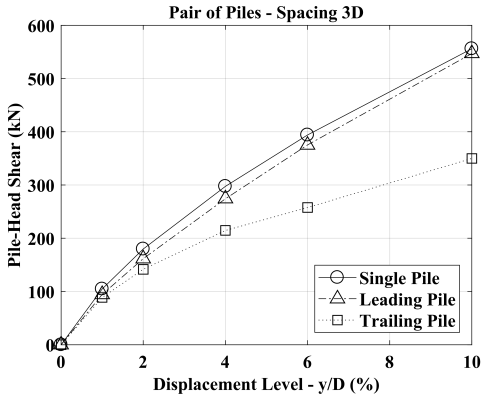

Figure 4.5: Pair of Piles Analysis – 'Horizontal Load-Displacement Level Curve' – Spacing 3D - $\phi = 33°$

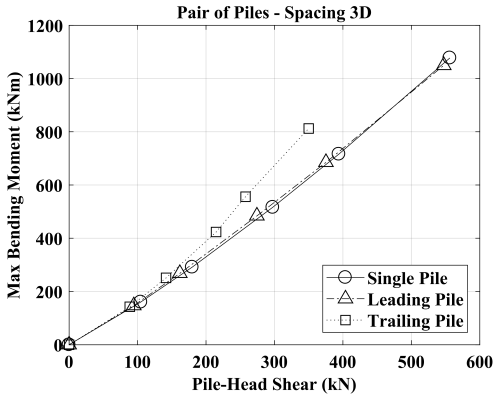

Figure 4.6: Pair of Piles Analysis – 'Maximum Bending Moment-Horizontal Load Curve' – Spacing 3D - $\phi = 33°$

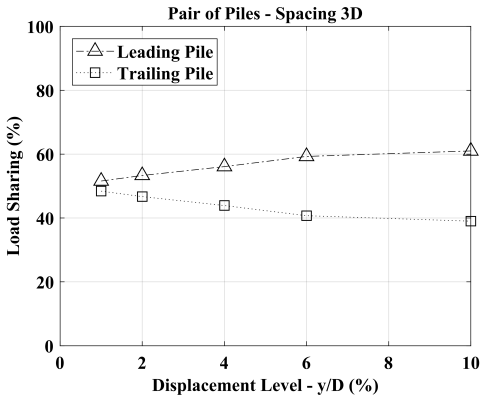

Figure 4.7: Pair of Piles Analysis – 'Load Distribution-Displacement Level' – Spacing 3D - $\phi = 33°$

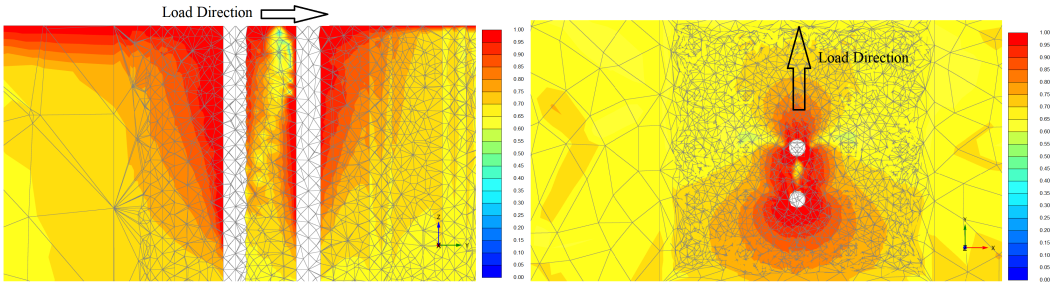

Figure 4.8: Pair of Piles Analysis – τ_{rel} Vertical and Horizontal Section (Displacement Level 2%) – Spacing 3D - $\phi = 33°$

The pair of piles response with a spacing ratio s/D = 6 (fixed-head) are presented in terms of 'load - deflection' curve (Figure 4.9), 'maximum bending - load' curve (Figure 4.10) and 'load distribution' (Figure 4.11) between the front and the rear pile at each displacement level investigated during the analyses. Again, a vertical section and a horizontal section (at the depth of 2D) representing the relative shear stress (τ_{rel}) color map, at a displacement level equal to y/D = 2% (1 cm), is shown (Figure 4.12).

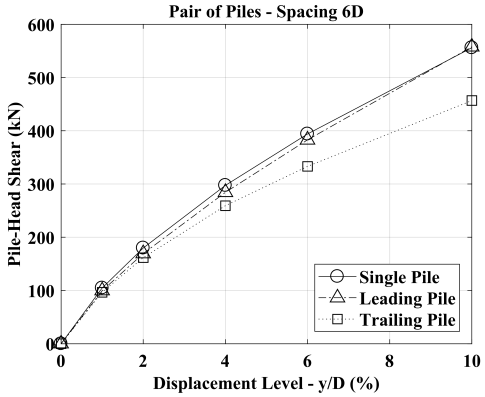

Figure 4.9: Pair of Piles Analysis – 'Horizontal Load-Displacement Level Curve' – Spacing 6D - $\phi = 33°$

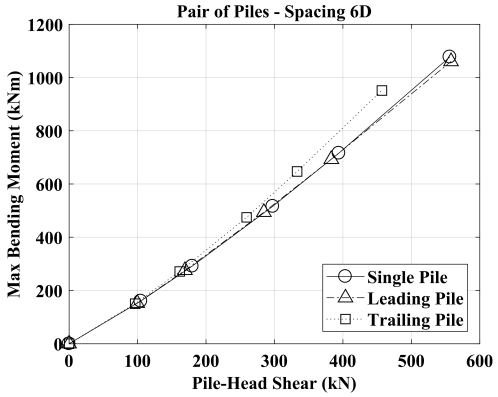

Figure 4.10: Pair of Piles Analysis – 'Maximum Bending Moment-Horizontal Load Curve' – Spacing 6D - $\phi = 33°$

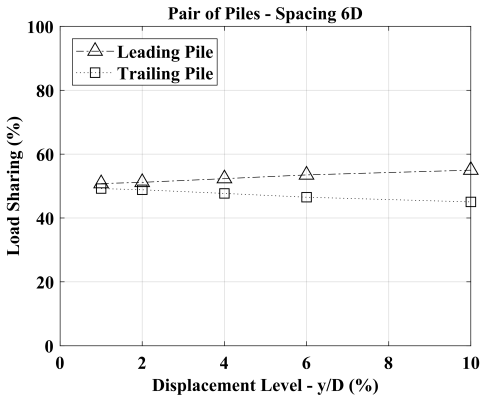

Figure 4.11: Pair of Piles Analysis – 'Load Distribution-Displacement Level' – Spacing 6D - $\phi = 33°$

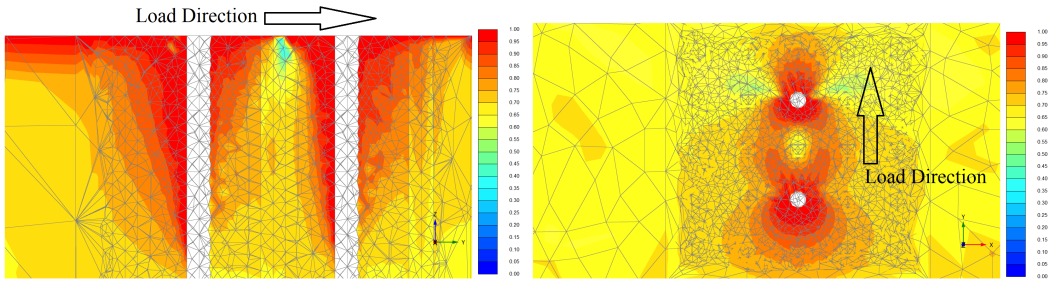

Figure 4.12: Pair of Piles Analysis – τ_{rel} Vertical and Horizontal Section (Displacement Level 2%) – Spacing 6D - $\phi = 33°$

Observing at the results, it's clear how the different responses, due to different spacing values, are affected by the development of the active and the passive soil wedges, respectively behind and in front of the pile shaft.

It is observed that the front pile response is basically the same of the single isolated pile. This was already noted in the past, and the reason for this behaviour can be explained by the fact that the front pile is in contact (at the front side) with an undisturbed soil that can mobilize all the passive resistance available as in the single isolated pile. The rear pile, instead, has a completely different response, for spacing values less than 6D, because while the front pile starts to move, the soil positioned at its back side undergoes immediately a decreasing in the confinement stress state.

For this reason, the rear pile is in contact with a disturbed soil that can't fully mobilize the passive resistance. Therefore, it's evident that only for spacing values bigger than 6D, the decrease in the confinement stress in the back side of the front pile doesn't affect anymore the response of the rear pile.

Moreover, looking at the 'maximum bending - load' curves (Figure 4.6 and Figure 4.10), it's possible to see that, for spacing values ranging between 3D and 6D, the rear pile: a) is subjected to a horizontal load lower than the leading pile at the same displacement level, but, b) is subjected to a bigger maximum bending moment compared to the front pile for a given horizontal load.

In order to complete the investigation on pair of piles response, some analyses were performed on pair of piles positioned side by side (center-to-center line perpendicular to the load direction), having spacing values equal to 3D, 6D, 9D. However, already for a pair with a spacing of 3D, it was observed that the response of the two piles is approximately equal to that observed in the single isolated pile. Not significant interaction mechanisms between active and passive wedges have been noted.

4.5 Pile group analyses

This 3D model layout permits to study pile groups having different spacing and number of piles. The main aim of these analyses was to better understand the group effects. All the analyses were performed with fixed-head restraint conditions and in displacement control (all the pile-heads are subjected to the same displacement). The displacement sequence, for each pile, was: 0, 5, 10, 20, 30 and 50 mm, corresponding to a displacement level (defined as y/D) of 0, 1, 2, 4, 6 and 10%. Two pile lengths ($L = 10$ m and L = 20 m) were used in the analyses. However, no significant differences were observed, thus the results reported here are about pile groups having a pile length equal to 10 m. The pile group layouts investigated were:

- Pile Group: 5x5 (25 piles) – Spacing = 3D;

- Pile Group: 3x3 (9 piles) – Spacing = 6D;
- Pile Group: 3x3 (9 piles) – Spacing = 3D;
- Pile Group: 2x2 (4 piles) – Spacing = 6D;

Neverthless, in the next are described the results obtained for the 3x3 pile-group with a spacing of 3D and for the 3x3 pile-group with a spacing of 6D.

4.5.1 Pile group 3x3 (fixed-head) - s/D = 3

The Figures 4.13 and 4.14 represent the response of a 'representative pile' in each row in terms of load-displacement and maximum bending-horizontal load curves. Figure 4.15, instead, represents the load sharing between the pile rows.

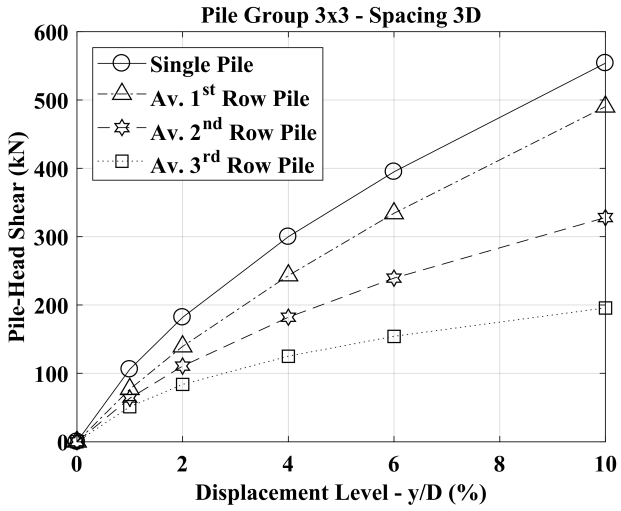

Figure 4.13: 3x3 P.G. $s/D = 3D$: 'Load - Displ. Level' curve for each representative pile

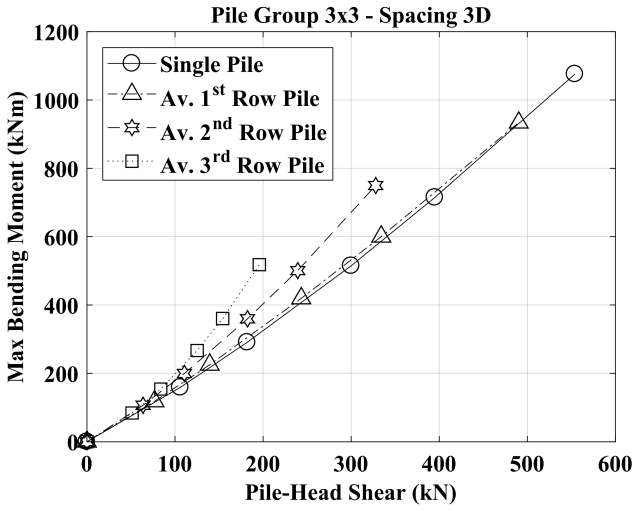

Figure 4.14: 3x3 P.G. $s/D = 3D$: 'Max Moment - Load' curve for each representative pile

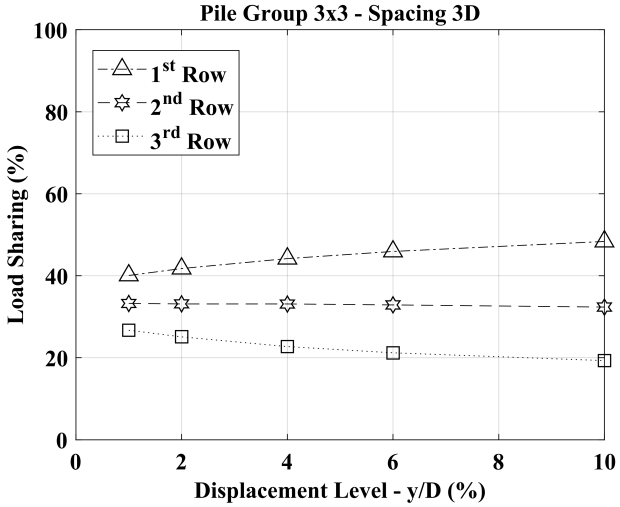

Figure 4.15: 3x3 P.G. $s/D = 3D$: Load Sharing between the rows

It can be noted, as expected, that the 1^{st} row carries the bigger rate of the horizontal load, while the 3^{rd} row the lower, due to the shadowing effect, that is relevant for small spacing values.

Moreover, looking at the maximum bending moment-load curves, the piles located in the rows behind the first row, even if they carry a horizontal load lower than the piles in the leading row for a same displacement level, they are subjected to a bigger maximum bending moment compared to the front piles for a same horizontal load.

In Figures 4.16, 4.17 and 4.18 are shown the vertical stress σ_{zz}, the τ_{rel} and the horizontal displacement colormaps, respectively, for a vertical section along the horizontal load direction at a pile-head displacement level, y/D, equal to 4% (2 cm).

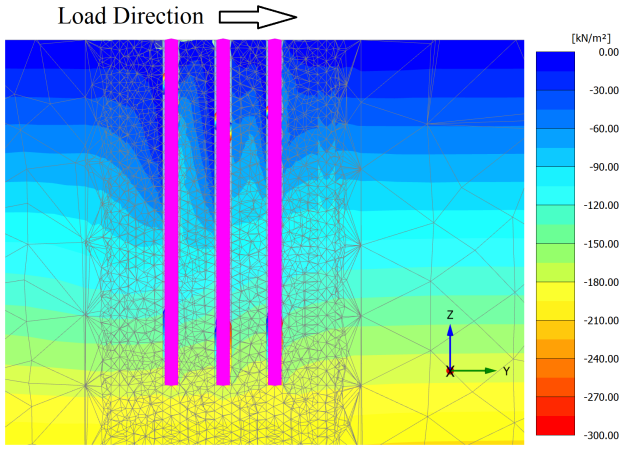

Figure 4.16: 3x3 Pile Group (Spacing = 3D) – Vertical stress σ_{zz}

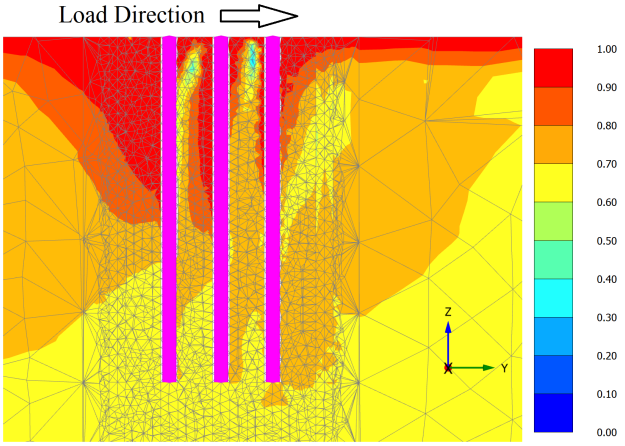

Figure 4.17: 3x3 Pile Group (Spacing = 3D) – τ_{rel}

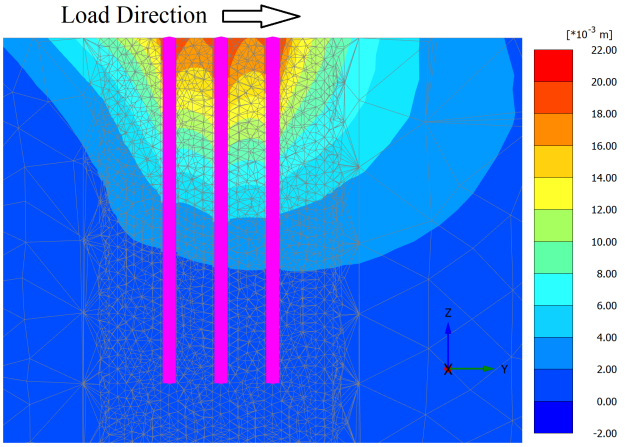

Figure 4.18: 3x3 Pile Group (Spacing = 3D) – Horizontal displacements

4.5.2 Pile group 3x3 (fixed-head) - s/D = 6

The Figures 4.19 and 4.20 represent the response of a 'representative pile' in each row in terms of load-displacement and maximum bending-horizontal load curves. Figure 4.21, instead, represents the load sharing between the rows.

As expected, with a spacing of 6D, all the interaction mechanisms start to become negligible compare to the analogous 3x3 pile-group studied before (with a spacing equal to 3D). In this case, the piles in the first row exhibit the same behaviour of the single pile. This result confirms that, not only is necessary to decrease the number of piles, to reduce interactions, but also to increase the pile spacing.

It can be noted that, the load distribution between the three rows becomes more homogeneous compared to the same rows in the pile group seen before. The rows are subjected to loading rates ranging between 30 and 36%, so they behave essentially at the same way.

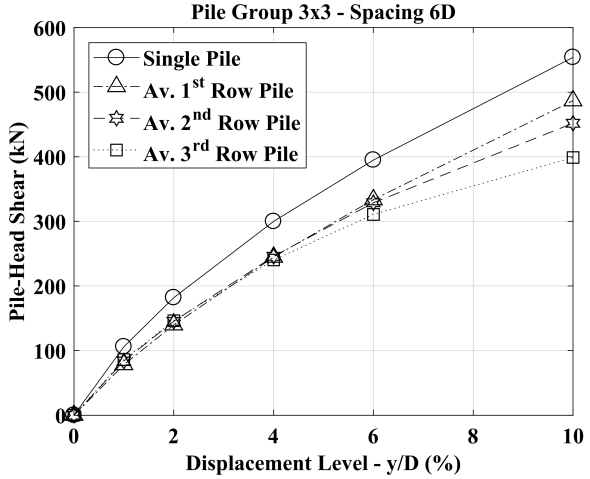

Figure 4.19: 3x3 P.G. $s/D = 6D$: 'Load - Displ. Level' curve for each representative pile

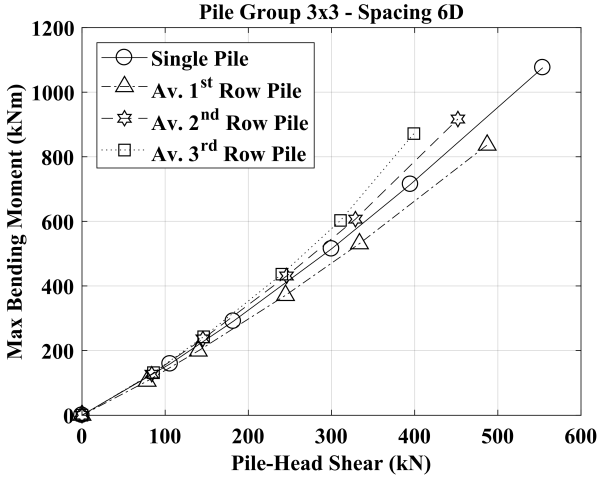

Figure 4.20: 3x3 P.G. $s/D = 6D$: 'Max Moment - Load' curve for each representative pile

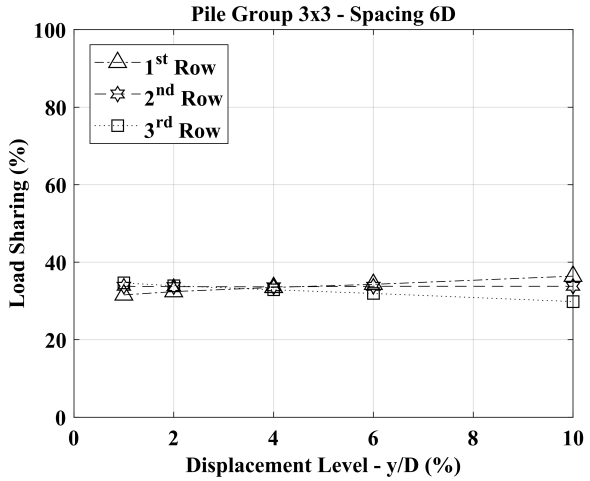

Figure 4.21: 3x3 P.G. $s/D = 6D$: Load Sharing between the rows

Looking at the maximum bending moment-load curves, all the piles behave practically as the single isolated pile.

In Figures 4.22, 4.23 and 4.24 are shown the vertical stress σ_{zz}, the τ_{rel} and the horizontal displacement colormaps, respectively, for a vertical section along the horizontal load direction at a pile-head displacement level, y/D, equal to 4% (2 cm).

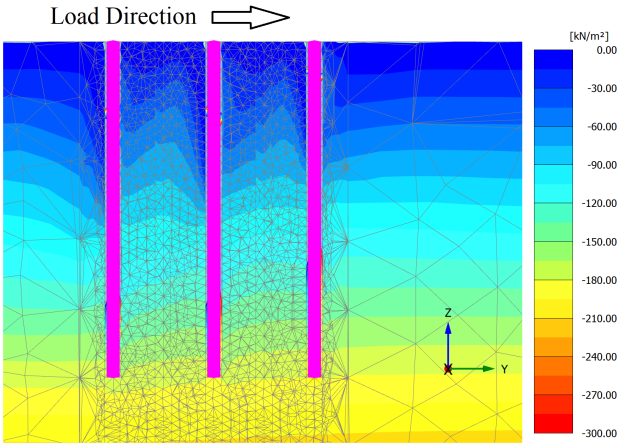

Figure 4.22: 3x3 Pile Group (Spacing = 6D) – Vertical stress σ_{zz}

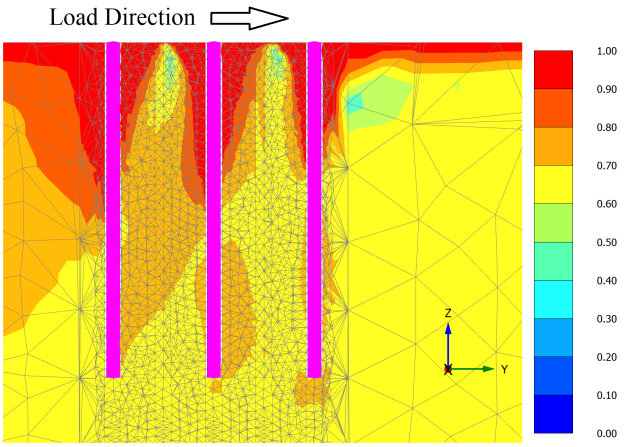

Figure 4.23: 3x3 Pile Group (Spacing = 6D) – τ_{rel}

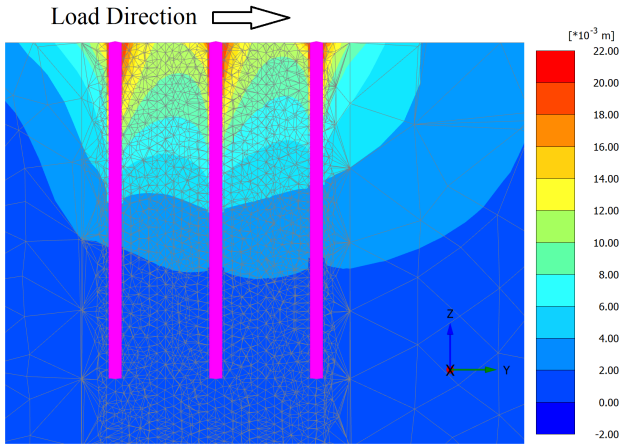

Figure 4.24: 3x3 Pile Group (Spacing = 6D) – Horizontal displacements

4.6 Piled raft analyses under vertical and horizontal loading

The analyses performed on piled-rafts take into account of the influence of a vertical load acting on the raft. The latter, in the Plaxis 3D model, was modelled using a fictitious unit weight value for the raft-concrete material. The vertical load was chosen starting from the bearing capacity of the raft foundation under this loading condition. This value was divided three times, as if it was used a safety factor equal to 3. The vertical load, evaluated as described before, is approximately 15000 kN, and corresponds to a uniform load of (15000 kN) / (7.0 m x 7.0 m) = 306 kPa. The fictitious unit weight value, thus was assumed equal to (306 kPa) / (0.7 m) = 437.3 kN/m^3. The horizontal displacement of the raft was applied after the application of the vertical load, when the soil stress state underneath the raft was completely changed by the vertical load. The lateral displacement sequence was: 0, 5, 10, 20, 30, 50 mm. The piled-raft systems investigated are the following:

- Piled-Raft with a 5x5 pile-group (25 piles) – Spacing = 3D;
- Piled-Raft with a 3x3 pile-group (9 piles) – Spacing = 6D;
- Piled-Raft with a 3x3 pile-group (9 piles) – Spacing = 6D;
- Piled-Raft with a 2x2 pile-group (4 piles) – Spacing = 6D;
- Raft alone.

In the next are described in detail the results obtained for the 3x3 piled raft with a 3x3 pile group and a spacing of 3D and for the piled raft with a 3x3 pile group and a spacing of 6D, in order to compare these results with those described previously for the simple pile groups without the raft and the vertical load.

4.6.1 Piled raft with a 3x3 pile-group (s/D=3)

After the application of the vertical load the average contact pressure at the raft-soil interface was approximately equal to 100 kPa (Figure 4.25). The vertical stress σ_{zz} in a vertical section is shown in Figure 4.26. In this case the raft carries a significant rate of the vertical load. For this reason, it is expected an improvement of the pile-group

performance caused by the increased stress state in the soil surrounding the pile group beneath the raft.

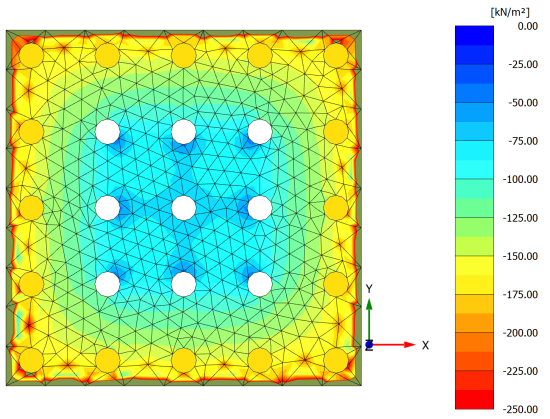

Figure 4.25: Piled Raft with a 3x3 Pile-Group (Spacing = 3D) – Contact pressure at the raft-soil interface after the vertical load application

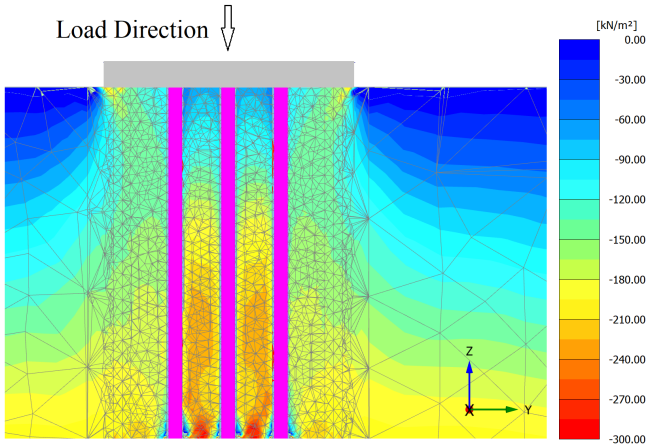

Figure 4.26: Piled Raft with a 3x3 Pile-Group (Spacing = 3D) – Vertical stress σ_{zz} after the vertical load application

In Figure 4.27 and in Figure 4.28 are shown the response of the piled raft system and its components in terms of lateral load - deflection curves and the horizontal load distribution between the pile group and the raft, respectively. In Figure 4.27 are also presented the response of the raft alone (subjected to the total vertical load) and of the simple pile group (where no vertical load was applied).

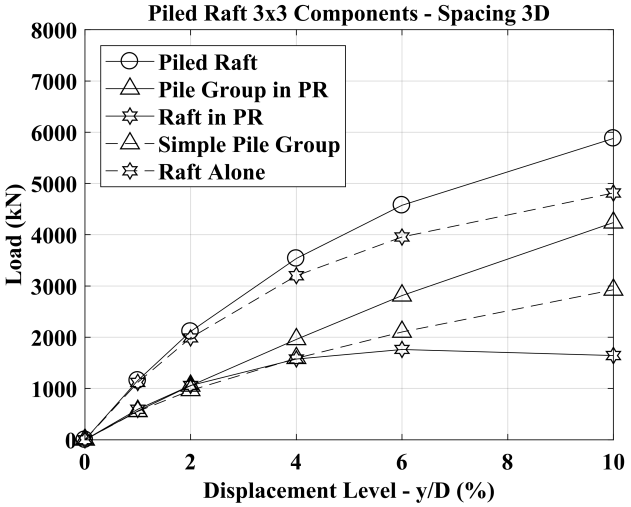

Figure 4.27: Piled-Raft with a 3x3 Pile-Group (Spacing 3D)

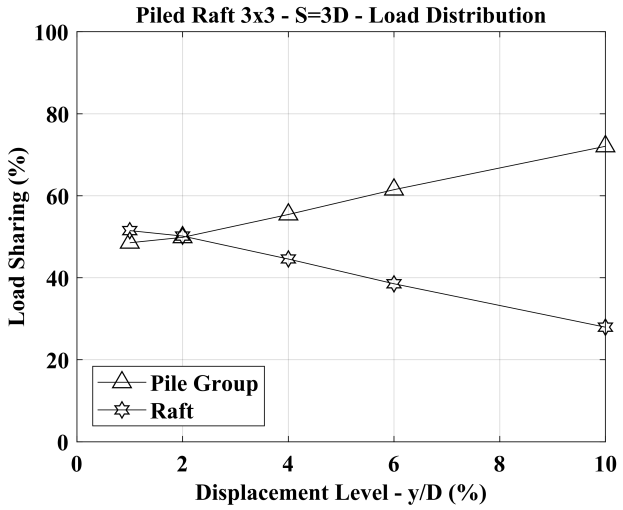

Figure 4.28: Piled Raft with a 3x3 Pile-Group (Spacing 3D) Load sharing between the Pile Group and the Raft

It was noted that the response of the pile rows in the group beneath the raft looks different compared to that in the simple pile group as can be seen looking at the differences between the results in Figure 4.13, Figure 4.14 and Figure 4.15, and those in Figure 4.29, Figure 4.30 and Figure 4.31.

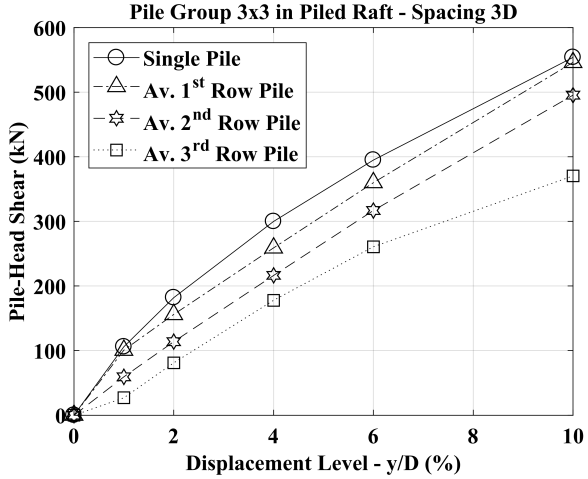

Figure 4.29: 'Load-Displacement Level' curve for each representative pile

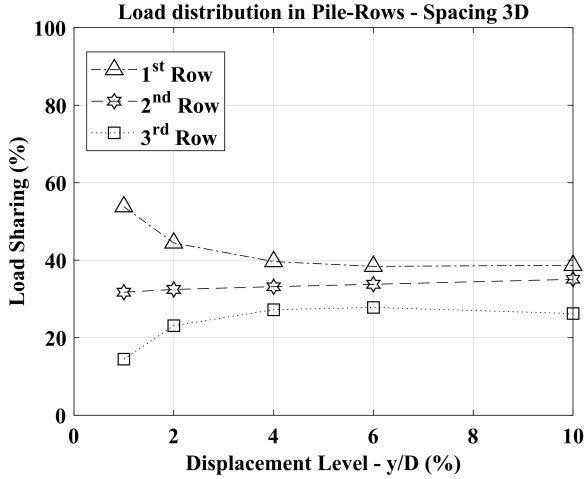

Figure 4.30: Load-Sharing between the rows

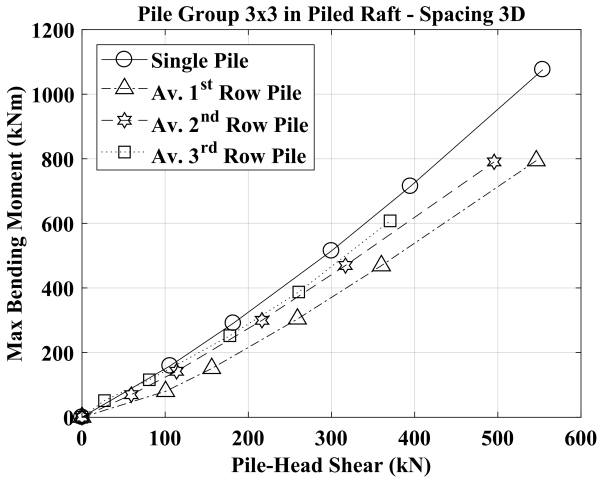

Figure 4.31: 'Max Bending Moment-Load' curve for each representative pile

The load distribution between the pile rows of the pile group in the piled raft is characterized, for small displacement levels, by a higher contribution of the first row compared to the simple pile group case. For higher displacement levels, instead, it was observed a decreasing trend for the loading rate carried by the first row and an increasing trend for the loading rate carried by the 3^{rd} row, while the 2^{nd} row seems to be unaffected by the increase of the displacement level.

Looking at the 'maximum bending moment-horizontal load' curves, it's important to note that the piles in the group in the piled raft system are subjected to bending moments lower than the analogous piles in the simple pile group, for a same value of the horizontal load.

The contact pressure distribution at the raft-soil interface (Figures 4.25 and 4.32) and the vertical stresses beneath the raft (Figures 4.26 and 4.33), can explain the load distribution between the pile rows. In fact, it was observed a significant increase of the stress state of the soil beneath the raft, especially in front of the 1^{st} pile row. For this reason the stiffness and resistance of this soil volume was increased.

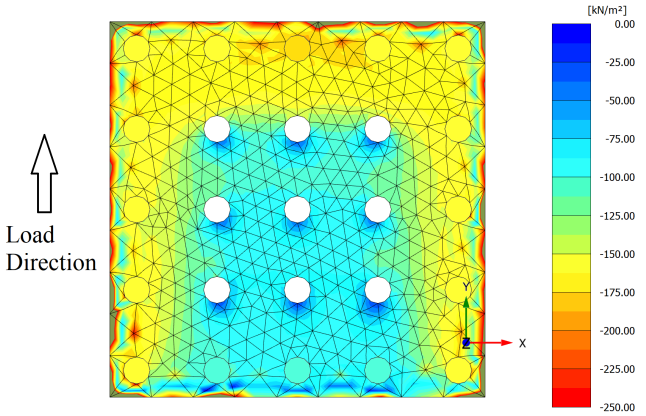

Figure 4.32: Piled Raft with a 3x3 Pile-Group (Spacing = 3D) – Contact pressure at the raft-soil interface at a piled raft horizontal displacemement level y/D = 4% (2 cm)

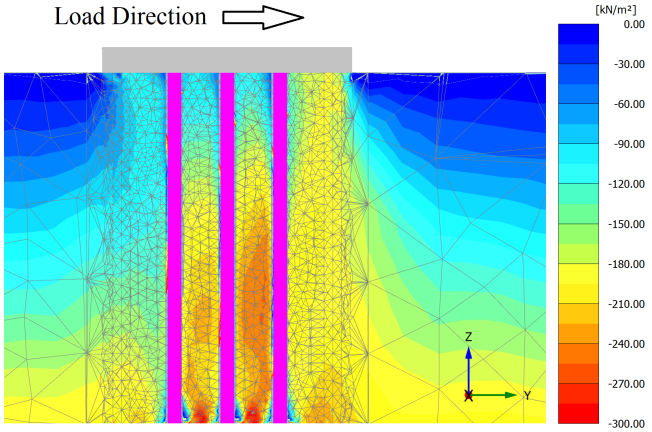

Figure 4.33: Piled Raft with a 3x3 Pile-Group (Spacing = 3D) – Vertical stress σ_{zz} at a piled raft horizontal displacemement level y/D = 4% (2 cm)

The results of this analysis show that, with this layout, the piled raft has a better response compared to the raft alone. The raft can mobilize a significant resistance, while the pile group beneath the raft has an improved overall response compared to the simple one. Moreover, the increase of the soil stress state and stiffness beneath the raft leads to a reduction of the maximum bending moments in the piles.

In Figures 4.34 and 4.35 are shown the horizontal displacements and the vertical displacements, respectively, for a vertical section along the horizontal load direction at a piled raft displacement level, y/D, equal to 4% (2 cm).

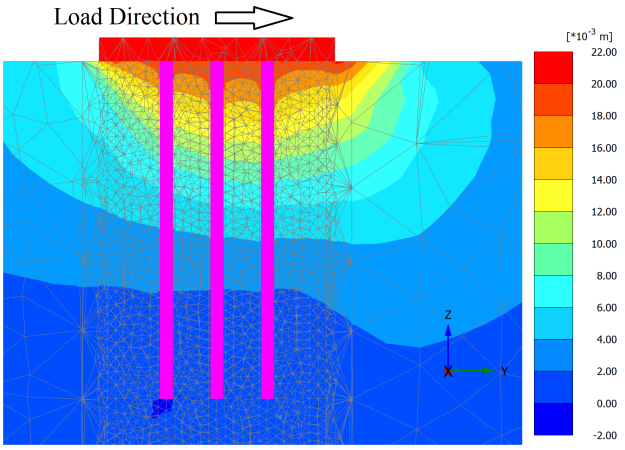

Figure 4.34: Piled Raft with a 3x3 Pile-Group (Spacing = 3D) – Horizontal displacements at a piled raft horizontal displacemement level y/D = 4% (2 cm)

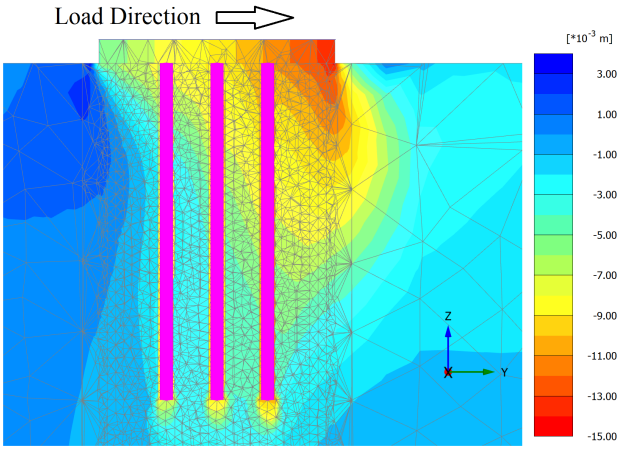

Figure 4.35: Piled Raft with a 3x3 Pile-Group (Spacing = 3D) – Vertical displacements at a piled raft horizontal displacemement level y/D = 4% (2 cm)

4.6.2 Piled raft with a 3x3 pile-group (s/D=6)

After the application of the vertical load the average contact pressure at the raft-soil interface was approximately equal to 140 kPa (Figure 4.36). The vertical stress σ_{zz} in a vertical section is shown in Figure 4.37. The raft carries a significant rate of the vertical load. Again, it is expected an improvement of the pile-group performance caused by the increased stress state in the soil surrounding the pile group beneath

the raft. Nevertheless, this improvement is reduced, compared to the previous case studied.

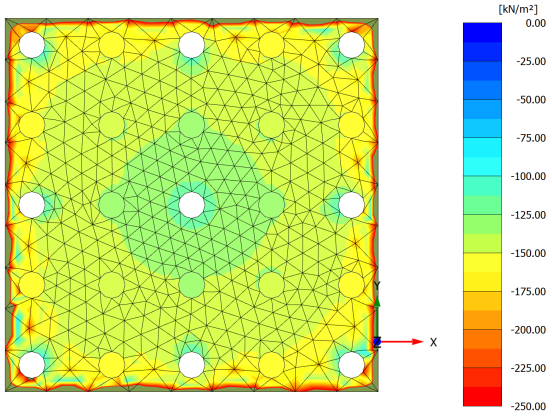

Figure 4.36: Piled Raft with a 3x3 Pile-Group (Spacing = 6D) – Contact pressure at the raft-soil interface after the vertical load application

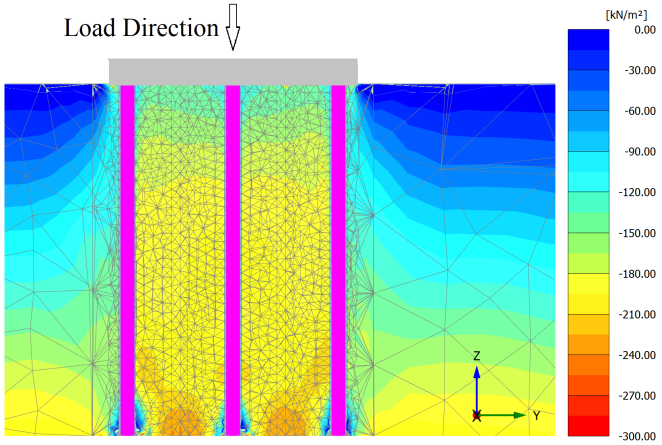

Figure 4.37: Piled Raft with a 3x3 Pile-Group (Spacing = 6D) – Vertical stress σ_{zz} after the vertical load application

In Figure 4.38 and in Figure 4.39 are shown the response of the piled raft system and its components in terms of lateral load - deflection curves and the horizontal load distribution between the pile group and the raft, respectively. In Figure 4.38 are also presented the response of the raft alone (subjected to the total vertical load) and of the simple pile group (where no vertical load was applied).

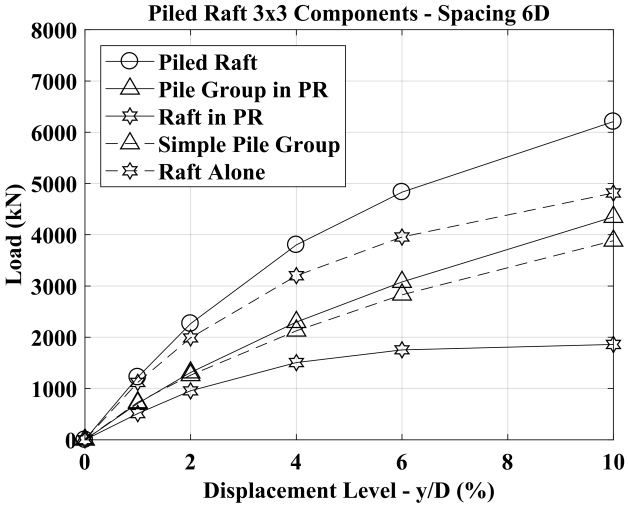

Figure 4.38: Piled-Raft with a 3x3 Pile-Group (Spacing 6D)

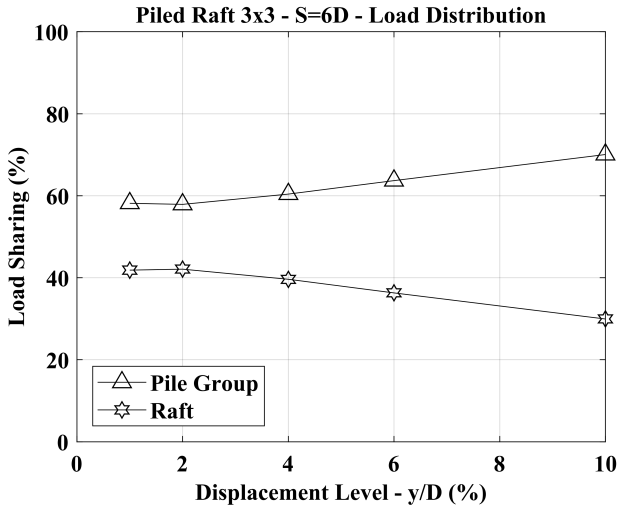

Figure 4.39: Piled Raft (3x3) Load sharing between the Pile Group and the Raft

It was observed that the response of the pile rows in the group beneath the raft looks different compared to that in the simple pile group as can be seen looking at the differences between the results in Figure 4.19, Figure 4.20 and Figure 4.21 and those in Figure 4.40, Figure 4.41 and Figure 4.42.

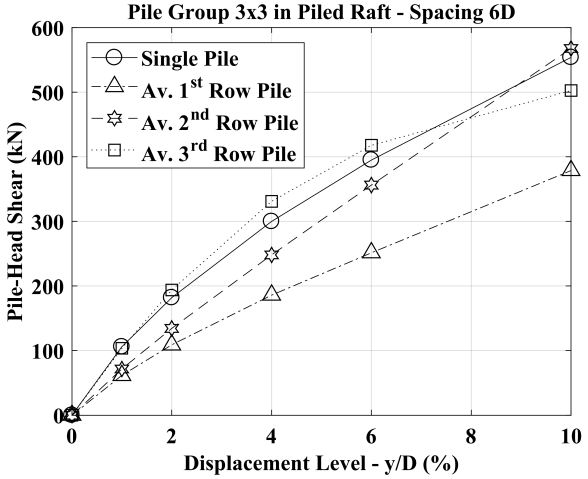

Figure 4.40: 'Load-Displacement Level' curve for each representative pile

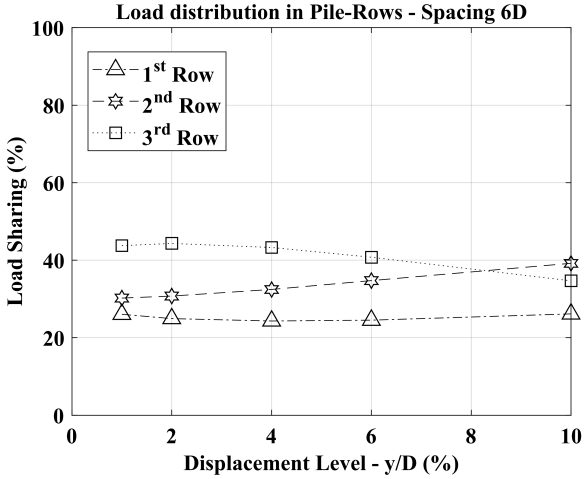

Figure 4.41: Load-Sharing between the rows

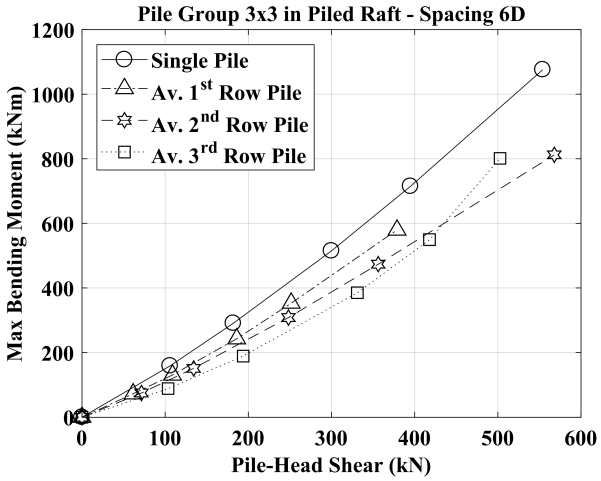

Figure 4.42: 'Max Bending Moment-Load' curve for each representative pile

The load distribution between the pile rows of the pile group in the piled raft is characterized for small displacement levels by a higher contribution of the rear row. For higher displacement levels, instead, it was observed a decreasing trend for the loading rate carried by the rear row and an increasing trend for the loading rate carried by the middle row, while the first row carried the same loading rate at each displacement level.

Looking at the 'maximum bending moment-horizontal load' curves, the piles in the group in the piled raft system are subjected to bending moments lower than the single pile, for the same value of the horizontal load.

The contact pressure distribution at the raft-soil interface (Figures 4.36 and 4.43) and the vertical stresses beneath the raft (Figures 4.37 and 4.44), can explain the load distribution between the pile rows. It was observed a significant increase of the stress state of the soil beneath the raft. However, compared to previous case, the increase of the vertical stress is low in the soil volume in front of the 1^{st} pile-row, while is high for the soil volume in front of the other two rows. This is due to the piled-raft layout, in fact, the 1^{st} pile-row is placed close to the edge of the raft.

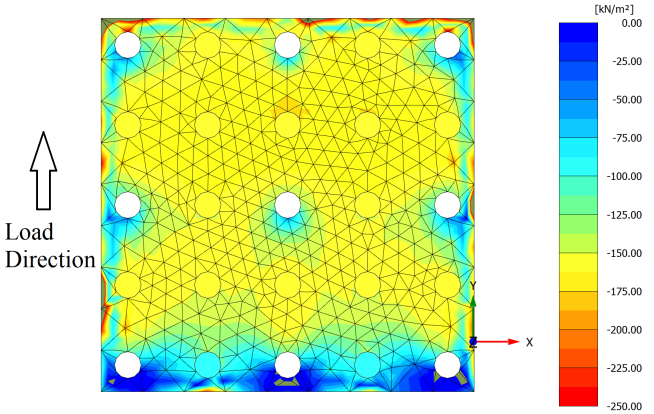

Figure 4.43: Piled Raft with a 3x3 Pile-Group (Spacing = 6D) – Contact pressure at the raft-soil interface at a piled raft horizontal displacemement level y/D = 4% (2 cm)

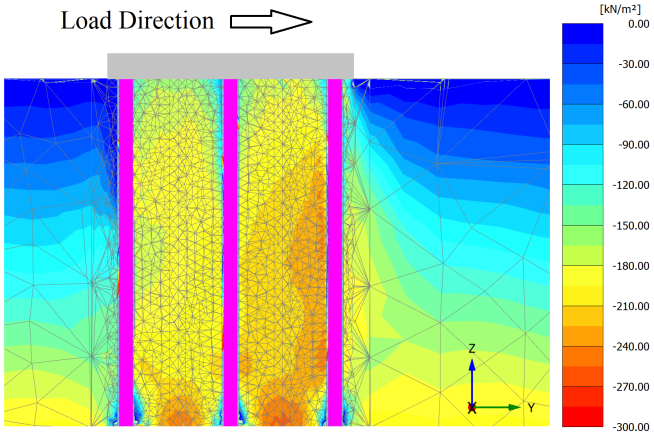

Figure 4.44: Piled Raft with a 3x3 Pile-Group (Spacing = 6D) – Vertical stress σ_{zz} at a piled raft horizontal displacemement level y/D = 4% (2 cm)

The results of this analysis show that the piled raft has a better response compared to the raft alone. Neverthless, the pile group beneath the raft has an overall response similar to the simple pile group.

In Figures 4.45 and 4.46 are shown the horizontal displacements and the vertical displacements, respectively, for a vertical section along the horizontal load direction at a piled raft displacement level, y/D, equal to 4% (2 cm).

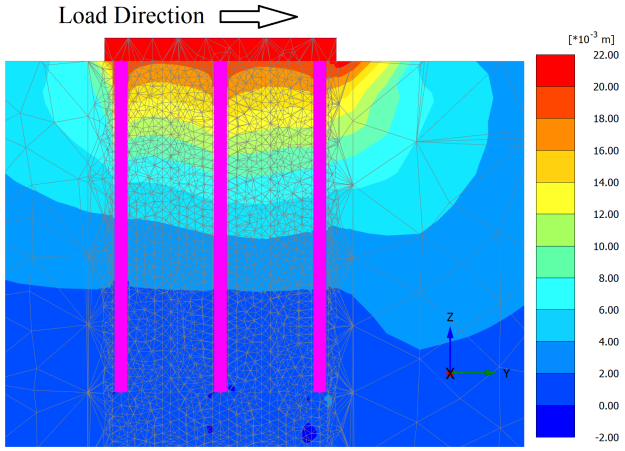

Figure 4.45: Piled Raft with a 3x3 Pile-Group (Spacing = 6D) – Horizontal displacements at a piled raft horizontal displacemement level y/D = 4% (2 cm)

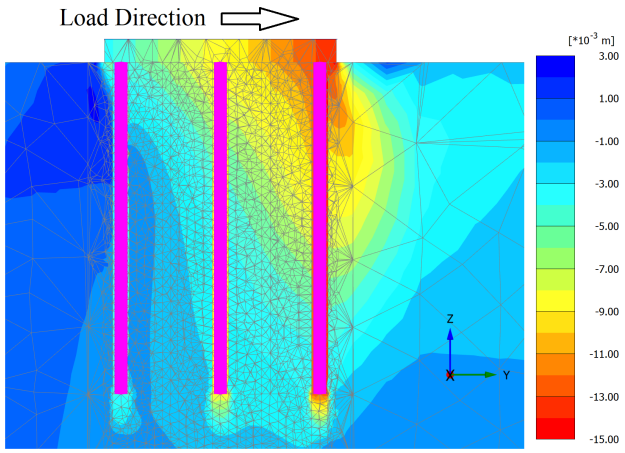

Figure 4.46: Piled Raft with a 3x3 Pile-Group (Spacing = 6D) – Vertical displacements at a piled raft horizontal displacemement level y/D = 4% (2 cm)

4.6.3 Piled-rafts and components responses

In Figures 4.47, Figure 4.48 and 4.49 are shown for comparison, all the load-displacement curves of the piled-raft systems, of the rafts in the piled-rafts and of the pile-groups in the piled-rafts analysed, respectively. In Figure 4.49 are shown, also, for comparison the results of the analogous simple pile-groups. It was observed, in general, that the global response of the simple pile-groups is very close to that of the pile-groups in piled-raft systems. Only few improvements in the performance were noted.

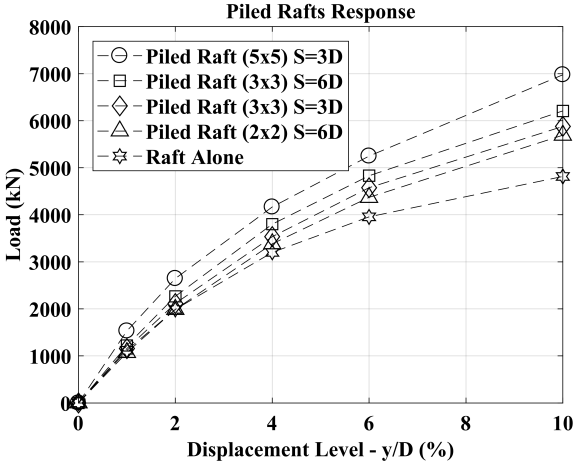

Figure 4.47: Piled-Raft Response – 'Load-Displ. Level Curve' – Vertical Load = 15 MN

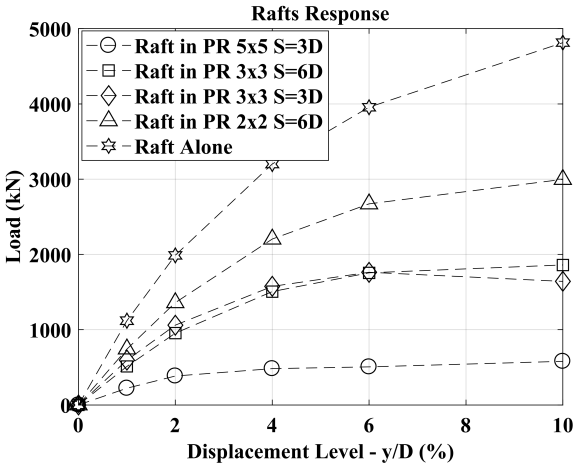

Figure 4.48: Raft Response – 'Load-Displ. Level Curve' – Vertical Load = 15 MN

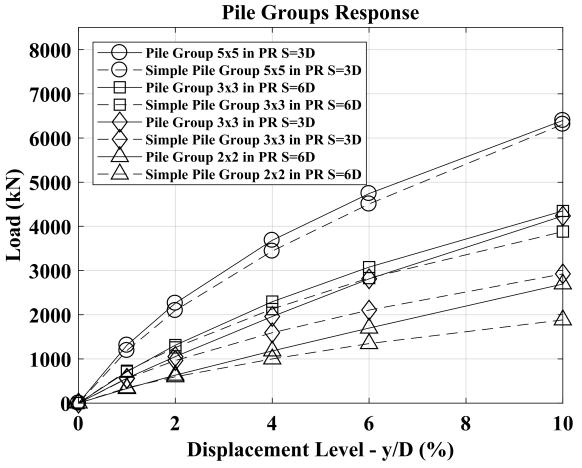

Figure 4.49: Pile Group Response – 'Load-Displ. Level Curve' – Vertical Load = 15 MN and Vertical Load = 0 kN

4.7 Remarks on the numerical experiments

In this section all the analysis results (on piled-rafts) are compared. In Figure 4.50 and Figure 4.51 the simple pile groups and the pile groups in piled raft efficiencies (defined as $H_{group}/(nH_{single})$) are plotted against the displacement level y/D. Where H_{group} is the load carried by the pile group for a given displacement level, n is the number of piles in the group and H_{single} is the load carried by a single isolated pile at the same displacement level.

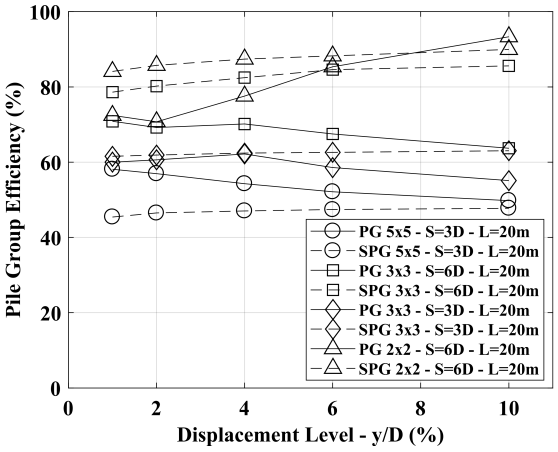

Figure 4.50: Pile groups efficiencies against the displacement level (Pile length = 20 m)

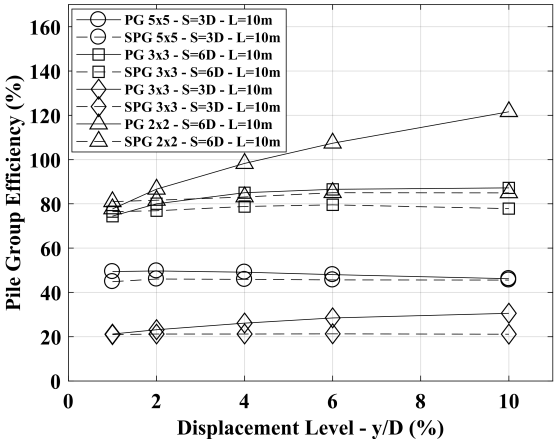

Figure 4.51: Pile groups efficiencies against the displacement level (Pile length = 10 m)

In Figure 4.52 the piled raft efficiencies (defined as H_{PR}/H_R) are plotted against the displacement level y/D. Where H_{PR} is the load carried by the piled raft for a given displacement level, and H_R is the load carried by the raft alone at the same displacement level.

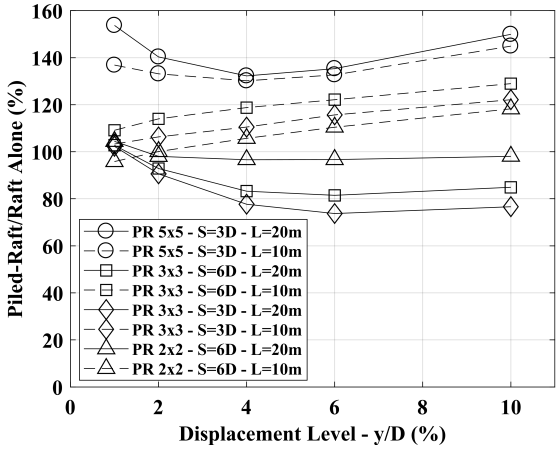

Figure 4.52: Piled raft efficiencies against the displacement level

Looking at the results, the following considerations can be drawn:

- not always the efficiency of the piled raft (defined as the ratio between the horizontal load carried by the piled raft and the load carried by the raft alone at a given displacement level and subjected to the same vertical load (=15 MN)) is bigger than that of the raft alone. It was noted that the piled raft efficiency is higher when the piles in the pile-group have a length of 10 m compared to the same piled-raft system with a pile length equal to 20 m. When the piles are shorter a bigger vertical load rate is transferred by the raft directly to the soil beneath the raft. In this case the raft can contribute in a better way to the overall lateral response. However, if the raft carries a bigger rate of the vertical load even the vertical settlement of the foundation increases. In order to define the best design solution, in terms of performance and costs, it is necessary to find the solution that can reduce properly the settlement (to guarantee the requirements of the superstructure) and that can improve the performance as much as possible under lateral loads;

- the efficiency factor of the pile group in the piled-raft and the efficiency factor of the simple pile group (no raft in contact with the ground and no vertical load applied) are basically the same for the soil condition and piled-raft layouts studied in this work;

- the percentage of the horizontal load carried by the raft decreases with the increase of the lateral displacement, while the vertical load distribution between the raft and the piles remains, basically, unchanged during the lateral load phases. Increasing the horizontal load, the front pile rows are subjected to an increase of the axial load while the rear rows to a decrease because the raft starts to rotate;

- when the contact pressure between the raft and the soil is small, the pile group response in the piled-raft and the load distribution between the pile rows is basically the same as observed in the simple pile group case. The well-known shadowing effect affects the pile group behaviour;

- when the contact pressure between the raft and the soil is high, the pile group response in the piled-raft and the load distribution between the pile rows can be in some cases completely different compared to that observed in the simple pile

group case. The pile rows located at the rear of the foundation can sometimes carry a bigger horizontal load rate compared to the front pile row. This result can be justified, as observed in this work and in the work of Katzenbach and Turek (2005), by the increase of stresses and stiffness in the soil beneath the raft (the highest increase occurred beneath the center of the raft), due to the high vertical load transferred by the raft. Moreover, for a given horizontal load applied at the pile-head, the maximum bending moment is less than that observed in the single isolated pile;

- almost always, the piled raft systems have a slightly lower initial lateral stiffness and lateral resistance (at the same displacement level) compared to the sum of the raft alone and the simple pile group responses (note: raft alone analyses were performed using vertical loads able to reproduce the average contact pressures between the raft and the soil like in the piled-raft systems; simple pile group analyses were realized without the vertical load).

Chapter 5

Analysis methods developed

5.1 Introduction to BEM-methods for pile foundation applications

Continuous elastic approaches model the soil as an elastic half-space, identified by E (Young's modulus) and ν (Poisson's ratio). The analysis methods based on the elastic theory have the quality, despite the Winkler model approach, to represent the soil as a continuum. This property is basically useful when the study is extended to the pile-group case.

The elastic continuous models presented, here, are solved with the boundary element method (BEM); adopting this method to study the pile-soil system is sufficient to discretize only the interfaces of all the elements. The methodological approach that distinguishes the application of the boundary element method is the following: the element object of study (in this case, the pile-foundation embedded within the soil and subjected to an external action) is divided into a certain number of elements, considered appropriate to describe the problem with an acceptable approximation; the solution equation system is obtained imposing the compatibility between the pile-elements displacements and the soil-movements, the overall equilibrium and the boundary conditions. The Green's function used in this work, to study the pile-soil interaction problem, is the Mindlin's equation (Appendix). This function, that defines the displacement at a point of an elastic half-space caused by a point-load acting within the same half-space, has to be integrated in an appropriate way on the pile surface.

5.2 Single pile analysis: 'Hybrid BEM-py curves' method

This is the first part of a more extensive work on the development of an analysis method to study combined piled raft foundations under lateral load. A hybrid method BEM - py curves approach has been developed for the analysis of single pile with free or fixed head restraint conditions. The proposed method includes:

- the non-linear behaviour of the soil by p-y curves, which describe the near field soil response, located in series to a multi-layered elastic half-space, which represents the far field soil response;
- the non linear response of reinforced concrete pile sections, also taking into account the influence of tension stiffening;
- the influence of suction by increasing the stiffness of shallow portions of soil. This effect is modelled using the Modified Kovacs Model.

The hybrid BEM - py curves method saves computational effort compared to more sophisticated FEM codes and provides reliable results using input data from a standard site investigation. The reliability of this simplified method was verified by comparing results from data from full scale and centrifuge tests on single piles (in Chapter 6).

5.2.1 Pile modelling

The proposed method was developed to capture the response of a single pile subjected to horizontal load. It consists of a Hybrid BEM - py curves approach. The analysis is performed using a non-linear incremental tangent method. The pile is modelled as a vertical strip, geometrically defined by the outer diameter D and the length L of the actual pile, discretized in 60 blocks of variable length with depth (Figure 5.1).

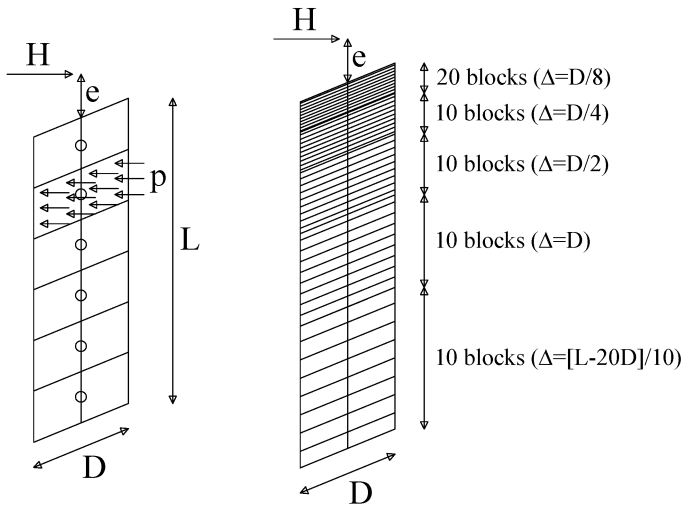

Figure 5.1: Pile discretization (Landi, 2006)

With this kind of discretization, it is possible to minimize the calculation-time. Neverthless, the accuracy of the solution is guaranteed by the thinner dimension of the blocks, in which the pile is discretized, in the upper part of the problem domain.

The definition of the discretization criterion was suggested by Landi (2006) on the basis of results obtained with a parametric study on a free-to-rotate single pile embedded in a homogeneous and isotropic elastic half-space.

In such condition the solution of the problem can be expressed in the following dimensionless form, for the displacement at the pile head:

$$\frac{yE_sD}{H} = f(\frac{L}{D}, \frac{e}{D}, \frac{E_p}{E_s}, \nu_s) \tag{5.1}$$

similarly, for the maximum bending moment along the pile shaft:

$$\frac{M_{max}}{HD} = f(\frac{L}{D}, \frac{e}{D}, \frac{E_p}{E_s}, \nu_s) \tag{5.2}$$

These expressions are obtained assuming as independent mechanical properties: the pile diameter D and the elastic modulus E_s of the elastic half-space. The numerical solution of the boundary problem depends on the discretization method adopted.

Adopting a homogeneous discretization with depth when the number of blocks (n) gradually increases, the solution becomes increasingly accurate, reaching an n^* value

beyond which the solution remains unchanged. The parametric study (Landi, 2006) showed that by decreasing the pile-soil relative stiffness $K = E_p/E_s$ the dependence of the response on the number of blocks starts to increase. Using an n^* value equal to 60 leads to an error (the error can be evaluated comparing this solution against that obtained with a theoretically infinite number of blocks) that varies as a function of the relative stiffness $K = E_p/E_s$: for K = 10^1, 10^2, 10^3, 10^4 the error is 20%, 10%, 5%, 2% respectively, in the evaluation of the pile-head deflection and the maximum bending moment.

Evangelista and Evangelista (1976) have shown the usefulness of a non homogeneous pile discretization. Since the displacements are mainly localized up to depth corresponding to 10-15 pile diameters, a suitable discretization is when the element height is sufficiently small for depths close to the ground surface.

On the basis of these observations, Landi (2006) introduced the discretization shown in 5.1, and in this case for K = 10^1, 10^2, 10^3, 10^4 the error was 8%, 7%, 4%, 2% respectively, in the prediction of the pile-head deflection. For the maximum moment along the pile shaft, the error was 8%, 5%, 2.5%, 1% respectively.

The resulting discretization is the following (5.1):

- 20 blocks with a thickness $\Delta = D/8$, starting from the ground level up to a depth of $2.5D$;
- 10 blocks with a thickness $\Delta = D/4$, starting from a depth of $2.5D$ up to a depth of $5D$;
- 10 blocks with a thickness $\Delta = D/2$, starting from a depth of $5D$ up to a depth of $10D$;
- 10 blocks with a thickness $\Delta = D$, starting from a depth of $10D$ up to a depth of $20D$;
- 10 blocks with a thickness $\Delta = (L - 20D)/10$, starting from a depth of $20D$ up to the pile base depth;

This type of discretization remains unchanged even for a pile with a reduced slenderness ($L/D < 20$). In such case, the total number of blocks is automatically reduced. If the horizontal load is applied with an eccentricity, the program inserts an additional block to the pile head, whose height is equal to the load eccentricity.

Pile flexibility matrix definition

The pile flexibility matrix, in case of a linear elastic behaviour of the pile, is obtained using the elastic beam theory, and each coefficient of this matrix can be expressed using the following expression (Figure 5.2).

$$\begin{aligned} &if\ z_i < z_j \\ &a_{ij} = (z_i^3)/(3E_pI_p) + (z_i^2(z_j - z_i))/(2E_pI_p) \\ &if\ z_i \geq z_j \\ &a_{ij} = (z_j^3)/(3E_pI_p) + (z_j^2(z_i - z_j))/(2E_pI_p) \end{aligned} \tag{5.3}$$

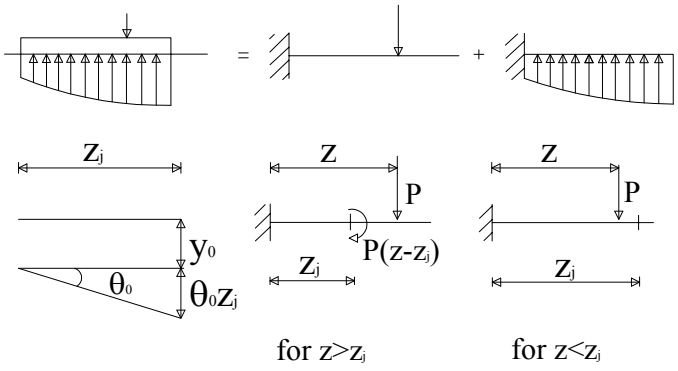

Figure 5.2: Pile flexibility matrix using the elastic beam theory (auxiliary restraint method)

In this way, the horizontal displacement of each pile-block assumes the expression as in Eq. 5.4.

$$y_i = -\sum_{j=1}^{n} a_{ij} P_j + y_0 + \theta_0 z_i \tag{5.4}$$

in which P_j represents the load applied at the generic pile-block j (located at the depth z_j), and y_0 and θ_0 are the unknown displacement and rotation at the pile-head. Obviously if the pile-head is fixed, the rotation becomes a known term. Each pile-point displacement is a function of $n + 2$ (or $n + 1$, for fixed condition) unknowns, n pile-soil interface pressures, y_0 and θ_0.

The proposed method analyses both steel-pipe and reinforced concrete piles. For the analysis of steel piles, the flexural rigidity $E_p I_p$ is assumed to be constant (which means hypothesizing a linear-elastic behaviour of the section until the ultimate bending moment occurs).

For reinforced concrete sections, the development of cracks, even at low values of the bending moment, requires a different modelling of the pile response. For this material, in fact, it is also necessary to know the mechanical properties of both the concrete and steel, the number of longitudinal bars, and the spacing of the transverse reinforcement. These data provides the basis for the moment-curvature relationship (for each axial load value) for the reinforced concrete cross-section.

The 'moment-curvature-axial load' relationship is obtained by imposing the equilibrium equations to the translation and rotation at the geometric center of gravity of the section, varying the curvature and the deformation at the most compressed fiber in the section. This model has the additional feature of taking the influence of tension stiffening into account (Morelli et al., 2017). This model has been realized in the context of this PhD thesis with the cooperation of researchers and Professors of the Department of Civil and Industrial Enginnering of the University of Pisa.

The main assumptions of the tension stiffening model are:

- the conservation of planar sections;
- concrete tension strength equal to zero for cracked sections;
- perfect bonding between steel bars and surrounding concrete;
- the constitutive model proposed by Mander, Priestley, and Park (1988) for confined concrete in compression;

- the constitutive model proposed by Popovics (1973) for unconfined concrete in compression;
- the constitutive model proposed by Ceb-Fip (1993) for concrete in tension;
- a simple strain-hardening model or a bilinear model for steel reinforcement;
- a bond-slip law as suggested by Sigrist (1995);
- the tension stiffening is considered using a variable elastic modulus for the concrete in tension along a pile-block between two consecuttive cracks;
- the crack spacing can be estimated using the expression suggested by the CEB-FIP (1993);
- no other secondary cracks develop between two consecutive cracks.

Using these assumptions, the 'average moment-curvature' relationship for a representative pile-section can be estimated as the weighted average of the moment-curvature relationships computed in the middle, at a quarter, at three quarters and at the cracked section of a block between two cracks.

Details about this model will be presented in the next paragraph. Once the average moment-curvature relationship has been obtained, the coefficients of the pile flexibility matrix need to be defined using the Eq. 5.5 for the reinforced concrete pile, which is modelled in this case as a step-tapered beam with a variable flexural rigidity, E_pI_p, along the pile shaft. In Eq. 5.5, the variation of both E_p and I_p along the shaft is fully considered changing the moment of inertia, I_p, of the section, while E_p is kept constant. Consequently, in an incremental analysis, the pile flexibility matrix needs to be updated at each load increment.

$$\begin{aligned} a_{ij} = \sum_{1}^{i-1} k[(&\frac{(l_k - l_{k-1})^3}{3E_pI_k} + \frac{(z_j - l_k)(l_k - l_{k-1})^2}{2E_pI_k})+ \\ &(\frac{(l_k - l_{k-1})^2}{2E_pI_k} + \frac{(z_j - l_k)(l_k - l_{k-1})}{E_pI_k})(z_i - l_k)] \\ &+ (\frac{(z_i - l_{i-1})^3}{3E_pI_i} + \frac{(z_j - z_i)(z_i - l_{i-1})^2}{2E_pI_i}) \end{aligned} \tag{5.5}$$

In Eq. 5.5, z_i and z_j represent respectively, the distance between the fixed node in Figure 5.2 and the point along the beam in which the displacement is considered and the distance between the same fixed node and the point where the load is applied. On the other hand, l_k, represents the distance between the fixed node and the lower part of block k, and E_pI_k is the flexural rigidity of the block k.

Reinforced concrete sections: considering the influence of the tension stiffening

Introduction

Reinforced concrete elements are characterized, even for low force values, by a non-linear behaviour mainly due to the stress-strain relationship of the two forming materials: concrete and steel. The exact modelling of such behaviour can prove to be a very hard issue and, for this reason, several simplifications are usually adopted in order to take into account only the most important non-linear aspects affecting the particular studied problem.

However, it can be recognized that, among all the non-linearity sources, the most influencing and also the one that originally gave birth to the idea of the composite material 'reinforced concrete' is the low, in most cases negligible, tensile strength of the concrete. If it does not influence so much the ultimate resistance of a reinforced concrete element, on the other hand it can modify its stiffness also for high value of the external force due the 'tension stiffening'. The tension stiffening can be defined as the phenomenon leading to an increasing of the stiffness of the concrete section due to the transmission of stresses from the reinforcing bar to the boundary concrete in tension between two adjacent cracks, see Figure 5.3.

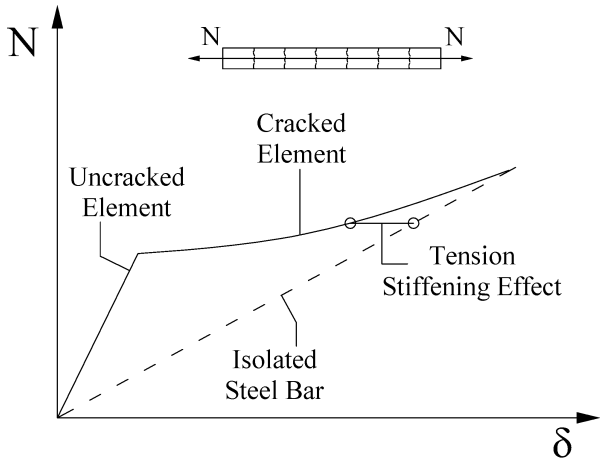

Figure 5.3: Effect of the tension stiffening on an isolated reinforcing bar

The way of modelling this phenomenon is, up to date, codified by different standards and several researches have been done in the last decade on this topic. Eurocode 2 (EC2-1, 2005) and CEB-fib Model Code 2010 consider the tension stiffening in terms of strain, curvature or deflection, interpolating the computed parameter evaluated on the uncracked section and on the fully cracked one adopting the following expressions.

$$\alpha = \zeta\alpha_2 + (1-\zeta)\alpha_1 \tag{5.6}$$

$$\zeta = 1 - \beta(\frac{\sigma_{SF}}{\sigma_s}) \tag{5.7}$$

where α is the mean value of the parameter of interest (strain, curvature or deflection) of the element segment comprised between two consecutive cracks; α_1 and α_2 are the corresponding values computed in the uncracked and fully cracked section respectively; ζ is the distribution coefficient, β is a factor that takes into account long term effects (β=1.0 for short term effects, β=0.5 for sustained loads or many cycles of repeated loading); σ_s is the stress in the reinforcement in tension calculated on a cracked section while σ_{SF} is the evaluated under the loading conditions causing first cracking. Eurocode 2 (EC2-1, 2005) proposes also an expression for the evaluation of the cracks interaxis mean value, s_{rm}:

$$s_{rm} = 50 + 0.25K_1K_2\frac{\Phi_s}{\rho_{p,eff}} \tag{5.8}$$

where:

- Φ_s is the mean value of the reinforcing bars diameter;
- K_1 is a coefficient that takes into account the bond properties of bond reinforcement;
- K_2 is a coefficient that takes into account the distribution of strain (pure tension or bending);
- $\rho_{p,eff} = A_{st}/A_{ct}$ is the effective reinforcement ratio evaluated as the ratio between the area of the reinforcing bars, A_{st}, contained within the concrete cross section portion effectively influenced by the bars in the formation of cracks.

The effects of tension stiffening on the flexural behaviour of r.c. elements are considered in many other studies. Salvatore et al. (2007) studied its effect on the flexural behaviour, with particular attention to the ductility evaluation, of rectangular concrete sections reinforced with special, dual-phase (Maffei, Salvatore, and Valentini, 2007), steel bars.

Stramandinoli and La Rovere (2008) developed a model in which the tensile stress strain curve of concrete displays an exponential decay in the post-cracking range, defined by a parameter that depends on the reinforcement ratio and on the steel-to-concrete modular ratio. The numerical results obtained by the model show good agreement with several experimental results on simply supported beams with rectangular cross sections tested under 4-point bending.

Lee, Cho, and Vecchio (2011) presented a tension stiffening model able to calculate average tensile stresses in concrete after yielding of reinforcement in r.c. elements subjected to uniaxial tension, shear or flexure.

Kaklauskas, Gribniak, and Bacinskas (2009) studied the effects of the shrinkage on the tension stiffening on rectangular sections with symmetrically or asymmetrically reinforcement, providing free-of-shrinkage tension stiffening relationships.

An important aspect to consider in the study of the tension stiffening phenomenon is the definition of the 'effective area', defined as the portion of concrete surrounding the reinforcing bar involved in the transmission of stresses from the bar to the concrete itself.

Eurocode 2 defines the effective area only for typical rectangular sections as the area having the same width of the section and a height $h_{c,eff}$ equal to the minimum between $2.5(h-d)$, $((h-x))/3$ or $h/2$, where the meaning of the symbols is well explained by Figure 5.4.

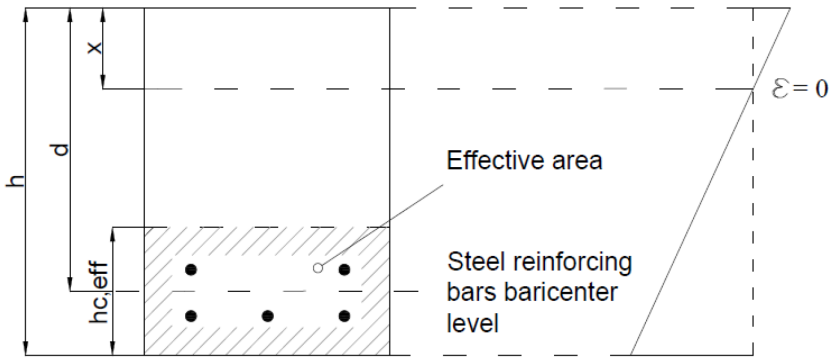

Figure 5.4: Effective area for rectangular section defined by Eurocode 2

CEB-fib Model Code 2010 suggests similar values, stating that, in the absence of a more refined model, the effective concrete area in tension can be assessed as $2.5(h - d) < ((h - x))/3$.

Several authors proposed different expressions for the evaluation of the effective area. Manfredi and Pecce (1998) proposed a refined fiber model for the analysis of r.c. beams that include an explicit formulation of bond–slip relationship in which employ an effective area around the reinforcement that occupies the whole width of the section and has a height $h_{c,eff} = (c + 8.5\phi)$, with c being the concrete cover and ϕ the reinforcing bar diameter.

Kwak and Song (2002) in their study on an analytical model, which can simulate the post-cracking behaviour and tension stiffening effect in a r.c. tension member, proposed that the effective area of concrete in tension can be represented by, $A_{c,eff} \cong 1/4(1 + n\rho)bh$ with b and h the width and height of the section respectively, $n = E_s/E_c$ and ρ the ratio of steel reinforcement (A_s/bh).

Castel, Vidal, and François (2007) came up with the following expression for $A_{c,eff}$ which is based on a multi-linear stress profile in the full depth of the concrete section between the flexural cracks. The meaning of the symbols is explained in Figure 5.5.

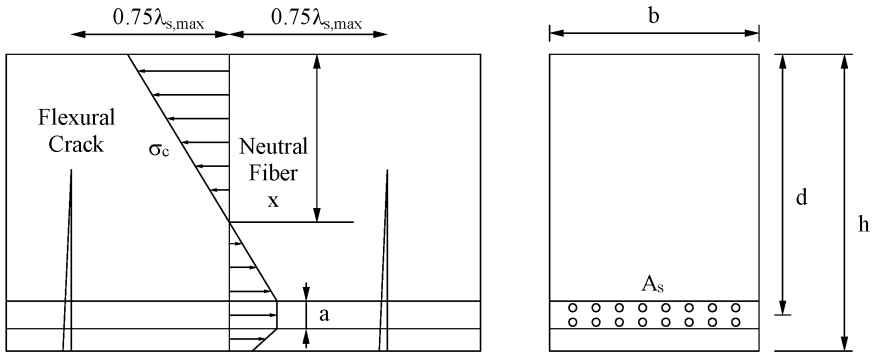

Figure 5.5: Model of stress distribution in the concrete and effective area of concrete in tension proposed by Castel et al. (2007)

$$A_{ct,eff} = \frac{b(d - x - a/2)}{2} + ba + b(h - d - a/2)[1 - \frac{b(h - d - a/2)}{2(d - x - a/2)}] - A_s \qquad (5.9)$$

All of these works deals with the definition of the effective area on rectangular r.c. section. Very few works have been done on circular sections, even if they represent important elements in the field of r.c. construction. It is in fact sufficient to think about the bridge piers or pile foundations that are, often the former and practically always the latter, realized with circular sections. Wiese et al. supply an expression for the determination of the effective area of symmetrically reinforced circular section idealizing the reinforcement as a continuous ring.

Carbonell-Marquez et al. (2014) presented a definition of the effective area in circular cross sections for both symmetric and asymmetric layout and demonstrate the validity of the proposed expression comparing it with the experimental results on r.c. members subjected to pure flexure.

Mondal and Prakash (2015) propose an improved analytical model for r.c. circular columns under combined axial-torsional load conditions demonstrating that neglecting tension stiffening can lower sensibly the accuracy of numerical/analytical models in predicting test data.

The influence of tension stiffening on the global behaviour of elements with circular cross section and subjected to the combined axial-flexural action has not however, as far as the Authors know, been never quantified and the question if, or in which conditions, it is necessary to model the tension stiffening still remains without clear answers. Moreover, the influence on tension stiffening effects of the axial force, to which circular cross section elements such as bridge piers and pile foundations are usually subjected to, or of the reinforcement ratio are never been quantified.

Within this work the modelling approach adopted by Salvatore et al. (2007) for rectangular sections is analysed, enhanced in some definition and adapted to circular, symmetrically reinforced, cross section. The reliability of the model results is then tested comparing them with experimental results of tests carried out on circular elements characterized by different reinforcements ratios and subjected to combined axial and bending forces. Finally, a parametric analysis, using the proposed model, is executed to estimate the influence of various parameters (axial force, reinforcement ratio, slenderness) on the global behaviour of r.c. elements having circular cross section.

Modelling of the tension stiffening

Salvatore et al. (2007) proposed a model based on CEB-fib Model Code (1998) approach upholding the classical hypotheses of plane cross-sections and perfect adherence between steel bars and the surrounding concrete, even after cracking, in all sections (cracked and uncracked ones). The bond–slip relation is assumed to be rigid–plastic, as illustrated in Figure 5.6a, where τ_{b1} is the bond stress when the reinforcing bar is in the elastic phase and τ_{b2} the bond stress when the bar is yielded.

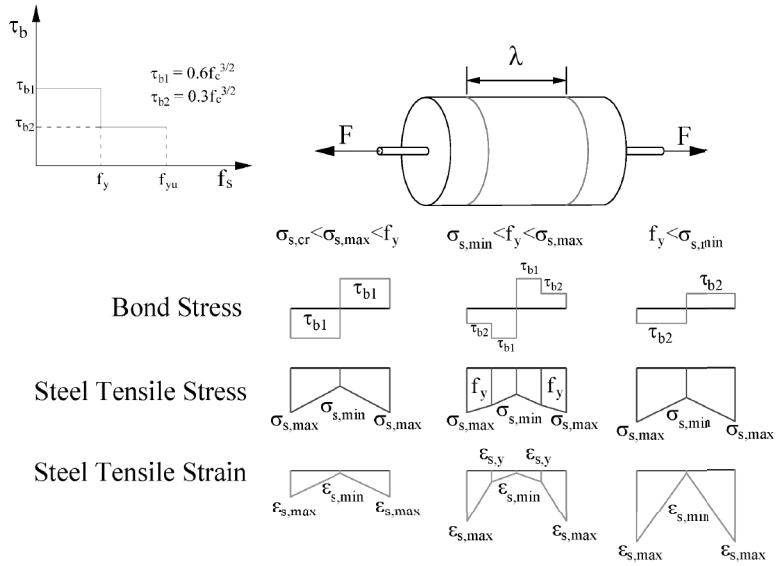

Figure 5.6: a) Bond–slip relation for the steel–concrete interface; b) adherence, stress and strain in the steel

The bond and steel tensile stresses, together with the steel tensile strain resulting from the application of an increasing force to the steel bar are schematically shown in Figure 5.6b. To consider the deformational effects consequent to sliding between the steel and the concrete and the consequent redistribution of stresses, a fictitious elasticity modulus, E_{ct}, for the concrete in tension in the post-cracking phase is defined.

The definition of E_{ct} is derived from the equilibrium equation of an infinitesimal length of bar surrounded by the portion of concrete involved in the transmission of stresses from the bar to the concrete itself. On the base of the stress condition of the steel bar, Salvatore et al. (2007) derived the following expression of E_{ct}:

For $\sigma_{scr} \leq \sigma_{s,max} < f_y$:

$$E_{ct}(x) = \frac{4A_s}{\phi_s A_c}\tau_{b1}x\frac{1}{\frac{\sigma_{s,max}}{E_s} - \frac{4}{\phi_s E_s}\tau_{b1}x} \tag{5.10}$$

For $\sigma_{s,min} \leq f_y < \sigma_{s,max}$ and $x \geq x_y$:

$$E_{ct}(x) = \frac{(\frac{4}{\phi_s}\tau_{b1}x - \frac{4}{\phi_s}(\tau_{b1}+\tau_{b2})x_y)A_s}{(\frac{\sigma_{s,max}}{E_s} - \frac{4}{\phi_s E_s}(\tau_{b1}+\tau_{b2})x_y + \frac{4}{\phi_s}\tau_{b1}x)A_c} \tag{5.11}$$

For $f_y < \sigma_{s,min}$ or $\sigma_{s,min} \leq f_y < \sigma_{s,max}$ and $x < x_y$:

$$E_{ct}(x) = \frac{\frac{4A_s}{\phi_s A_c}\tau_{b2}x}{\varepsilon_y + \frac{\sigma_{s,max}(\varepsilon_u-\varepsilon_y)}{f_u-f_y} - \frac{4(\varepsilon_u-\varepsilon_y)}{\phi_s(f_u-f_y)}\tau_{b2}x - f_y\frac{(\varepsilon_u-\varepsilon_y)}{(f_u-f_y)}} \tag{5.12}$$

Where $\sigma_{s,min}$ and $\sigma_{s,max}$ are the minimum and maximum stresses in the bar occurring respectively in the mid-line section and in the cross-sections of the element where the crack forms, σ_{scr} is the stress in the steel upon first cracking and, finally, x_y the distance from the cracked section where the stress in the steel begins to be lower than the yield stress.

Observations

The modelling approach adopted by Salvatore et al. (2007) briefly described in the previous paragraph suffers, however, of some inaccuracies. In the case of reinforcing bar subjected to stresses lower than the yield one, the elasticity modulus in tension E_{ct} would be defined by the respective equation but the following observations can be made:

- For $\frac{\sigma_{s,max}}{E_s} - \frac{4}{\phi E_s}\tau_{b1}x$, $E_{ct}(x) \to \infty$. This result is unrealistic given that the upper limit of $E_{ct}(x)$, $E_{ct,lim}$, should be at least equal to elastic modulus of the concrete in compression, E_c.
- For $\frac{\sigma_{s,max}}{E_s} - \frac{4}{\phi_s E_s}\tau_{b1}x < 0$, $E_{ct}(x) < 0$. Also this result has no physical meaning. The lower limit of E_{ct} should be equal to zero (in correspondence of the cracked section).

In Figure 5.7, the first equation is plotted for different values of σ_{scr}. It is immediate to understand that, in order to have some real physical meaning, the fictitious elasticity modulus in tension E_{ct} should respect the following limits:

$$0 \leq E_{ct}(x) \leq E_{ct,lim} \tag{5.13}$$

where $E_{ct,lim}$ represents the likely maximum value of the elasticity modulus in tension, assumed in the present study, equal to the concrete elasticity modulus in compression.

For this reason, we assumed for $\sigma_{scr} \leq \sigma_{s,max} < f_y$:

for $x < \frac{\sigma_{s,max}}{E_s} \frac{\phi_s E_s}{4\tau_{b1}}$:

$$E_{ct}(x) = \frac{4}{\phi_s} \frac{A_s}{A_c} \tau_{b1} x \frac{1}{\frac{\sigma_{s,max}}{E_s} - \frac{4}{\phi_s E_s} \tau_{b1} x} \tag{5.14}$$

for $x \geq \frac{\sigma_{s,max}}{E_s} \frac{\phi_s E_s}{4\tau_{b1}}$:

$$E_{ct}(x) = E_{ct,lim} \tag{5.15}$$

In Figure 5.8 the trend of the elasticity modulus in tension, E_{ct}, evaluated adopting Eq. 5.14 and Eq. 5.15 is shown.

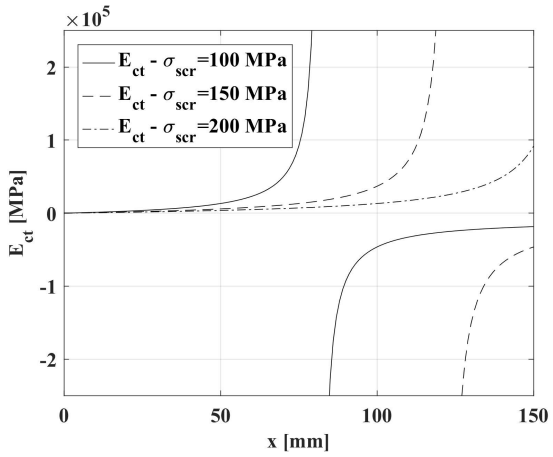

Figure 5.7: Elasticity modulus in tension, E_{ct}, as a function of the distance from the cracked section, x, for different values of the stress in the steel upon first cracking, σ_{scr}

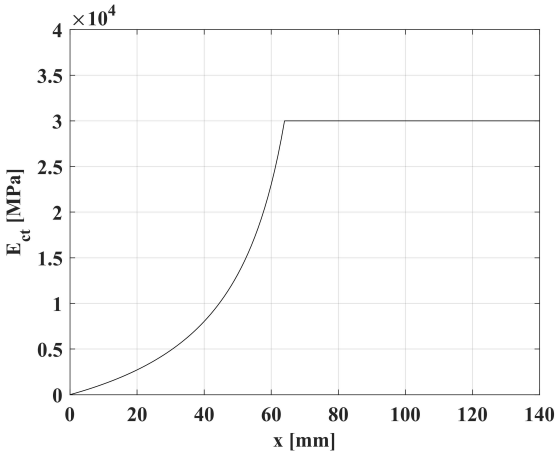

Figure 5.8: Trend of the elastic modulus in tension, E_{ct}, as a function of the distance, assumed within this work

Flexural behaviour of circular section considering the tension stiffening

The moment-rotation behaviour of the circular cross section portion of element comprised between two consecutive cracks can be obtained integrating the moment vs curvature relationship along the length of the element itself and adopting, for the concrete in tension, the fictitious elasticity modulus. Alternatively, as assumed in the present study, the element can be discretized in smaller elements and the curvature considered constant within each element. The rotation, θ_{A-B}, between the two consecutive cracked sections can be thus evaluated as follows:

$$\theta_{A-B} = \chi_A \frac{\lambda}{8} + \chi_{\frac{\lambda}{4}A} \frac{\lambda}{4} + \chi_{\frac{\lambda}{2}A} \frac{\lambda}{4} + \chi_{\frac{\lambda}{4}B} \frac{\lambda}{4} + \chi_A \frac{\lambda}{8} \tag{5.16}$$

To evaluate the moment curvature relationship, each section is discretized into a finite number of longitudinal fibers, see Figure 5.9, distinguishing the confined and unconfined concrete zones in compression and the concrete part influenced by the tension stiffening.

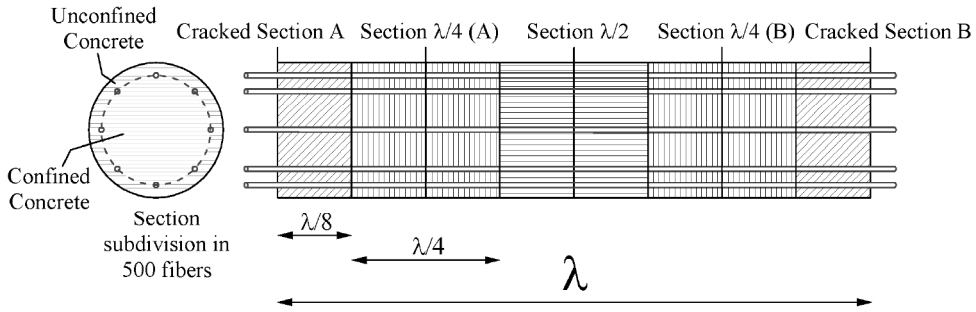

Figure 5.9: Element portion comprised between two consecutive cracks: a) Fibers of the circular section; b) sections studied for the evaluation of the total rotation

The hypotheses of plane sections and absence of slip between steel bars and the surrounding concrete are adopted. The effective area of concrete in tension was obtained following the Eurocode 2 approach. The concrete behaviour in compression is modelled using the Mander (1988) approach for the confined zone, the Popovics (1973) one for the unconfined concrete, while the concrete in tension with a brittle linear elastic behaviour, as proposed by CEB MC90. A bilinear hardening behaviour is assumed for steel reinforcing bars. An example of the resulting moment-curvature curve, evaluated in correspondence of a cracked section, is shown in Figure 5.10.

The effects of the tension stiffening are evident when the moment-curvature curve, evaluated on the cracked section, at $\lambda/4$ and at $\lambda/2$ are compared, see Figure 5.10. It can be seen that, thanks to the presence of concrete in tension between two cracks, the ultimate bending moment of the $\lambda/4$ and $\lambda/2$ sections are greater than the cracked section one, meaning that the plastic rotation of the element tends to accumulate within the cracked sections.

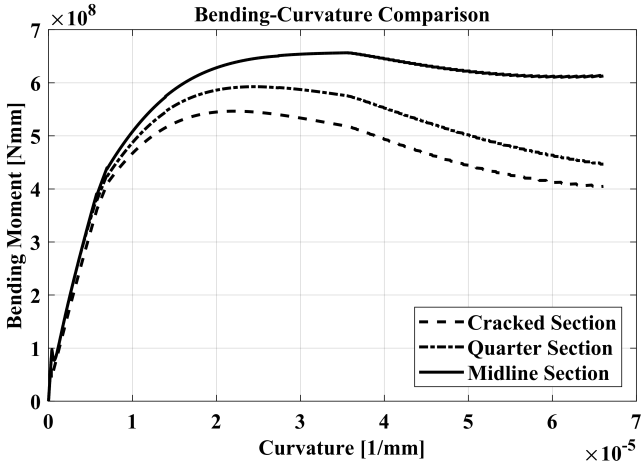

Figure 5.10: Examples of the moment-curvature curve computed for the circular pile studied by Therani (2014): comparison between the cracked, $\lambda/4$ and $\lambda/2$ sections

The displacements of a circular cross section element in bending was then easily estimated subdividing it in blocks, whose length, in the cracked portion of the element, should be equal to the cracks distance, while in the uncracked portion should depend on the flexural moment gradient. The relative displacement between two sections, Δ_{tot}, was then computed by summing the displacements, δ_i, of each block comprised between the two sections.

$$\Delta_{tot} = \sum_{i=1}^{N} \delta_i = \sum_{i=1}^{N} (H_i \sum_{j=1}^{i} \theta_j) \tag{5.17}$$

where H_i, is the length of the i block, N is the number of blocks in which the portion of element is divided into, θ_i is the relative rotation between the two faces of the i block evaluated using the equation:

$$\theta_{A-B} = \chi_A \frac{\lambda}{8} + \chi_{\frac{\lambda}{4}A} \frac{\lambda}{4} + \chi_{\frac{\lambda}{2}A} \frac{\lambda}{4} + \chi_{\frac{\lambda}{4}B} \frac{\lambda}{4} + \chi_A \frac{\lambda}{8} \tag{5.18}$$

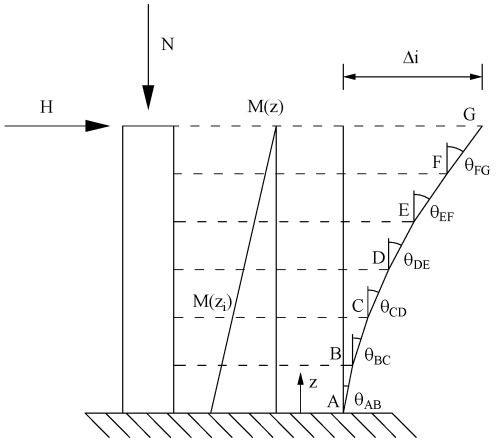

Figure 5.11: Evaluation of the relative displacement between two sections of an element in bending

Experimental validation

The procedure described in the previous paragraphs was validated applying it to evaluate the load-deflection curves of several r.c. circular cross section elements and comparing them with the experimental results.

Description of the experimental results

For this purpose, the experimental tests conducted by Lehman and Moehle (2000) and by Calderone, Lehman, and Moehle (2000) are used. Both publications provide a lot of details regarding the geometrical and mechanical characteristics of the section, on the loading mode and the cracks pattern during the test and on its completion. In both cases the test setup is equal: the column is fixed to the base and loaded transversely by a cyclic force and axially by a constant one, see Figure 5.12.

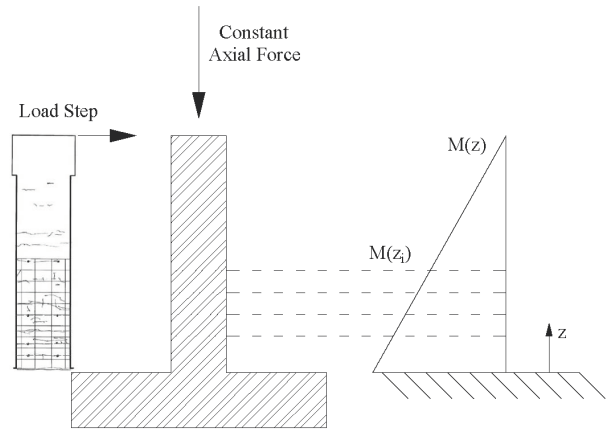

Figure 5.12: Bending Moment Profile $M(z_i)$

Lehman and Moehle (2000) tested a total of 5 specimens, whose main geometrical and mechanical characteristics are resumed in Table 5.1, focusing the study on the influence of the slenderness ratio on the column behaviour. Calderone and Lehman (2000), tested 4 specimen varying the column slenderness and the transversal reinforcement, see Table 5.2.

Table 5.1: Main geometrical and mechanical properties of specimens tested by Lehman and Moehle (2000)

Column ID	Height [mm]	Section Diameter [mm]	Concrete Cover [mm]	Long. Reinforc. d [mm]	Transverse Reinforc. d [mm] - s [mm]	Concrete f'_c [MPa]	Long. Reinforc. f_y [MPa]	Trans. Reinforc. f_y [MPa]
407	2438	609.6	33.4	10 – 16	6 – 32	43.4	471.6	668.1
415	2438	609.6	33.4	22 - 16	6 – 32	43.4	471.6	668.1
430	2438	609.6	33.4	22 - 23	6 – 32	43.4	471.6	668.1
815	4877	609.6	33.4	22 - 16	6 – 32	43.4	471.6	668.1
1015	6096	609.6	33.4	22 - 16	6 – 32	43.4	471.6	668.1

Table 5.2: Main geometrical and mechanical properties of specimens tested by Calderone and Lehman (2000)

Column ID	Height [mm]	Section Diameter [mm]	Concrete Cover [mm]	Long. Reinforc. d [mm]	Transverse Reinforc. d [mm] - s [mm]	Concrete f'_c [MPa]	Long. Reinforc. f_y [MPa]	Trans. Reinforc. f_y [MPa]
328	1829	609.6	41.3	28 – 19	6 – 25	27.6	483	483
328T	1829	609.6	41.3	28 – 19	6 – 76	27.6	483	483
828	4877	609.6	41.3	28 – 19	6 – 76	27.6	483	483
1028	6096	609.6	41.3	28 – 19	6 – 51	27.6	483	483

In both cases, the transverse load is applied cyclically and with an increasing amplitude. With the intent of comparing the monotonic experimental behaviour with the numerical one, the envelope curve of each test is taken into consideration, assuming that, given the low values of the imposed displacements (the maximum value of interest is around 5 cm), phenomena such as low cycle fatigue do not influence the response of the column.

Comparison of numerical and experimental results

The cracks pattern recorded by Lehman and Moehle (2000) and Calderone and Lehman (2000) allowed a preliminary validation of the mean cracks distance value given by Eq. 5.17.

Table 5.3 shows the comparison between the numerical and experimental results. Assuming that the identification of 'cracks' is characterized by high uncertainties and that their actual interaxis is strongly influenced by the actual mechanical characteristics of component materials, the Table 14 shows a good mean agreement between numerical and experimental results.

$$\lambda = \frac{3}{2}\lambda_{min} = \frac{3\phi_s A_c f_{ct}}{8\tau_{b1} A_s} \tag{5.19}$$

Table 5.3: Comparison between the experimental and numerical values of the mean cracks distance

Column ID	Experimental mean crack distance [mm]	Mean cracks distance evaluated by eq. 5.17 [mm]	Column ID	Experimental mean crack distance [mm]	Mean cracks distance evaluated by eq. 5.17 [mm]
407	167	204	328	78	74
415	93	112	328T	77	74
430	114	79	828	114	74
815	147	112	1028	84	74
1015	102	112			

Using the bending moment profile $M(z)$ along the column, calculated at each loading step, the corresponding deflections are obtained adopting the procedure described in the previous paragraphs.

The comparison between the experimental and numerical results, showed in Figure 5.13 and Figure 5.14, testifies the optimal capacity of the proposed model in evaluating the flexural behaviour of the circular cross section columns, especially from

a stiffness point of view. A lower accuracy was obtained from the resistance point of view but this issue is practically independent from the tension stiffening phenomenon and can be mainly ascribed to the low information regarding the hardening of the material. The figures show also the equivalent force-displacement curve obtained not considering the contribution of the concrete in tension.

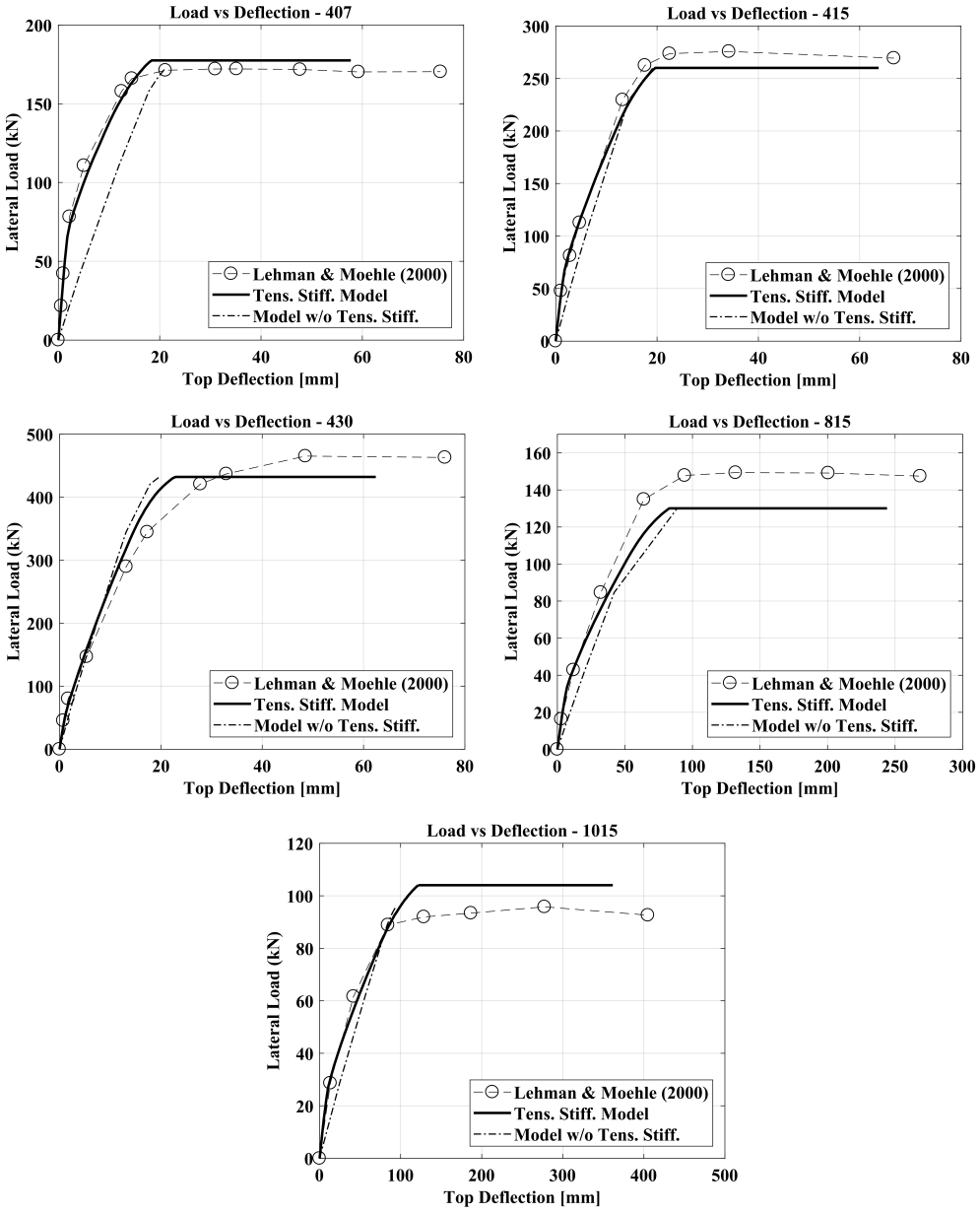

Figure 5.13: Comparison between the experimental results of Lehman and Moehle (2000) and the numerical ones

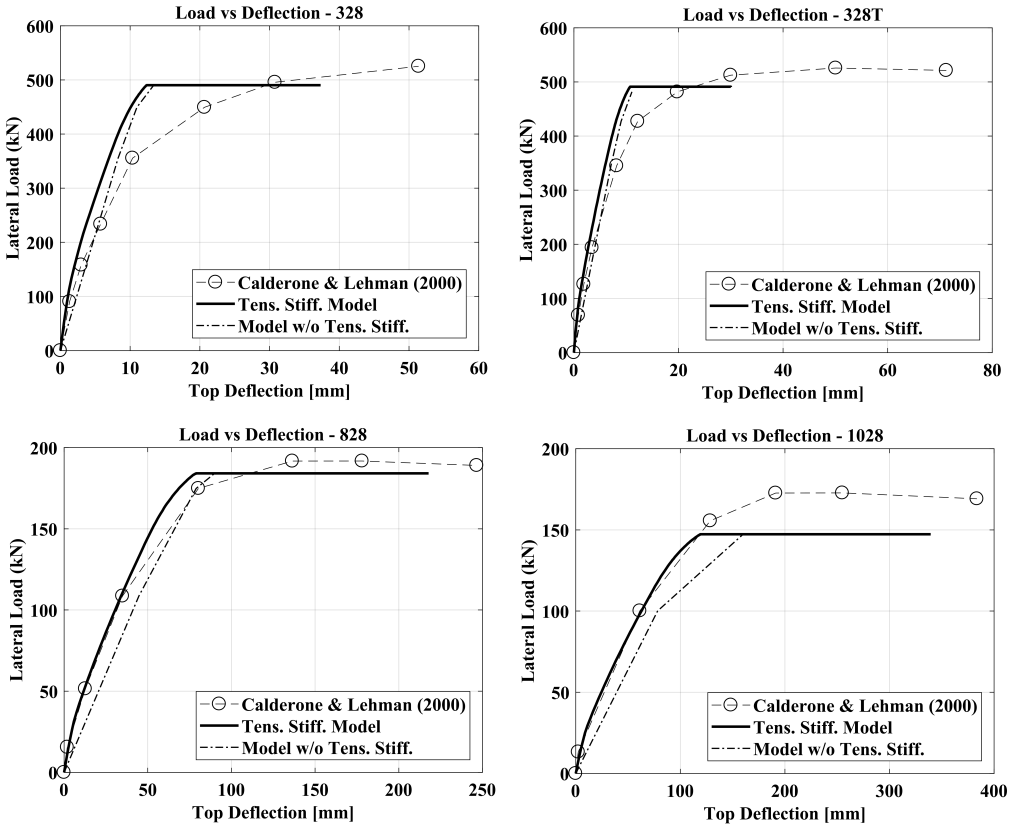

Figure 5.14: Comparison between the experimental results of Calderone and Lehman (2000) and the numerical ones

From the comparison of the proposed method curves (considering so the tension stiffening effects), the numerical curve obtained ignoring the tension stiffening and the experimental results, it was preliminary possible to observe that:

- for column 407, not considering the tension stiffening can lead to a sensible error in evaluating the element stiffness;
- for more slender columns (828 and 1028) the tension stiffening effects are more evident than shorter ones (328 and 328T).

Parametric analyses

To study the influence of the tension stiffening on the global behaviour, in this section it was executed a parametric analysis performed for different sections varying: the section diameter, the longitudinal reinforcing ratio and the compressive force. The cases considered in the parametric analysis are resumed in Table 5.4. Three different diameter, with values typical of the pile foundations (60 cm, 100 cm and 150 cm), and three longitudinal reinforcing bar ratios (1%, 2% and 3%) were considered. For each of these sections, the influence of 4 levels of the external compressive force, corresponding to the 5%, 10%, 25% and 35% of the ultimate axial resistance of the section (N_u), evaluated with the expression: $N_u = f_c A_c$, was studied. The results presented herein were obtained in two ways: taking into account the influence of the tension stiffening, adopting the model proposed in the previous paragraphs, or neglecting it. It was

thus possible to point out how the tension stiffening can affect the performance of a reinforced concrete element with a circular section.

Table 5.4: Circular reinforced concrete sections used for the parametric study

Diameter (m)	Longitudinal Bars	As/Ac	N/Nu (1)	N/Nu (2)	N/Nu (3)	N/Nu (4)
0.6	14ϕ16	1%	0.05	0.1	0.25	0.35
0.6	18ϕ20	2%	0.05	0.1	0.25	0.35
0.6	22ϕ22	3%	0.05	0.1	0.25	0.35
1	30ϕ18	1%	0.05	0.1	0.25	0.35
1	42ϕ22	2%	0.05	0.1	0.25	0.35
1	44ϕ26	3%	0.05	0.1	0.25	0.35
1.5	40ϕ24	1%	0.05	0.1	0.25	0.35
1.5	44ϕ32	2%	0.05	0.1	0.25	0.35
1.5	66ϕ32	3%	0.05	0.1	0.25	0.35

Assumed that the concrete elastic modulus remains constant, the influence of tension stiffening was evaluated in terms of equivalent moment of inertia. For each diameter considered and listed in Table 5.4 two plots were then presented, the former referring to a normalized moment of inertia defined as the ratio between the secant flexural rigidity $(E_cI)_{sec,y}$ at the first steel bar yielding and the intact flexural rigidity of the section ($(E_cI)_{intact} = (E_c\pi D^4)/64$) and the second referring to a normalized moment of inertia defined as the ratio between the secant flexural rigidity at the maximum bending moment, $(E_cI)_{sec,u}$, and the intact flexural stiffness. Figures 5.15, 5.16 and 5.17 show that the influence of the tension stiffening is:

- less evident on the secant stiffness at the first bar yielding than on the evaluated at the maximum bending moment;
- increasing as the reinforcement ratio decreases;
- not so much influenced by the axial force, except for low values of the reinforcement ratio
- higher for smaller diameter.

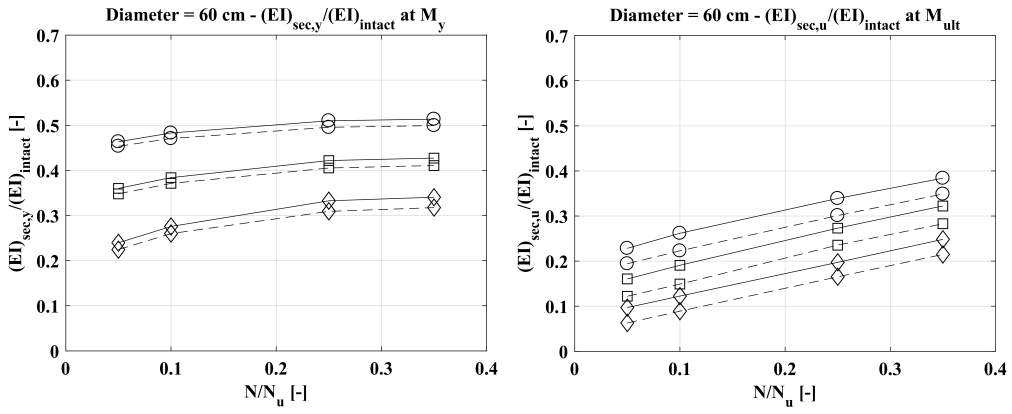

Figure 5.15: Diameter 60 cm: normalized secant flexural rigidity at first steel bar yielding (left) and at maximum bending moment (right)

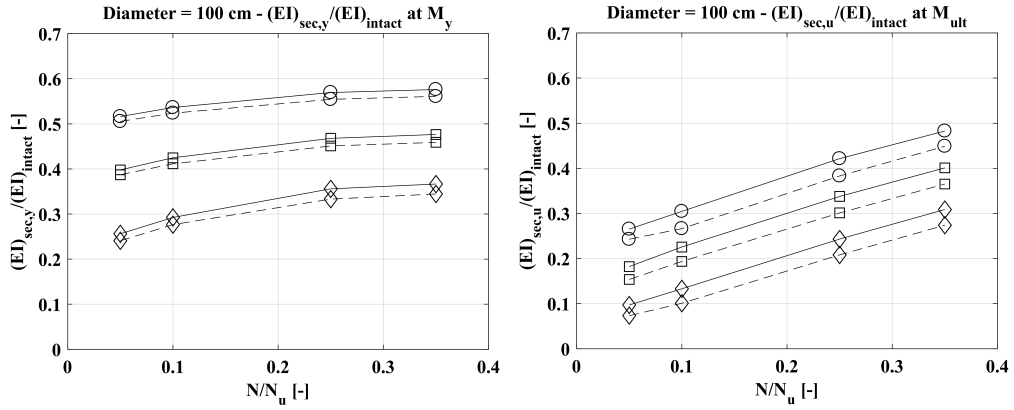

Figure 5.16: Diameter 100 cm: normalized secant flexural rigidity at first steel bar yielding (left) and at maximum bending moment (right)

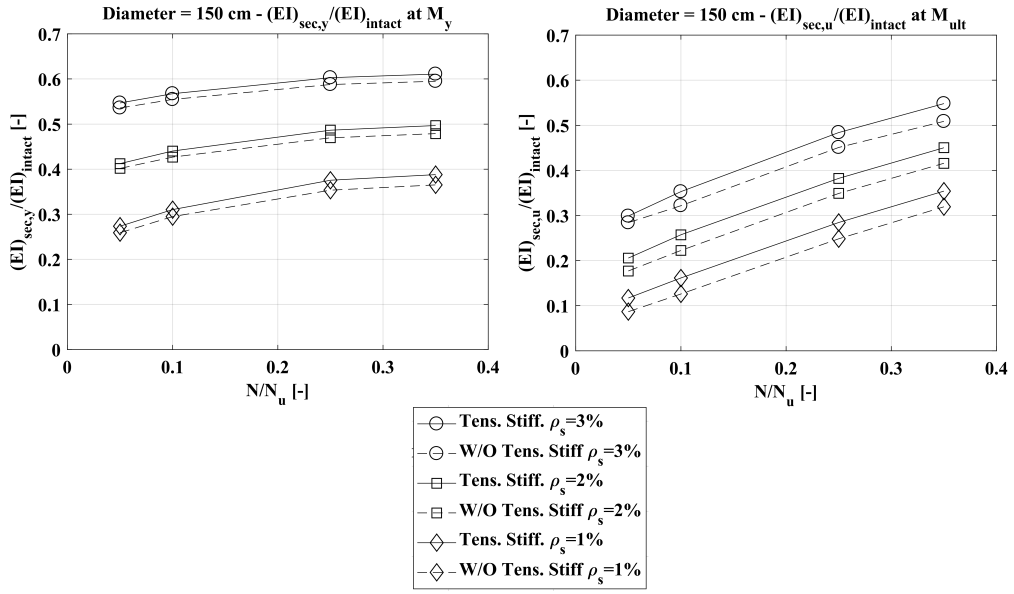

Figure 5.17: Diameter 150 cm: normalized secant flexural rigidity at first steel bar yielding (left) and at maximum bending moment (right)

These results suggest that for r.c. elements characterized by circular section with diameter higher than 1 m and with a reinforcement ratio higher than 1%, such as usual bridge piers, the influence of the tension stiffening can be neglected.

The influence of the tension stiffening becomes sensible for low diameter (around 60 cm, such as some foundation piles) and low values of the reinforcement ratio (lower than 1%). However, in general, in the case of foundation piles, it can be easily assumed that the influence of the tension stiffening on the global behaviour is absorbed by the uncertainties in the definition of the soil mechanical properties.

5.2.2 Soil modelling

Far-field soil

The 'far-field' soil (far from the pile shaft) is modelled as a multi-layered elastic half-space. BEM analysis requires an appropriate elementary singular solution to be integrated on the surface of the problem domain. In the case of piles subjected to horizontal loading, the elastic Mindlin solution (1936) is generally used (Appendix). This solution, which evaluates the pile-soil interactions, is valid and rigorous only in the case of a homogeneous elastic half-space, however it can still be considered valid in the case of a multi-layered elastic half-space (Poulos and Davis, 1980).

The horizontal displacement s_{ij} induced at a point i, belonging to the half space by a horizontal load P_j applied at point j can be expressed as in the following equation (Figure 5.18). Where the term b_{ij} represents the general expression for each 'far-field soil' flexibility matrix coefficient.

$$\begin{aligned} s_{ij} =& \frac{P_j(1+\nu)}{8\pi E(1-\nu)}[\frac{3-4\nu}{R_1}+\frac{1}{R_2}+\frac{x^2}{R_1^3}+\frac{3-4\nu}{R_2^3}x^2+ \\ & \frac{2cz}{R_2^3}(1-\frac{3x^2}{R_2^2})+\frac{4(1-\nu)(1-2\nu)}{R_2+z+c}(1- \\ & \frac{x^2}{R_2(R_2+z+c)})] = b_{ij}P_j \end{aligned} \tag{5.20}$$

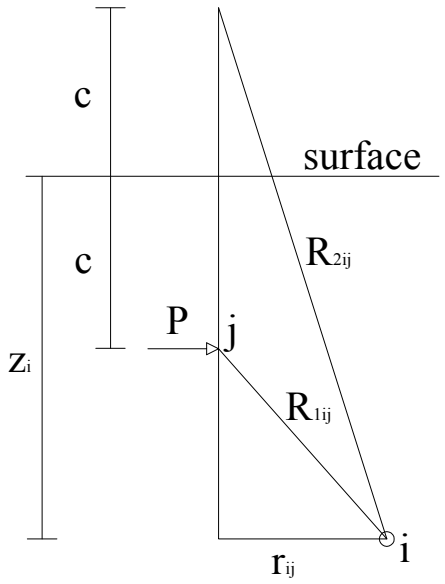

Figure 5.18: Mindlin solution scheme

Secondary discretization of blocks in sub-blocks

The numerical integration of the Mindlin equation (1936) is more accurate as higher is the number of sub-blocks in which the block j-th is divided. The need for a more refined discretization in sub-blocks, however, becomes less important as the distance, between the point at which the induced displacement is evaluated (middle-point of the generic block i-th) and the block j-th at which the soil reaction acts, increase. This

aspect is taken into account by using a variable discretization in sub-blocks, on the basis of the relative position between the block i-th and the block j-th: when this relative distance increases, the sub-discretization may be less refined.

In order to optimize the discretization of the pile-blocks in sub-blocks, a parametric study was carried out by Landi (2006). The coefficients of the soil flexibility matrix are evaluated changing the number of sub-blocks (r x s). The parameters considered in this parametric analysis are the slenderness ratio L/D and the pile-soil relative stiffness $K = E_p/E_s$. The subdivisions in sub-blocks studied are (r = the number of sub-blocks in the y direction; s = the number of sub-blocks in the z direction): 4 x 3; 6 x 4; 10 x 5; 20 x 10; 40 x 20; 50 x 25; 60 x 30; 80 x 40, that correspond to a total sub-blocks number equal to: 12; 24; 50; 200; 800; 1250; 1800; 3200.

The results of the parametric study suggest that a proper subdivision in r x s sub-blocks is that presented in Figure 5.19.

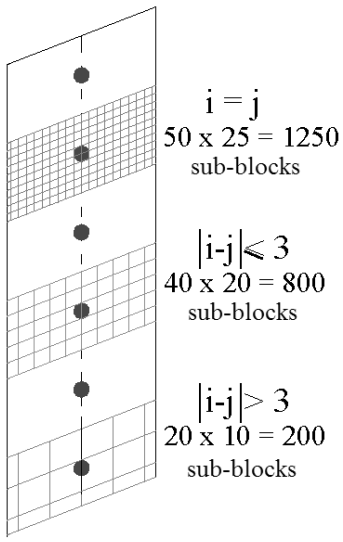

Figure 5.19: Pile-discretization in sub-blocks to carry out the numerical integration of Mindlin's equation (Landi, 2006)

If the point where the displacement is evaluated (middle-point of the block i-th) and the point at which the soil reaction acts (center of gravity of the block j-th) belong to same pile k:

- 50 x 25 = 1250 sub-blocks for the calculation of b_{ii} coefficients;
- 40 x 20 = 800 sub-blocks for the calculation of b_{ij} coefficients with $|i - j| \leq 3$;
- 20 x 10 = 200 sub-blocks for the calculation of b_{ij} coefficients, $|i - j| > 3$.

A similar parametric analysis was carried out for a pair of piles. The results suggest that for the evaluation of the soil flexibility matrix coefficients, b_{ij}, related with blocks belonging to different piles, a subdivision into 20 x 10 = 200 sub-blocks can be enough.

Near-field soil

The 'near-field' soil and its non-linear response is introduced by placing non-linear springs in series to each pile-half-space node (Figure 5.20), with a shape dependent on

the soil type. In the present study, the 'p-y' curves proposed by Matlock (1970), Reese et al. (1974), Welch and Reese (1972) and Reese et al. (1975) are used.

The input data required for the soil are: the elastic modulus E_{max} at small strain levels (which can be estimated starting with the maximum shear modulus G_{max}, the Poisson ratio, and the angle of internal friction (and the relative density D_R) or the undrained shear resistance if the soil is cohesionless or cohesive, respectively.

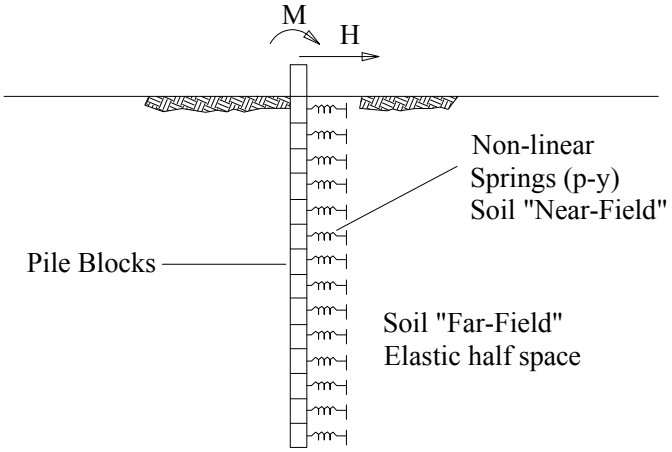

Figure 5.20: Hybrid BEM-py curve method

Calculation of non-linear springs

In this paragraph is described the procedure to compute the non-linear springs used in the proposed Hybrid BEM - py curves method.

Non-linear springs for soft clay

The procedure to define the 'p-y' curves for soft clay needs the following steps (Matlock, 1970):

- obtain the best estimate of the variation of undrained shear strength and submerged unit weight with depth. Also obtain the value of ε_{50}, the strain corresponding to one-half the maximum principal stress difference. If no stress-strain curves are available, typical values of ε_{50} are given in Table 5.5;
- compute the ultimate soil resistance per unit length of pile, using the smaller of the values given by the equations below,

$$p_{ult} = [3 + \frac{\gamma'}{c_u}z + \frac{J}{b}z]c_u b \tag{5.21}$$

$$p_{ult} = 9c_u b \tag{5.22}$$

- where γ' = average effective unit weight from ground surface to the depth z analysed; z = depth from the ground surface of the point investigated; c_u = shear strength at depth z; and b = width of the pile (= diameter). Matlock (1970) stated that the value of J was determined experimentally to be 0.5 for a soft clay and about 0.25 for a medium clay. A value of 0.5 is frequently used, thus will be used this value.

- compute the deflection, y_{50}, at one-half the ultimate soil resistance from the following equation:

$$y_{50} = 2.5\varepsilon_{50}b \tag{5.23}$$

- points describing the p-y curve are now computed from the following relationship.

$$\frac{p}{p_{ult}} = 0.5(\frac{y}{y_{50}})^{1/3} \tag{5.24}$$

- the value of p remains constant beyond $y = 8y_{50}$.

Table 5.5: Representative values of ε_{50} for normally consolidated clay

Consistency of clay	Average value of c_u (kPa)	ε_{50}
Soft	< 48	0.02
Medium	48-96	0.01
Stiff	96-192	0.005

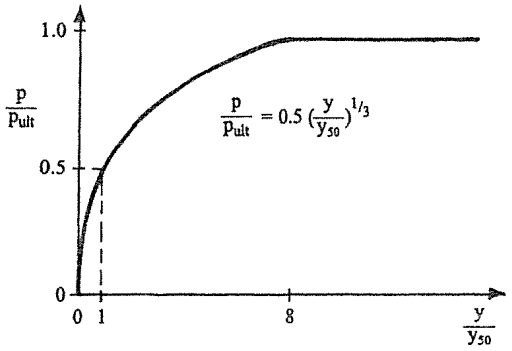

Figure 5.21: Characteristic shape of p-y curve for soft clay in the presence of free water (static loading) – (after Matlock, 1970)

Non-linear springs for stiff clay

The procedure to define the 'p-y' curves for stiff clay needs the following steps (Reese, Cox, and Koop, 1975):

- obtain values of undrained shear strength, c_u, soil submerged unit weight γ', and pile diameter b.
- compute the average undrained shear strength c_a over the depth z.
- compute the ultimate soil resistance per unit length of pile using the smaller of the value given by the equations below:

$$p_{ct} = 2c_a b + \gamma' bz + 2.83c_a z \tag{5.25}$$

$$p_{cd} = 11c_u b \tag{5.26}$$

- choose the appropriate value of A_s from Figure 5.22 for the particular non dimensional depth.

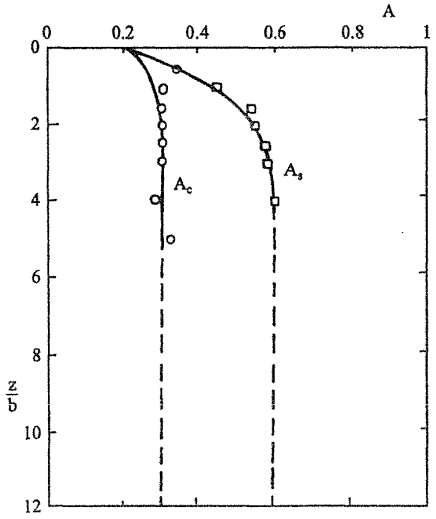

Figure 5.22: Values of constants A_s (Reese and Van Impe, 2001)

- establish the initial straight-line portion of the p-y curve, using the appropriate value of k_s from Table 5.6.

$$p = (k_s z)y \tag{5.27}$$

- compute y_{50}, using an appropriate value of ε_{50} from results of laboratory tests or in the absence of the laboratory tests, from Table 5.7.

$$y_{50} = \varepsilon_{50} b \tag{5.28}$$

- establish all the portions of the p-y curve as shown in Figure 5.23.

Table 5.6: Representative values of k_{py} for overconsolidated clays

Average undrained shear strength (kPa)	50-100	100-200	300-400
k_{pys} (MN/m^3)	135	270	540

Table 5.7: Representative values of ε_{50} for overconsolidated clays

Average undrained shear strength (kPa)	50-100	100-200	300-400
ε_{50}	0.007	0.005	0.004

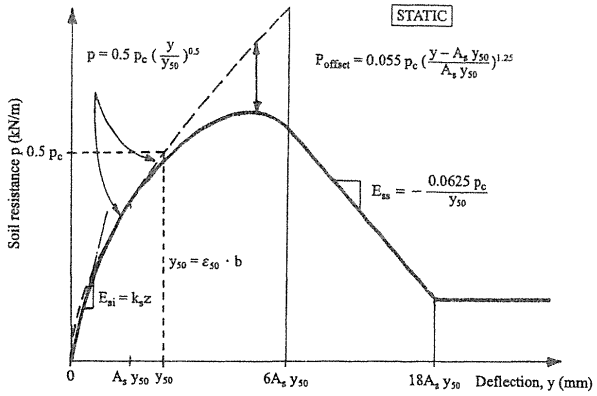

Figure 5.23: Characteristic shape of p-y curves for static loading in stiff clay in the presence of free water (Reese at al., 1975)

Non-linear springs for stiff clay with no free water

The procedure to define the 'p-y' curves for stiff clay with no free water needs the following steps (Welch and Reese, 1972):

- obtain values for undrained shear strength c_u, soil unit weight γ, and pile diameter b. Also obtain the values of ε_{50} from stress-strain curves. If no stress-strain are available, use a value for ε_{50} of 0.010 or 0.005 as given in Table 5.7, the larger value being more conservative.
- compute the ultimate soil resistance per unit length of pile, using the smaller of the values given by the equations below.

$$p_{ult} = [3 + \frac{\gamma}{c_u} z + \frac{J}{b} z] c_u b \tag{5.29}$$

$$p_{ult} = 9 c_u b \tag{5.30}$$

- where γ = average soil unit weight from ground surface to the depth z analysed; z = depth from the ground surface of the point investigated; c_u = average shear strength from ground surface to the depth z analysed; and b = width of the pile (= diameter). The value of J is taken generally equal to 0.5.
- compute the deflection, y_{50}, at one-half the ultimate soil resistance from the following equation:

$$y_{50} = 2.5 \varepsilon_{50} b \tag{5.31}$$

- points describing the p-y curve are now computed from the following relationship:

$$\frac{p}{p_{ult}} = 0.5(\frac{y}{y_{50}})^{0.25} \tag{5.32}$$

- the value of p remains constant beyond $y = 16y_{50}$

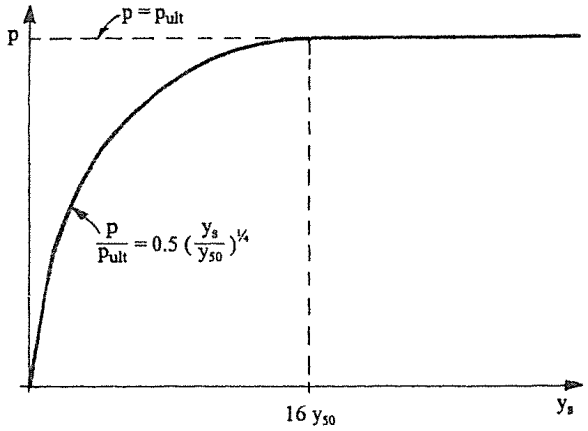

Figure 5.24: Characteristic shape of p-y curves for static loading in stiff clay with no free water (Welch and Reese, 1972)

Non-linear springs for sand

The procedure to define the 'p-y' curves for sand above and below the water table needs the following steps (Reese, Cox, and Koop, 1974):

- Obtain values for the friction angle ϕ, the soil unit weight γ, and pile diameter b (Note: use buoyant unit weight for sand below the water-table and total unit weight for sand above the water table).
- Make the following preliminary computations.

$$\alpha = \phi/2; \beta = 45 + \phi/2; K_0 = 0.4; K_a = tan^2(45 - \phi/2) \tag{5.33}$$

- Compute the ultimate soil resistance per unit length of pile using the smaller of the values given by the following equations (for derivation from analysis of a wedge).

$$\begin{aligned} p_{st} =& \gamma z[\frac{K_0 z tan\phi sin\beta}{tan(\beta - \phi)} + \frac{tan\beta}{tan(\beta - \phi)}(b + z tan\beta tan\alpha) + \\ & K_0 z tan\beta(tan\phi sin\beta - tan\alpha) - K_a b] \end{aligned} \tag{5.34}$$

$$p_{sd} = K_a b\gamma z(tan^8\beta - 1) + K_0 b\gamma z tan\phi tan^4\beta \tag{5.35}$$

- establish y_u as $3b/80$. Compute p_{ult}, using the appropriate value of $(\bar{A}_s)$ from Figure 5.25 for the particular non-dimensional depth, with the following expression:

$$p_{ult} = \bar{A}_s p_s \tag{5.36}$$

- establish y_m as $b/60$. Compute p_m, using the appropriate value of B_s from Figure 5.26 for the particular non-dimensional depth, with the following expression:

$$p_m = B_s p_s \tag{5.37}$$

- the two straight-line portions of the p-y curve, beyond the point where y is equal to $b/60$ can now be established.
- establish the initial straight-line portion of the p-y curve, using the appropriate value of k_{py} from Table 5.8 or Table 5.9.

$$p = (k_{py} z) y \tag{5.38}$$

- establish the parabolic section of the p-y curve,

$$p = \bar{C} y^{1/n} \tag{5.39}$$

- fit the parabola between points k and m as follows: a) get the slope of the line between points m and u by:

$$m = \frac{p_u - p_m}{y_u - y_m} \tag{5.40}$$

b) obtain the power of the parabolic section by:

$$n = \frac{p_m}{m y_m} \tag{5.41}$$

c) obtain the coefficient $\bar{C}$ as follows:

$$\bar{C} = \frac{p_m}{y_m^{1/n}} \tag{5.42}$$

d) determine point k as:

$$y_k = \left(\frac{\bar{C}}{k_{py} z}\right)^{\frac{n}{n-1}} \tag{5.43}$$

e) compute appropriate number of points on the parabola by using: $p = \bar{C} y^{1/n}$.

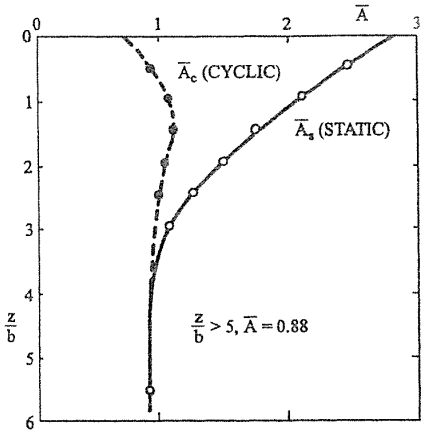

Figure 5.25: Values of coefficient $\bar{A}_s$ (Reese and Van Impe, 2001)

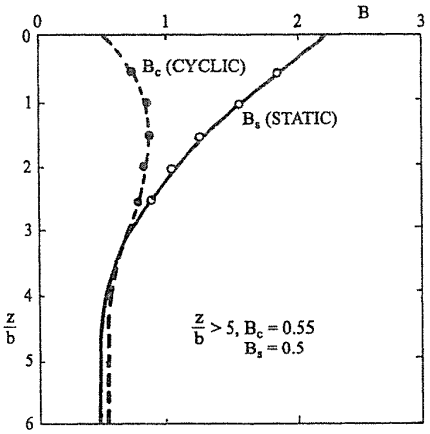

Figure 5.26: Non-dimensional coefficient B_s for soil resistance versus depth (Reese and Van Impe, 2001)

Table 5.8: Representative values of k_{py} for submerged sand

Relative density	Loose	Medium	Dense
Recommended k_{py} (MN/m^3)	5.4	16.3	34

Table 5.9: Representative values of k_{py} for sand above the water table

Relative density	Loose	Medium	Dense
Recommended k_{py} (MN/m^3)	6.8	24.4	61

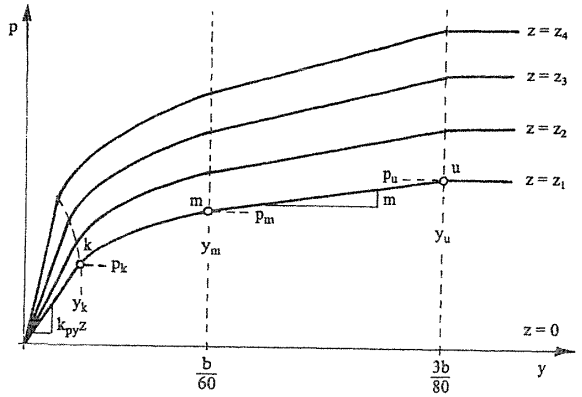

Figure 5.27: Characteristic shape of p-y shape curves for static loading in sand (Reese et al, 1974)

5.2.3 Influence of suction on pile lateral response

Suction is an important aspect in pile foundation subjected to lateral loads because the response of this foundation system is mainly affected by the shallower soil layers. The proposed method uses the 'MK-Model' (Modified-Kovacs Model) proposed by Aubertin et al. (2003).

This model makes use of a parameter defined as the equivalent capillary rise h_{c0} in the porous medium. The role of this parameter is the same as the average capillary rise in the original model developed by Kovacs and is calculated using the expression for the rise of water in a capillary tube (h_c) having a diameter d. For the sake of convenience, the expressions to estimate the equivalent capillary rise in granular soils (Eq. 5.44) and in cohesive/plastic soils (Eq. 5.45) are reported below.

$$h_{c0}(cm) = \frac{0.75}{eD_{10}[1 + 1.17logC_U]} \tag{5.44}$$

where D_{10} (in cm) is the diameter corresponding to 10% passing on the grain-size distribution curve, C_U is the coefficient of uniformity (= D_{60}/D_{10}) and e is the void ratio.

$$h_{c0}(cm) = \frac{0.15\rho_s}{e} w_L^{1.45} \tag{5.45}$$

where w_L is the liquid limit, and ρ_s is the solid grain density (kg/m^3).

The MK-Model uses the equivalent capillary rise as a reference parameter to define the relationship between the degree of saturation S_r (or volumetric water content Θ) and matrix suction ψ.

The model consider that water is held by capillary forces, responsible for capillary saturation S_c, and by adhesive forces, causing saturation by adhesion S_a. The S_c component is more important at relatively low suction values, while the S_a component becomes dominant at higher suction when most capillary water has been withdrawn.

The relationship proposed in the MK-Model is written as in Eq. 5.46 for the degree of saturation:

$$S_r = \Theta/n = S_c + S_a^*(1 - S_c) \tag{5.46}$$

In this equation, to ensure that this component does not exceed unity at low suction a truncated value of the adhesion component S_a^* is introduced in place of S_a used in the original model. The contribution of the capillary and the adhesion components to the total degree of saturation is defined as function of h_{c0} and ψ using the equations reported in Aubertin et al. (2003).

Implementing the 'MK-Model' in the Hybrid BEM - py curves method takes suction into account and increases the effective stress state of the upper soil layers. This thus increases both the stiffness and the resistance of the non-linear springs (described in the previous paragraph) located close to the ground surface which are expressed as a function of the soil stress state.

5.2.4 Non-linear solution procedure

The solution system is defined as: $[F][X] = [P]$. $[X]$ is the unknowns vector composed of $k + 2$ terms or $k + 1$ terms for free and fixed head conditions, respectively, where k is the number of pile blocks, p are the k unknown pressures acting at the pile-soil interface, y_0 is the single pile displacement at the pile-head, θ_0 is the pile-head rotation. $[P]$ is the known-term vector, which has the same dimension as the vector $[X]$.

$[F]$ is a $(k+2)x(k+2)$ or $(k+1)x(k+1)$ matrix, obtained by adding the k x k pile flexibility matrix $[F_P]$ (containing the a_{ij} coefficients), the k x k soil ('far field') flexibility matrix $[F_{SFF}]$ (composed of the b_{ij} coefficients), and the k x k soil ('near field') flexibility matrix $[F_{SNF}]$ (composed of the c_{ii} coefficients, representing the flexibility of each non-linear spring). The final two (or one in the fixed-head condition) rows and columns of the matrix $[F]$ are necessary to impose the equilibrium and to complete the compatibility equations at each pile-spring-half-space node, respectively.

$$\begin{bmatrix} a_{11}+b_{11}+c_{11} & a_{1j}+b_{1j} & a_{1k}+b_{1k} & -1 & -z_1 \\ a_{i1}+b_{i1} & a_{ii}+b_{ii}+c_{ii} & a_{ik}+b_{ik} & -1 & -z_i \\ a_{k1}+b_{k1} & a_{kj}+b_{kj} & a_{kk}+b_{kk}+c_{kk} & -1 & -z_k \\ 1 & 1 & 1 & 0 & 0 \\ z_1 & z_j & z_k & 0 & 0 \end{bmatrix} \begin{bmatrix} p_1\Delta_1 D \\ p_i\Delta_i D \\ p_k\Delta_k D \\ y_0 \\ \theta_0 \end{bmatrix} = \begin{bmatrix} 0 \\ 0 \\ 0 \\ H \\ M \end{bmatrix} \tag{5.47}$$

In the equation 5.47, H is the horizontal load applied and M is the bending moment applied.

The $[F_{SNF}]$ is a diagonal matrix, and each coefficient represents the 'p-y' tangent flexibility evaluated at each spring displacement y value reached at each pile-spring node at the previous load increment step. Elements of the soil 'far-field' matrix $[F_{SFF}]$ always remain constant, and are used to consider the interaction between the non-linear springs. The pile flexibility matrix, $[F_P]$, only in the case of a non-linear 'moment-curvature' relationship for the pile section, is updated at each step, using the tangent flexural rigidities of the section, according to the bending moments reached at each pile node in the previous load increment.

In addition, at each load step a check is carried out to determine whetheher the ultimate soil resistance at the pile-soil interface has been reached.

Once the initial flexibility matrix has been calculated, the total horizontal load is applied in the first step of the solution procedure. At each generic load increment h_k, an iterative process is performed where two solutions are obtained, the first using h_k (full step) as the load increment, the second using two load steps equal to $h_k/2$ (two half step).

The solution scheme is described in Figure 5.28, which, for the sake of simplicity, refers to the explicit Euler method with step-doubling and adaptive step-size control. However, a fourth order Runge-Kutta method can also be used to obtain some improvement in the accuracy of the solution.

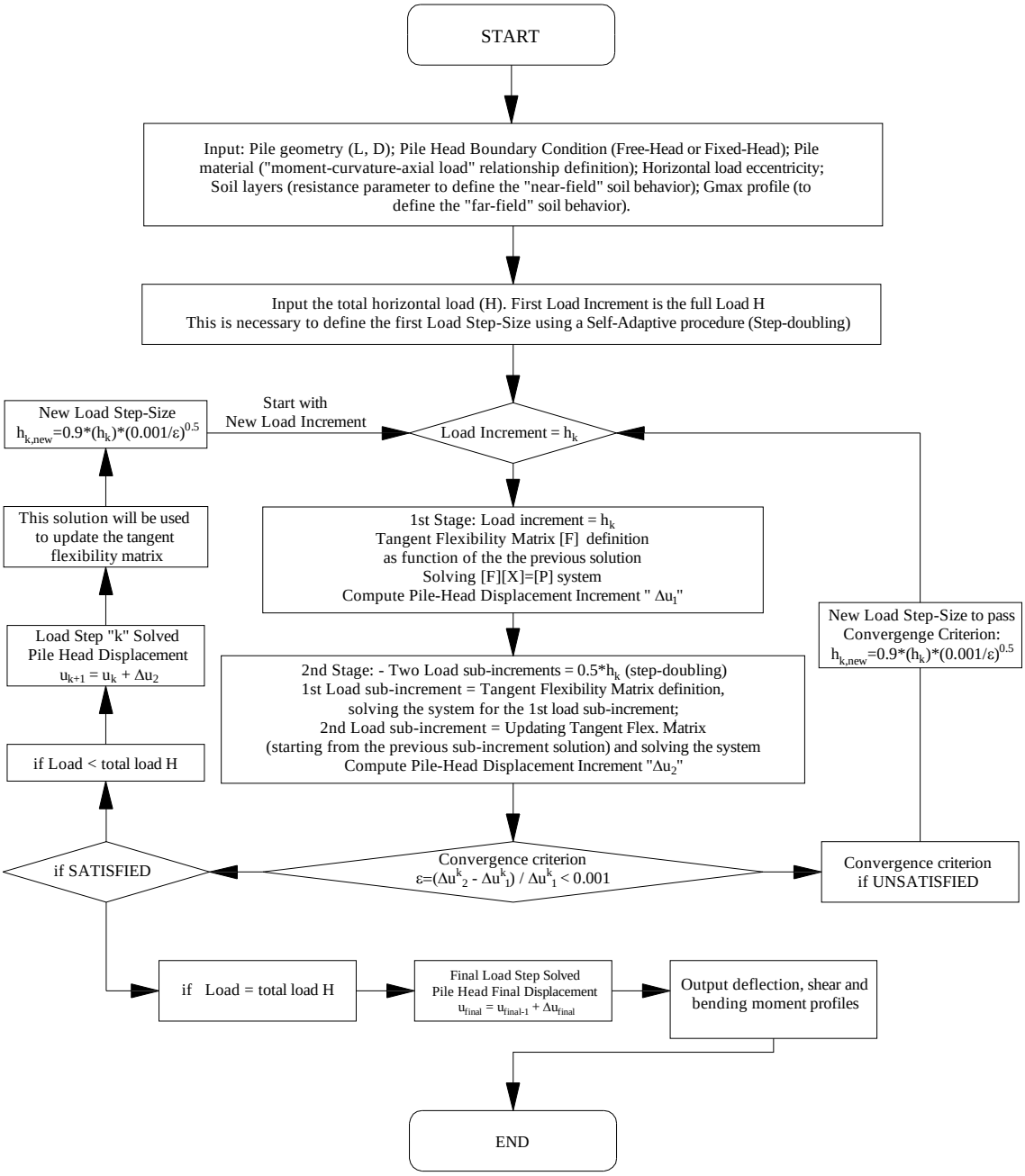

Figure 5.28: Flow-chart of the proposed non-linear adaptive step size method

Once these two solutions have been computed, the incremental ratio (ε), is computed according to Eq. 5.48.

$$\varepsilon = \frac{\Delta u_2 - \Delta u_1}{\Delta u_1} \tag{5.48}$$

where Δu_1 and Δu_2 are the incremental displacement at the pile-head evaluated using one and two steps, respectively. The ε value is compared with a predefined tolerance taken equal to 0.001 (Figure 5.29). When this converge criterion is exceeded, the iterative process starts again with an updated load increment h_k^{new} which should be able to achieve the desired accuracy. h_k^{new} can be estimated using the Eq. 5.49.

$$h_k^{new} = SF h_k (\frac{tol}{\varepsilon})^{\frac{1}{p+1}} \tag{5.49}$$

where p is the order of the method used (in the Euler method $p = 1$, in the Runge-Kutta method $p = 4$), and SF is a safety factor (taken as equal to 0.90) to guarantee the success in the next attempt. When this converge criterion is passed, expression 5.49 is used again to estimate the next step-size. The procedure stops when the final lateral load H is reached. Finally, the entire load-deflection curve and the deflection, shear, bending moment and pile-soil interface pressure profiles along the pile shaft at each load-step can be evaluated.

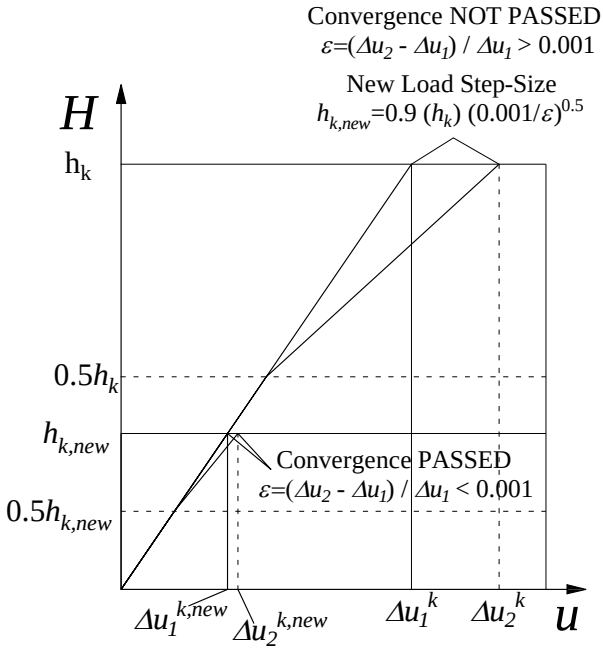

Figure 5.29: Adaptive Step-Size Control

Currently, it is only possible to analyse free-to-rotate or fixed-head single piles, however a different restraint can be added. The computation process ends with the calculation of the unknowns, which in this case are the pressures acting at the pile-soil interfaces, the rotation, and the horizontal displacement at the pile-head section. The analyses are performed in an incremental manner, using an adaptive step-size control.

5.3 Pile group and Piled raft analysis: BEM method

5.3.1 Main features of the proposed method

The proposed method to describe the behaviour of single piles, pile groups and piled rafts subjected to horizontal loads consists of a BEM approach. The safe and economic design of piled rafts requires non-linear methods of analysis which have the capability of simulating all relevant interactions between the foundation elements and the subsoil, specifically:

- pile-soil-interaction (i.e. single pile response);
- pile-pile-interaction (i.e. group effects);

- raft-soil-interaction;
- pile-raft interaction.

The originality of the proposed approach lies in its ability to provide a complete BEM analysis of the soil continuum (in which all four of the above interactions are modelled). Indeed, compared to FEM or FDM analyses, BEM provides a complete problem solution in terms of boundary values only, specifically at the raft-soil and pile-soil interfaces.

This leads to a drastic reduction in unknowns to be solved for, thereby resulting in substantial savings in computing time and data preparation effort. This feature is particularly significant for three-dimensional problems such as piled rafts and makes the analysis suitable not only for the design of piled rafts supporting high rise buildings (generally based on complex and expensive 3D FEM or FDM analyses) but also for that of bridges and ordinary buildings.

The approach has been extended to include the raft analysis (including its reciprocal interaction with the piles) by discretizing the raft-soil interface into a number of rectangular elements, whose behaviour is evaluated using the traditional Mindlin (Appendix) and Cerutti solutions.

The non-linear soil response is modelled, in an approximate manner, by adopting a quasi-hyperbolic elastic modulus reduction curve; to obtain the solution an incremental tangent method is used (by means of a fourth order Runge-Kutta numerical method with a self-adaptive step-size control), with a procedure which ensures that the specified limiting stresses at the raft-soil interface are not exceeded. The limiting values of the raft-soil shear resistance at the raft-soil interface are based on a simple frictional law that is expressed as a function of the vertical stress acting on each raft-soil interface element (computed with a vertical load analysis).

The analysis is currently restricted to the assumption of a perfectly rigid raft (under horizontal loading), thus each pile-head and each point of the raft move the same quantity at each step. While in the analysis under vertical loads, the raft flexibility is taken into account in an approximate, but reasonable, way (using the approach suggested by Mayne and Poulos (1999)).

The proposed method, relies upon the following assumption:

- horizontally layered elastic soil;
- the pile is modelled in the same way as described in the section of the Hybrid BEM - py curves method;
- non-linear soil behaviour (incremental analysis);
- pile-soil, pile-pile, raft-pile interactions (Mindlin's solution);
- pile-raft and soil-raft interactions (Cerutti's solution);
- constraint conditions at the pile-heads: hinged or fixed head;
- influence of vertical loads, using an improved version of the Poulos-Davis-Randolph (PDR) method. With this is possible to estimate the load distribution between the pile-group and the raft and thus, the induced vertical stresses, caused by a vertical load acting on the raft, at each pile-soil and raft-soil interface block (specifically, at the center point of each block in which the entire foundation-system has been discretized);

- the influence of suction in the same way as described in the section of the Hybrid BEM - py curves method

In the analysis of pile groups and piled-rafts, the program adopts the following further assumptions:

- non-symmetrical extinction distance for the interaction between a couple of blocks belonging to different piles in the group; this distance is defined according to the suggestion by Reese and Van Impe (2001) and is sketched in Figure 5.30,
- group effects (shadowing - overlapping passive soil wedges (Figure 5.31)) for small spacings. The so-called shadowing effect has been implemented in the algorithm, using an approach similar to that described in Ashour and Norris (2004) for the definition of group interactions effect caused by the overlapping of passive wedges of soil.

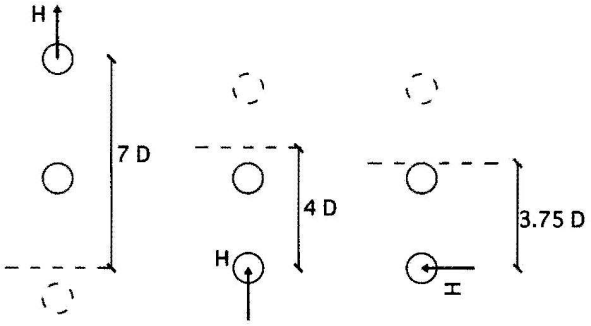

Figure 5.30: Extinction distance as defined by Reese and Van Impe (2001)

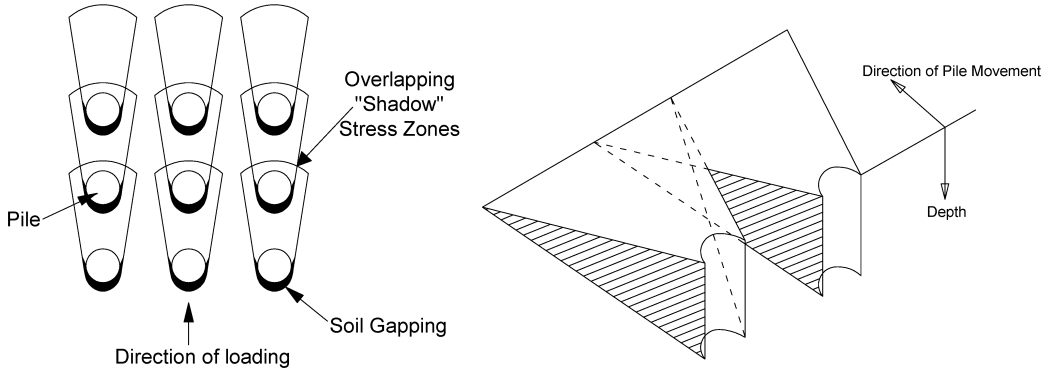

Figure 5.31: Group Effects (Shadowing and Overlapping Passive Soil Wedges)

To validate the program with its main assumptions, available case histories have been collected and a prediction exercise has been carried out. The number of piles in the group is generally rather small (the largest field test studied is on a 15 piles group). In all the examined cases, a load test on a single pile was also available. The program was applied both on the single pile and on the pile groups. Some judgement was applied in the simplification of the soil profile to predict the behaviour of the pile group.

5.3.2 Soil modelling

Pile-soil, pile-pile and raft-pile interactions

The soil is modelled as an multi-layered elastic half-space and the Mindlin's solution (Mindlin, 1936) is used (Appendix). In this work the approximation suggested by Poulos and Davis (1980) is used, thus the soil elastic modulus introduced in the Mindlin equation is the average between the elastic modulus at the point where the displacement is evaluated and the elastic modulus at the point where the force is applied: $E = (E_i + E_j)/2$. The horizontal displacement s_{ij} at a point i belonging to the half space by a horizontal load P_j applied at point j can be expressed as in the Eq. 5.50 (Figure 5.32). Where the term b_{ij} represents the general expression for each soil flexibility matrix coefficient.

$$\begin{aligned} s_{ij} =& \frac{P_j(1+\nu)}{8\pi E(1-\nu)}[\frac{3-4\nu}{R_1} + \frac{1}{R_2} + \frac{x^2}{R_1^3} + \frac{3-4\nu}{R_2^3}x^2 + \\ & \frac{2cz}{R_2^3}(1 - \frac{3x^2}{R_2^2}) + \frac{4(1-\nu)(1-2\nu)}{R_2+z+c}(1- \\ & \frac{x^2}{R_2(R_2+z+c)})] = b_{ij}P_j \end{aligned} \tag{5.50}$$

Pile-raft and soil-raft interactions

The raft is modelled as a thin plate discretized in blocks having a square or a rectangular shape and subjected to uniform shear stresses at each block. Cerutti's solution is adopted to model 'pile-raft' and 'soil-raft' interactions. Even in this case, the approximation suggested by Poulos is used, thus the soil elastic modulus introduced in the Cerutti's equation is the average value between the elastic modulus at the point where the displacement is evaluated and the elastic modulus at the point where the force is applied: $E = ((E_i + E_j))/2$.

The horizontal displacement ρ_{ij} at the point i belonging to the half-space caused by a load P_j applied at the point j along the raft-soil interface is given by Eq. 5.51 (see Figure 5.33).

$$\rho_x = \frac{P(1+\nu)}{2\pi ER}[1 + \frac{x^2}{R^2} + (1-2\nu)(\frac{R}{R+z} - \frac{x^2}{(R+z)^2})] \tag{5.51}$$

At the raft-soil interface the sliding mechanism will initiate when the shear stress at the interface exceeds a value defined by a simple frictional law (Eq. 5.52).

$$\tau_f = \sigma_n tan\delta \tag{5.52}$$

Where σ_n, in this simplified approach, can be defined after the vertical load analysis carried out following the procedure described in the next paragraph. δ is the angle of friction at the raft-soil interface, that in absence of specific information can be taken reasonably equal to 2/3 of the angle of internal friction of the shallower soil layer. Once reached the ultimate shear stress at a raft-soil interface block sliding starts and for the block in question the compatibility equation is removed.

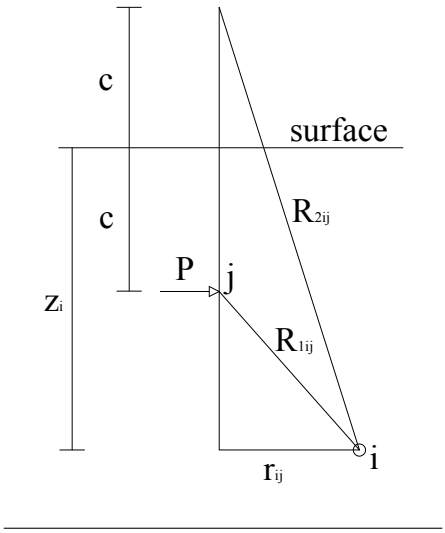

Figure 5.32: Mindlin solution scheme

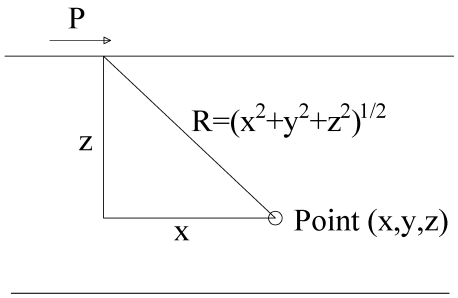

Figure 5.33: Cerutti's solution

Soil non-linear behaviour

Kondner (1963), Duncan and Chang (1970) and Hardin and Drnevich (1972) used hyperbolae to model shear stress-strain curves, with the tangent equal to G_{max} at zero strain and where the tangent is asymptotic to τ_{max} at infinite strain. By defining a reference strain ($\gamma_{ref} = \tau_{max}/G_{max}$) it is possible to rewrite the equation of a hyperbola as a normalized secant shear modulus (G_{sec}/G_{max}) that is reduced with a normalized shear strain (γ/γ_{ref})(Eq. 5.53).

$$\frac{G_{sec}}{G_{max}} = \frac{1}{(1 + \frac{\gamma}{\gamma_{ref}})} \tag{5.53}$$

On the other hand, Fahey and Carter (1993) adopted the formulations in Eq. 5.54 and Eq. 5.55 for the secant and the tangent elastic modulus reduction respectively.

$$\frac{G_{sec}}{G_{max}} = 1 - R_f(\frac{\tau}{\tau_{max}})^g \tag{5.54}$$

$$\frac{G_{tan}}{G_{max}} = \frac{(G_{sec}/G_{max})^2}{[1 - R_f(1-g)(\frac{\tau}{\tau_{max}})^g]} \tag{5.55}$$

These represent a quasi-hyperbolic relation written in terms of shear stress rather than shear strain, and employing an exponent g to adjust the shape of the curve. To model the non-linear behaviour of the soil, therefore, a modified version of the formulation proposed by Fahey and Carter (1993) was adopted. The vertical stresses (at the pile-soil interface points) are assumed not to vary during the horizontal load analysis, thus only the horizontal stresses change.

An analogy can thus be assumed between the 'interface pressure - ultimate soil resistance' ratio and the 'shear stress - maximum shear stress' ratio ($p/p_{ult} \sim \tau/\tau_{max}$). With this assumption, at each step of the analysis the value of the tangent elastic modulus is updated at each pile-soil interface point using Eq. 5.56.

$$\frac{G_{tan}}{G_{max}} = \frac{(G_{sec}/G_{max})^2}{[1 - R_f(1-g)(\frac{p}{p_{ult}})^g]} \tag{5.56}$$

In the proposed method, R_f is taken equal to 1, while the parameter g ranges between 0.25 and 1. The appropriate value for g, to perform the analysis, can be easily estimated by trying to obtain the best-fit with the load-deflection curve of a lateral load test on a single pile or with the load-deflection curve obtained with other available codes, like for example the commercial code LPILE (software for the analysis of single pile under horizontal loading based on p-y curves method), the open-source code OpenSees (that has been implemented with the p-y curves recommended by the American Petroleum Institute) or using the 'Hybrid BEM-p-y curve' method presented before.

The input data required for the soil, are: the elastic modulus E_{max} at small strain level (value that can be estimated starting from the maximum shear modulus G_{max} (SCPT or down-hole tests)), the Poisson's ratio, and the angle of internal friction (and the relative density D_R) or the undrained shear resistance, respectively in case of cohesionless or cohesive soil. The solving scheme, is typical of BEM methods, and requires the imposition of: a) compatibility equations between the soil and pile displacements and the raft and the soil displacements and b) local and global equilibrium equations to the translation and rotation.

Calculation of the ultimate lateral soil resistance profile

The p_{ult} values in the Eq. 5.56 can be evaluated using the following expressions.

Ultimate soil resitance for soft clay

For soft clays, the ultimate soil resistance per unit length of pile, can be computed using the smaller of the values given by the equations below (Matlock, 1970).

$$p_{ult} = [3 + \frac{\gamma'}{c_u}z + \frac{J}{b}z]c_u b \tag{5.57}$$

$$p_{ult} = 9c_u b \tag{5.58}$$

where γ' = average effective unit weight from ground surface to the depth z analysed; z = depth from the ground surface of the point investigated; c_u = shear strength at depth z; and b = width of the pile (= diameter). Matlock (1970) stated that the value of J was determined experimentally to be 0.5 for a soft clay and about 0.25 for a medium clay. A value of 0.5 is frequently used, thus will be used this value.

Ultimate soil resitance for stiff clay

For stiff clays, the ultimate soil resistance per unit length of pile, can be evaluated using the smaller of the value given by the equations below (Reese, Cox, and Koop, 1975):

$$p_{ct} = 2c_a b + \gamma' b z + 2.83 c_a z \tag{5.59}$$

$$p_{cd} = 11 c_u b \tag{5.60}$$

where c_a is the average undrained shear strength over the depth z.

Ultimate soil resistance for sand

For sands, the ultimate soil resistance per unit length of pile, can be computed using the smaller of the values given by the following equations (Reese, Cox, and Koop, 1974).

$$\begin{aligned} p_{st} =& \gamma z[\frac{K_0 z tan\phi sin\beta}{tan(\beta-\phi)} + \frac{tan\beta}{tan(\beta-\phi)}(b + z tan\beta tan\alpha) + \\ & K_0 z tan\beta(tan\phi sin\beta - tan\alpha) - K_a b] \end{aligned} \tag{5.61}$$

$$p_{sd} = K_a b\gamma z(tan^8\beta - 1) + K_0 b\gamma z tan\phi tan^4\beta \tag{5.62}$$

where ϕ = the friction angle, γ = the soil unit weight, b = pile diameter, $\alpha = \phi/2$, $\beta = 45 + \phi/2$, $K_0 = 0.4$ and $K_a = tan^2(45 - (\phi/2))$ (Note: use buoyant unit weight for sand below the water-table and total unit weight for sand above the water table).

5.3.3 Vertical load acting on the piled raft

In the proposed BEM method the lateral contribution offered by the raft in a piled raft system is activated when the raft is in contact with the ground and when a vertical load is applied over that. Currently, the method assumes that:

- the vertical load is applied prior to the lateral one;
- the vertical load distribution among piles and raft is evaluated using the PDR method concepts, this point is fully described in this section;
- the vertical load analysis is performed before and it is not coupled with the lateral load analysis. This means that the vertical load analysis is performed only to evaluate the vertical load distribution between raft and piles, and in particular the induced vertical stress at each pile-soil and raft-soil interface block;
- the vertical stress induced at each raft-soil interface element is the σ_n value used in the Eq. 5.52. This permits to compute the available shear resistance at each raft-soil interface block;
- the vertical stress induced at each pile-soil interface point, instead, is added to the vertical geostatic stress at the same interface-point depth. This permits to increase the ultimate soil lateral resistance at each pile-soil interface-point, computed using the expressions presented previously;
- the vertical load distribution between the raft and the piles is kept constant during the lateral load analysis.

The vertical load analysis to obtain the vertical load distribution between the pile group and the raft is performed using an improved version of the PDR method that can take also into account of the piled raft non-linear response. The original method is described in an extended way in Poulos (2000). This one combines the BEM-method proposed by Poulos and Davis (1980) with the method for the evaluation of the load sharing between the raft and the piles described in Randolph (1994). For this reason, it has been called PDR (from the initials of the names of the three authors).

The improved version of the PDR approach used here can be applied starting from the values of the raft stiffness (K_R), the raft bearing capacity ($Q_{R,lim}$), the pile-group

stiffness (K_G) and the single pile bearing capacity ($Q_{P,lim}$). Even the entire 'load-settlement' curve of the piled-raft foundation can be evaluated. The bearing capacity of the raft and of the single pile can be computed using the most common analytical expressions available in literature or if available using load test data. The raft stiffness and the pile-group stiffness are evaluated considering the pile-group and the raft separately, and the piles in the pile-group are assumed to settle of the same vertical displacement (as rigidly linked by a connecting structure). This means that all the piles in the group are subjected to different vertical loads. Once evaluated the raft and the pile group stiffness, a vertical load incremental analysis is performed, where the pile-group and raft work as two springs in parallel. The analysis is carried out in an incremental way because the non-linear response of both the raft and the pile group is considered.

The raft stiffness (K_R) is evaluated using the Mayne and Poulos (1999) method because can take into account of many factors affecting the raft stiffness in terms of influence factors. The raft stiffness can be computed starting from the following final form of the settlement equation:

$$w_{raft} = \frac{qdI_G I_F(1-\nu^2)}{E_0} \tag{5.63}$$

where: q = applied stress; d = diameter of the raft foundation or an equivalent diameter if the raft is square/rectangular; the equivalent diameter can be defined as: $d_{eq} = 2\sqrt{A_{raft}/\pi}$. Where A_{raft} is the area in plan of the actual raft; E_0 = value of the soil modulus directly beneath the raft (at z = 0); ν = Poisson's ratio; I_G = influence factor for a Gibson soil profile (soil modulus linearly variable with depth) for both rigid and flexible footings (Figure 5.34).

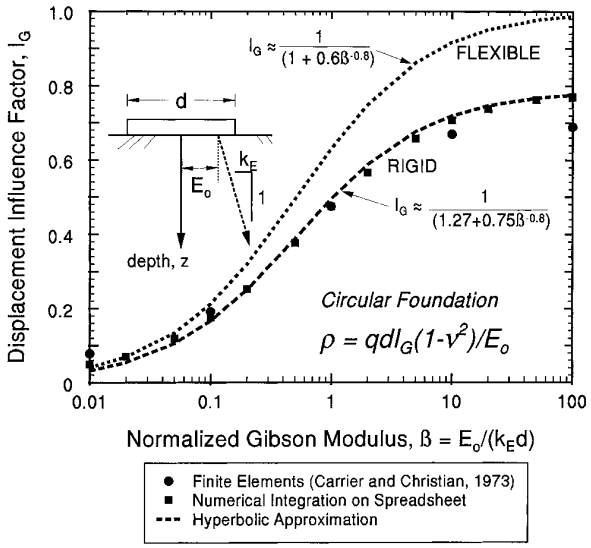

Figure 5.34: Influence factor for Gibson soil profile (Mayne and Poulos, 1999)

I_F = influence factor to consider the foundation flexibility (or rigidity) (Figure 5.35)

$$I_F \cong \frac{\pi}{4} + \frac{1}{(4.6 + 10K_F)} \tag{5.64}$$

where K_F is the foundation flexibility factor, defined in Mayne and Poulos (1999) as follows:

$$K_F \cong \frac{E_{fdn}}{E_{sAV}}(2t/d)^3 \tag{5.65}$$

where: d = foundation diameter; E_{fdn} = elastic modulus of foundation material; E_{sAV} = representative elastic soil modulus located beneath the foundation base (i.e. value of E_s at depth $z = 0.5D$); t = foundation thickness.

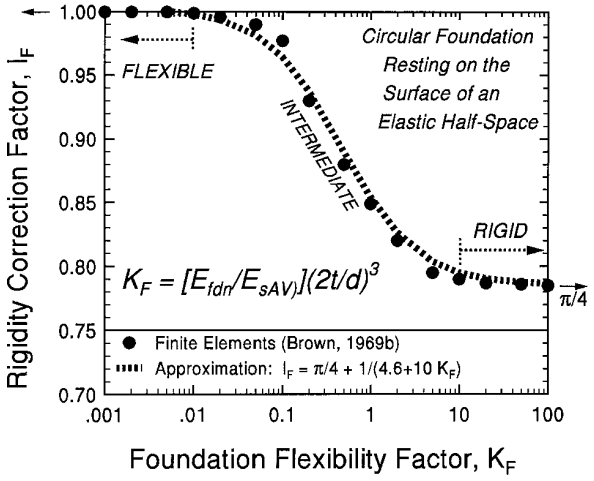

Figure 5.35: Effect of foundation rigidity on center-point settlement (Mayne and Poulos, 1999)

The pile-group stiffness (K_G), instead, can be evaluated using the well-known 'interaction-coefficients' approach (based on the BEM method primarily proposed by Poulos and Davis (1980)), which is a very reasonable compromise between ease of implementation, reduction in computation time and the goodness of the results.

Each interaction coefficient can be obtained studying a group of two identical, equally-loaded piles. The soil displacements may be equated to the pile displacements and the resulting system of equations solved.

The analysis of a two pile group is therefore identical to the single pile analysis, except that the soil-displacement matrix includes the influence of the second pile. The result of the above analysis is conveniently expressed in terms of an 'interaction coefficient' α.

$$\alpha_{ij} = \frac{\text{additional settlement caused by adjacent pile (j)}}{\text{settlement of pile under its own load (i)}} \tag{5.66}$$

Where the pile and the adjacent pile carry the same load. Solutions for α as a function of several variables are described in Poulos and Davis (1980). The 'pile-pile' interaction-coefficients (α_{ij}) have been applied only at the elastic component of the single pile settlement (computed considering a soil elastic modulus at small strain levels), and the non-linear component of the single pile settlement have been added using the 'interaction-coefficient' α_{ii}. The settlement w_i of the generic pile i can be expressed as:

$$w_i = w_{1,i}(Q_i\alpha_{ii} + \sum Q_j\alpha_{ij}) \tag{5.67}$$

where: $w_{1,i}$ = settlement of the single pile subjected to a unit load; Q_j = vertical load acting on the generic pile j.

The non-linear response is considered with an incremental analysis, following the suggestions of Caputo and Viggiani (1984), according to which the non-linearity is concentrated at the pile-soil interface, while the interaction between different elements (pile-pile, pile-raft and raft-soil) can be considered linear without any remarkable errors. It follows that, in an incremental analysis carried out using interaction-coefficients, all α_{ij} coefficients are kept constant, while the coefficients on the main diagonal of the global flexibility matrix are updated at each load increment according to the expression:

$$\alpha_{ii} = \frac{1}{(1 - \frac{Q_i}{Q_{P,lim}})^2} \tag{5.68}$$

The same concept is adopted also for the raft, this means that the raft stiffness is reduced at each load step of the incremental analysis dividing the initial raft stiffness K_R with the coefficient α_r:

$$\alpha_r = \frac{1}{(1 - \frac{Q_R}{Q_{R,lim}})^2} \tag{5.69}$$

in which Q_R is the vertical load acting on the raft at the previous load step and $Q_{R,lim}$ is the raft bearing capacity.

Finally, it is possible to define the entire 'load-mean settlement' curve (Figure 5.36) and to evaluate also the load distribution between the pile-group and the raft.

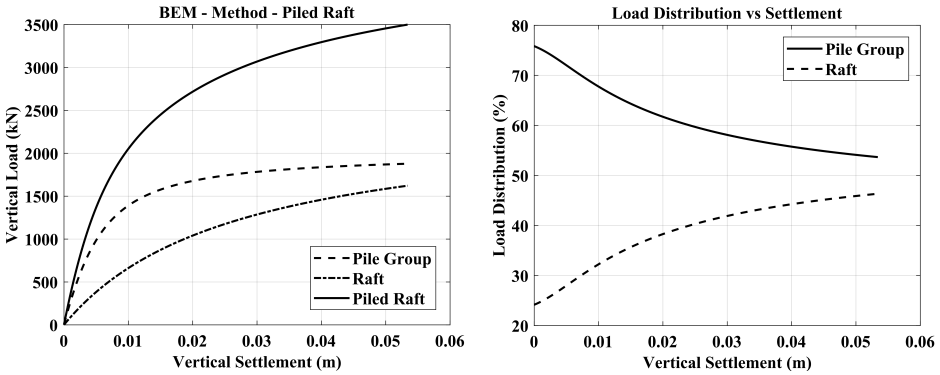

Figure 5.36: Load distribution between the raft and the pile group (using the improved PDR method)

Once computed the load transferred directly by the raft to the soil, the elastic-theory, and in particular the elastic solution for a uniform vertical load q (Poulos and Davis, 1974) acting on a rectangular area (solution beneath the corner of the rectangle having length l and width b), can be used:

$$\Delta\sigma_z = \frac{q}{2\pi}[tan^{-1}\frac{lb}{zR_3} + \frac{lbz}{R_3}(\frac{1}{R_1^2} + \frac{1}{R_2^2})] \tag{5.70}$$

where:

- $R_1 = \sqrt{l^2 + z^2}$;
- $R_2 = \sqrt{b^2 + z^2}$;
- $R_3 = \sqrt{l^2 + b^2 + z^2}$;

Equation 5.70 allows to evaluate the vertical stresses induced at each pile-soil interface point (Figure 5.37 in order to take into account of the influence of a vertical load, acting on a piled-raft foundation, on its response under horizontal loads.

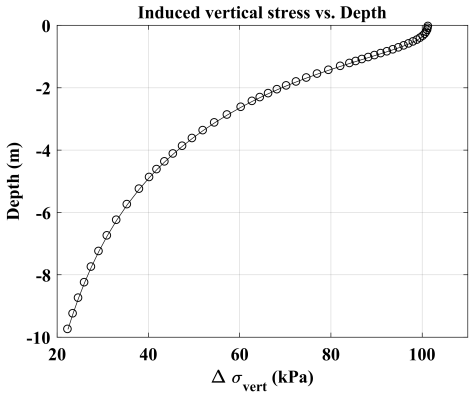

Figure 5.37: Vertical stresses induced at each pile-soil interface point

5.3.4 Pile group interaction (overlapping of soil passive wedges)

Experimental and numerical results revealed that for small spacing values the interaction between piles belonging to different rows cannot be studied only considering a non-linear reduction of the soil elastic modulus. This is because the movements of the front piles instantaneously cause an active state condition in the soil behind the shaft. This causes not only a reduction in the stiffness of the soil, responsible for the back piles response, but also a reduction in resistance. Therefore, the proposed simplified BEM method required of an approach to better capture the behaviour seen in FEM-analyses and in experimental data. The approach chosen, is similar to that proposed by Ashour et al. (2004) to permit the application of the so-called 'Strain Wedge Model' (SW) for pile groups analyses. In the latter work, the interaction among the piles in a group is determined based on the envisioned geometry of the developing passive wedge of soil in front of the pile in addition to the pile spacing. As shown in Figure 5.38, the soil passive wedge in front of a pile in the group overlaps horizontally with those of adjacent piles by an amount that varies with depth.

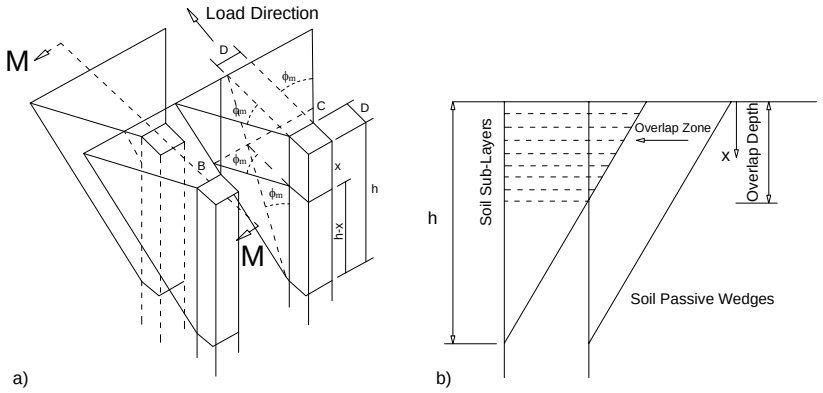

Figure 5.38: a) Mobilized passive wedges and associated pile group interaction; b) front overlap among soil sublayer in two adjacent passive wedges (section M-M) (Ashour et al, 2004)

The overlap of the wedges of neighbouring piles at depth x in different sublayers over the depth of the interaction is characterized as shown in Figure 5.39. According to classification of the piles in a group shown in Figure 5.39, the load carried by inner piles is less than the load carried by the outer piles in a given row. This behaviour was observed in several field tests. At a given depth (see Figure 5.39) overlapping areas exhibit larger values of soil strains and stresses compared to the isolated pile.

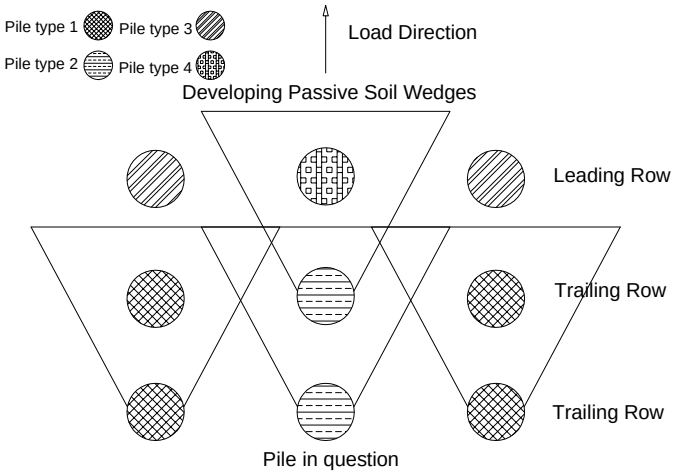

Figure 5.39: Horizontal (lateral and frontal) interaction for particular pile in pile group at given depth (Ashour et al, 2004)

The increase in the average soil stress attributable to the passive wedge of a given pile depends on the number and area of interfering wedges overlapping the wedge of the pile in question (Figure 5.40-a). The overlap of a uniform stress change is considered at the face of the passive wedge of the pile in question (Figure 5.40-b).

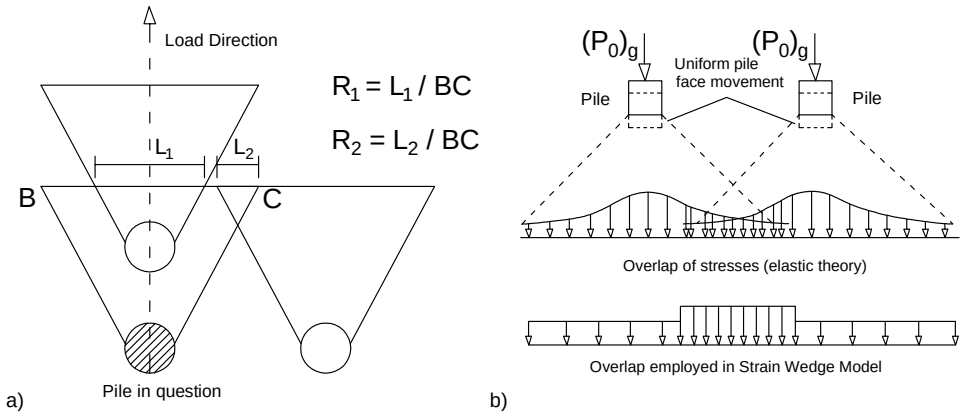

Figure 5.40: a) Overlapping ratios among piles in pile group and b) stress overlapping among piles in pile group (Ashour et al, 2004)

This overlap depends on the position of the pile in the group. Similar to the p-multiplier technique, the average stress level in a soil layer (SL_g) due to passive wedge interference is evaluated based on an empirical relationship (Eq. 5.71) which provides good agreement with field test results.

$$SL_g = SL_i(1 + \sum R_j)^{1.5} \leq 1 \tag{5.71}$$

Where j = number of neighbouring passive wedges in soil layer i that overlap the wedge of the pile in question; R = ratio between the length of the overlapped portion of the face of the passive wedge (L) and the total length of the face of the passive wedge (BC); and R_j is determined from all the neighbouring piles (sides and front piles) of the pile in question (Figure 5.39).

The SL_i value on the right-hand of Eq. 5.71, which represents the SL of the single isolated pile, for cohesionless soils in the Strain Wedge model, is defined in Eq. 5.72.

$$SL = \frac{\Delta\sigma_h}{\Delta\sigma_{hf}} = \frac{tan^2(45^\circ + \phi_m/2) - 1}{tan^2(45^\circ + \phi/2) - 1} \tag{5.72}$$

Where the horizontal stress change at failure ($\Delta\sigma_{hf}$) (or the deviatoric stress at failure in the triaxial test) is $\Delta\sigma_{hf} = \Delta\sigma_{v0}(tan^2(45^\circ + \phi/2) - 1)$. However, in the proposed method it is assumed that $SL_i = p/p_{ult}$, and thus:

$$\frac{p}{p_{ult}} = \frac{\Delta\sigma_h}{\Delta\sigma_{hf}} = \frac{tan^2(45^\circ + \phi_m/2) - 1}{tan^2(45^\circ + \phi/2) - 1} \tag{5.73}$$

The mobilized friction angle, ϕ_m, can be easily obtained if SL_i is known, which is assumed to be approximately equal to the ratio p/p_{ult}. The values of SL_g vary with depth and level of loading and can be used to evaluate the increased value of the pressure at each pile-soil interface (p_g) (where this increase is caused by the interferences of the passive wedges) with the equation Eq. 5.74 and Eq. 5.75.

$$SL_g = \frac{p}{p_{ult}}(1 + \sum R_j)^{1.5} \tag{5.74}$$

$$SL_g = \frac{p_g}{p_{ult}} \tag{5.75}$$

The value assumed by p_g at each pile-soil interface is then used to update the value of the tangent elastic modulus of the soil at each depth using Eq. 5.76.

$$\frac{G_{tan}}{G_{max}} = \frac{(G_{sec}/G_{max})^2}{[1 - R_f(1-g)(\frac{p_g}{p_{ult}})^g]} \tag{5.76}$$

For cohesive soils, on the other hand, is assumed to be in an undrained-condition (total stress). Consequently, the value of ϕ is equal to 0° and also the value of ϕ_m is always 0°. This means that the base angle of the passive wedge, for cohesive soils, is constantly equal to 45° and only the dimension in depth (and thus on the plain) of the passive wedge changes when the load increases. However, in this way, only the interaction between the wedge of a pile positioned in a row different from the front row with the wedge of the pile located in front of it can be considered, and thus the interactions between the wedges of piles belonging to the same row are neglected (Figure 5.41). To overcome this limit, and thus to consider the interactions between the wedges of piles located side by side, we consider the extreme case in which a row of piles has a relative spacing s/D equal to 1. In this condition, theoretically, the ultimate soil resistance profile should be coincident to the one in a retaining wall, given by the difference of the passive earth pressure and the active earth pressure in an undrained condition.

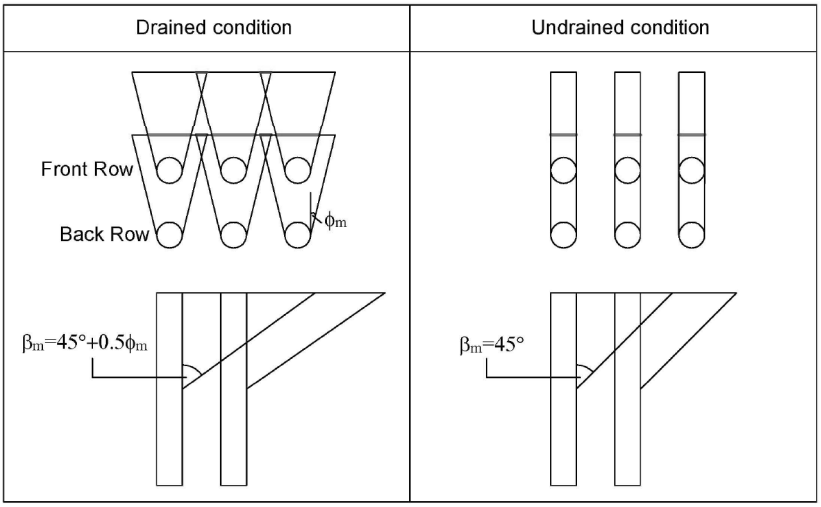

Figure 5.41: Pile group effect: shadowing modelling

In this case the active and passive soil pressure profiles (in terms of force per unit length) acting along the pile shaft are expressed by Eq. 5.77 and 5.78 respectively.

$$p_a(z) = (\sigma_{v0}(z) - 2c_u(z))D = (\gamma z - 2c_u(z))D \tag{5.77}$$

$$p_p(z) = (\sigma_{v0}(z) + 2c_u(z))D = (\gamma z + 2c_u(z))D \tag{5.78}$$

Note that the value of p_a, for shallow depths, could be negative and this means that the soil is in tension. Assuming reasonably that the soil cannot support tension all the values of $p_a < 0$ are corrected, and set equal to 0. The difference between p_p and p_a thus represents the ultimate soil pressure profile, p_r, (in terms of force per unit length) acting along a pile shaft in a row of piles having a spacing of 1D. For example, Figure 5.42 shows all these steps to define the resulting lateral pressure profile, p_r, considering a homogeneous cohesive soil with a constant c_u equal to 50 kPa, a soil unit weight γ equal to 20 kN/m^3 and a pile diameter D = 1 m.

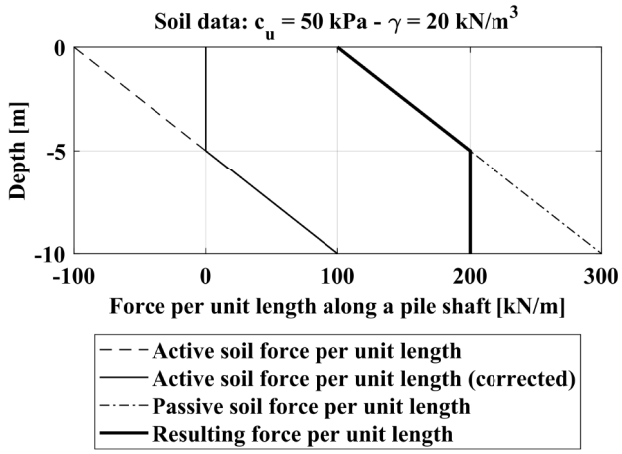

Figure 5.42: Soil pressure profile

The soil resistance profile is now considered, for the same soil condition shown before, as defined by Matlock (1970) for a single isolated pile in soft clay, and thus expressed by the minimum values of Eq. 5.79.

$$min[(3 + \frac{\gamma'}{c_u}z + \frac{J}{D}z)c_uD; 9c_uD] \tag{5.79}$$

Figure 5.43 compares the values of p_r (for a spacing of 1D) and p_{ult} (for a single isolated pile).

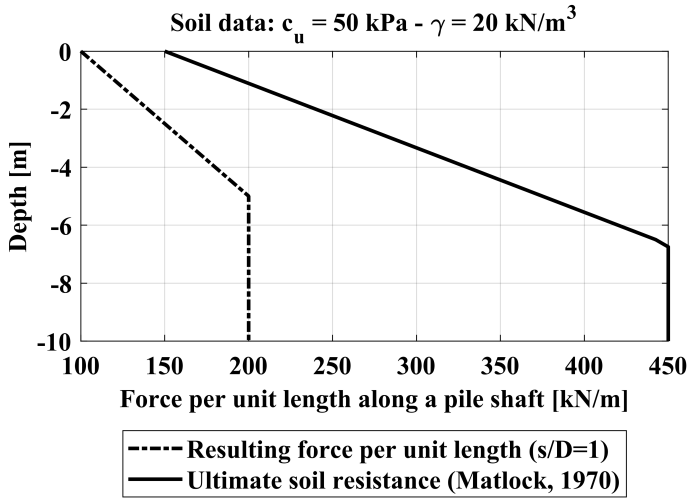

Figure 5.43: Resulting soil pressure profile

Based on all the experimental data studied, it is assumed that the ultimate soil resistance profile for the single isolated is valid only for pile spacing $s/D \geq 6$. For pile spacing ratio less than 6 it is considered that the ultimate soil resistance profile is intermediate to the profile p_r (assumed for spacing ratio $s/D = 1$) and the profile p_{ult} (assumed for spacing ratio $s/D \geq 6$).

To evaluate the definitive soil resistance profile ($p_{ult,def}$), for spacing ratio between 1 and 6, it is assumed that $p_{ult,def}$ can be expressed as a function of the actual spacing ratio s/D and the depth, z, using the relationship in Eq. 5.80.

$$p_{ult,def}(z) = p_r(z) + F(s/D)(p_{ult}(z) - p_r(z)) \tag{5.80}$$

Where, $F(s/D)$ is a factor defined as a function of the relative spacing ratio according to Eq. 5.81.

$$F(s/D) = \frac{s/D - 1}{5} \tag{5.81}$$

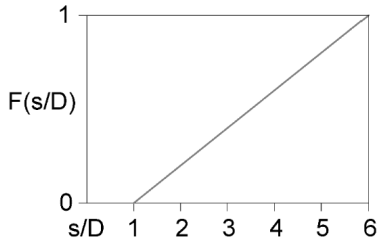

Figure 5.44: F(s/D) factor

With this procedure, even for cohesive soil in undrained condition, it is possible to consider the interactions between the piles located side by side, simply by substituting the ultimate soil resistance evaluated with the expressions defined by Matlock (1970) with the $p_{ult,def}$ values.

In the proposed approach (which is obviously different from the original method to consider pile group interaction in Ashour et al. (2004)), the mobilized soil passive wedge starts to develop at a depth, along the pile shaft, which is different from pile to pile, where the pressure at the pile-soil interface changes from a positive to a negative value, passing from a passive to an active state.

5.3.5 Rotational restraint of the pile-cap

The piled-raft tests studied in this work (Horikoshi et al., 2003; Matsumoto et al., 2010; Unsever, Matsumoto, and Ozkan, 2015; Hamada et al., 2015) and practically all the tests carried out in the past were realized on foundation systems that can be defined as 'small piled-raft' systems. These are piled-rafts where the pile length is bigger compared to the raft width. In practical applications these are adopted as foundation system when it is necessary to use piles not only to reduce settlement but even to improve the bearing capacity. In this case, in general, the raft can be considered rigid.

No significant experimental results, instead, are available in literature on 'large piled-raft' systems. These are piled-rafts where the piles are used only to reduce average settlement or to solve localized problem related to differential settlements. For this type of piled-raft, instead, the flexibility of the raft should be appropriately considered in the design process and in the analyses. Experimental works, thus, are needed on large piled-raft foundations in order to understand better the real influence of the raft flexibility on the response under combined vertical/lateral loading.

For this reason, the proposed BEM method can be considered appropriate for the analysis of 'small piled-rafts'. The raft, herein, is considered to be rigid. Moreover, the tests realized by Horikoshi et al. (2003), Matsumoto et al. (2010), Unsever et al. (2015) and Hamada et al. (2015) were carried out on piled-rafts with pile-heads having a hinged or a rigid connection.

During the lateral load tests in piled-raft 'hinged' it was observed, in general, that the vertical load distribution between the raft and the piles remained constant and that the rotation of the raft was negligible, thus the raft was simply moving along the direction of the horizontal load applied.

In the horizontal load tests in piled-raft 'rigid', instead, it was noted again that the vertical load distribution between the raft and the piles remained the same, but the raft, because of the rigid connection of the pile-heads, started to rotate. In this case, thus, the raft was moving and rotating during the lateral load tests, but keeping constant the vertical load sharing with the piles.

To take into account of this rotation (observed in these tests on piled-rafts, with piles rigidly connected to the raft) in the proposed method, it has been introduced a rotational stiffness of the pile cap. This rotational stiffness can be theoretically estimated (assuming: a) the raft as a rigid body and b) no significant variations on the vertical load distribution between the raft and the piles during the application of the horizontal load) starting from the evaluation of the axial stiffness of the piles in compression and of the piles in tension according to the simple formulation of Randolph and Wroth (1978) for an axially loaded pile. For the piles in compression the axial stiffness takes into account of both the shaft stiffness and the pile base stiffness, while for the piles in tension only the shaft stiffness is considered. Therefore, the following expressions can be used.

For pile in compression:

$$K_{\Delta c} = \frac{\Delta P_{base}}{\Delta y} + \frac{\Delta P_{shaft}}{\Delta y} = \frac{\Delta P_{tot,c}}{\Delta y} = \frac{4Gr_p}{(1-\nu)} + \frac{2\pi GL}{ln(\frac{r_m}{r_p})} \tag{5.82}$$

For pile in tension:

$$K_{\Delta t} = \frac{\Delta P_{shaft}}{\Delta y} = \frac{\Delta P_{tot,t}}{\Delta y} = \frac{2\pi GL}{ln(\frac{r_m}{r_p})} \tag{5.83}$$

Where:

- ΔP_{base}= variation of the axial load carried by the pile tip (or base);
- ΔP_{shaft}= variation of the axial load carried by the pile-shaft;
- G = average shear modulus of the soil along the pile shaft;
- $r_m = 2.5L(1-\nu)$ = 'magic radius' as defined by Randolph and Wroth (1978);
- r_p = pile radius;
- L = pile length;
- Δy = vertical displacement of the pile.

The rotation of the raft can be expressed as (Figure 5.45):

$$\Delta\theta = tan^{-1}\frac{\Delta y_i}{x_i - a} \tag{5.84}$$

The variation of the axial load for the pile i in compression beneath the raft can expressed, as:

$$\Delta P_c = K_{\Delta c}\Delta y_i \tag{5.85}$$

and for the pile i in tension as:

$$\Delta P_t = K_{\Delta t}\Delta y_i \tag{5.86}$$

Then, it is necessary to evaluate the position of the point of rotation of the rigid raft, by means of the following vertical equilibrium equation:

$$\sum_{i=1}^{n}[K_{\Delta c}(x_i - a)] - \sum_{i=1}^{n}[K_{\Delta t}(x_i - a)] = 0 \tag{5.87}$$

Once evaluated the position a of the point of rotation of the raft, the pile-cap rotational stiffness can be expressed as:

$$K_{M\theta} = \frac{\Delta M}{\Delta \theta} = \sum_{i=1}^{n} [K_{\Delta c}(x_i - a)^2] + \sum_{i=1}^{n} [K_{\Delta t}(x_i - a)^2] \tag{5.88}$$

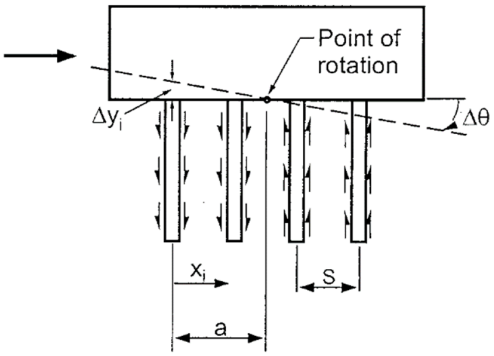

x_i = Distance from last row of trailing piles to center of pile i.
(x_i - a) = Distance from point of rotation to pile i.
S = Pile row spacing.

Figure 5.45: Scheme for the determination of the rotational stiffness of the raft (Mokwa and Duncan, 2003)

The rotational stiffness of the raft can be then used as a boundary condition for the pile-heads in the piled raft system. In particular, this value should be added in the rotational-equilibrium equations of the solution-system of the proposed method.

Obviously, this procedure is based on a very simplified evaluation of the axial stiffness of the pile in compression and in tension. In order to consider the interactions between the piles a full BEM method approach should be considered. Otherwise it can be used the approach suggested by Mokwa and Duncan (2003) in the evaluation of the axial stiffness of the pile in compression and of the pile in tension.

5.3.6 Non-linear solution procedure

The solution system is defined as: $[F][X] = [P]$. $[X]$ is the unknowns vector composed of $km + n + 2m + 2$ terms or $km + n + m + 2$ terms for free or fixed head conditions, respectively, where m is the number of piles, k and n are the number of pile blocks for each pile and the number of raft elements, respectively, p are the $km+n$ unknown pressures acting at the pile-soil and soil-raft interfaces, y_0 is the piled-raft displacement, θ_m are the m pile-heads rotations, H_m are the m horizontal loads at the pile-heads and H_{raft} is the horizontal load carried by the raft. $[P]$ is the known term vector, which has the same dimension as the vector $[X]$. $[F]$ is a $(km + n + 2m + 2)$ x $(km+n+2m+2)$ or $(km+n+m+2)$ x $(km+n+m+2)$ matrix, obtained by adding:

- the km x km pile flexibility matrix $[F_P]$, composed of the a_{ij} coefficients;
- the km x km flexibility matrix $[F_S]$, composed of the b_{ij} coefficients that represent the displacements induced by a load acting at the pile-soil interface j to the pile-soil interface i;

- the km x n flexibility matrix $[F_{RS}]$, composed of the c_{ij} coefficients that represent the displacements induced by a load acting at a raft-soil interface j to the pile-soil interface i;
- the n x km flexibility matrix $[F_{SR}]$, composed of the d_{ij} coefficients that represent the displacements induced by a load acting at the pile-soil interface j to the raft-soil interface i;
- the n x n flexibility matrix $[F_{RR}]$, composed of the e_{ij} coefficients that represent the displacements induced by a load acting at the raft-soil interface j to the raft-soil interface i.

Obviously, in the case of a pile group analysis, all the coefficients related with the raft-soil interface elements are not considered and the system is composed by the $[X]$ and $[P]$ vectors (having now $km + 2m + 1$ or $km + m + 1$ terms) and by the matrix $[F]$ ($(km + 2m + 1)$ x $(km + 2m + 1)$ or $(km + m + 1)$ x $(km + m + 1)$) obtained summing $[F_P]$ and $[F_S]$. The final $2m + 2$ or $m + 2$ (or $2m + 1$ and $m + 1$ in the case of a pile group) rows and columns, of the matrix $[F]$ are necessary to impose the local and global equilibrium and to complete the compatibility equations at each pile-soil and raft-soil interface node. In the Eq. 5.89, H is the horizontal load applied and f is the load eccentricity.

The flexibility matrix $[F]$ is updated at each step of the procedure, with the pile flexibility sub-matrix, $[F_P]$, that is updated only in case of a non-linear 'moment-curvature' relationship for the pile section. $[F_P]$ is updated using the tangent flexural rigidities of the section, according to the bending moments reached at each pile-node in the previous load increment. In addition, at each load step a check is carried out to determine whether the ultimate soil resistance at the pile-soil and at the raft-soil interfaces has been reached. When it happens at that node the compatibility equation is removed.

$$\begin{bmatrix}
a_{1,1}+b_{1,1} & \cdots & a_{1,km}+b_{1,km} & c_{1,1} & \cdots & c_{1,n} & -1 & -z_{1,1} & \cdots & \cdots & 0 & \cdots & 0 & 0 \\
\vdots & \ddots & \vdots & \vdots & \ddots & \vdots & \vdots & \vdots & \ddots & \vdots & \vdots & \ddots & \vdots & \vdots \\
a_{km,1}+b_{km,1} & \cdots & a_{km,km}+b_{km,km} & c_{km,1} & \cdots & c_{km,n} & -1 & \cdots & \cdots & -z_{km,m} & 0 & \cdots & 0 & 0 \\
d_{1,1} & \cdots & d_{1,km} & e_{1,1} & \cdots & e_{1,n} & -1 & 0 & \cdots & 0 & 0 & \cdots & 0 & 0 \\
\vdots & \ddots & \vdots & \vdots & \ddots & \vdots & \vdots & \vdots & \ddots & \vdots & \vdots & \ddots & \vdots & \vdots \\
d_{n,1} & \cdots & d_{n,km} & e_{n,1} & \cdots & e_{n,n} & -1 & 0 & \cdots & 0 & 0 & \cdots & 0 & 0 \\
1 & \cdots & 1 & 1 & \cdots & 1 & 0 & 0 & \cdots & 0 & 0 & \cdots & 0 & 0 \\
z_{1,1} & \cdots & \cdots & 0 & \cdots & 0 & 0 & 0 & \cdots & 0 & 0 & f & f & f \\
\vdots & \ddots & \vdots & \vdots & \ddots & \vdots & \vdots & \vdots & \ddots & \vdots & f & 0 & f & f \\
\cdots & \cdots & z_{m,km} & 0 & \cdots & 0 & 0 & 0 & \cdots & 0 & f & f & 0 & f \\
1_{1,1} & \cdots & \cdots & 0 & \cdots & 0 & 0 & 0 & \cdots & 0 & -1 & 0 & 0 & 0 \\
\vdots & \ddots & \vdots & \vdots & \ddots & \vdots & \vdots & \vdots & \ddots & \vdots & 0 & -1 & 0 & 0 \\
\cdots & \cdots & 1_{m,km} & 0 & \cdots & 0 & 0 & 0 & \cdots & 0 & 0 & 0 & -1 & 0 \\
0 & \cdots & 0 & 1 & \cdots & 1 & 0 & 0 & \cdots & 0 & 0 & \cdots & 0 & -1
\end{bmatrix}
\begin{bmatrix}
p_1^p \Delta_1 D \\ \vdots \\ p_{km}^p \Delta_{km} D \\ p_1^r \Delta_r^2 \\ \vdots \\ p_n^r \Delta_r^2 \\ y_0 \\ \theta_1 \\ \vdots \\ \theta_m \\ H_1 \\ \vdots \\ H_m \\ H_{raft}
\end{bmatrix}
=
\begin{bmatrix}
0 \\ \vdots \\ 0 \\ 0 \\ \vdots \\ 0 \\ H \\ fH \\ \vdots \\ fH \\ 0 \\ \vdots \\ 0 \\ 0
\end{bmatrix}
\tag{5.89}$$

Once the initial flexibility matrix has been calculated, the total horizontal load is applied in the first step of the solution procedure. At each generic load increment h_k, an iterative process is performed where two solutions are obtained, the first using h_k (full step) as the load increment, the second using two load steps equal to $h_k/2$ (two half step).

The solution scheme is described in Figure 5.46, which, for the sake of simplicity, refers to the explicit Euler method with step-doubling and adaptive step-size control. However, a fourth order Runge-Kutta method can also be used to obtain some improvement in the accuracy of the solution.

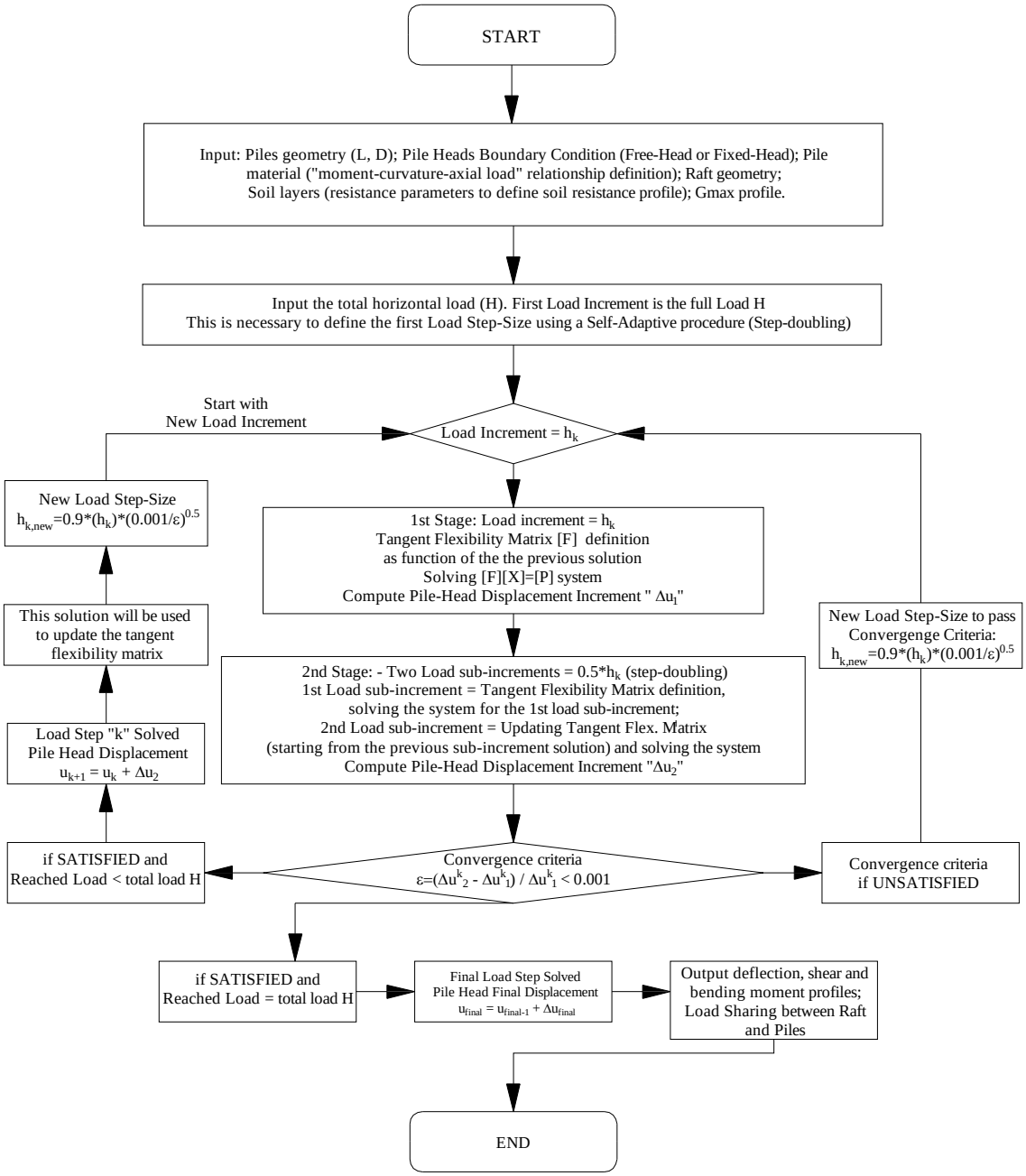

Figure 5.46: Flow-chart of the proposed non-linear adaptive step size method

Once these two solutions have been computed, the incremental ratio (ε), is computed according to Eq. 5.90.

$$\varepsilon = \frac{\Delta u_2 - \Delta u_1}{\Delta u_1} \tag{5.90}$$

where Δu_1 and Δu_2 are the incremental displacement at the pile-head evaluated using one and two steps, respectively. The ε value is compared with a predefined tolerance taken equal to 0.001 (Figure 5.47). When this converge criterion is exceeded, the iterative process starts again with an updated load increment h_k^{new} which should be able to achieve the desired accuracy. h_k^{new} can be estimated using the Eq. 5.91.

$$h_k^{new} = SFh_k(\frac{tol}{\varepsilon})^{\frac{1}{p+1}} \tag{5.91}$$

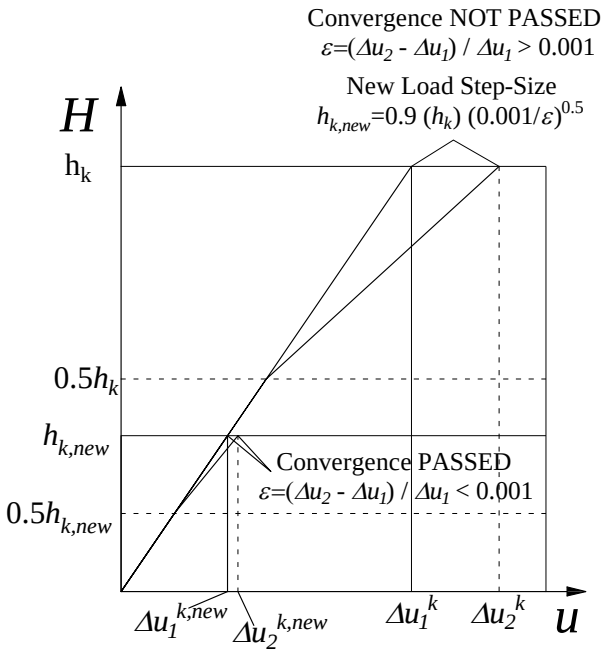

Figure 5.47: Adaptive step-size control

Chapter 6

Validation of the developed methods

In the case histories studied, the soil input parameters used to perform the analyses (with the proposed methods) were or data provided directly by the authors or data obtained using the set of correlations for the interpretation of in-situ tests (CPT, SPT) presented in the next paragraph.

In addition, the elastic modulus used as an input is a Young Modulus at small strain levels E_{max}, that can be obtained starting with the G_{max} (Shear Modulus at small strain levels) value, using the elastic relationship: $E = 2G(1 + \nu)$. For the centrifuge-test case histories (Remaud, Garnier, and Frank, 1998; McVay, Casper, and Shang, 1995), instead, the G_{max} values was obtained using the formulation:

$$G_{max} = 625F(e)(OCR)^k(p_a)^{1-n}(\sigma'_m)^n \tag{6.1}$$

Where:

- $F(e)$ = is a function of the void ratio – Jamiolkowski et al. (1991) suggested: $F(e) = 1/e^{1.3}$;
- OCR = is the overconsolidation ratio;
- k = an overconsolidation ratio exponent that in the case histories has been set to 0;
- p_a = the atmospheric pressure;
- $\sigma'_m = (\sigma'_1 + 2\sigma'_3)/3$;
- n = a stress exponent that has been taken equal to 0.5.

6.1 Interpretation of the in-situ test data

In this work, for the interpretation of the in-situ test data (CPT and SPT tests) the correlations listed in Table 6.1 and in Table 6.2 were used.

Table 6.1: Set of correlations - CPT data

Correlations	Author
$\phi' = arctan[0.1 + 0.38log_{10}(\frac{q_t}{\sigma'_{v0}})]$	(Robertson and Campanella, 1983)
$\phi' = 17.6 + 11log_{10}(\frac{q_t - \sigma_{v0}}{\sqrt{\sigma'_{v0} p_a}})$	(Mayne, 2006)
$\phi' = 16D_R^2 + 0.17D_R + 28.4$	(API, 2007)
$D_R = -98 + 66log_{10}[\frac{q_t}{\sqrt{\sigma'_{v0}}}]$	(Jamiolkowski, 1985)
$D_R = (\frac{q_t/p_a}{305\sqrt{\sigma'_{v0}/p_a}})$	(Kulhawy and Mayne, 1990)
$G_0 = q_t 1634(\frac{q_t}{\sqrt{\sigma'_{v0}}})^{-0.75}$ (Sand)	(Rix and Stokoe, 1992)
$V_s = 1.75(q_t)^{0.627}$ (Clay)	(Mayne and Rix, 1995)
$OCR = 0.37(\frac{q_t - \sigma_{v0}}{\sigma'_{v0}})^{1.01}$	(Mayne and Kemper, 1988)
$c_u = \frac{q_t - \sigma_{v0}}{N_k}$	

Table 6.2: Set of correlations - SPT data

Correlations	Author
$N_{SPT} = (17 + 24(\frac{\sigma'_{v0}}{p_a}))D_R^2$	(Gibbs and Holtz, 1957)
$D_R = 1.5(\frac{N_{SPT}}{0.65(\sigma'_{v0}/p_a)^2 + 16.8(\sigma'_{v0}/p_a) + 14})^{0.222} - 0.6$	(Gibbs and Holtz, 1957)
$D_R = 0.21\sqrt{\frac{N_{SPT}}{\frac{\sigma'_{v0}}{p_a} + 0.7}}$	(Meyerhof, 1957)
$D_R = \sqrt{\frac{C_N N_{SPT}}{60}}$	(Skempton, 1986)
$\phi' = 27.1 + 0.3C_N N_{SPT} - 0.00054(C_N N_{SPT})^2$	(Wolff, 1989)
$\phi' = arctan[\frac{N_{SPT}}{12.2 + 20.3(\sigma'_{v0}/p_a)}]^{0.34}$	(Kulhawy and Mayne, 1990)
$c_u = f_1 N_{SPT}$	(Stroud, 1974)

6.2 Single piles

This section shows the prediction results of the single pile responses using the proposed Hybrid BEM - py curves method. The solutions obtained with the analyses are compared with the experimental results observed in lateral load tests on single piles both in coarse soils (sand and gravel) and cohesive soils (clays and silts) and both in steel pipes and reinforced concrete piles. The experimental results refer to well-documented lateral load tests found in literature (a total of 22 case histories for single pile analyses, Table 6.3).

Table 6.3: Case histories studied: Single piles

Case study	Pile material	Diameter D (m)	Length L (m)	Soil type	H_{max} (kN)
(Brown, Reese, and O'Neill, 1987)	Steel w/GF	0.273	13.11	OC Clay	92.7
(Brown, Morrison, and Reese, 1988)	Steel w/GF	0.273	13.11	Sand	133.5
(Cox, Reese, and Grubbs, 1974)	Steel pipe	0.61	21	Sand	263.4
(Dunnavant and O'Neill, 1989)	Steel	0.273	11.8	Clay	116.8
(Dunnavant and O'Neill, 1989)	Steel	1.22	11.4	Clay	1074.7
(Huang and Hsueh, 2001)	Bored RC	1.5	34.9	Sand	2945.7
(Khalili-Tehrani et al., 2014)	Drilled RC	0.6	11.68	OC Clay	104.7
(Mandolini and Viggiani, 1992)	Multiton	0.457	17.5	Clay	119.8
(Mandolini and Viggiani, 1992)	Multiton	0.406	17.5	Clay	119.9
(Matlock, 1970)	Steel-pipe	0.319	12.8	Clay	105.0
(McVay, Casper, and Shang, 1995)	Aluminium	0.43	13.3	Sand	109.5
(McVay, Casper, and Shang, 1995)	Aluminium	0.43	13.3	Sand	134.1
(Ng, Zhang, and Nip, 2001)	Bored RC	1.5	30	Sand	2950.4
(Portugal and Sêco e Pinto, 1993)	Drilled RC	1.20	40	Clay	300.74
(Price and Wardle, 1981)	Steel-pipe	0.406	16.5	Clay	100.0
(Price and Wardle, 1987)	Drilled RC	1.50	12.5	Sand	2394.1
(Remaud, Garnier, and Frank, 1998)	Aluminium	0.72	12	Sand	804.7
(Reese, Cox, and Koop, 1975)	Steel-pipe	0.641	15.2	Clay	596.7
(Reese and Welch, 1975)	Drilled RC	0.762	12.8	Clay	443.5
(Rollins, Peterson, and Weaver, 1998)	Steel w/GF	0.305	8.7	Clay	178.3
(Rollins, Lane, and Gerber, 2005)	Steel-pipe	0.324	11.5	Sand	112.3
(Rollins et al., 2006)	Steel-pipe	0.324	11.9	Clay	210.8

The aim of the analyses is to validate the proposed method. They are conducted not as a back-analysis but as a class A prediction, directly using the actual pile mechanical and geometrical properties and the soil strength and stiffness parameters according to the interpretation of the in-situ and laboratory tests data.

The results obtained highlight the possibility of providing a good forecast of the most representative aspects (pile-head displacement and rotation and maximum bending moment) of the single pile response.

Figure 6.1 shows a comparison between measured and computed results. In these plots, the ratio between the measured horizontal load for a given displacement level (y/D) and the measured maximum lateral load during the test (H_{max}) is on the x-axis, while the ratio between the computed and the measured load at the same displacement level is on the y-axis. The error in the load prediction at each displacement level reached during the tests is generally included in a range of $\pm 20\%$.

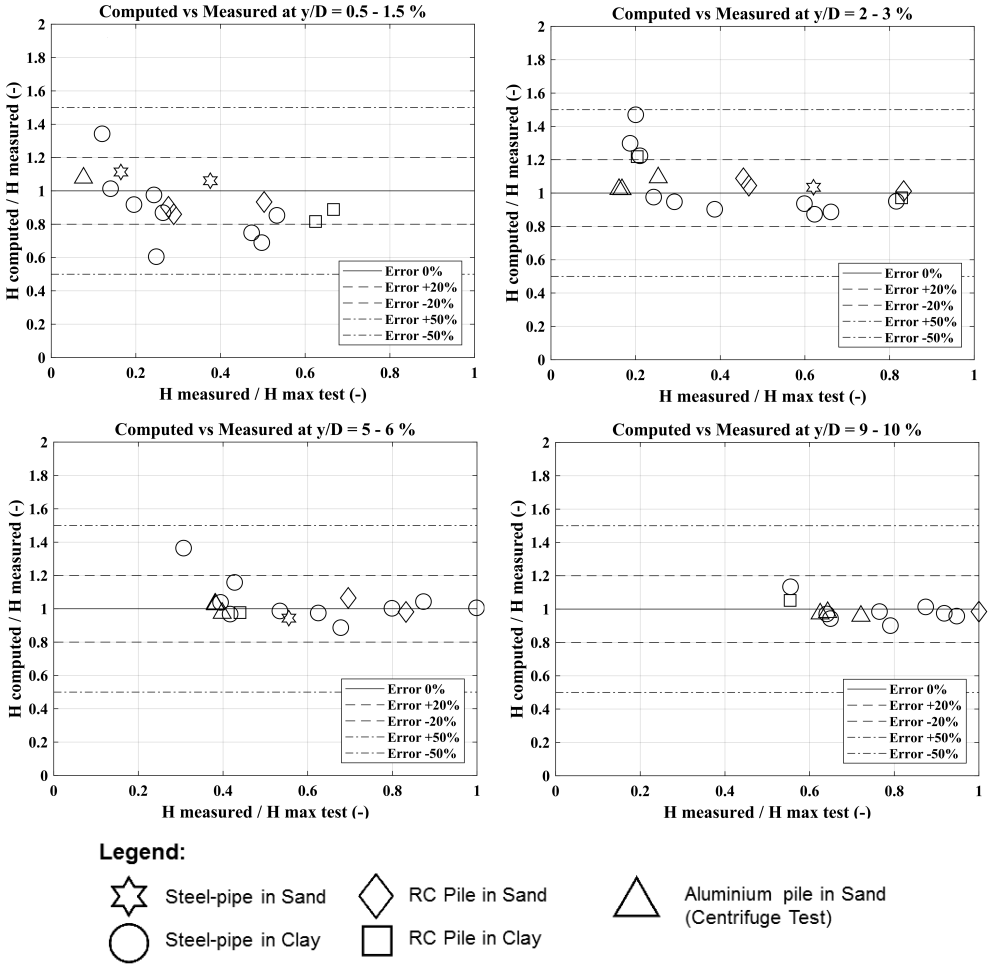

Figure 6.1: Single pile - Comparison between computed and measured load at different displacement levels y/D

6.2.1 Analysis results of a specific case study

A full-scale test program (Huang and Hsueh, 2001), set up in Taiwan, is discussed and described here to show the capability of the Hybrid BEM - py curves method with all its features to predict the single pile response under lateral load. Two pile groups, one consisting in bored piles and the other in driven piles, were subjected to horizontal loading tests. The tests were also conducted on single piles installed using the same two techniques. The response of the groups is described in the next section.

Soil conditions and pile properties

In order to evaluate the effects induced by the installation technology on the soil properties, the in-situ tests were conducted before and after installing the pile-groups. Before installation, eight boreholes and eight SPT tests were performed, up to a depth of 80 m below the ground level (G.L.). Three CPT tests and DMT tests were also conducted. The two CPT tests included the measurement of the shear wave velocity (SCPT). After installing the piles, but before the load tests, three DMT and three CPT tests were carried out.

A comparison of the results obtained highlighted the most evident effects of the installation on soil properties occurring within the first 15 m of depth. The soil at the

site, on the basis of samples and laboratory tests, was generally classified as silty sand (SM in the USCS classification) or silt (ML), with occasional layers of silty clay (CL). The water table was located at approximately 1 m below the ground level, and did not vary significantly during the tests. Figure 6.2 shows the CPT, SPT and the shear modulus, G_{max}, profile.

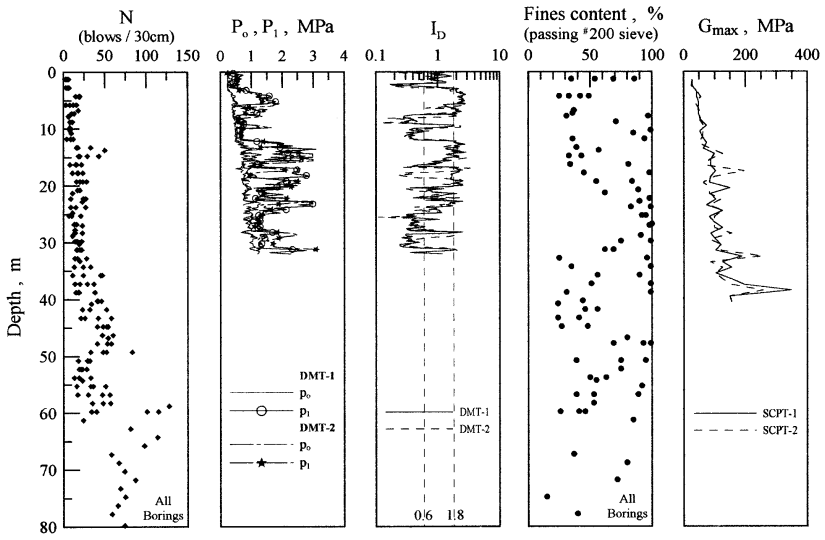

Figure 6.2: Cone Penetration Test (CPT), Standard Penetration Test (SPT) and Seismic CPT Data – Huang et al. 2001

The single bored pile had a diameter D equal to 1500 mm, a length, L, of 34.9 m and an intact flexural rigidity, E_pI_p, equal to 6.86 GNm^2. The strain guages and inclinometers were connected to the longitudinal reinforcement bars. Pile properties are summarized in Table 6.4.

Table 6.4: Structural properties of bored pile (Huang et al., 2001)

Pile diameter D (mm)	1500
Pile length (m)	34.9
Cross sectional area (cm^2)	17672
Reinforcement yield stress f_y (MPa)	471
Steel ratio ρ_s	0.025
Intact flexural rigidity $EI(GNm^2)$	6.86

Single bored pile B7: analysis results

Since the soil unit weight values of the site were not reported in the article of Huang and Hsueh (2001), it was assumed a $\gamma = 18.5\ kN/m^3$. Along the depth of interest, approximately equal to the first 15 meters, corresponding to 10 pile diameters, the mean tip resistance was approximately 5 MPa. The mechanical properties of the pile used in the analysis were the same as those indicated in Table 6.4. Figure 6.3 presents the average moment-curvature relationship used in the analysis and computed using the model that considers also the tension stiffening.

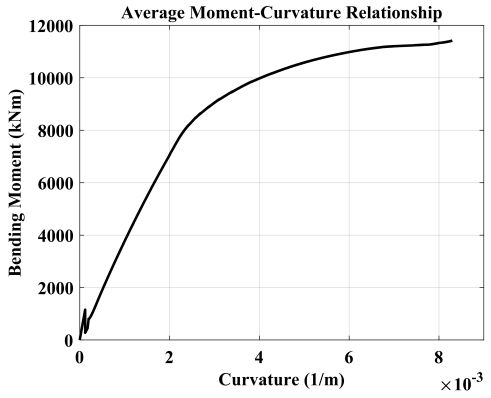

Figure 6.3: Computed average 'bending moment - curvature' relationship for B7 pile section

On the basis of the data provided by the CPT tests, a friction angle ϕ' of $34°$ was used, obtained with the correlation proposed by Mayne (2006).

$$\phi' = 17.6 + 11 \cdot log_{10}(\frac{q_t - \sigma_{v0}}{\sqrt{\sigma'_{v0} p_a}}) \tag{6.2}$$

The shear modulus profile at small strain levels was that provided by the authors in the SCPT data (Figure 6.2), but was simplified in the analysis, and thus a G_{max} profile linearly increasing from 15 to 150 MPa was adopted. The Poisson ratio was taken as equal to 0.35, thus E_{max} linearly increased from 40 to 400 MPa. The non-linear p-y curve adopted, to model the near field soil response, was that proposed by Reese, Cox, and Koop (1974).

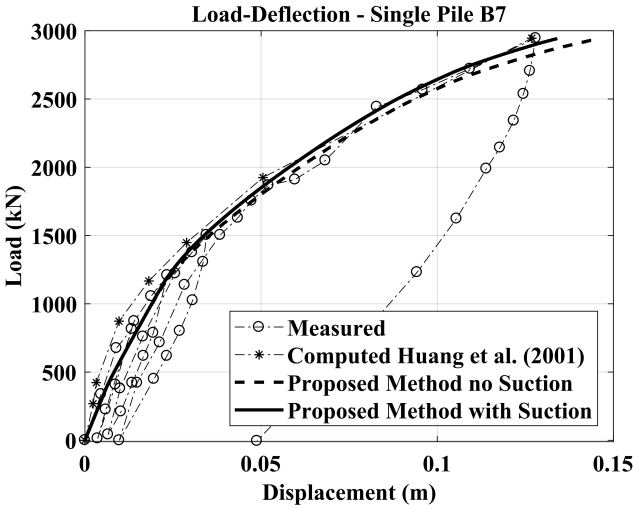

Figure 6.4: Comparison of measured, computed by Huang et al. (2001) and with the proposed method 'Lateral Load vs Head Deflection curve'

Since the water table was located 1 meter below the ground surface, approximate suction effects were considered, because of the lack of information to use the MK-Model rigorously, thus increasing the vertical effective soil stresses at the first meter in depth. In fact, a linearly increasing suction value was assumed from 0 to 10 kPa starting from one meter depth up to the ground surface.

This results in an increase in the ultimate pile-soil interface pressure, computed using the relationships suggested by Reese, Cox, and Koop (1974), only in the first meter depth. Figure 6.4 compares the measured and computed load-deflection curves.

Pile deflection profiles versus depth are shown (computed and measured) for three different lateral load values at the pile-head, considering suction in Figure 6.5 and without suction in Figure 6.6. The agreement is good in both cases however considering suction, there was an improvement in the prediction of the measured data.

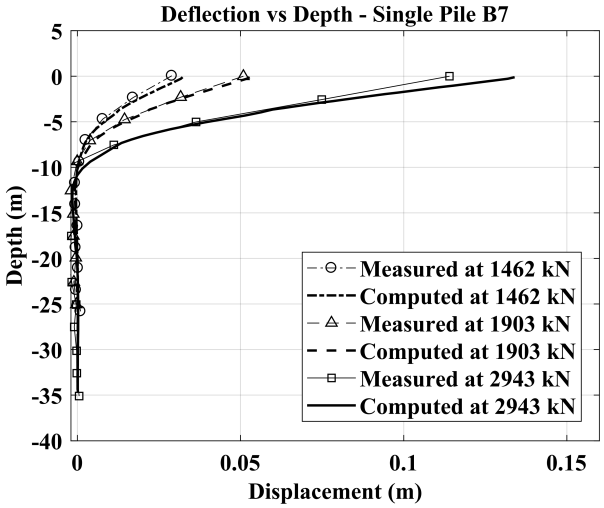

Figure 6.5: Pile deflections versus depth for B7 single pile under various load levels: Computed data obtained considering suction

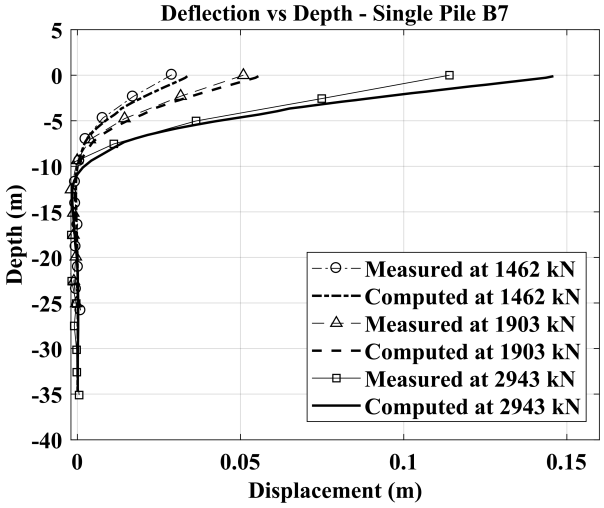

Figure 6.6: Pile deflections versus depth for B7 single pile under various load levels: Computed data obtained without considering suction

In addition, Figure 6.7 shows the computed bending moments profile versus depth for various load values. Note that the authors identify the load of 1462 kN as the value at which corresponds the beginning of cracking in the concrete, and therefore there is a progressive decrease in the flexural rigidity E_pI_p.

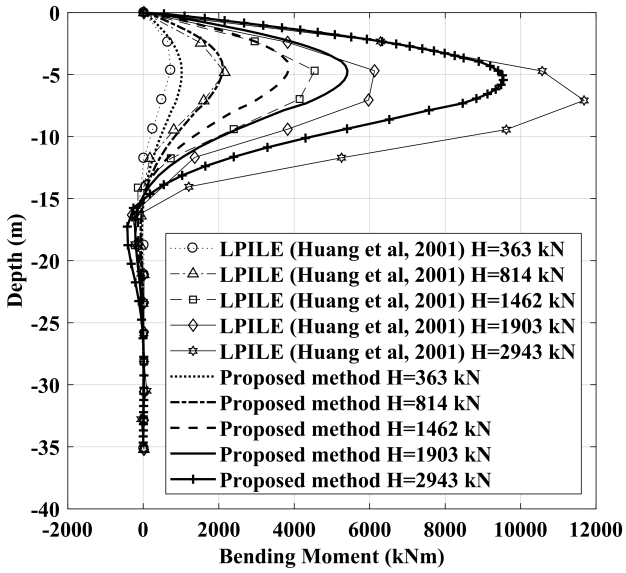

Figure 6.7: Computed bending moments of B7 single pile at various load levels

Huang and Hsueh (2001) and more recently Wu, Finn, and Dowling (2015) thus assigned a reduced flexural rigidity to the relevant section of this pile in order to simulate cracking. The reduced values of E_pI_p were necessary in both cases to obtain a suitable match between the analyses and the data measured during the tests.

The software used in these two studies were LPILE version 4.0 (p-y curves code, (Reese and Wang, 1993)) and VERSAT-P3D (a quasi-3D-FEM, (Wu, 2006)), respectively. The proposed Hybrid BEM - py curves method, instead, automatically updates the flexural rigidity along the pile shaft according to the bending moment - curvature relationship, computed on the basis of the geometrical and mechanical properties of the pile section.

6.3 Pile groups

This section shows the prediction results of the pile-group responses using the proposed BEM-method. The solutions obtained with the analyses are compared with the experimental results observed in lateral load tests on pile-groups both in coarse soils (sand and gravel) and cohesive soils (clays and silts) and both in steel-pipes and r.c. piles. The experimental results refer to well-documented load tests found in literature (a total of 15 case histories for pile-group analyses, Table 6.5). The number of piles in the group is generally rather small (the largest field test studied is on a 15 piles group). In all the examined cases, a load test on a single pile was also available. The aim of the analyses is to validate the proposed computational model. They are conducted again not as a back-analysis but as a class A prediction, directly using the actual pile mechanical and geometrical properties and the soil strength and stiffness parameters according to the interpretation of the in-situ and laboratory tests data.

Table 6.5: Case histories studied: Pile groups

Case study	Pile material	Diameter D (m)	Length L (m)	Soil type	H_{max} (kN)
(Brown, Reese, and O'Neill, 1987) 3x3-3D	Steel w/GF	0.273	13.11	OC Clay	695
(Brown, Morrison, and Reese, 1988) 3x3-3D	Steel w/GF	0.273	13.11	Sand	808.5
(Huang and Hsueh, 2001) 3x2-3D	Bored RC	1.5	34.9	Sand	11043
(McVay, Casper, and Shang, 1995) $\phi = 34°$ -3x3-3D	Aluminium	0.43	13.3	Sand	761.2
(McVay, Casper, and Shang, 1995) $\phi = 39°$ -3x3-3D	Aluminium	0.43	13.3	Sand	1508.2
(McVay, Casper, and Shang, 1995) $\phi = 34°$ -3x3-5D	Aluminium	0.43	13.3	Sand	1110.5
(McVay, Casper, and Shang, 1995) $\phi = 39°$ -3x3-5D	Aluminium	0.43	13.3	Sand	1424
(Remaud, Garnier, and Frank, 1998) 2x1-2D	Aluminium	0.72	12	Sand	1183
(Remaud, Garnier, and Frank, 1998) 2x1-4D	Aluminium	0.72	12	Sand	1220.1
(Remaud, Garnier, and Frank, 1998) 2x1 6D	Aluminium	0.72	12	Sand	1030.72
(Rollins, Peterson, and Weaver, 1998) 3x3-3D	Steel w/GF	0.305	8.7	Clay	927.05
(Rollins, Lane, and Gerber, 2005) 3x3-3D	Steel-pipe	0.324	11.5	Sand	488.6
(Rollins et al., 2006) 3x3-5.65D	Steel-pipe	0.324	11.9	Clay	1407
(Rollins et al., 2006) 3x4-4.4D	Steel-pipe	0.324	11.9	Clay	1353.8
(Rollins et al., 2006) 3x5-3.3D	Steel-pipe	0.324	11.9	Clay	1942.5

It needs to be remembered that (as explained in the description of the proposed BEM method) in the analyses of pile-groups the value of the exponent g of the elastic modulus reduction curve has to be defined. The appropriate g value to be considered can be easily estimated trying to obtain the best-fit with the load-deflection curve of the horizontal test on a single pile or with the load-deflection curve obtained with the 'Hybrid BEM-py curve' approach.

Figure 6.8 shows the comparison between measured and computed results. In these plots, the ratio between the measured horizontal load for a given displacement level (y/D) and the measured maximum lateral load during the test (H_{max}) is on the x-axis, while the ratio between the computed and the measured load at the same displacement level is on the y-axis. The error in the load prediction at each displacement level reached during the tests is included in a range of $\pm 30\%$.

The results obtained have shown the possibility of providing a really good prediction of the most representative aspects (pile-head displacement and rotation and maximum bending moment) of the pile-group response. The calculation program correctly reproduces all the typical aspects of the response of piles in a group, as the shadowing effect, so the load distribution between different pile rows is captured.

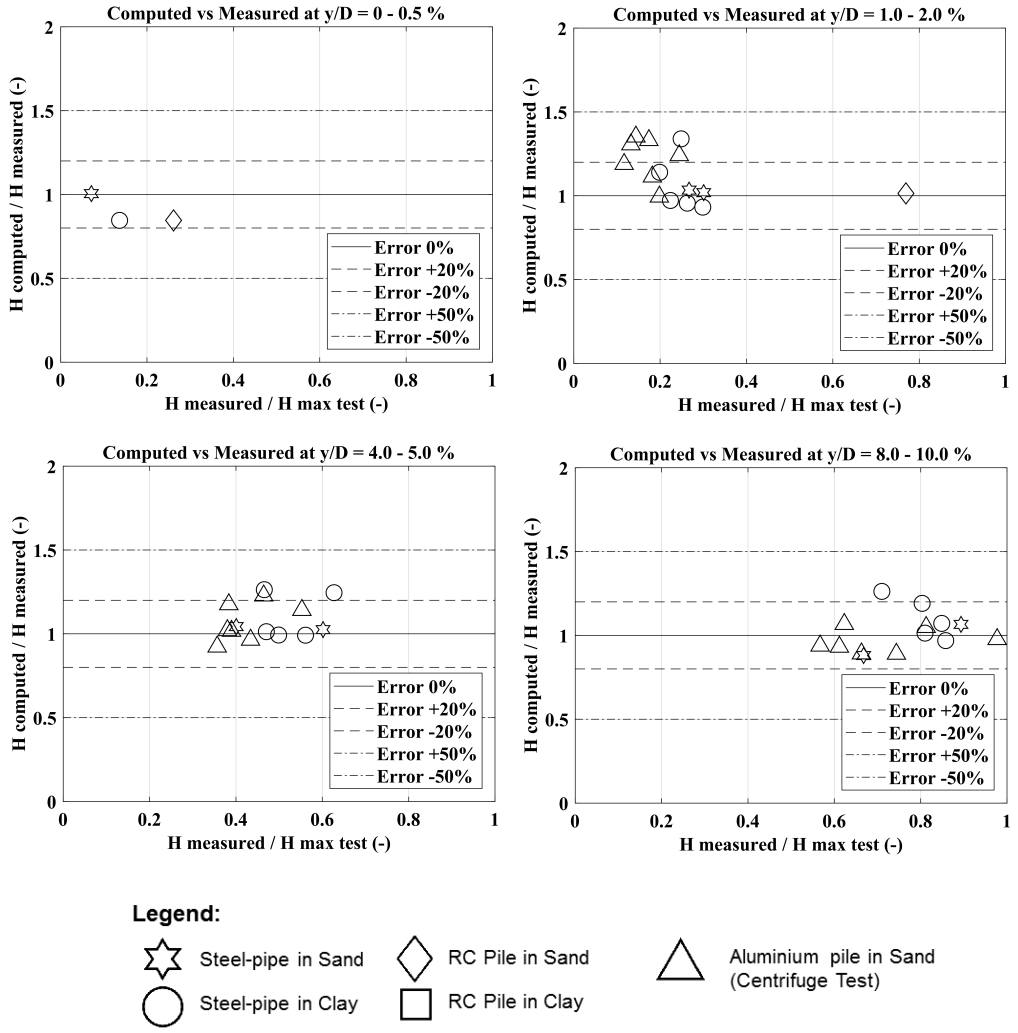

Figure 6.8: Pile groups - Comparison between computed and measured load at different displacement levels y/D

6.3.1 Analysis results of two specific case studies

Case study n.1: Huang et al. (2001)

The full-scale test program (Huang et al, 2001) carried out in Taiwan was presented before for the validation of Hybrid BEM - py curves method. Two pile-groups, one consisting of bored piles and the other consisting of driven piles, were subjected to horizontal loading test. Here are presented the analysis results, using the proposed BEM-method for pile groups, that refer to the bored pile-group. The soil condition are shown in Figure 6.2.

In the site were placed, 13 cast-in-situ bored piles. Eleven of the 13 bored piles (D = 1500 mm, L = 34.9 m; E_pI_p = 6.86 GNm^2) were realized using bentonite-mud with reverse circulation. Bored pile properties are summarized in Table 6.4. The fixed-head pile group was a 3x2 pile group (3 pile rows) and the pile spacing ratio (s/D) was equal to 3.

Since the soil unit weight values of the site were not reported in the article of Huang et al. (2001), for silty sands, it was assumed a unit weight γ equal to 18.5 kN/m^3. On the basis of the data provided by CPT tests a friction angle ϕ' of 34° was

used, obtained using the correlation proposed by Mayne (2006). The 'bending moment - curvature' relationship shown in Figure 6.3 was used in the analysis. The comparison between measured and computed results for the fixed-head pile group are shown in Figure 6.9, in Figure 6.10 and in Figure 6.13. In Figure 6.10 the group efficiency in the pile-group analysis results is defined as: $H_{group}/(nH_{single})$. Where, H_{group} = the total horizontal load in the pile group, H_{single} = the horizontal load in the single isolated pile (at the same displacement level) and n is the number of piles in the group. Figures 6.11 and 6.12 show the computed 'Load - Deflection' and 'Maximum Moment - Load' curves for each pile-row.

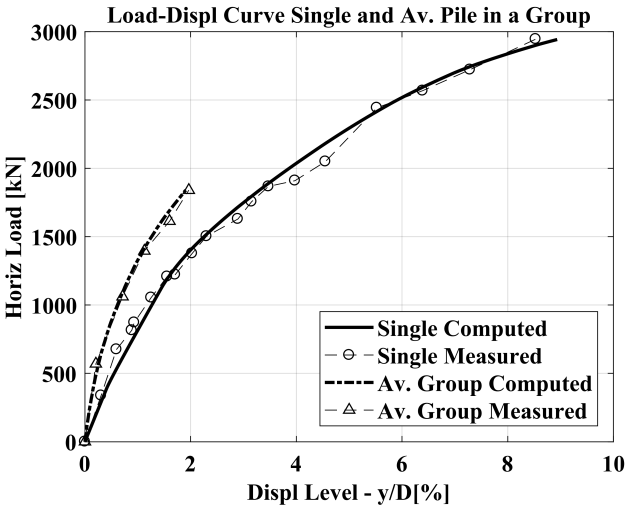

Figure 6.9: Computed vs measured: 'Load-Deflection' curves

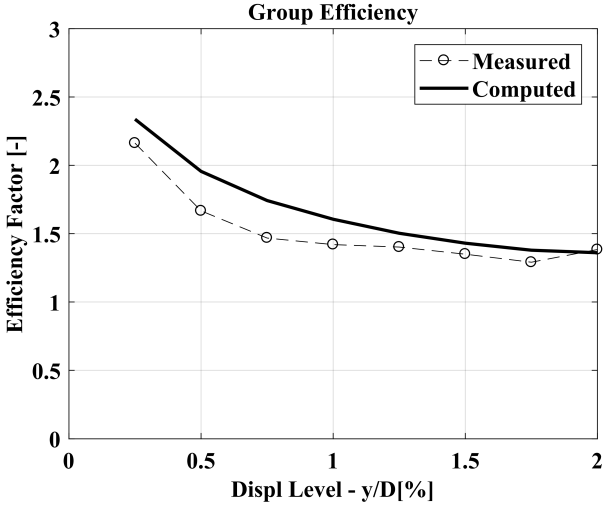

Figure 6.10: Computed vs measured: Pile Group Efficiency

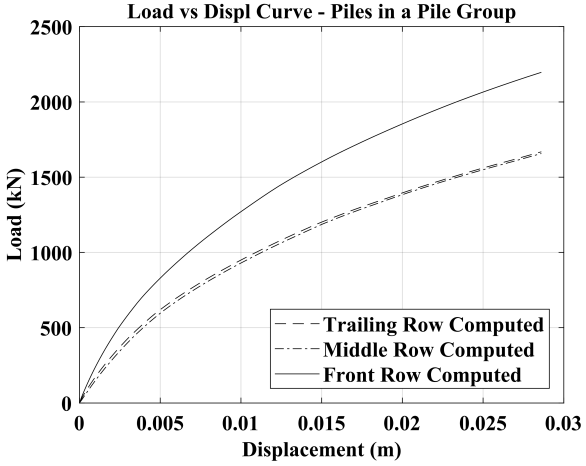

Figure 6.11: Computed 'Load - Deflection' curves of piles in different rows

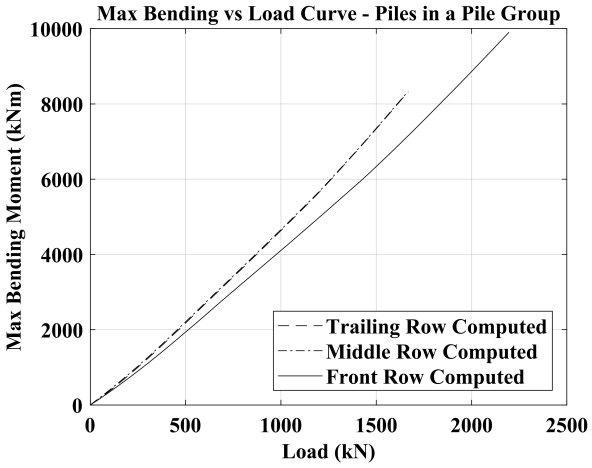

Figure 6.12: Computed 'Maximum Moment - Load' curves of piles in different rows

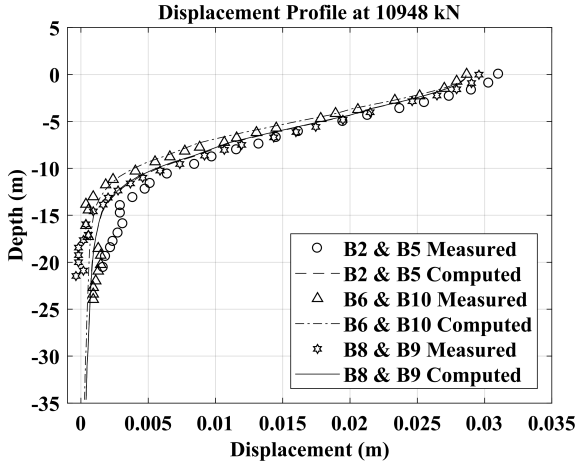

Figure 6.13: Computed vs measured deflection profiles at H=10948 kN of piles B2, B5, B6, B8, B9, B10

Case study n.2: Rollins et al. (2005)

The tests were conducted as part of a research program aimed to the evaluation of the single pile and pile-groups behaviour under horizontal loads in liquefied sands. It was also investigated, for comparison purposes, the piles response before the soil liquefaction. The test layout is shown in Figure 6.14.

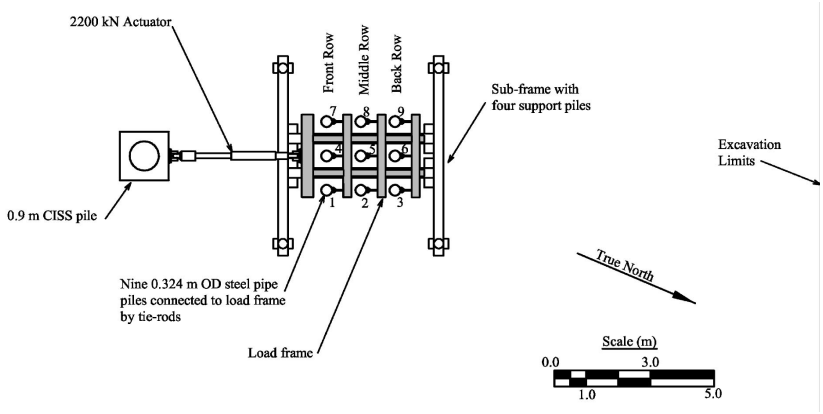

Figure 6.14: Test layout (Rollins et al., 2005)

The test was performed on the artificial island of Treasure Island, located in the San Francisco Bay. The site consisted of soil deposited by sedimentation and native sands up to a depth of about 6 m. This depth refers to the new ground level because, prior to the tests, was removed a layer having a thickness of 1.2 m. The filling consisted of loose-fine sands or silty sands. Silty sand and mud were arranged below the layers of sand. The sands were classified as SP - SM according to the USCS classification system. In Figure 6.15 the soil profile is presented.

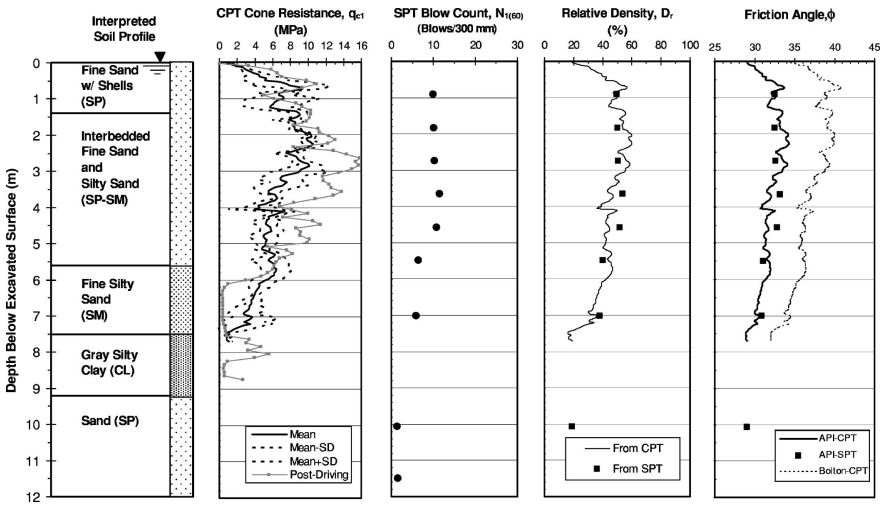

Figure 6.15: Soil profile (Rollins et al., 2005)

SPT and CPT tests were performed. A CPT test was carried out after the driving of the pile-group. On average the tip resistance values, q_c, obtained with CPT tests after the driving of the pile-group are 1.56 times higher than those obtained before the piles installation. These results are also shown in Figure 6.15. The $(N_1)_{60}$ (number

of normalized blows) value was about 10 in the clean sands and about 7 in the layer underlying the silty sands.

During the test conducted on the single pile, the water table was located at 0.5 m below the ground level. The pile-group test was carried out with the water table at 0.1 m below the ground level.

Soil characterization

According to the profile shown in Figure 6.15, the soil was composed (along the pile shaft) by 4 soil layers: 1) clean fine sands (up to a depth of 5.60 m); 2) fine silty sands (up to a depth of 7.50 m); 3) grey silty clays (up to 9.20 m); 4) sand (at higher depth). The authors provided the soil unit weight values adopted in their analyses for the layers mentioned: for sandy layers: $\gamma' = 10.3kN/m^3$ (buoyant unit weight, or effective unit weight) and $\gamma = 19.5kN/m^3$ (soil unit weight). For the clays: $\gamma' = 9.5kN/m^3$. To capture the pile response to horizontal loads the most significant layer was basically the first.

Pile properties

The pile was a steel-pipe driven open-ended up to a depth of 11.5 meters below the ground level. The outer diameter was 0.324 m and the wall thickness 9.5 mm. The pile was internally filled with the soil starting from the depth of 5.5 m onwards. The yield strength of the steel was of 404.6 MPa. The moment of inertia of the section was $1.16 * 10^8\ mm^4$, that became equal to $1.43 * 10^8\ mm^4$ considering the angle iron arranged to protect strain gauges, useful for the measurement of bending moments.

The strain gauges were placed at 17 different depths, with a spacing of 0.38 m up to 2.54 m in depth, and with a spacing of 0.76 m below. A further transducer was placed near the pile-tip.

On the single pile, the test was conducted in displacement control. The actuator was controlled by a servo-electro valve and an electrohydraulic pump. The maximum displacement was of 38 mm, with an increase of loads of 9 mm/s. This was a test mode in which the loads were applied very quickly. The movements were measured with spring potentiometers attached to independent references. Load cells measured the applied force. The load was applied with an eccentricity of 0.69 m.

Analysis results

The analyses were carried out using, for the pile, the geometrical and mechanical properties provided by the authors. For the soil properties, the indications derived from the interpretation of CPT tests were considered more reliable than those derived from SPT tests. It was therefore assigned to the first soil layer an angle of internal friction of $40°$. Completely irrelevant was the characterization of the underlying layers. The comparison between measured and computed results are shown in Figures 6.16, 6.17 and 6.18 in terms of load-deflection curves, group efficiency and load-deflection curves for each pile-row, respectively. Figure 6.19 shows the computed 'Maximum Moment - Load' curves for each pile-row.

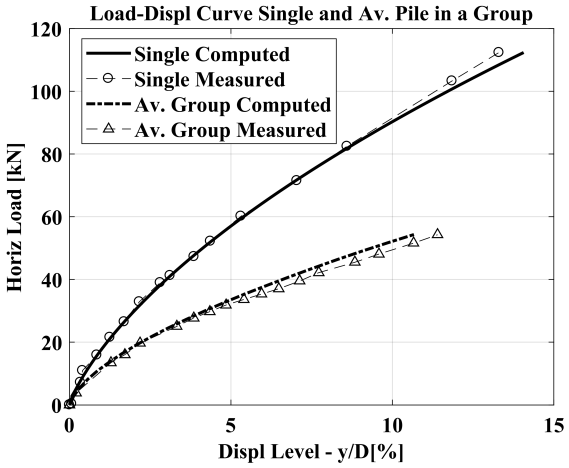

Figure 6.16: Computed vs measured load-deflection curves

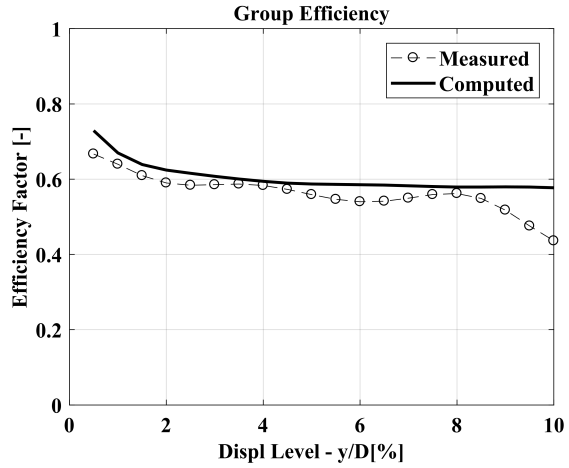

Figure 6.17: Computed vs measured group efficiency

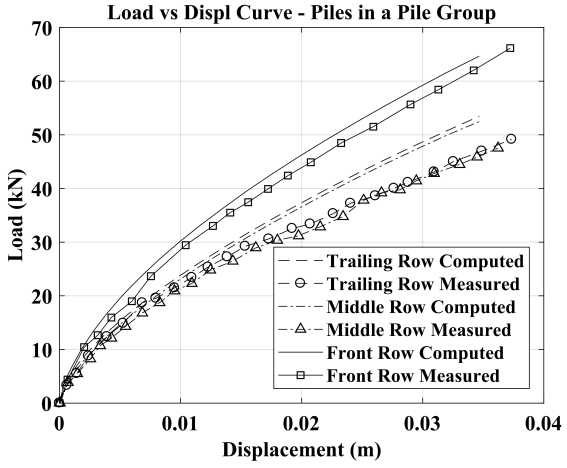

Figure 6.18: Computed vs measured load-deflection curves of average piles in different rows

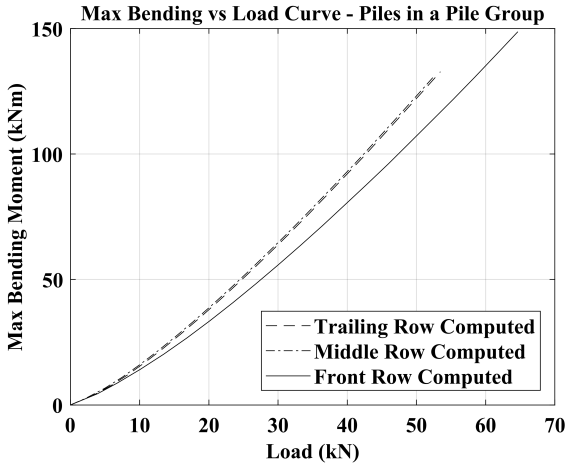

Figure 6.19: Computed maximum bending moment-load curves of average pile in different rows

6.4 Piled rafts

This section shows the prediction results of piled raft responses using the proposed BEM-method. The solutions obtained with the analyses are compared with the experimental results observed in lateral load tests on piled-rafts in coarse soils (centrifuge and $1-g$ tests). The experimental results refer to well-documented load tests found in literature (a total of 6 case histories for piled-raft analyses). In all the examined cases, a load test on a single pile was also available.

The aim of the analyses is to validate the proposed method. The analyses were conducted again not as a back-analysis but as a class A prediction, directly using the actual pile mechanical and geometrical properties and the soil strength and stiffness parameters according to the interpretation of the laboratory tests data provided by the authors. As for the pile-groups analyses it needs to be remembered that the value of the exponent g of the elastic modulus reduction curve has to be defined. The appropriate g value to be considered can be easily estimated trying to obtain the best-fit with the load-deflection curve of the horizontal load test on a single pile or with the load-deflection curve obtained with the 'Hybrid BEM-py curve' approach.

The results obtained show the potential of the model to provide a really good prediction of the most representative aspects (displacements, rotations and maximum bending moments) of the pile-groups in the piled-raft system. The calculation program correctly reproduces all the typical aspects of the response of the piled raft that in this case is affected not only by the well-known group effects and soil non-linear behaviour but even by all the interactions between all the components of the foundation system and by the vertical load acting on the raft. It should be highlighted, in particular, the capability of the proposed method to capture the load distribution between the piles in the group and the raft.

6.4.1 Horikoshi et al. (2003) - Sand ($D_R = 60\%$) - Centrifuge 50g

A series of static loading tests were conducted vertically and laterally on piled raft models and their components (single piles and rafts alone) on sand by using a geotechnical centrifuge. The effects of the rigidity at the pile head connection on the piled raft behaviour were in particular investigated.

In this study all the models (single piles, rafts alone and piled rafts) were loaded in separate tests. The centrifuge used in this study has an effective radius of 2.65 m and a centrifugal acceleration of 50g was applied to a 1/50 model. A rigid box with a length of 700 mm, a width of 400 mm and a height of 700 mm was used. Teflon sheets were attached to the side-walls to reduce the wall friction.

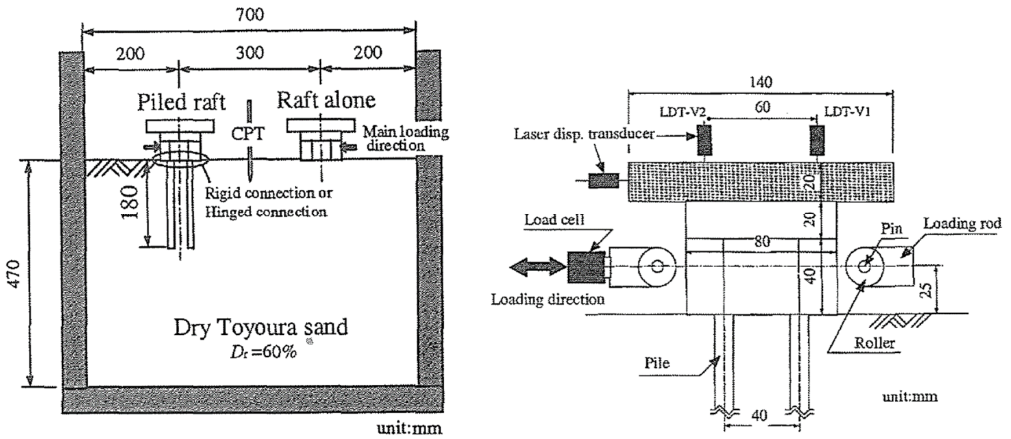

Figure 6.20: Centrifuge package and horizontal loading system (Horikoshi et al., 2003)

Soil characterization

Air-pluviated dry Toyoura sand was used in this study, having the properties summarised in Table 6.6. The relative density reached was about 60% after applying the centrifugal acceleration of 50g (before starting with the horizontal test).

Table 6.6: Properties of the model ground (Horikoshi et al.,2003)

Density of soil particle, ρ_s (t/m^3)	2.661
Maximum dry density, $\rho_{d,max}$ (t/m^3)	1.654
Minimum dry density, $\rho_{d,min}$ (t/m^3)	1.349
Median grain size, D_{50} (mm)	0.162

A series of triaxial consolidated drained shear tests (CD) were carried out with soil specimens having D_R = 95% and D_R = 65%, because also a 1g-model was studied by the authors, where the Toyoura sand had a relative density of 95%.

These triaxial CD tests were conducted using 4 different confining pressures (50, 100, 200, 300 kPa) and it was essential to carry out the triaxial tests at very low stress levels such as 5, 10 or 20 kPa, since the stresses at pile tip level was 2.78 kPa, but it was very difficult for the authors to conduct these tests because of the available equipment. For this reason, the stress dependency of the shear modulus, G, at very low stress levels was extrapolated from the test results at relatively high stress levels. The angle of internal friction, ϕ', was obtained as 45 degrees.

It was seen that the normalised deviatoric stress versus shear strain (divided by $\sqrt{p_0}$) converge on a unique line in both cases D_R = 95% and D_R = 65%. This result means that the shear stiffness of Toyoura sand at a given shear strain is proportional to the square root of the confining pressure (p_0). From the initial tangential gradient

of each curve, the initial shear modulus was estimated as $G_0 = q/\gamma$. The measured values of G_0 are closely fitted by the lines expressed in this form:

$$G_0 = G_{ref}(\frac{p}{p_{ref}})^{0.5} \tag{6.3}$$

Where p_{ref} is a reference value of confining pressure (= 100 kPa) and G_{ref} is the value of G_0 at $p = p_{ref}$. The value of G_{ref} are 29.16 MPa and 21.08 MPa for D_R = 95% and D_R = 65% respectively.

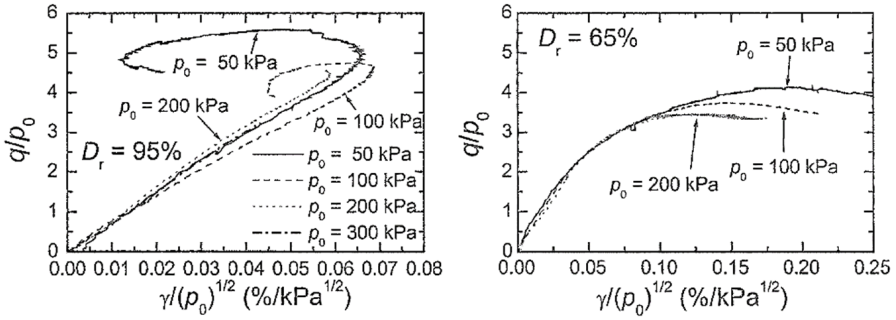

(a) D_r = 95% (b) D_r = 65%

Nomalised deviator stress versus shear strain obtained from CD tests of Toyoura sand

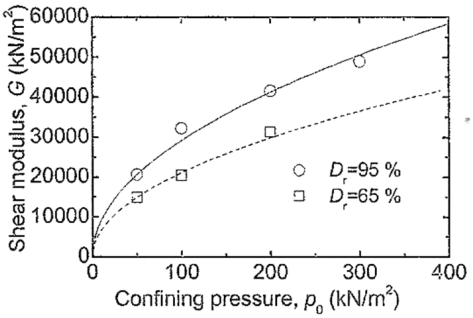

Shear modulus versus confining pressure, together with the fitting line

Figure 6.21: Triaxial CD tests results (Horikoshi et al., 2003)

Pile and raft properties

Square aluminium raft with width of 80 mm (4 meters at prototype scale) was used. The vertical load was applied by using a raft mass in the horizontal loading tests. The model pile was an aluminium pipe with an outer diameter of 10 mm, an inner diameter of 8 mm and a total embedded length of 180 mm. The pile toe was closed by using an aluminium plate. The pile was instrumented with foil strain gauges to measure axial forces and bending moments. The properties of the model and prototype pile are summarised in Table 6.7. The model pile is approximately equivalent to a solid concrete pile with a diameter of 500 mm at prototype scale. It was confirmed that the pile stress was below the yield stress in the majority of the loading tests. The material yield stress was 149 MN/m^2 and the failure stress was 243 MN/m^2. In this paper, the pile head connections were set at in the two extreme conditions: rigid and hinged.

Table 6.7: Properties of model pile and corresponding prototype pile (Horikoshi et al., 2003)

Item	Centrifuge model	Prototype
Material	Aluminium	Concrete
Outer diameter, D (mm)	10	500
Wall thickness, t (mm)	1	Solid
Length, L (mm)	180	9000
Cross sectional rigidity, EA (GN)	0.002	5.0
Bending rigidity, EI (GNm^2)	$2.0*10^{-8}$	0.13
Young's modulus E (GN/m^2)	71	41.7

The Figure 6.22 show the design of piled raft model with hinged pile head connections.

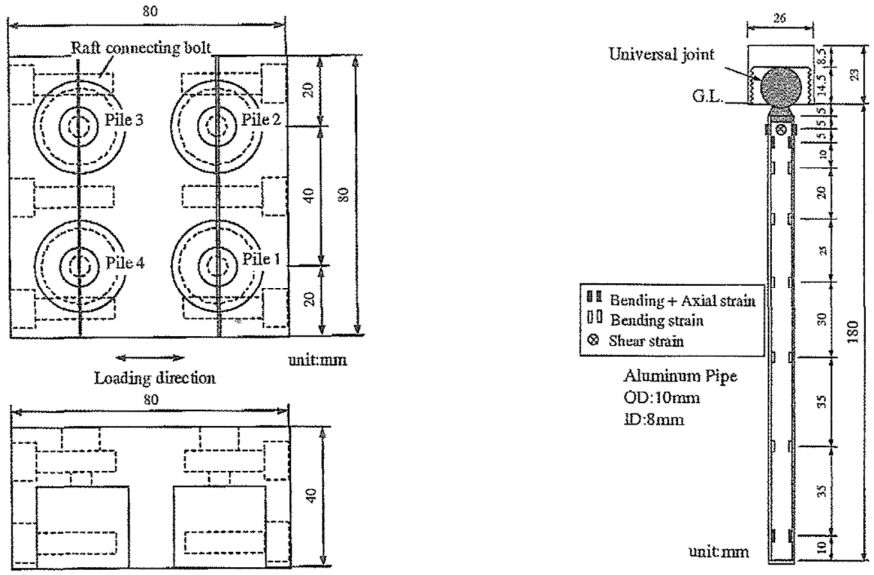

Figure 6.22: Design of model raft and pile for hinged pile head connection (Horikoshi et al., 2003)

Commercially available universal joint (THK Corp. type TBS8) was attached at each pile head. The joint can rotate in any direction with essentially negligible resistance. The degree of the pile head rigidity of the pile head connection model was examined by a separate loading test, and it was confirmed that the pile head was substantially rigid. The raft designed for piled raft models consisted of 3 separable aluminium plates, which enabled the raft to be connected to the piles after the first flight allowing for the self-weight settlement of the soils. The raft base was roughened to increase the frictional resistance. Four piles having an embedment length of 180 mm were installed beneath the raft at a relative spacing of 4 diameters.

The piled raft was horizontally (cyclically) loaded at a height of 25 mm above the soil surface using stainless rollers to minimize the friction between the rods and the

piled raft model. Added mass was set on the raft to give the intended vertical load to the piled raft.

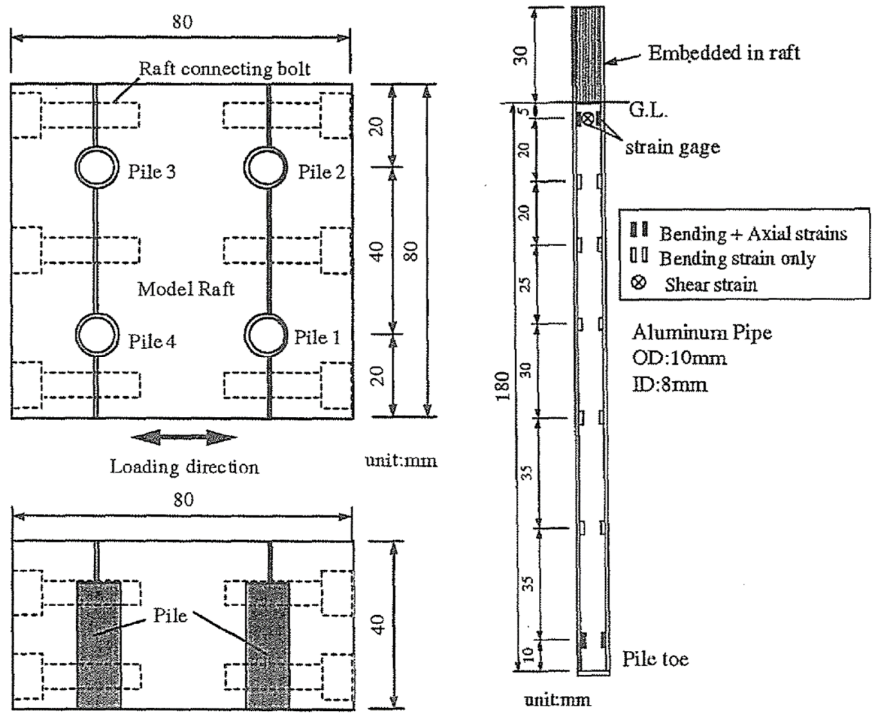

Figure 6.23: Design of model raft and pile for rigid pile head connection (Horikoshi et al., 2003)

Test procedure

The procedures for the horizontal loading tests were as follows: 1) set four piles at the corresponding positions by using an adjusting apparatus; 2) pour dry sand into the rigid box; 3) apply centrifugal acceleration up to 50g to allow for self-weight settlement of the soil and the piles; 4) check soil strength distribution through cone penetration tests; 5) place model raft on sand after halting the first flight; 6) connect the model raft and the piles, and place added mass on the raft; 7) set all instrumentations and apply centrifugal acceleration up to 50g again and 8) apply horizontal load to the piled raft. Therefore, it was not possible to model actual construction procedures.

It was considered that the most important factor was to simulate reasonable and consistent pile raft vertical load sharing before loading horizontally at an enhanced gravity level of 50g. Experimental cases and their conditions are summarised in Table 6.8.

Table 6.8: Experimental cases and their conditions (Horikoshi et al., 2003)

Model type	Horizontal loading
Single pile	
Length, L (mm)	170
Raft alone	
Width, B (mm)	80
Mass, M (kg)	4.69
Piled raft (rigid or hinged)	
Pile length, L (mm)	180
Raft width, B (mm)	80
Raft mass, M (kg)	4.69

Experimental test results

Single pile

The pile head boundary was set at in a free condition. During the test, a constant displacement rate of 0.01 mm/s was applied to the pile at 25 mm above the soil surface. The distributions of the bending moments along the pile shaft at the initial stage are shown. The maximum moment was observed at a depth of about 50 mm below the soil surface. The position of the maximum bending moment was slightly lower compared with the typical free-headed single pile response.

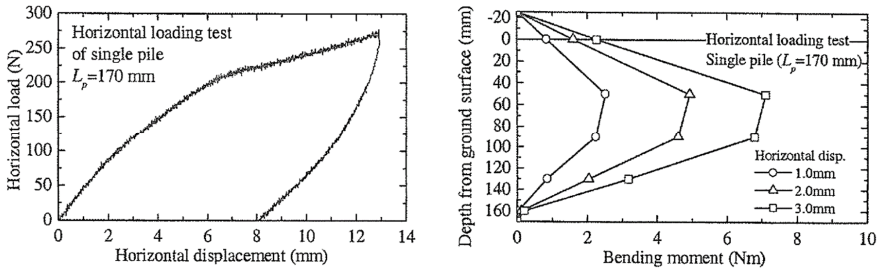

Figure 6.24: Single pile test results (Horikoshi et al., 2003)

Raft alone

The raft weight was the same as that used for the horizontal loading test on piled raft model (2298 N at 50g). The horizontal load-displacement relationship shows the ultimate resistance of the raft of 973 N at a displacement of about 5 mm, which corresponds to the coefficient of friction of 0.423 (interface friction angle of 22.9 degrees).

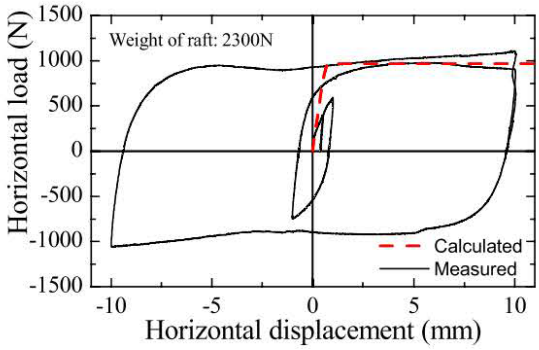

Figure 6.25: Raft alone test results (Horikoshi et al., 2003)

Piled rafts

In this study the vertical load was applied by increasing the initial raft mass to 2298 N at 50g, so as to simplify the experimental apparatus and procedures, and because the main objective of this study was to compare the behaviour of different piled raft models with consideration of the component behaviours, rather than to simulate the behaviour during the construction of prototype, achieving the consistent vertical load-sharing between the raft and the piles was the most important concern, rather than applying the vertical load in a strict manner.

Figure 6.26 shows the vertical loads carried by each component of the piled rafts during the stage of increase in g level to 50g. About 40% of the vertical loads were carried by the 4 piles before performing the horizontal test in both cases.

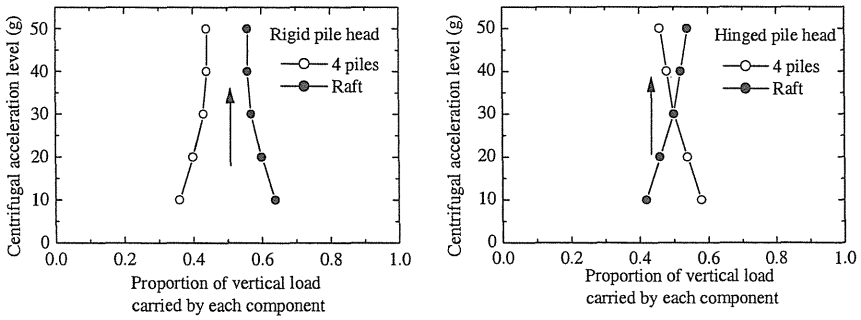

(a) Rigid connection model **(b) Hinged connection model**

Figure 6.26: Proportion of vertical load carried by each component during the stage of increase in g level to 50g (Horikoshi et al., 2003)

Comparison between measured and computed results

Raft alone

In figure 6.27 is shown the comparison between the measured and computed load-displacement curve of the raft alone.

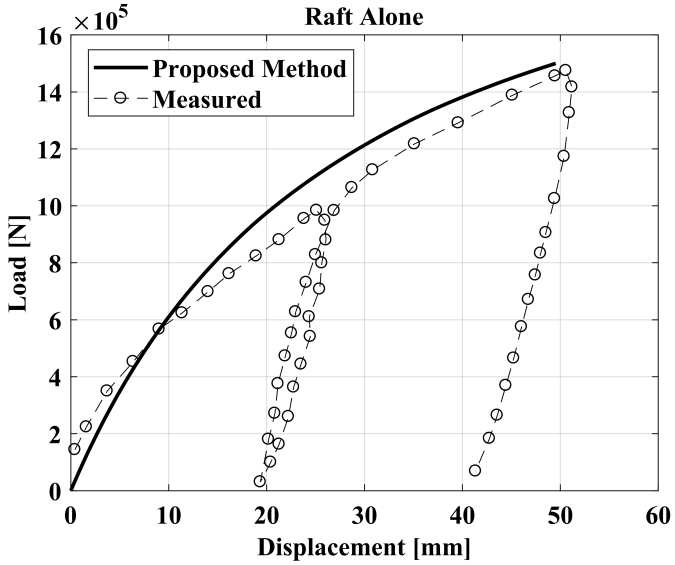

Figure 6.27: Computed vs measured load-deflection curve of the raft alone

Piled raft rigid

The comparison between measured and computed results is presented in terms of: a) load-displacement curves of the rigid piled-raft and its components (raft and pile group) (see Figure 6.28); b) load-displacement curves of the representative piles located in the front row and in the back row (see Figure 6.29); c) bending moment profiles, at a displacement equal to 12.5 mm, of the representative piles located in the front row and in the back row (see Figure 6.30). In these figures the comparison is shown even against the results obtained by the authors using the software PRAB.

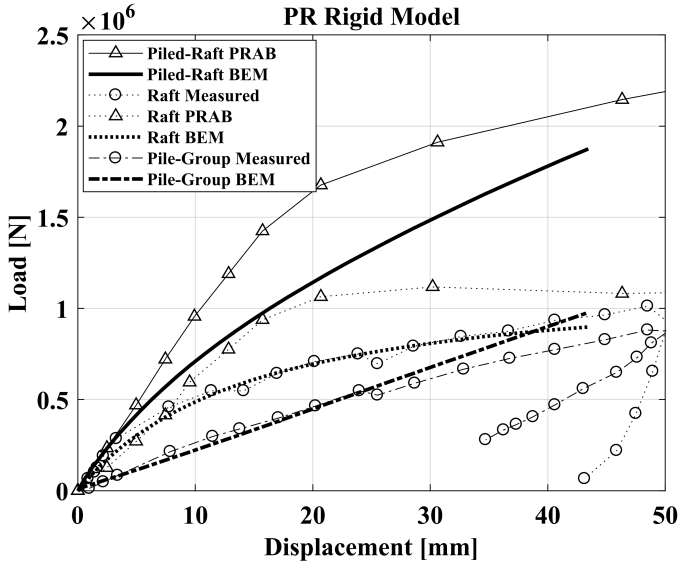

Figure 6.28: Computed vs measured horizontal load-displacement relationships of rigid piled-raft

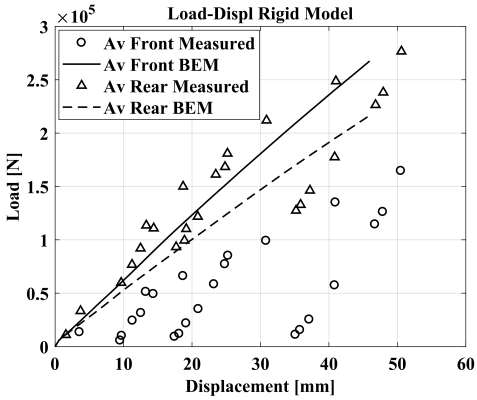

Figure 6.29: Computed vs measured horizontal load-displacement relationships of piles in rigid pile head model

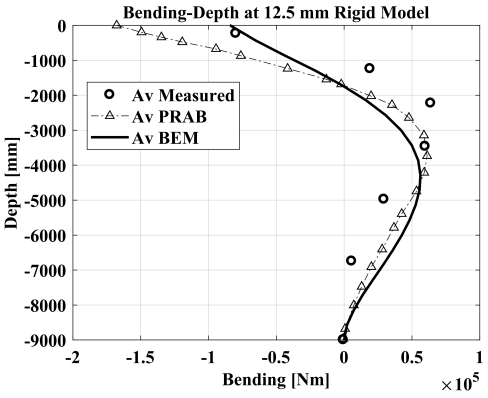

Figure 6.30: Computed vs measured distributions of bending moments along the pile shaft of an average pile in the rigid piled raft model

Piled raft hinged

The comparison between measured and computed results is presented in terms of: a) load-displacement curves of the hinged piled-raft and its components (raft and pile group) (see Figure 6.31); b) load-displacement curves of the representative piles located in the front row and in the back row (see Figure 6.32); c) bending moment profiles, at a displacement equal to 12.5 mm, of the representative piles located in the front row and in the back row (see Figure 6.33). In these figures the comparison is shown even against the results obtained by the authors using the software PRAB.

All the results shown reveal the ability of the proposed method to reproduce qualitatively and quantitatively the piled-raft response to horizontal loading.

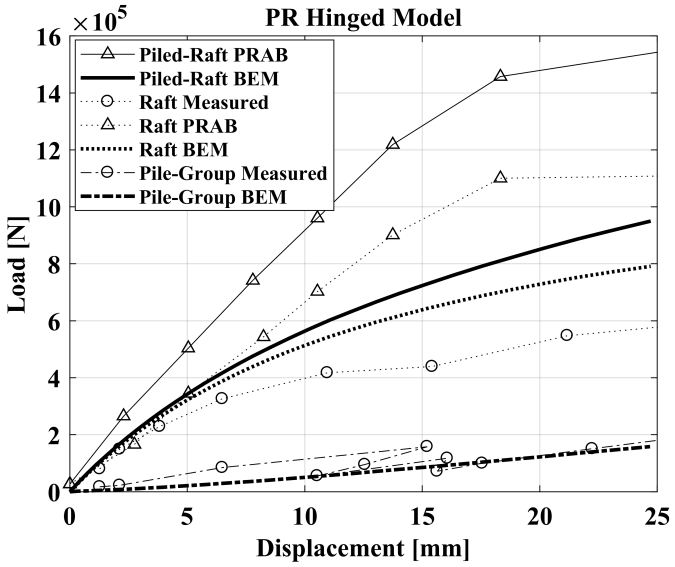

Figure 6.31: Computed vs measured horizontal load-displacement relationships of hinged piled-raft

It's important to remember, again, that the analyses with the developed BEM method were carried out not as back-analysis but as class A prediction, using the actual pile

mechanical properties and the soil strength and stiffness parameters according to the interpretation of the laboratory tests data. The analysis results of the authors were obtained using a plate-beam-spring model (software PRAB) where the soil is treated as springs and the non-linear behaviour is modelled using a bi-linear (elastic - perfectly plastic) response of soil springs. Moreover, the PRAB results are the outcomes of a back-analysis process where the Young modulus of the soil was varied in order to obtain the fitting with the measured load-deflection curves.

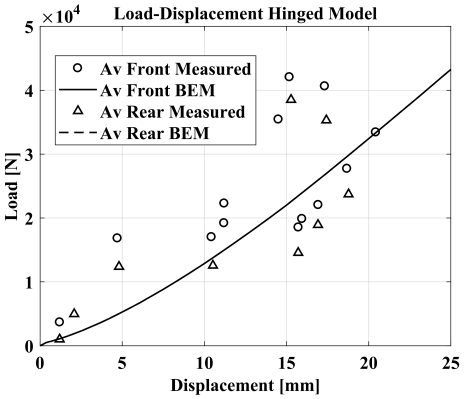

Figure 6.32: Computed vs measured horizontal load-displacement relationships of piles in hinged pile head model

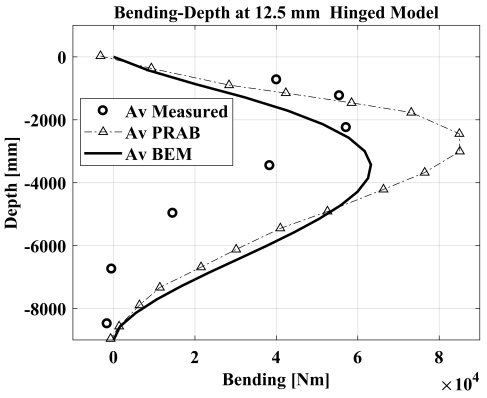

Figure 6.33: Computed vs measured distributions of bending moments along the pile shaft of an average pile in the hinged piled raft model

6.4.2 Matsumoto et al. (2010) - Sand ($D_R = 80\%$) - 1g field test

In this work a series of experimental activities were carried out in order to investigate what is the influence of different pile head connection conditions between raft and piles on the behaviour of piled-raft foundation systems in dry sand subjected to static vertical loading and static cyclic horizontal loading. The focus was on cyclic horizontal loading, and behaviour such as horizontal stiffness and rotation of the foundation, the load proportions between the raft and the piles.

Soil characterization

Dry Toyoura sand was used for the model ground in this study. The physical properties of the Toyoura sand are reported in Table 6.9. A series of triaxial CD tests were conducted to find the stress dependency of the shear modulus, G, and the internal angle of friction, ϕ'. These tests were carried out with specimens having a relative density of 80%, with different confining pressures.

Table 6.9: Properties of the model ground (Matsumoto et al., 2010)

Density of soil particle, ρ_s (t/m^3)	2.673
Maximum dry density, $\rho_{d,max}$ (t/m^3)	1.621
Minimum dry density, $\rho_{d,min}$ (t/m^3)	1.328
Median grain size, D_{50} (mm)	0.17
Internal friction angle, ϕ'	40°

From initial linear part of the measured deviatoric stress, q, versus shear strain, γ, the shear modulus was estimated as $G = q/\gamma$, and was plotted against the confining pressure, p_0. The measured values of G are fitted by the lines expressed by:

$$G_0 = G_{ref}(\frac{p}{p_{ref}})^{0.5} \tag{6.4}$$

Where p_{ref} is a reference value of pressure (= 100 kPa) and G_{ref} is the value of G at $p_0 = p_{ref}$. From the tests data an internal angle of friction, ϕ', of 40 degrees was found.

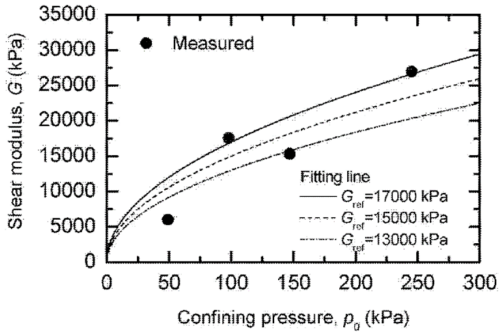

Figure 6.34: Shear modulus vs confining pressure of the Toyoura sand together with the fitting lines (Matsumoto et al., 2010)

Pile and raft properties

The sand was prepared in a steel cubic box of 1500 mm in length. The base bricks were set at the bottom of the soil box to a level of 500 mm from the bottom, thus, the effective height of the model ground was 1000 mm. The square model raft was made of stainless steel plate having a width of 400 mm and a thickness of 40 mm ('rigid plate'). The sand was glued at the bottom base of the model raft to increase the coefficient of friction at the raft-soil interface.

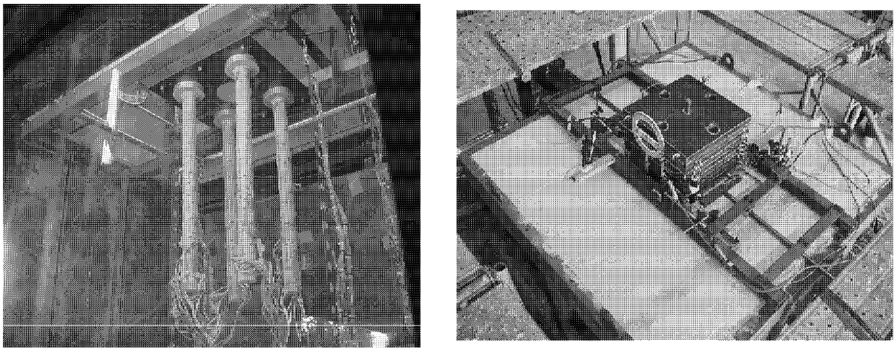

Figure 6.35: Model foundation with instruments and Test set-up prior cyclic horizontal load tests (Matsumoto et al., 2010)

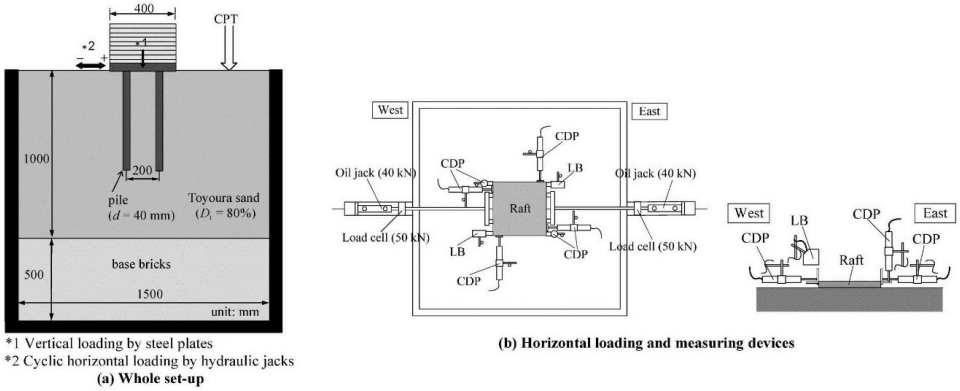

Figure 6.36: Illustration of test set-up (Matsumoto et al., 2010)

Aluminium pipes with an outer diameter of 40 mm having a wall thickness of 2 mm and a length of 600 mm were used. The model pile properties are presented in (Table 6.10). The Toyoura sand was also glued on the outer shaft of the model pile to increase the shaft resistance. Four different pile head connection conditions were investigated in this study using connection bars with a length of 5 mm between the top steel cap and the raft.

Table 6.10: Properties of model pile (Matsumoto et al., 2010)

Property	Value
Material	Aluminium
Outer diameter, D (mm)	40
Wall thickness, t (mm)	2
Length, L (mm)	600
Cross sectional rigidity, EA (kN)	$1.67{*}10^4$
Bending rigidity, EI (kNm^2)	3.03
Young's modulus E (GN/m^2)	70

The connection bars had different diameters, 30.5 mm, 13.0 mm and 10 mm. The bending rigidities of these connection bars are 2974, 0.098 and 0.034 kNm^2, respectively. A ball joint was used to simulate the hinged pile head connection condition. These pile head connection conditions are called 'Rigid', 'Semi-Rigid', 'Semi-Hinged' and 'Hinged' respectively. Note that the bending rigidities of the connection bars are about 1, 1/30 and 1/90 of the pile bending rigidity (= 3.03 kNm^2).

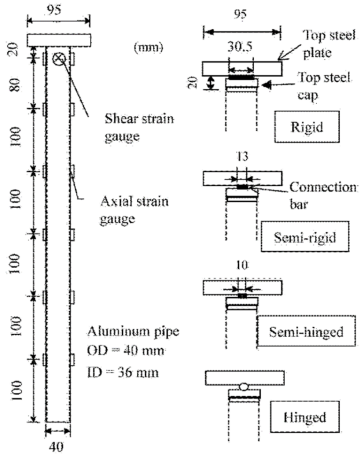

Figure 6.37: Model piles with different pile head connection conditions (Matsumoto et al., 2010)

Test procedure

A total of 7 test cases were carried out as reported in Table 6.11.

Table 6.11: Experimental cases (Matsumoto et al., 2010)

Test Cases	Total vertical Load (kN)	Load sharing Pile (%)	Load sharing Raft (%)
Raft alone			
Case 1 Raft	3.384	0	100
Pile group			
Case 2 (Rigid) PG-R	3.384	100	0
Case 3 (Hinged) PG-H	3.384	100	0
Piled Raft			
Case 4 (Rigid) PR-R	3.384	51	49
Case 5 (Semi-rigid) PR-SR	3.384	73	27
Case 6 (Semi-hinged) PR-SH	3.384	65	35
Case 7 (Hinged) PR-H	3.384	72	28

The method of setting-up of the model foundation in the model ground was: 1) four model piles were set in the soil box at the prescribed positions with a spacing of 200 mm using specially designed rings; 2) the sand was poured into the soil box to have a thickness of 100 m, and was compacted using a vibrator until it had a relative

density of about 80%, this procedure was repeated until the model ground was 1000 mm thick; 3) the model raft was placed on the model piles, and at the top steel plate on each pile was bolted to the raft.

Note that, in the cases of pile groups, a gap of 5 mm between the raft base and the ground was made before to the start of the load test. The loading process on the model foundation was divided in two phases, the vertical load phase and the cyclic horizontal loading phase.

The vertical load was applied by placing 9 steel plates with a weight of 0.376 kN each on the model raft one by one. A maximum vertical load of 3.384 kN was applied. The average contact pressure at the raft-soil interface was about 21.2 kPa for the case of raft alone. After the completion of vertical loading stage, cyclic horizontal loads were applied to the model raft by means of two oil jacks.

Experimental test results

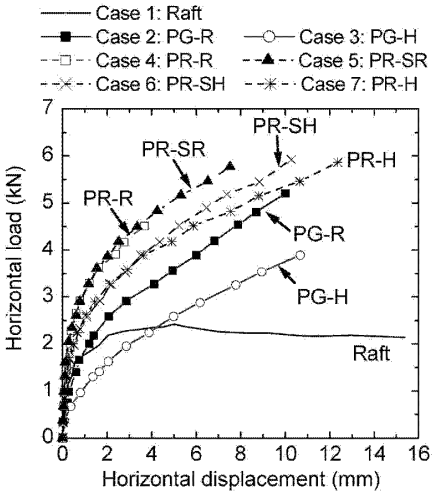

Figure 6.38: Horizontal load vs horizontal displacement at maximum load in each cycle for all the test cases (Matsumoto et al., 2010)

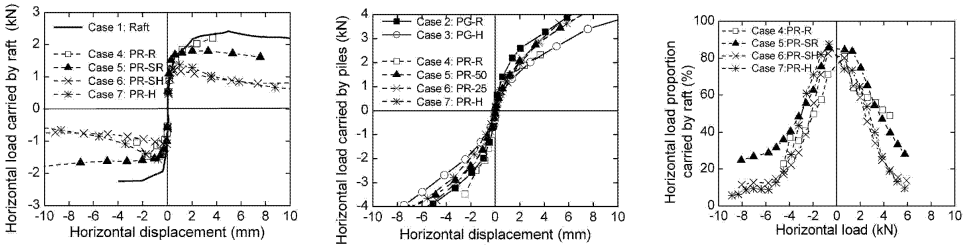

Figure 6.39: Load carried by 1) raft, 2) piles versus horizontal displacement and 3) Load proportion carried by raft (Matsumoto et al., 2010)

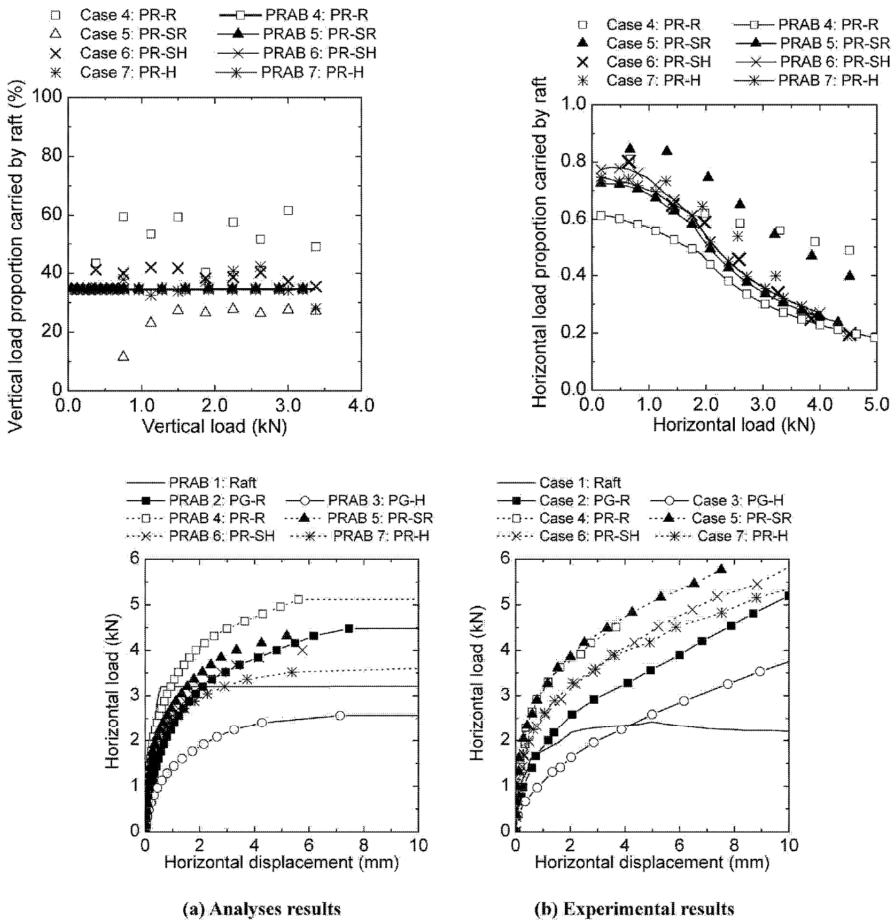

Figure 6.40: Comparison of calculated (by authors) and measured results (Matsumoto et al., 2010)

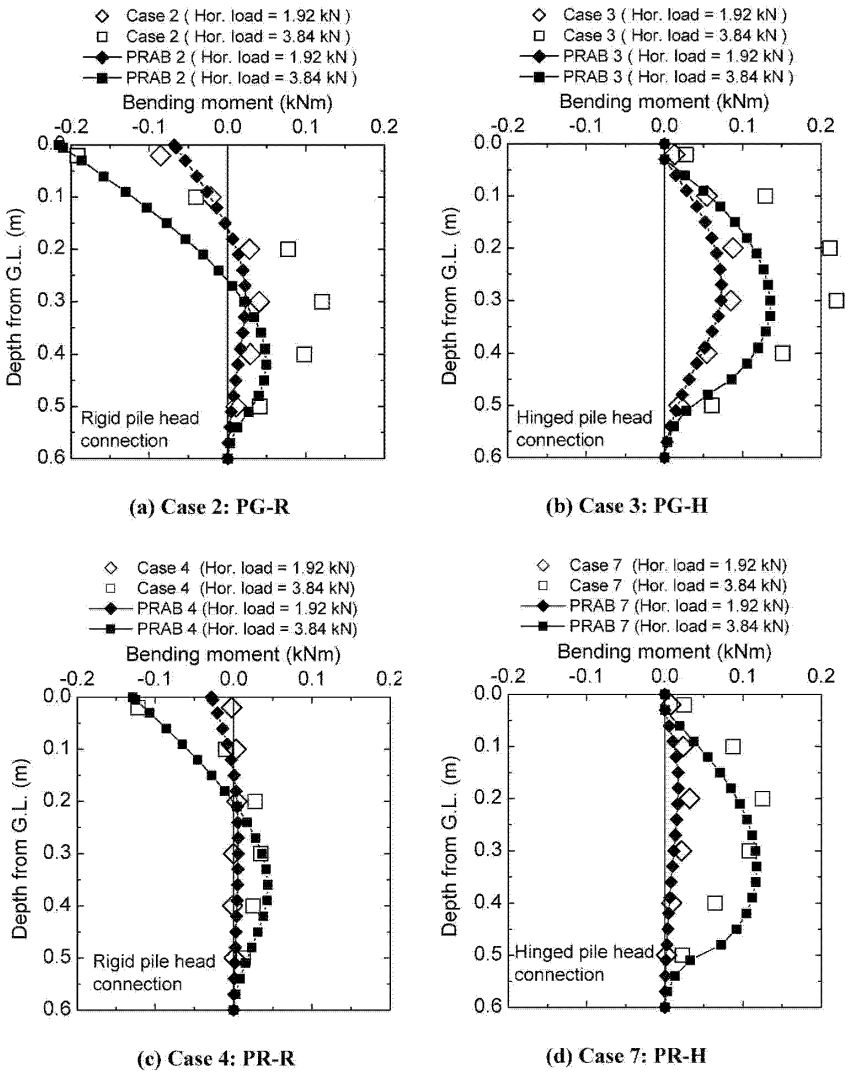

Figure 6.41: Comparison of calculated (by authors) and measured distributions of bending moments in pile (Matsumoto et al., 2010)

Comparison between measured and computed results

Raft alone

In figure 6.42 is shown the comparison between the measured and computed load-displacement curve of the raft alone. The comparison is presented even against the results obtained by the authors using the software PRAB.

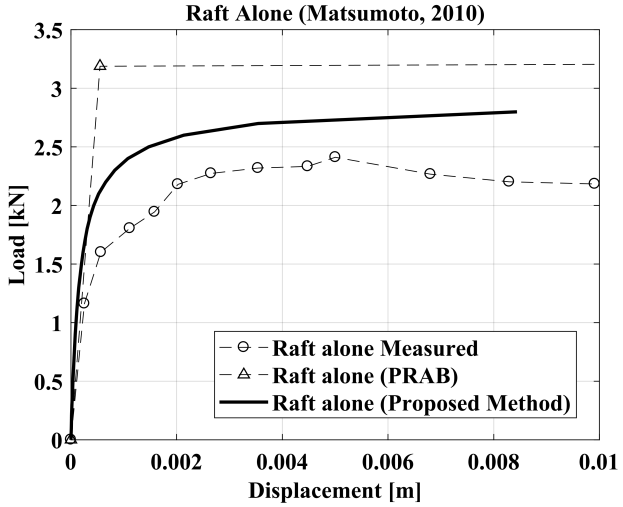

Figure 6.42: Computed vs measured load-deflection curve of the raft alone

Pile group hinged

The comparison between measured and computed results is presented in terms of: a) load-displacement curves of the hinged pile-group (see Figure 6.43); b) bending moment profiles, at two load levels, of an average pile of the hinged group (see Figure 6.43). In these figures the comparison is shown even against the results obtained by the authors using the software PRAB.

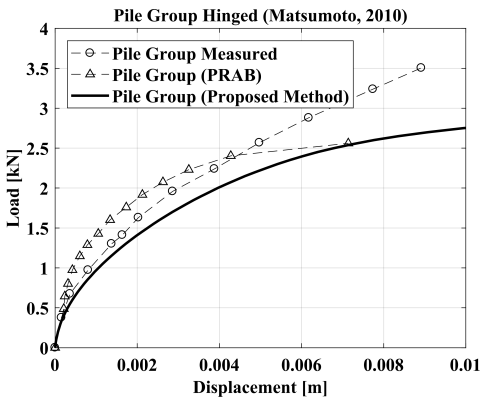

Figure 6.43: Computed vs measured load-deflection curve of the pile group (hinged)

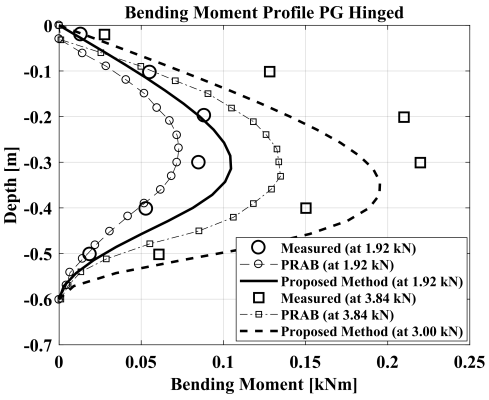

Figure 6.44: Computed vs measured bending moment profiles at H=1.92 kN and H=3.84 kN of an average pile of the pile group (hinged)

Pile group rigid

The comparison between measured and computed results is presented in terms of: a) load-displacement curves of the rigid pile-group (see Figure 6.45); b) bending moment profiles, at two load levels, of an average pile of the rigid group (see Figure 6.46). In these figures the comparison is shown even against the results obtained by the authors using the software PRAB.

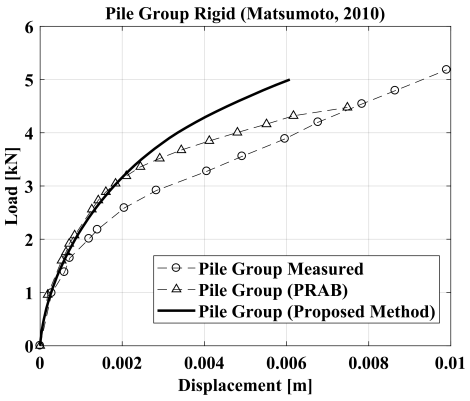

Figure 6.45: Computed vs measured load-deflection curve of the pile group (rigid)

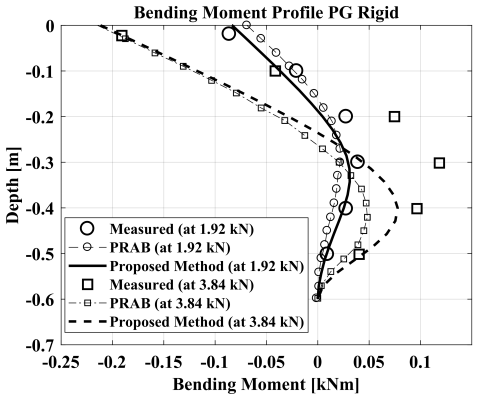

Figure 6.46: Computed vs measured bending moment profiles at H=1.92 kN and H=3.84 kN of an average pile of the pile group (rigid)

Piled raft hinged

The comparison between measured and computed results is presented in terms of: a) load-displacement curves of the hinged piled-raft and its components (raft and pile group) (see Figure 6.47); b) percentage of the load carried by raft (see Figure 6.48); c) bending moment profiles, at two load levels, of an average pile in the piled raft system (see Figure 6.49). In these figures the comparison is shown even against the results obtained by the authors using the software PRAB.

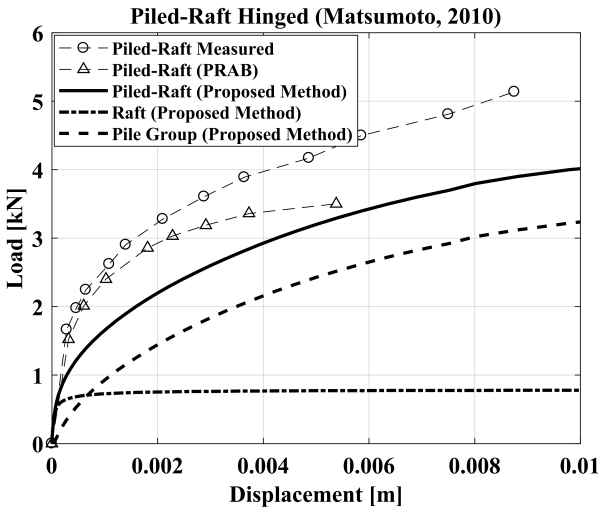

Figure 6.47: Computed vs measured load-deflection curve of the piled-raft (hinged)

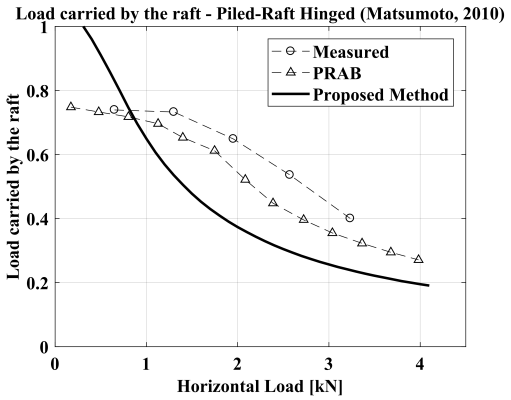

Figure 6.48: Computed vs measured load proportion carried by the raft in the piled-raft (hinged)

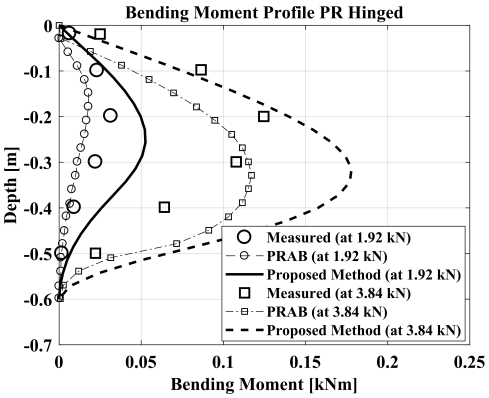

Figure 6.49: Computed vs measured bending moment profiles at H=1.92 kN and H=3.84 kN of an average pile in the piled-raft (hinged)

Piled raft rigid

The comparison between measured and computed results is presented in terms of: a) load-displacement curves of the rigid piled-raft and its components (raft and pile group) (see Figure 6.50); b) percentage of the load carried by raft (see Figure 6.51); c) bending moment profiles, at two load levels, of an average pile in the piled raft system (see Figure 6.52). In these figures the comparison is shown even against the results obtained by the authors using the software PRAB.

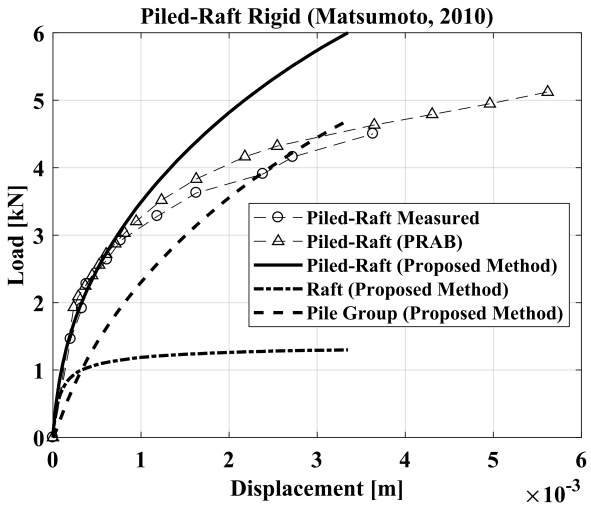

Figure 6.50: Computed vs measured load-deflection curve of the piled-raft (rigid)

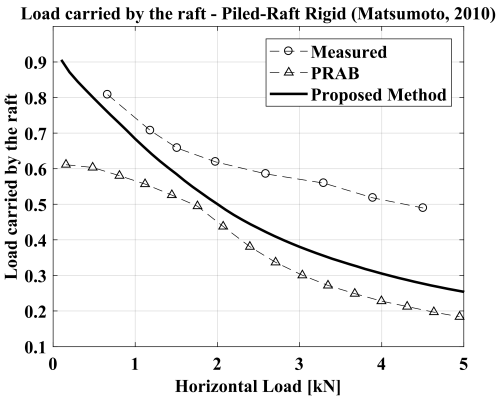

Figure 6.51: Computed vs measured load proportion carried by the raft in the piled-raft (rigid)

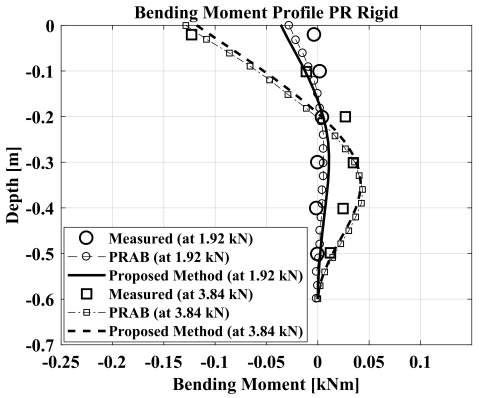

Figure 6.52: Computed vs measured bending moment profiles at H=1.92 kN and H=3.84 kN of an average pile in the piled-raft (rigid)

The results point out the capability of the proposed method to reproduce the raft alone response, while the hinged pile-group and the hinged piled-raft behaviours are correctly captured starting from the initial part of the load-displacement curves (initial stiffness of the foundation system) and up to a displacement level (y/D, D = 40 mm) approximately equal to 2%. For bigger displacement levels the load-deflection responses are underestimated. The rigid pile-group and the rigid piled-raft behaviours are captured starting from the initial part of the load-displacement curves (initial stiffness of the foundation system) and up to a displacement level (y/D, D = 40 mm) approximately equal to 3-5%, while for bigger displacement levels the load-deflection responses are overestimated. It's important to remember, that the analyses with the developed BEM method were carried out not as back-analysis but as class A prediction, using the actual pile mechanical properties and the soil properties according to the data provided by the authors. The analysis results of the authors were obtained using PRAB where the soil is treated as springs with a bi-linear (elastic - perfectly plastic) response. PRAB results are the outcomes of a back-analysis process where the soil Young modulus was found trying to obtain the fitting with the experimental results.

6.4.3 Unsever et al. (2015) - Sand ($D_R = 70\%$) - 1g field test

In order to understand the behaviour of piled raft foundations under vertical and horizontal loading, a series of vertical load test and horizontal load test (static and cyclic) on a 3-pile piled raft model were carried out in dry sand model ground 1-g field. Load test of the components of the piled raft model, such as raft alone and single pile, were also carried to investigate their interaction in the piled raft.

Numerical modelling of the load tests was conducted, aiming at obtaining more insight into the behaviour of the piled raft subjected to vertical and horizontal loading. A FEM software, PLAXIS 3D, was used for this purpose. The hardening soil model was used for modelling the sand behaviour.

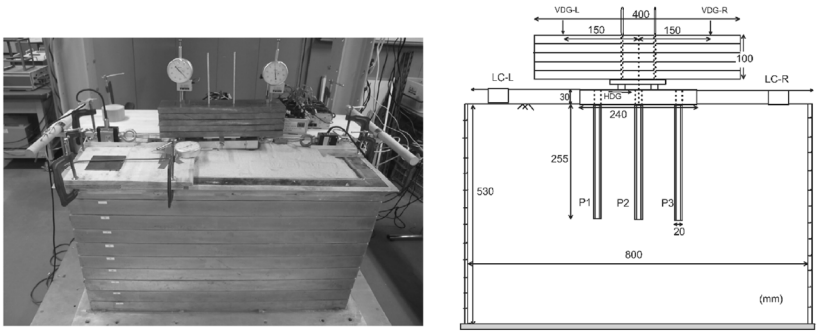

Figure 6.53: Test setup for horizontal loading of piled raft (Unsever et al., 2015)

Soil characterization

Dry silica sand #6, having a relative density, D_R, of about 70% was used as a model ground. The physical properties of the sand are summarised in Table 6.12. The mechanical properties of the sand were obtained from triaxial CD tests. Model ground was prepared, in a laminar box that had dimension of 800 mm x 500 mm with a depth of 530 mm, by layers (10 layers of 50 mm and one of 30 mm) in order to control the density, in this way each layer reached a DR of 70%. Triaxial CD tests of the sand were carried out under four different confining pressures (p_0). The soil specimens had a height of 100 mm with a radius of 50 mm.

Table 6.12: Properties of the model ground (Unsever et al., 2015)

Density of soil particle, ρ_s (t/m^3)	2.66
Maximum dry density, $\rho_{d,max}$ (t/m^3)	1.542
Minimum dry density, $\rho_{d,min}$ (t/m^3)	1.28
Maximum void ratio, e_{max} (-)	1.079
Minimum void ratio, e_{min} (-)	0.725
Median grain size, D_{50} (mm)	0.423
Coefficient of uniformity, U_C (-)	1.880

Test results are shown in Figure 6.54. It was observed that initial stiffness increases with increasing confining pressure and that stress-strain relations exhibit non-linearity and a relatively large dilatancy occurs.

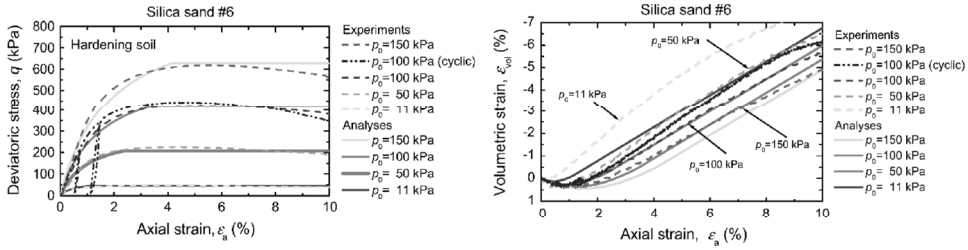

Figure 6.54: Triaxial CD test results. Deviatoric stress vs axial strain and Volumetric strain vs axial strain (Unsever et al., 2015)

To model the observed sand behaviour, the Hardening soil model was used. The FEM-model parameters were selected from the cyclic CD test with a confining pressure of 100 kPa. It was assumed by the authors that $E_{oed} = E_{50}/1.20$. The values of m and R_f were determined so that the results of numerical simulations fit to the measured results. The results of the numerical simulations of the CD tests are compared with the measured results in Figure 6.54.

Table 6.13: Properties of the sand (Plaxis 3D - HS model) (Unsever et al., 2015)

Secant stiffness at $p_{ref} = 100kPa$, $E_{50}(kPa)$	29560
One-dimensional stiffness at $p_{ref} = 100kPa$, $E_{oed}(kPa)$	23650
Unloading/reloading stiffness at $p_{ref} = 100kPa$, $E_{ur}(kPa)$	99590
Stress dependency parameter for stiffness, m (-)	0.5
Non-linear factor. R_f (-)	0.75
Poisson's ratio, ν (-)	0.19
Internal friction angle, ϕ' (°)	43.2
Dilatancy angle, Ψ (°)	15.8

The authors underline that the post-peak softening behaviours measured in the CD tests are not simulated using numerical modelling. In the FEM model interface elements were arranged along the pile shafts and at the raft base. The interface friction angle for the pile shaft and the raft base was estimated as 31.1 degrees from the horizontal loading test of the raft alone model on the model ground. The raft and the piles were assumed to be linearly elastic.

Although the model piles were hollow cylinders with an end plate, they were modelled by combination of beam elements surrounded by solid elements, following Kimura and Zhang (2000). In the hybrid modelling of pile, a large portion of the bending stiffness, EI, and axial stiffness, EA, of the pile are shared by the beam elements, still keeping large enough stiffness of the solid pile elements compared to the stiffness of the surrounding ground. The big advantage of the hybrid modelling of pile is that axial forces, bending moments and shear forces of the pile can be estimated easily from the factored values of those of the beam elements.

Pile and raft properties

The single pile model (SP), made of aluminium, properties are summarised in Table 6.14. This was instrumented with six strain gauges at different levels (see Figure 6.55) to obtain axial forces, bending moments and shear forces induced in the pile during loading tests. Piled raft (PR) model was composed of three piles and a rectangular raft of stainless steel having dimensions of 240 x 80 mm and a thickness of 30 mm. Pile relative-spacing was of 4 diameters (D = 20 mm, Spacing = 80 mm). The 3 piles were rigidly connected to the raft.

The authors underline that the sand particles were adhered on the pile shaft and the raft base to increase their friction resistance. In horizontal loading test of the piled-raft the vertical load was applied by placing 5 plates (497 N in total, see Figure 6.53) before start the lateral load test. The horizontal load was then applied using rotating wooden rods and wires in displacement control.

Table 6.14: Properties of model pile (Unsever et al., 2015)

Property	Value
Outer diameter, D (mm)	20
Wall thickness, t (mm)	1.1
Length, L (mm)	255
Cross sectional area, A (mm^2)	65.31
Moment of inertia, I (mm^4)	2926.2
Young's modulus E (N/mm^2)	64000
Poisson's ratio, ν (-)	0.31

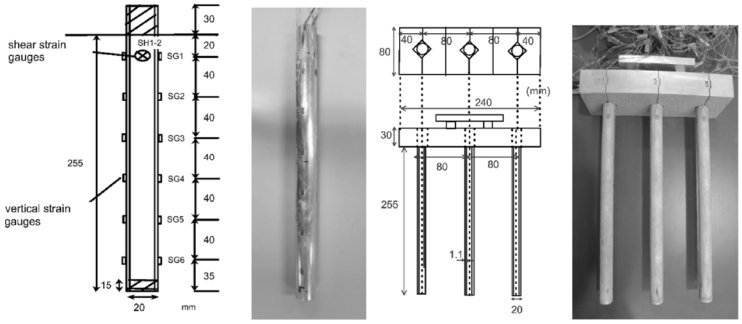

Figure 6.55: Single pile model and piled-raft model (Unsever et al., 2015)

Comparison between measured and computed results

The comparison between measured and computed results is presented in terms of: a) load-displacement curves of the rigid piled-raft and its components (raft and pile group) (see Figure 6.56); b) bending moment profiles, at three displacement levels (2%, 6% and 10%), of all the piles in the group (see Figures 6.57, 6.58 and 6.59). In the first figure, the comparison is shown even against the prediction realized by the authors using the FEM software Plaxis 3D.

The results shown reveal the ability of the proposed method to reproduce well the global piled-raft response to horizontal loading. However, looking at the results about the bending moment profiles along the pile-shafts, it seems that the proposed method is able to capture quite good the bending moment at the pile-heads while the positive bending moments are largely underestimated. The prediction of the bending moment profile is, neverthless, good for a displacement level of 2% that is the displacement level (among the experimental bending profiles) closer to those generally required by an ordinary superstracture.

It's important to remember, that the analyses with the developed BEM method were carried out not as back-analysis but as class A prediction, using the actual pile mechanical properties and the soil properties according to the data provided by the authors.

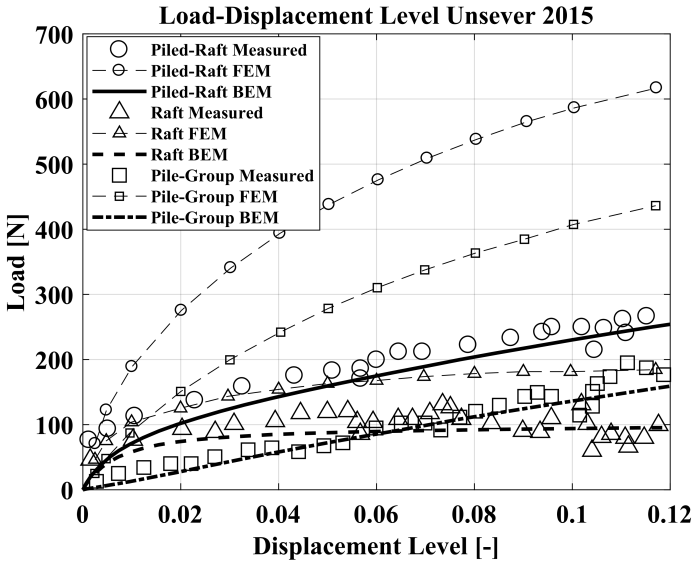

Figure 6.56: Computed vs measured - 'Horizontal load vs Normalised displacement'

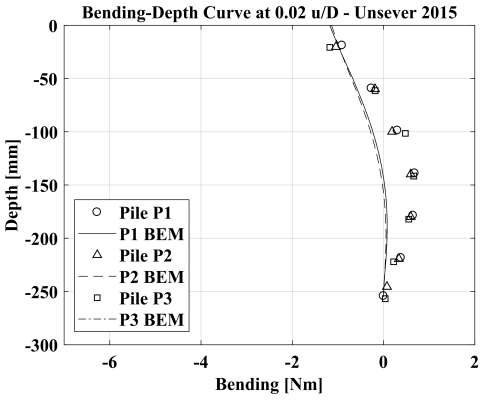

Figure 6.57: Bending moment distribution along each pile shaft (P1, P2 and P3) at u/D=0.02

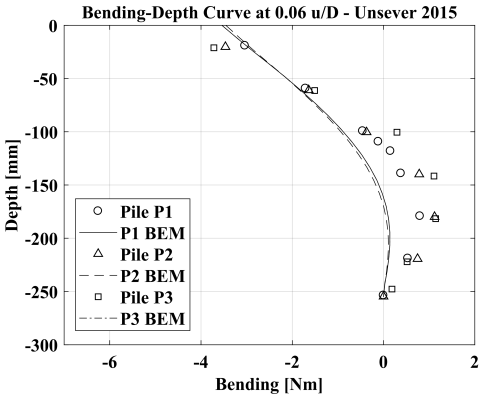

Figure 6.58: Bending moment distribution along each pile shaft (P1, P2 and P3) at u/D=0.06

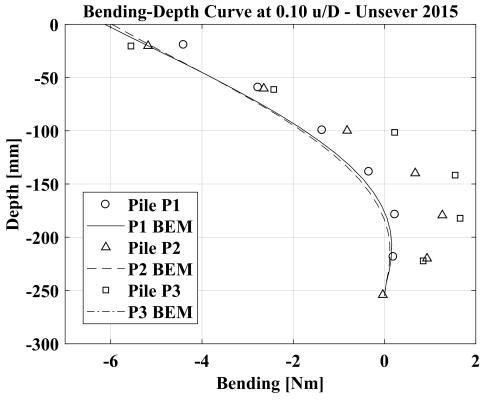

Figure 6.59: Bending moment distribution along each pile shaft (P1, P2 and P3) at u/D=0.10

6.4.4 Hamada et al. (2015) - Sand ($D_R = 60\% - 80\%$) - 1g field test

The authors presented the results of static cyclic lateral loading tests on large-scale piled-raft foundations carried out to investigate the influence of vertical load and pile spacing ratios during extreme events such as earthquakes. The test models were pile groups and piled rafts with a concrete footing supported by a 4x4 pile group in 1g field.

Soil characterization

Silica sand #6 was used in this study. The physical properties of this material are presented in Table 6.15.

Table 6.15: Properties of the model ground (Hamada et al., 2015)

Specific gravity of soil particles, G_s (-)	2.64
Maximum dry density, $\rho_{d,max}$ (t/m^3)	1.74
Minimum dry density, $\rho_{d,min}$ (t/m^3)	1.35
Median grain size, D_{50} (mm)	0.28
Coefficient of uniformity, U_C (-)	1.9

The internal angle of friction evaluated by means of triaxial CD tests was 42 degrees at relative density of 60%. It was found that the initial shear modulus at a relative density of 80% was related to the square root of the confining pressure as in the following equation experimentally defined by the authors from the initial shear stiffness in a cyclic triaxial test:

$$G_0 = 8800\sigma_c^{0.53}[kN/m^2] \tag{6.5}$$

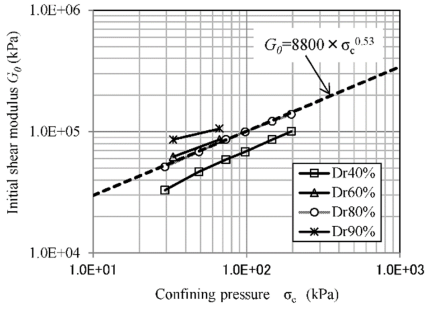

Figure 6.60: Confining pressure versus initial shear modulus of model sand (Hamada et al., 2015)

Pile and raft properties

The footing was 1.00 m long, 1.00 m wide, a thickness of 0.50 m and was sustained by a 4x4 pile-group. The piles were embedded in the concrete footing.

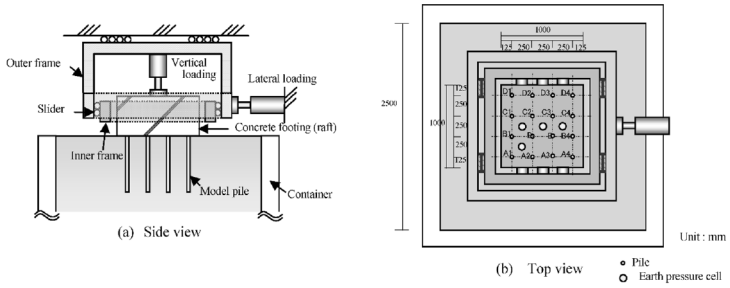

Figure 6.61: Tests model and loading apparatus (Hamada et al., 2015)

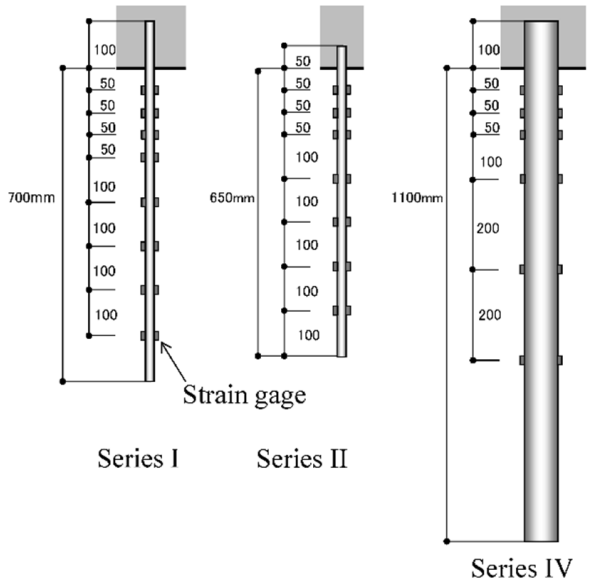

Figure 6.62: Model piles (Hamada et al., 2015)

Two different pile spacing ratios (s/d) were adopted by using two different diameter values. The spacing was the same in both the configurations, and equal to 0.25 m. One model, representing small pile group effect (s/d = 13), was made of aluminium pipes having an outer diameter of 19 mm and a wall thickness of 1 mm. The other model, representing large pile group effect (s/d = 3.3), was made of vinyl chloride pipes with an outer diameter of 76 mm and a wall thickness of 2.5 mm. The surface between the raft and the soil surface was rough because the raft was cast in place on model sand. According to the authors the piles were realized not to be rigid, and they were not short because their lengths were close to the footing dimension. In Table 6.17 the piles properties are shown.

Table 6.16: Properties of model pile (Hamada et al., 2015)

Item	Pile 1	Pile 2
Material	Aluminium	Vinyl chloride
Outer diameter, D (mm)	19	76
Wall thickness, t (mm)	1	2.5
Length, L (mm)	650	1100
Second moment of area, I (m^4)	$2.3{*}10^{-9}$	$3.9{*}10^{-7}$
Young's modulus E (GPa)	70	3.25

The evaluated coefficient of friction was 0.63, calculated by the authors as the ratio between the maximum horizontal load and the vertical load during raft alone tests (see Figure 6.63).

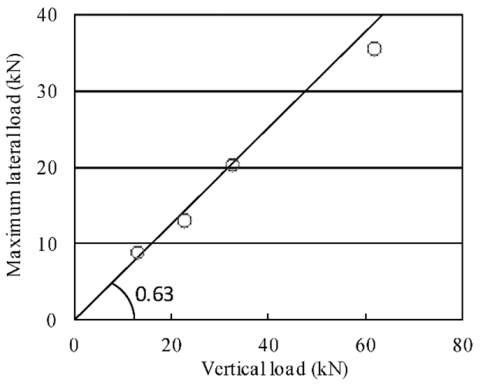

Figure 6.63: Vertical load versus maximum lateral load of raft foundations (Hamada et al., 2015)

Test procedure

Test cases were conducted (listed in Table 6.17) on pile groups (a steel plate was used to restrict vertical displacement), piled rafts (no vertical displacement restrictions) and raft alone (where the vertical load was varied). The footing was subjected to reverse cycles of lateral loads with increasing amplitudes, in displacement control. Two cycles at each displacement amplitude were realized. The shares of the vertical load carried by each component was monitored during the tests and in the table are shown the load sharing values before and after the lateral loading.

The procedures for setting up the model ground, model piles and model foundations were: 1) a 7.3 m thick layer of dry sand was poured into the soil container and compacted using a vibrator; 2) the 16 model piles were set at their prescribed positions; 3) dry sand was poured in 0.3 m thick layers into the container from a height of 2.4 m above the model ground surface; 4) for each layer, water was poured into the container three or four times to strengthen the model ground; 5) when the model ground was finished, the concrete raft was cast in place. The relative density of the soil was between 60% and 80%.

Table 6.17: Experimental cases (Hamada et al., 2015)

Test Cases	Total vertical Load (kN)	Load sharing Pile (%)	Load sharing Raft (%)	Maximum Lateral Displacement (mm)
Raft alone				
Case 1-1	32.2	0	100	7
Case 1-2	12.6	0	100	7
Case 1-3	22.4	0	100	7
Case 1-4	61.6	0	100	5
Single pile (d=76mm)				
Case 5	0	100	0	-
Pile group				
Case 2-4 (s/d=13)	32.2	100	0	7
Case 2-3 (s/d=13)	0	100	0	7
Case 3-3 (s/d=3.3)	0	100	0	7
Piled Raft (s/d=13)				
Case 2-1	32.2	32-42	68-58	7
Case 2-2	8.2	26-18	74-82	7
Piled Raft (s/d=3.3)				
Case 3-1	32.2	53-55	47-45	7
Case 3-2	64.5	28-38	72-62	7

Experimental test results

Piled Raft foundations of small pile diameter (s/d = 13)

In the test case 2-1 (vertical load = 32.2 kN), the friction resistance at the raft-soil interface was much higher than the pile's shear forces. The pile's shear forces were proportional to the lateral displacement, while the total lateral load behaviour was non-linear. The rear and the intermediate piles carried much more lateral load than the front piles, particularly at large lateral displacements. During loading, the sum of the axial forces of the piles changed considerably at large displacements. The piles experienced pulling forces and the contact pressure beneath the raft became larger (the initial value was 22.0 kPa). Therefore, it's possible that the soil modulus in front of the rear and intermediate piles probably increased.

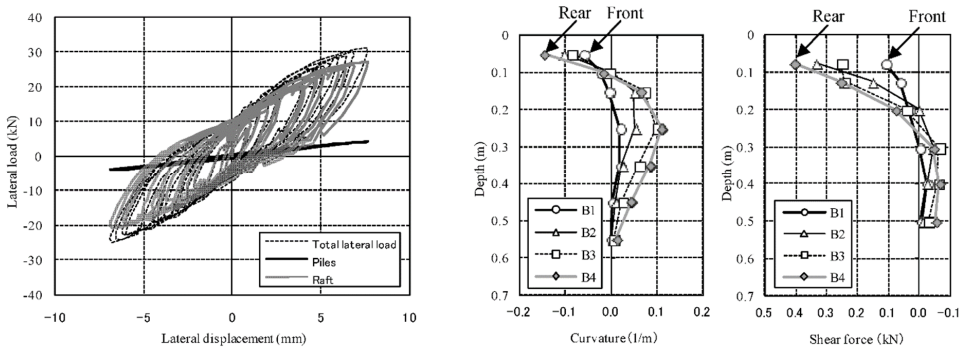

Figure 6.64: Case 2-1 results (Hamada et al., 2015)

Comparison between measured and computed results

Here it is presented the comparison between measured and computed (with the proposed BEM method) results in terms of load-displacement curves of the rigid piled-raft (Case 2-1) and its components (raft and pile group) (see Figure 6.65). In Case 2-1 the pile diameter was equal to 19 mm and the pile spacing ratio (s/D) was 13. The comparison is shown even against the prediction realized by the authors using a simplified analytical method. The results point out the capability of the proposed method to reproduce well the piled-raft response to horizontal loading. The analyses with the developed BEM method were carried out not as back-analysis but as class A prediction, using the actual pile mechanical properties and the soil properties according to the data provided by the authors.

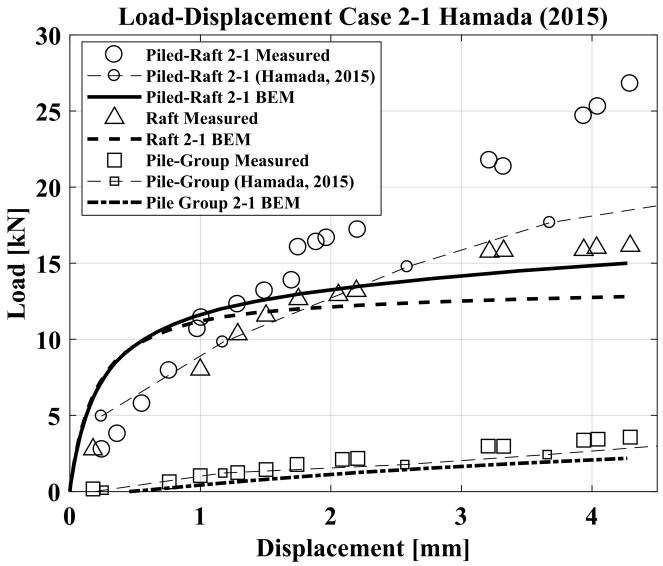

Figure 6.65: Computed vs measured - Horizontal load-displacement relationships of piled-raft Case 2-1

Chapter 7

Parametric studies

7.1 Single pile: parametric study

The most significant parametric studies on single pile under horizontal loads, realized with the continuous elastic model and solved with the boundary element method were conducted by Poulos (1971a), Poulos (1971b), Poulos (1973a), Poulos and Davis (1980), Banerjee and Davies (1978), Dente and Gullà (1983), El Sharnouby and Novak (1985), El Sharnouby and Novak (1986), Davies and Budhu (1986), Budhu and Davies (1987) and Budhu and Davies (1988). Kuhlemeyer (1979), Randolph (1981), Krishnan, Gazetas, and Velez (1983) and Chow (1987) carried out studies based on the continuous elastic model solved by finite elements.

7.1.1 Elastic analysis: literature overview

The most significant quantities that can represent the pile-soil system response in an elastic analysis, for a free-to-rotate single pile, are:

- the displacement at the pile-head;
- the rotation at the pile head;
- and the maximum bending moment (value and position).

For a fixed-head, are:

- the displacement at the pile head;
- the maximum negative bending moment (at the pile-head).

The displacement and rotation trends are usually presented in terms of dimensionless coefficients defined 'influence factors' and represented in graphs or by analytical formulas. In a homogeneous medium for a free-to-rotate pile subjected simultaneously to a horizontal load, H, and a moment, M, the horizontal displacement at the pile-head, y, and the pile-head rotation, θ, are expressed respectively by (Poulos, 1971; Banerjee and Davies, 1978):

$$y = I_{yH}\frac{H}{E_s L} + I_{yM}\frac{M}{E_s L^2} \tag{7.1}$$

$$\theta = I_{\theta H}\frac{H}{E_s L^2} + I_{\theta M}\frac{M}{E_s L^3} \tag{7.2}$$

For a fixed-head pile (Poulos, 1971; Banerjee and Davies, 1978):

$$y = I_{yF}\frac{H}{E_s L} \tag{7.3}$$

The coefficients (I_{yH}; I_{yM}; $I_{\theta H}$; $I_{\theta M}$ and I_{yF}) are the 'influence factors'. In a soil medium having a soil modulus linearly variable with depth (Gibson soil profile), displacements and rotations for a free-to-rotate pile are expressed by (Poulos, 1971; Banerjee and Davies, 1978):

$$y = \frac{H}{mL^2}(I'_{yH} + I'_{yM}\frac{e}{L}) \tag{7.4}$$

$$\theta = \frac{H}{mL^3}(I'_{\theta H} + I'_{\theta M}\frac{e}{L}) \tag{7.5}$$

Where e is the horizontal load eccentricity (= M/H). For a fixed-head pile:

$$y = \frac{H}{mL^2}I'_{yF} \tag{7.6}$$

m defines the slope of the soil modulus increase with depth, according to the law:

$$E(z) = mz \tag{7.7}$$

By the theorem of reciprocity, the values of $I_{\theta H}$ (pile-head rotation due to the horizontal load, H) must be equal to the values assumed by I_{yM} (displacement at the pile-head due to the moment, M); at the same way, it must be $I'_{\theta H}$ = I'_{yM}.

The 'influence factors' trends are generally expressed as a function of the most significant geometrical and mechanical properties of the pile-soil system; the most important factors are: the pile-soil relative stiffness, and the pile slenderness ratio L/D (Poulos, 1971). Pile-soil relative stiffness is the parameter that most affects the pile response in the elastic range. In older studies (Poulos 1971; 1973; Banerjee and Davies, 1978) the pile-soil relative stiffness was defined as:

$$K_R = \frac{E_p I_p}{E_s L^4} \tag{7.8}$$

for a homogeneous medium. For a medium having a modulus linearly increasing with depth, instead:

$$K_R = \frac{E_p I_p}{mL^5} \tag{7.9}$$

Parametric studies by Kuhlemeyer (1979) and Randolph (1981) showed that, in practical applications, rarely horizontally loaded piles are deformed along their entire length. The deformations, and consequently the moment and shear stresses induced on piles, become negligible at few pile-diameters below the ground surface, typically less than 10. Therefore, the total pile length is rarely a relevant parameter to be considered.

Kuhlemeyer (1979), in fact, introduced the concept of 'pile effective length', defining it as the maximum length that can affect the pile-head response. The author comparing the results of the parametric analysis conducted in a homogeneous medium by Poulos (1971; 1972) in the cases of floating pile and rock socketed pile, respectively, observed that the pile-head response, in terms of displacement and rotation, showed coincident values for a wide range of K_R values (up to a maximum value approximately equal to K_R =10^{-2} for I_{yH} and up to $K_R = 5 * 10^{-2}$ for $I_{\theta H}$ and $I_{\theta M}$).

Starting from these K_R values, the author obtained the effective slenderness L/r as a function of the ratio E_p/E_s. The piles with slenderness ratio greater than the effective one are not affected by the constraint condition at the pile base.

On the basis of the indications provided by Kuhlemeyer (1979), Randolph (1981) introduced the definition of flexible piles. The definition of Randolph (1981) took its origin from an analogy with the definition of infinitely long piles provided by Hetenyi (1946). In the case of a load acting at the head of an element, Hetenyi (1946) identified a critical length beyond which the actual length of the beam didn't influence the element-head response when the load (force or moment) was applied, causing the beam to behave like an infinitely long element.

In the work of Hetenyi (1946), realized with a Winkler method, the value of the critical length L_c was set equal to:

$$L_c = 4\sqrt[4]{\frac{E_p I_p}{k}} \tag{7.10}$$

Randolph (1981) introduced, instead, a critical length value referred this time to an elastic continuum model, the meaning of which was, however, analogous to that of his predecessors: piles having an actual length bigger than the critical one behave at the same way, when horizontally loaded.

The piles having an actual length bigger than the critical length are defined flexible. The critical length (defined, in dimensionless form, critical slenderness ratio) is provided by:

$$\frac{L_c}{D} = (\frac{E_p}{G^*})^{2/7} \tag{7.11}$$

for a homogeneous medium. In case of a medium having a modulus linearly increasing with depth, instead:

$$\frac{L_c}{D} = (\frac{E_p}{0.5mD})^{2/9} \tag{7.12}$$

Where G^* and m^* are corrected with the Poisson ratio using the expressions:

$$G^* = G(1 + \frac{3\nu}{4}) \tag{7.13}$$

$$m^* = m(1 + \frac{3\nu}{4}) \tag{7.14}$$

The considerations introduced by Randolph (1981) were confirmed by the subsequent parametric studies (for example: Krishnan et al. (1983), Davies and Budhu (1986) and Budhu and Davies (1987, 1988)).

The finding that most of the real piles behave as flexible piles has led to significant consequences on how to present the results of a parametric analysis. Regarding to the parameters identified by Poulos (1971), as those that most affect the response of a laterally loaded pile (slenderness ratio L/D and relative stiffness K_R), the following considerations can be drawn:

- the slenderness ratio L/D of the pile becomes an useless parameter, because the total length, L, is inappropriate to capture the response of the pile head; the piles behaviour, in terms of pile-head displacement and pile-head rotation or in terms of maximum bending moment, can be represented using a single curve (or a single analytical formula), without using as parameter the slenderness ratio L/D;

- the traditional relative stiffness parameter K_R (used by Poulos, 1971; 1973; Banerjee and Davies, 1978) is unnecessarily complicated and induces to represent different curves also for piles that behave similarly. The use of this parameter is misleading in the representation of the results and in their interpretation. More rational is the use of a relative stiffness parameter, K, which is simply defined as the ratio of the pile and soil stiffness:

$$K = \frac{E_p}{E_s} \tag{7.15}$$

for a homogeneous medium. In the case of a medium having a modulus linearly increasing with depth, instead:

$$K = \frac{E_p}{E_s(z = z^*)} \tag{7.16}$$

In the last expression the depth z^* means a conventional depth at which evaluate the soil modulus E_s.

In the light of these considerations a more rational definition of the 'influence factors' is, for example, that provided by Krishnan et al. (1983) or Budhu and Davies (1987). For free-to-rotate piles:

$$y = I_{yH}\frac{H}{E_s(z)D} + I_{yM}\frac{M}{E_s(z)D^2} \tag{7.17}$$

$$\theta = I_{\theta H}\frac{H}{E_s(z)D^2} + I_{\theta M}\frac{M}{E_s(z)D^3} \tag{7.18}$$

And for fixed-head piles:

$$y = I_{yF}\frac{H}{E_s(z)D} \tag{7.19}$$

Where for a non-homogeneous medium, $E_s(z)$, is the E_s value at a specific depth (usually one diameter, D): $E_s = mD$.

Conducting the study of the pile response to horizontal loads, the determination of bending moments and shears assumes an important relevance. At the design stage, in fact, the critical quantity to be considered (in most real cases) is the value of the maximum bending moment. The assessment of the internal forces and their distribution along the pile shaft are also necessary for the evaluation of the pile reinforcement.

Another significant quantity, for free-to-rotate piles, is the depth z at which the maximum moment occurs (usually at depths of few pile-diameters below the ground level and approximately at the 40% of the effective length). For fixed-head piles, the maximum moment is located at the pile head. Poulos (1971) and Banerjee and Davies (1978) identified a dimensionless moment, generated by a horizontal load, according to the expression:

$$M_{adim} = \frac{M}{HL} \tag{7.20}$$

7.1.2 Elastic analysis using the developed BEM-method

The following analysis results are about single piles. They were realized with the developed BEM method considering the following conditions:

- load at the pile-head: horizontal load (zero eccentricity);
- constraint condition at the pile-head: free-to-rotate and fixed;
- soil homogeneity: constant Young's modulus with depth, variable elastic modulus with depth (linearly increasing, Gibson soil profile);
- methods of analysis: linear elastic.

Free-head pile - homogeneous soil

The analysis results for a free-to-rotate single pile embedded in a homogeneous soil are presented in Fig. 7.1 in terms of the displacement and rotation influence factors (I_{yH} and $I_{\theta H}$) varying the pile-soil relative stiffness (E_p/E_s) and the pile slenderness ratio (L/D).

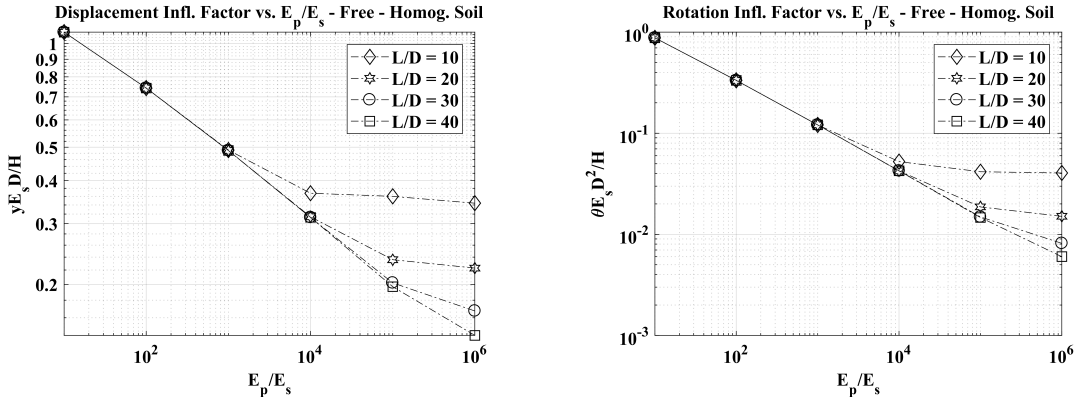

Figure 7.1: Displacement (I_{yH}, left) and rotation ($I_{\theta H}$, right) influence factors for a free-head pile in a homogeneous soil

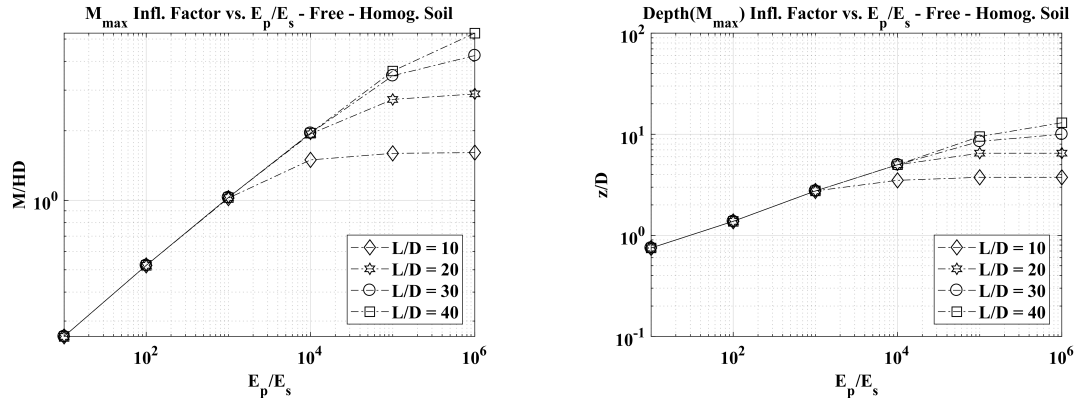

Figure 7.2: Normalized bending moment (M_{adim}, left) and Normalized maximum bending moment depth (z/D, right) for a free-head pile in a homogeneous soil

In Figure 7.3 and Figure 7.4, the deformations of piles subjected to lateral loading are shown in terms of elastic influence factor of displacement, I_{yH}. The effect of the pile slenderness ratio, L/D, on the factor I_{yH} is shown in Figure 7.3, while Figure 7.4 shows the effect of pile-flexibility factor K_R. Only in these analyses, the factors I_{yH} and K_R are defined as proposed by Poulos and Davis: $I_{yH} = (yE_sL)/H$ and $K_R = (E_pI_p)/(E_sL^4)$. Where y is the lateral displacement, H the lateral load, E_p the Young's modulus of the pile, and I_p the moment of inertia of the pile section.

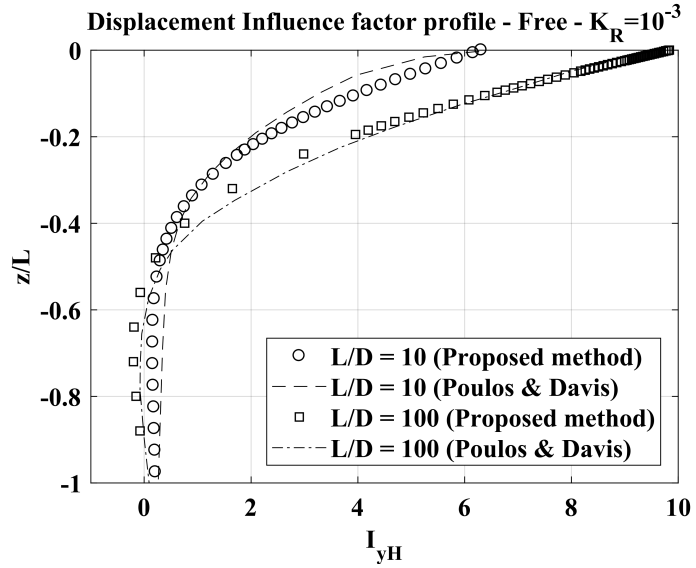

Figure 7.3: Displacement influence factor against the normalized depth for a free-head pile in a homogeneous soil ($K_R = 10^{-3}$)

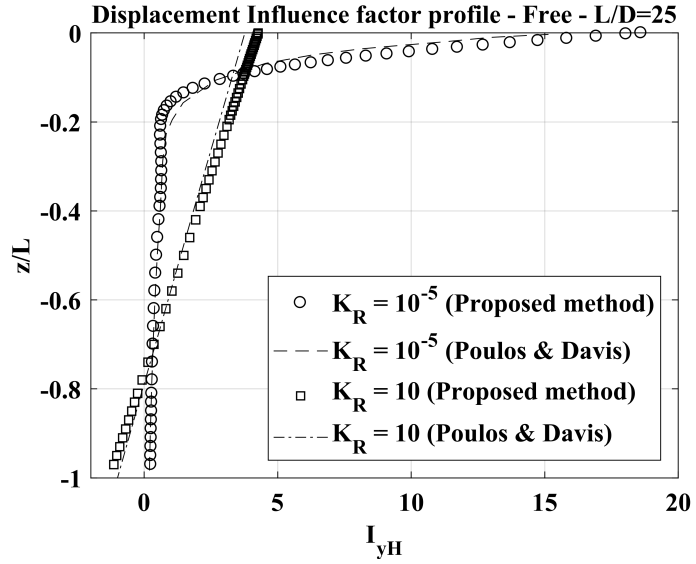

Figure 7.4: Displacement influence factor against the normalized depth for a free-head pile in a homogeneous soil ($K_R = 10^{-5}$; $K_R = 10$)

The Figure 7.5 shows the distributions of the normalised bending moments (M_z/HL) in a pile subjected to a lateral load, for two different values of K_R. These results are compared with those obtained by Poulos and Davis (1980).

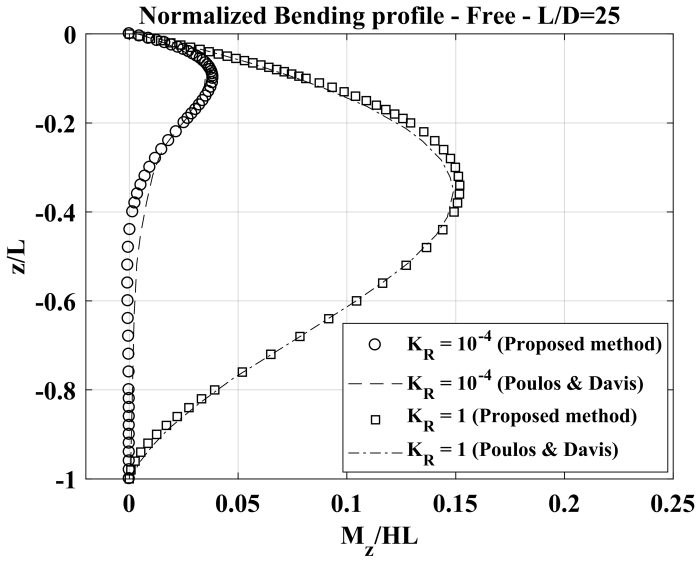

Figure 7.5: Normalised bending moment against the normalized depth for a free-head pile in a homogeneous soil ($K_R = 10^{-4}$; $K_R = 1$)

Free-head pile - Gibson's soil

The analysis results for a free-to-rotate single pile embedded in a Gibson soil are presented in Fig. 7.6 in terms of the displacement and rotation influence factors (I_{yH} and $I_{\theta H}$) varying the pile-soil relative stiffness (E_p/mD) and the pile slenderness ratio (L/D).

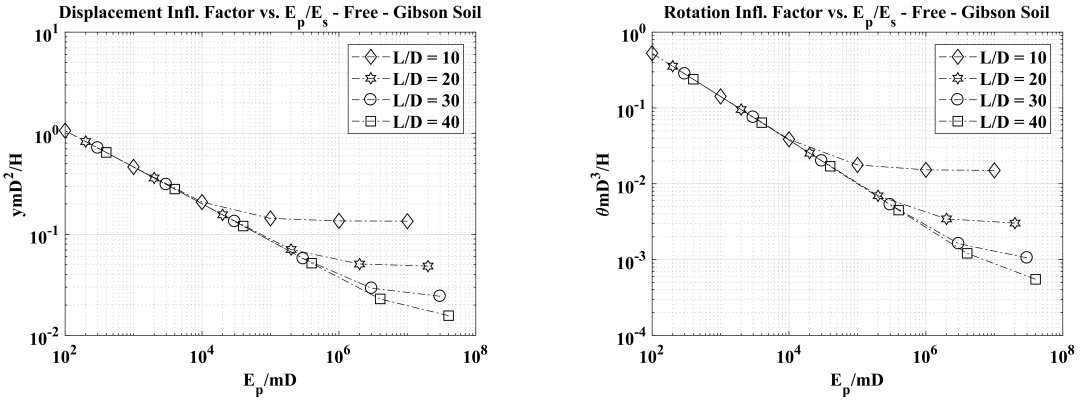

Figure 7.6: Displacement (I_{yH}, left) and rotation ($I_{\theta H}$, right) influence factors for a free-head pile in a Gibson soil

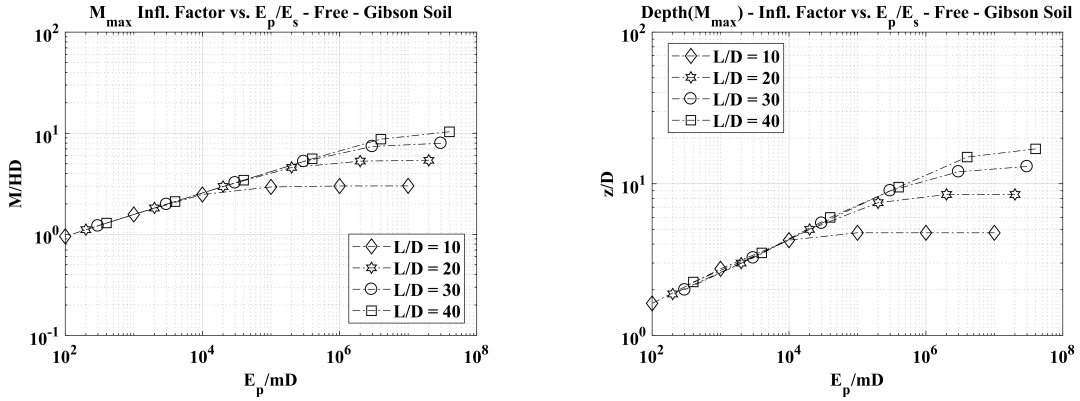

Figure 7.7: Normalized bending moment (M_{adim}, left) and Normalized maximum bending moment depth (z/D, right) for a free-head pile in a Gibson soil

Fixed-head pile - homogeneous soil

The analysis results for a fixed-head single pile embedded in a homogeneous soil are presented in Fig. 7.8 in terms of the displacement influence factor (I_{yH}) and of the dimensionless bending moment (M_{adim}) varying the pile-soil relative stiffness (E_p/E_s) and the pile slenderness ratio (L/D).

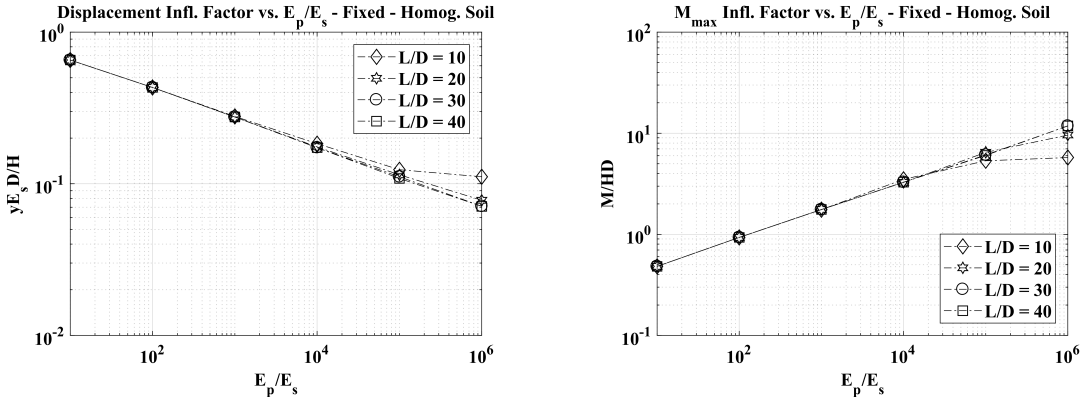

Figure 7.8: Displacement (I_{yH}, left) influence factor and Normalized bending moment (M_{adim}, right) for a fixed-head pile in a homogeneous soil

Fixed-head pile - Gibson's soil

The analysis results for a fixed-head single pile embedded in a Gibson soil are presented in Fig. 7.9 in terms of the displacement influence factor (I_{yH}) and of the dimensionless bending moment (M_{adim}) varying the pile-soil relative stiffness (E_p/mD) and the pile slenderness ratio (L/D).

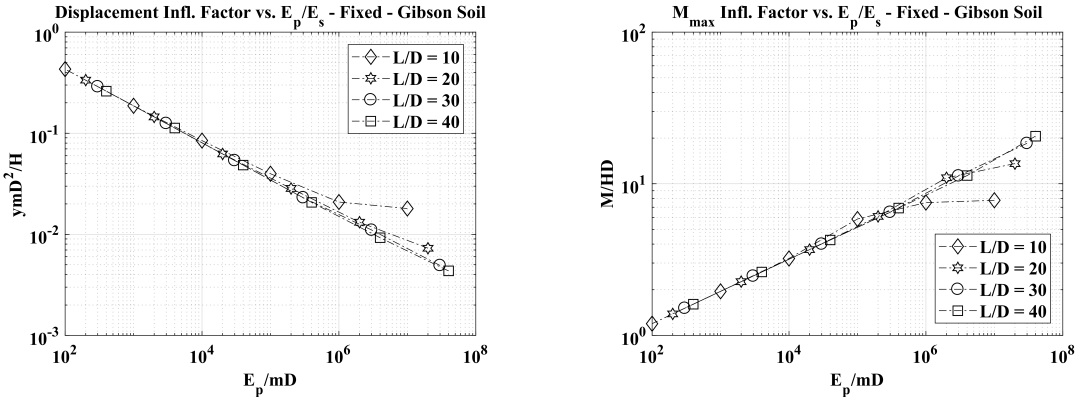

Figure 7.9: Displacement (I_{yH}, left) influence factor and Normalized bending moment (M_{adim}, right) for a fixed-head pile in a Gibson soil

7.1.3 Non-linear analysis: literature overview

In the available literature, the non-linear parametric analyses on single piles were carried out using an elastic-perfectly plastic procedure by means of a cut-off technique: 1) an ultimate soil resistance profile is defined, 2) once reached such limit value at one pile block (with the increase of the external loads), it is assumed that pile-soil relative displacement can occur at this plasticized pile block, 3) at that block, the soil pressure remains constant and equal to the ultimate resistance value, 4) further increases, in the external loads, are totally taken by the other blocks (those in elastic conditions).

Such an analysis, usually defined elasto-plastic analysis, was firstly performed by Poulos (1971, 1973) - the results are collected in Poulos and Davis (1980) - and subsequently by Davies and Budhu (1986) and Budhu and Davies (1987, 1988). These results (numerically obtained by these authors) are affected by the assumed ultimate soil resistance profiles.

The pile-soil relative displacements led to increments, often significant, of displacements, rotations and bending moments. The most significant quantities introduced in the elasto-plastic analyses are therefore:

- the increase of pile-head displacement;
- the increase of pile-head rotation (for free-to-rotate piles);
- the increase of the maximum moment acting on the pile.

These are expressed in terms of dimensionless factors, defined as the ratio between the value obtained in the elasto-plastic analysis and that obtained in the elastic one. The dimensionless factors values increase with the increase of the external forces, highlighting a non-linear trend of the pile response. Davies and Budhu (1986) defined the following parameters (for a free-to-rotate pile):

$$I_{yY}^{free} = \frac{y_Y}{y_E} \tag{7.21}$$

$$I_{\theta Y}^{free} = \frac{\theta_Y}{\theta_E} \tag{7.22}$$

$$I_{MY}^{free} = \frac{M_{max,Y}}{M_{max,E}} \tag{7.23}$$

where the subscript Y identifies the elasto-plastic analysis results (displacement, rotation and maximum bending moment, respectively) and the subscript E identifies the elastic analysis results. Similarly, for a fixed-head pile:

$$I_{yY} = \frac{y_Y}{y_E} \tag{7.24}$$

$$I_{MY} = \frac{M_{max,Y}}{M_{max,E}} \tag{7.25}$$

On the basis of the results obtained by Davies and Budhu (1986), Budhu and Davies (1987) and Budhu and Davies (1988) it is possible to make the following general considerations:

- as load increases, the difference with the values obtained in the elastic analysis becomes more evident;
- the displacement, rotation and moment increments are greater for flexible piles;
- the effects of the pile-soil relative displacements are less for fixed-head piles in terms of displacements and of bending moments;
- the effects due to non-linearity occur for higher loads in fixed-head piles compared to free-to-rotate piles.

Particularly significant is the consideration that the increase in maximum moments is bigger for flexible piles. In these works it was assumed that the maximum moment values, with increasing load level, become gradually independent on the pile-soil relative stiffness and depend essentially on the soil strength (Davies and Budhu, 1986).

Davies and Budhu (1986) and Budhu and Davies (1987, 1988) noted how the increase of the bending moment values is followed by an increase of the depth at which the maximum moment occurs.

The effective length values identified in the elastic analysis are no longer strictly valid. The effective length tends to assume, progressively, greater values with the increase of pile-soil relative displacements phenomena.

7.1.4 Non-linear analysis using the developed BEM-method

The following analysis results are about single piles. They were realized with the proposed BEM method considering the following conditions:

- load at the pile-head: horizontal load (zero eccentricity);
- constraint condition at the pile-head: fixed;
- soil homogeneity: initial Young modulus constant with depth;
- methods of analysis: non-linear (incremental analysis with the proposed BEM method);
- pile behaviour: linear-elastic, non-linear (reinfocerd concrete sections).

The non-linear analyses were performed considering the non-linear behaviour of the soil by means of the modified version of the quasi-hyperbolic relation proposed by Fahey and Carter (1993). It was assumed that the vertical stresses (at the pile-soil interface points) didn't vary during the horizontal load analysis. For this reason, can

be assumed an analogy between the 'interface pressure - ultimate soil resistance' ratio and the 'shear stress – maximum shear stress' ratio.

$$\frac{p}{p_{ult}} \sim \frac{\tau}{\tau_{max}} \tag{7.26}$$

At each step of the analysis, it was updated (at each pile-soil interface point) the value of the elastic modulus using the following relationship to obtain the normalized tangent shear-modulus:

$$\frac{G_{tan}}{G_{max}} = \frac{(G_{sec}/G_{max})^2}{[1 - R_f(1-g)(\frac{\tau}{\tau_{max}})^g]} \tag{7.27}$$

That, with the assumption done before, can be rewritten as:

$$\frac{G_{tan}}{G_{max}} = \frac{(G_{sec}/G_{max})^2}{[1 - R_f(1-g)(\frac{p}{p_{ult}})^g]} \tag{7.28}$$

Moreover, it was introduced a limit pressure profile, according to the ultimate soil resistance proposed by Matlock (1970) and Reese et al. (1974). Non-linear analyses were carried out considering both a linear-elastic behaviour and a non-linear behaviour of the pile section.

For each non-linear analysis the relative stiffness parameter ($K = E_p/E_s$), was dependent on the load-level, even if the pile was linear elastic (because in non-linear analysis the soil was subjected to a progressive elastic-modulus reduction). The relative stiffness parameter, $K = E_p/E_s$, therefore, increases compared to its initial value (indicated as K_0).

In the analyses on reinforced concrete single piles (fixed-head), not only the non-linear behaviour of the soil was taken into account, but also the influence of the pile non-linear response, considering two typical steel reinforcement ratio values, $\rho_s = A_s/A_c$, equal to 1% and 2%, and three compressive forces taken equal to 0%, 10% and 30% of the ultimate compressive load of the pile section ($N_u = A_c f_c$).

In order to better show the effect of the pile non-linear behaviour, the same analyses were performed even on a pile having the same properties, where the flexural rigidity was kept constant and equal to that of the intact section. The pile slenderness ratio, L/D, was taken equal to 20 and two pile diameter values were used (0.60 m and 1.0 m). For the soil instead, the following conditions were investigated:

- Cohesive soil: homogeneous soil condition, two values of the undrained shear resistance were used (equal to 50 kPa and 100 kPa). For the soil with $c_u = 50kPa$ the soil elastic modulus at small strain level $E_{max} = 60MPa$, thus the initial pile-soil relative stiffness was $K_0 = E_p/E_s = (30GPa)/(60MPa) = 500$; for the soil with $c_u = 100kPa$ the soil elastic modulus at small strain level $E_{max} = 150MPa$, so the initial pile-soil relative stiffness was $K_0 = E_p/E_s = (30GPa)/(150MPa) = 200$. The ultimate soil resistance profile was defined according to the relationship proposed by Matlock (1970). Two values of the exponent g (parameter that defines the shape of the soil modulus reduction curve) were used: 0.25 and 1.0.

- Cohesionless soil: homogeneous soil condition, two values of the angle of internal friction were used (equal to $30°$ (with a $D_R = 50\%$) and $40°$ (with a $D_R = 90\%$)). For the soil with $\phi = 30°$ the soil elastic modulus at small strain level $E_{max} = 30MPa$, thus the initial pile-soil relative stiffness was $K_0 = E_p/E_s = (30GPa)/(30MPa) = 1000$; for the soil with $\phi = 40°$ the soil elastic modulus at

small strain level $E_{max} = 60MPa$, so the initial pile-soil relative stiffness was $K_0 = E_p/E_s = (30GPa)/(60MPa) = 500$. The ultimate soil resistance profile was defined according to the relationship proposed by Reese et al. (1974). Two values of the exponent g (parameter that defines the shape of the soil modulus reduction curve) were used: 0.25 and 1.0.

The results of the analyses are presented in terms of non-linear dimensionless factors (I_{yY} and I_{MY}) against the normalised horizontal load applied and against the displacement level (y/D). Compared to the dimensionless factors defined in the technical literature described before in this case the dimensionless factors are obtained using a non-linear incremental analysis and not an elasto-plastic analysis as defined in the works of Davies and Budhu.

Fixed-head pile - cohesive soil - $g = 1.0$ **-** $c_u = 50kPa$**;** $c_u = 100kPa$ **- Pile diameter = 0.60 m and 1.0 m**

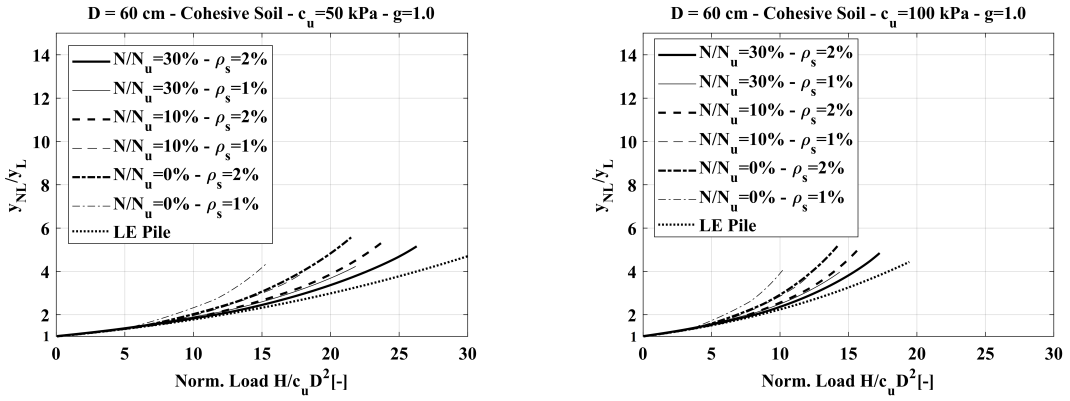

Figure 7.10: I_{yY} parameter against normalised horizontal load for a fixed-head pile in cohesive soils with parameter $g = 1$; D=60 cm

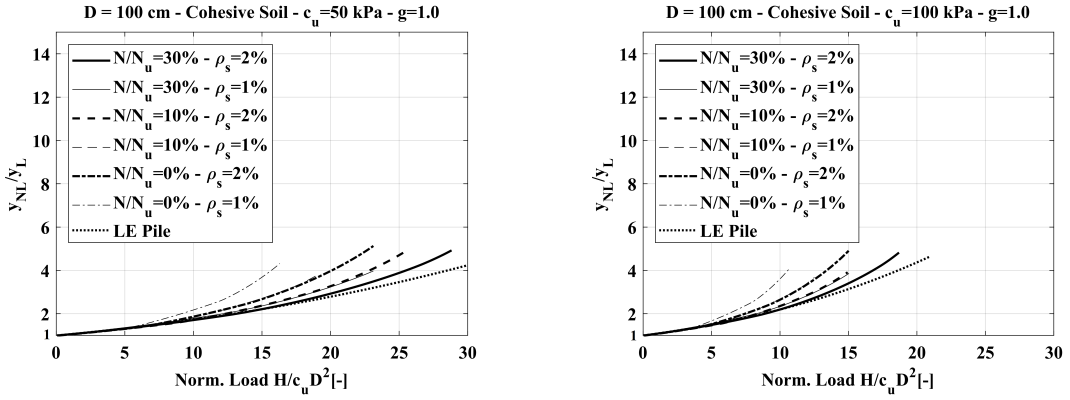

Figure 7.11: I_{yY} parameter against normalised horizontal load for a fixed-head pile in cohesive soils with parameter $g = 1$; D=100 cm

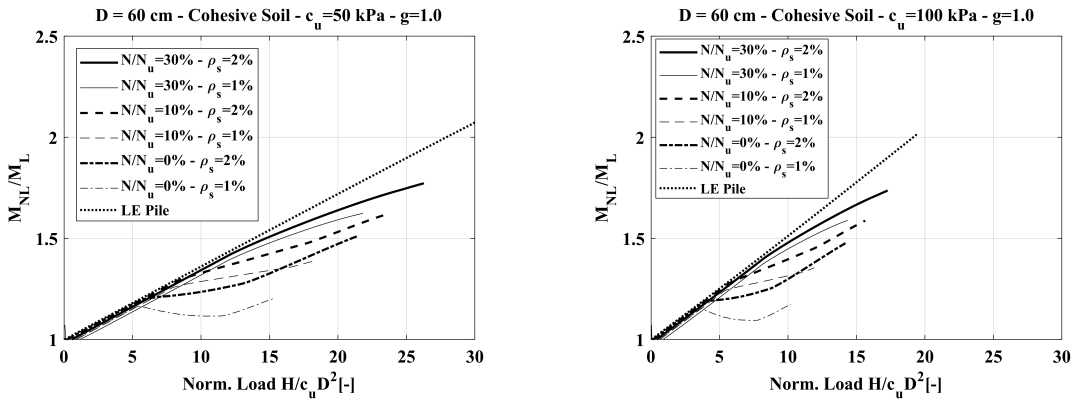

Figure 7.12: I_{MY} parameter against normalised horizontal load for a fixed-head in cohesive soils, with parameter $g = 1$; D=60 cm

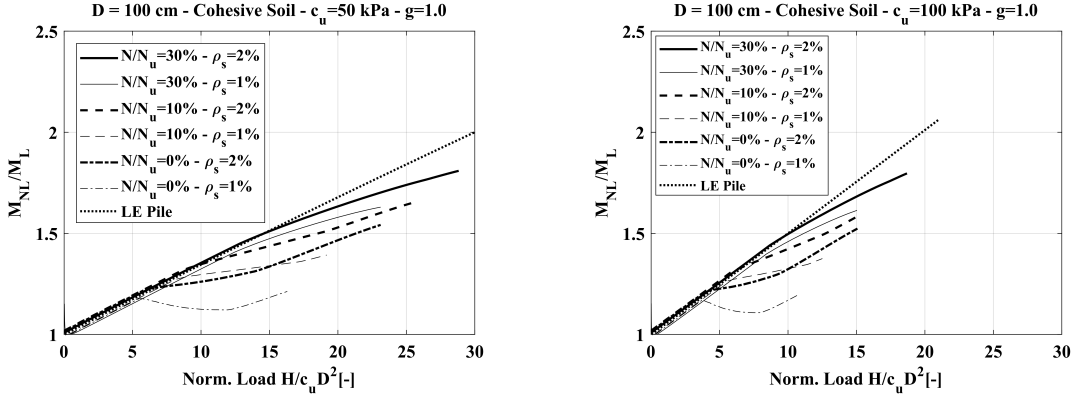

Figure 7.13: I_{MY} parameter against normalised horizontal load for a fixed-head in cohesive soils, with parameter $g = 1$; D=100 cm

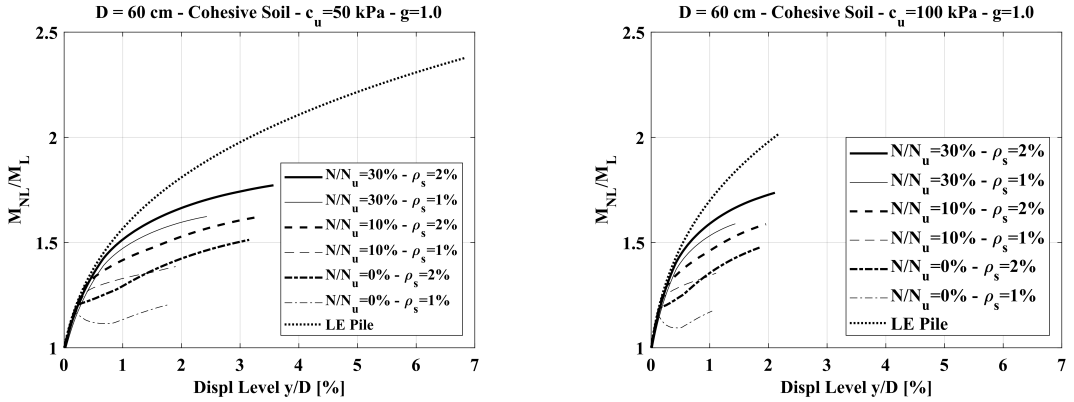

Figure 7.14: I_{MY} parameter against displacement level for a fixed-head in cohesive soils, with parameter $g = 1$; D=60 cm

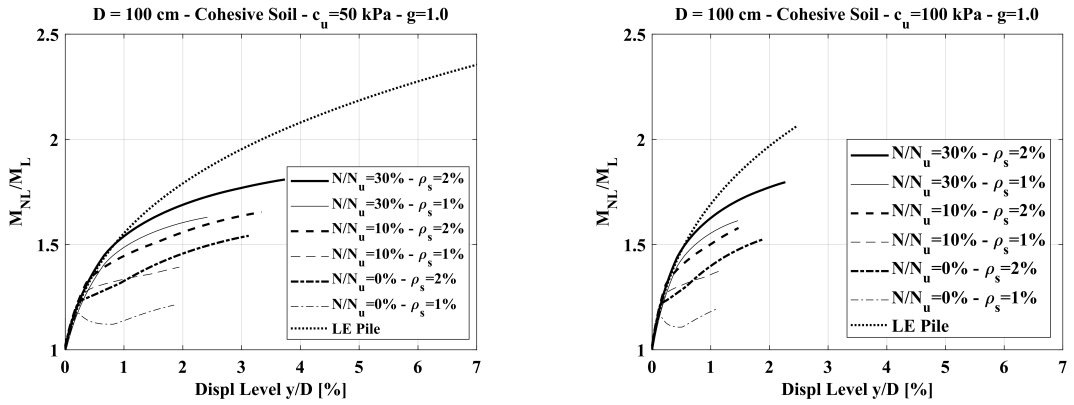

Figure 7.15: I_{MY} parameter against displacement level for a fixed-head in cohesive soils, with parameter $g = 1$; D=100 cm

Fixed-head pile - cohesive soil - $g = 0.25$ - $c_u = 50kPa$; $c_u = 100kPa$ - Pile diameter = 0.60 m and 1.0 m

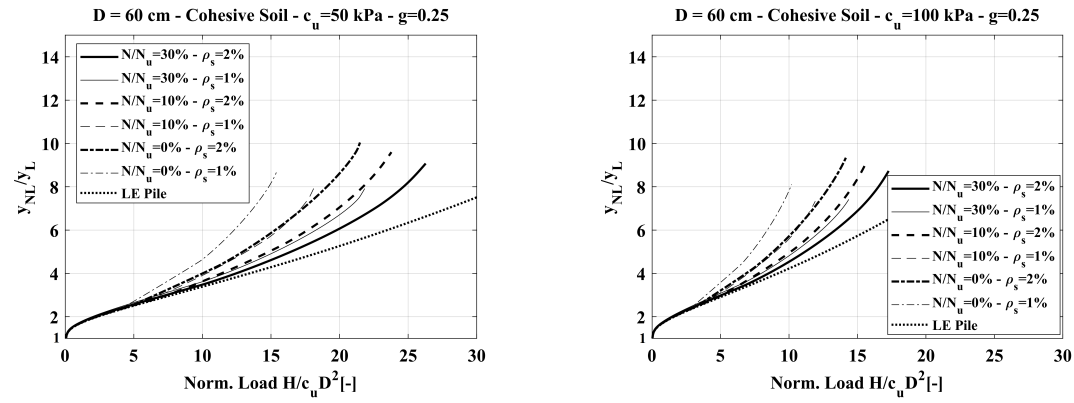

Figure 7.16: I_{yY} parameter against normalised horizontal load for a fixed-head pile in cohesive soils with parameter $g = 0.25$; D=60 cm

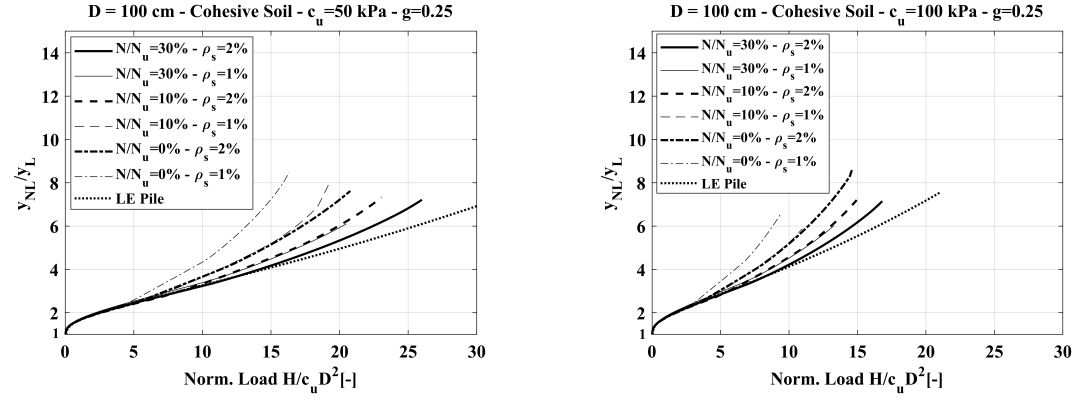

Figure 7.17: I_{yY} parameter against normalised horizontal load for a fixed-head pile in cohesive soils with parameter $g = 0.25$; D=100 cm

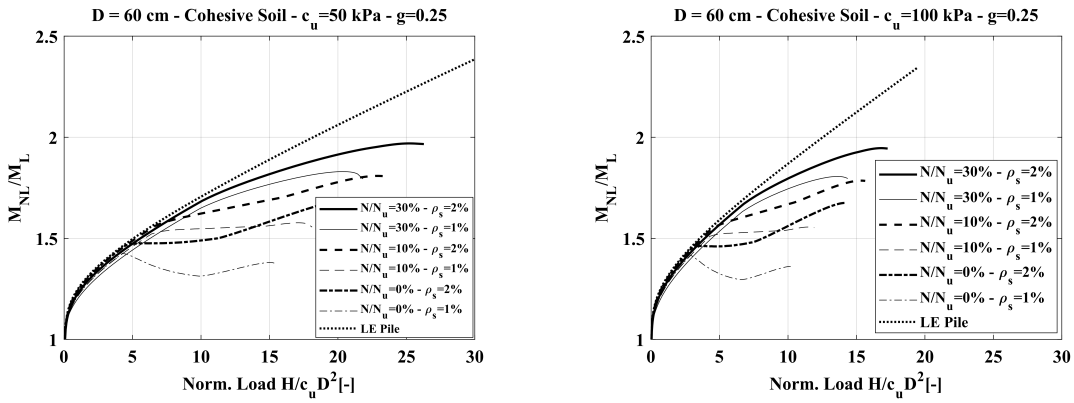

Figure 7.18: I_{MY} parameter against normalised horizontal load for a fixed-head in cohesive soils, with parameter $g = 0.25$; D=60 cm

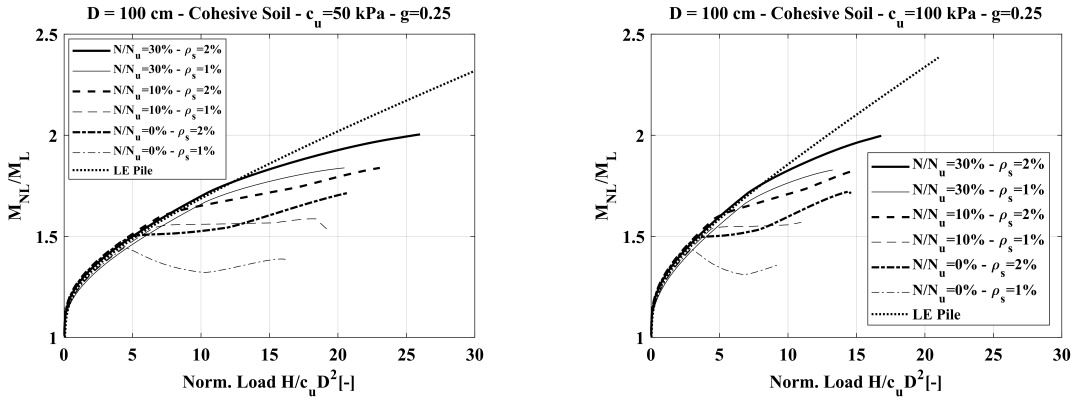

Figure 7.19: I_{MY} parameter against normalised horizontal load for a fixed-head in cohesive soils, with parameter $g = 0.25$; D=100 cm

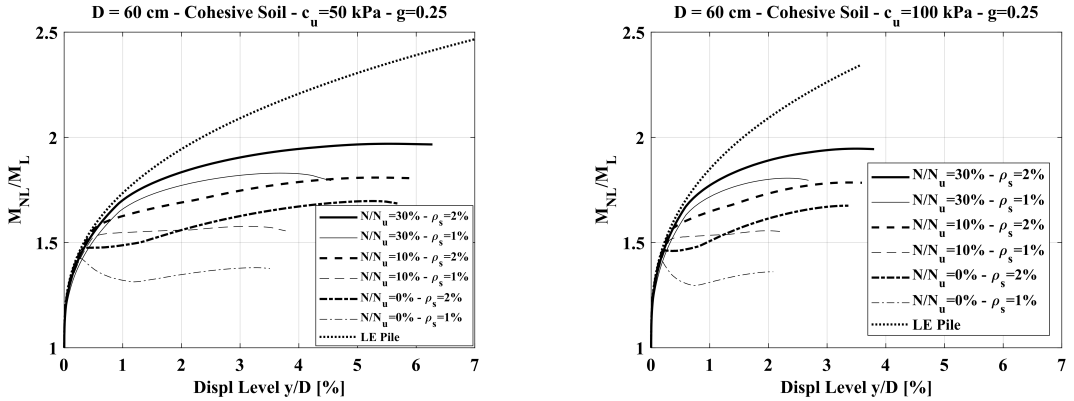

Figure 7.20: I_{MY} parameter against displacement level for a fixed-head in cohesive soils, with parameter $g = 0.25$; D=60 cm

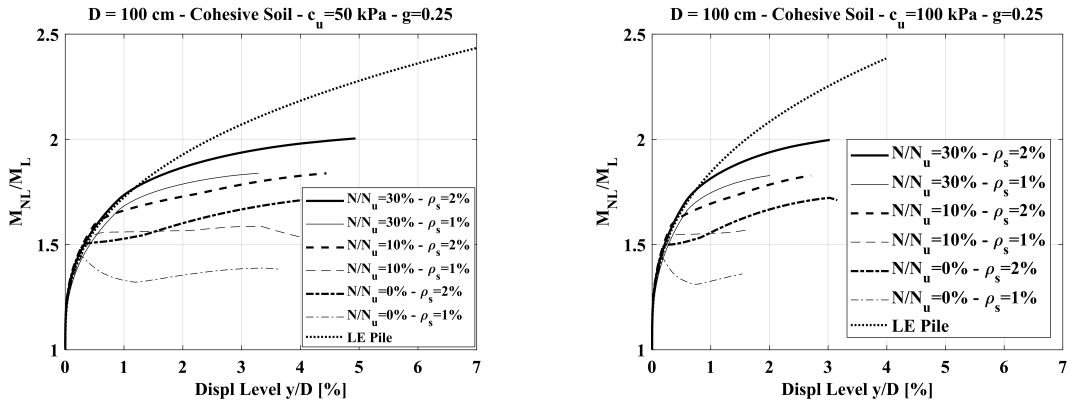

Figure 7.21: I_{MY} parameter against displacement level for a fixed-head in cohesive soils, with parameter $g = 0.25$; D=100 cm

Fixed-head pile - cohesionless soil - $g = 1.0$ - $\phi = 30°$; $\phi = 40°$ - Pile diameter = 0.60 m and 1.0 m

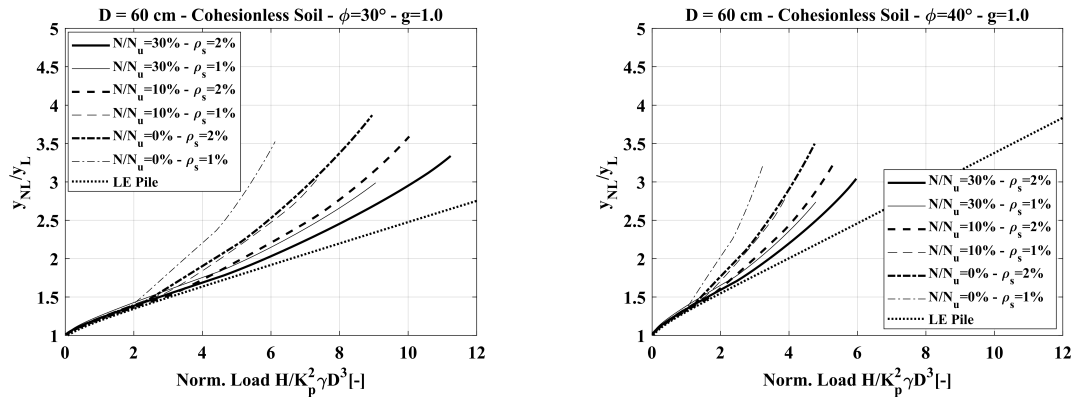

Figure 7.22: I_{yY} parameter against normalised horizontal load for a fixed-head pile in cohesionless soils with parameter $g = 1$; D=60 cm

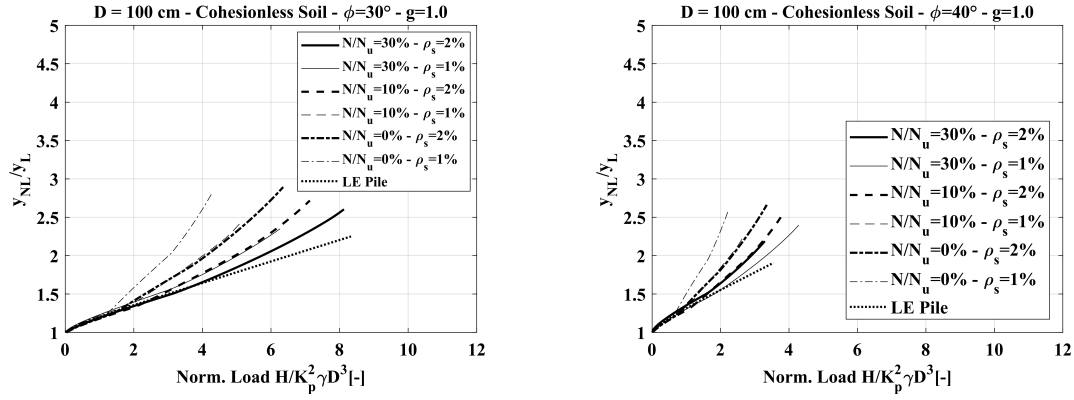

Figure 7.23: I_{yY} parameter against normalised horizontal load for a fixed-head pile in cohesionless soils with parameter $g = 1$; D=100 cm

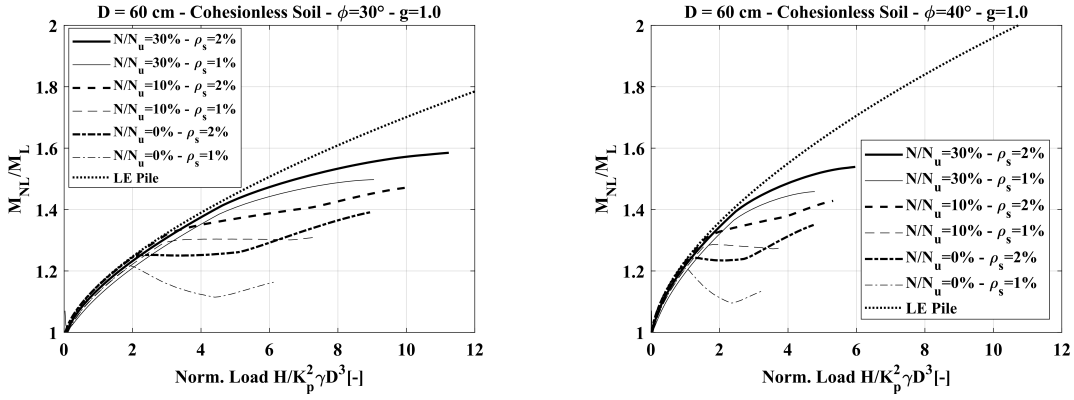

Figure 7.24: I_{MY} parameter against normalised horizontal load for a fixed-head in cohesionless soils, with parameter $g = 1$; D=60 cm

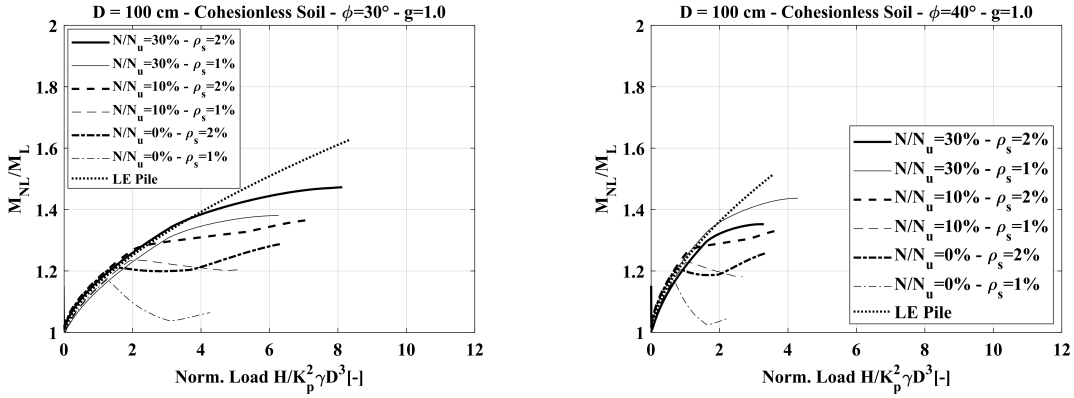

Figure 7.25: I_{MY} parameter against normalised horizontal load for a fixed-head in cohesionless soils, with parameter $g = 1$; D=100 cm

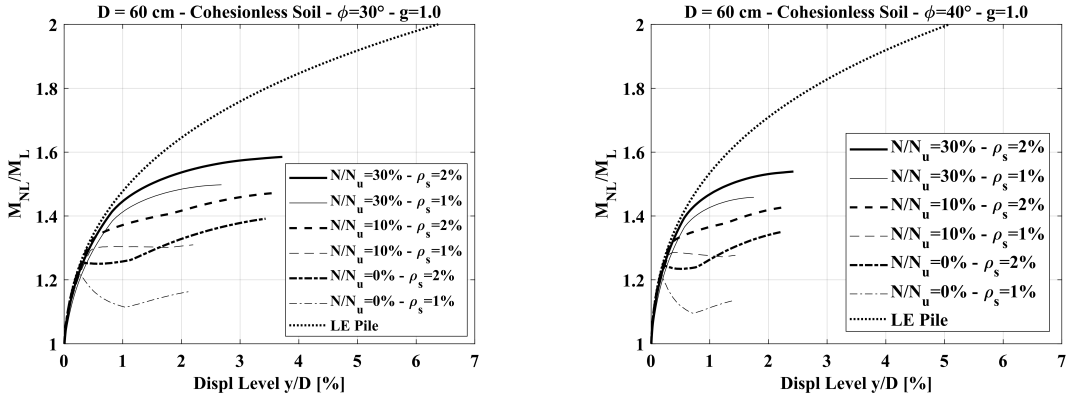

Figure 7.26: I_{MY} parameter against displacement level for a fixed-head in cohesionless soils, with parameter $g = 1$; D=60 cm

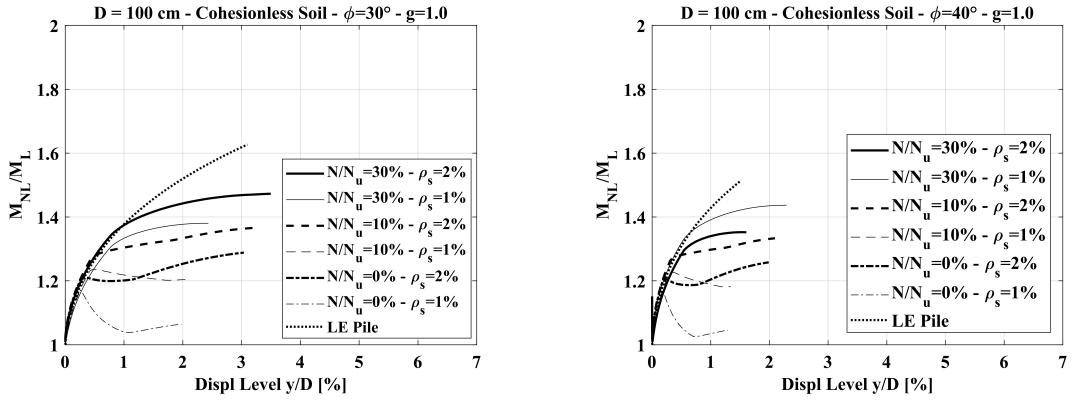

Figure 7.27: I_{MY} parameter against displacement level for a fixed-head in cohesionless soils, with parameter $g = 1$; D=100 cm

Fixed-head pile - cohesionless soil - $g = 0.25$ - $\phi = 30°$; $\phi = 40°$ - Pile diameter = 0.60 m and 1.0 m

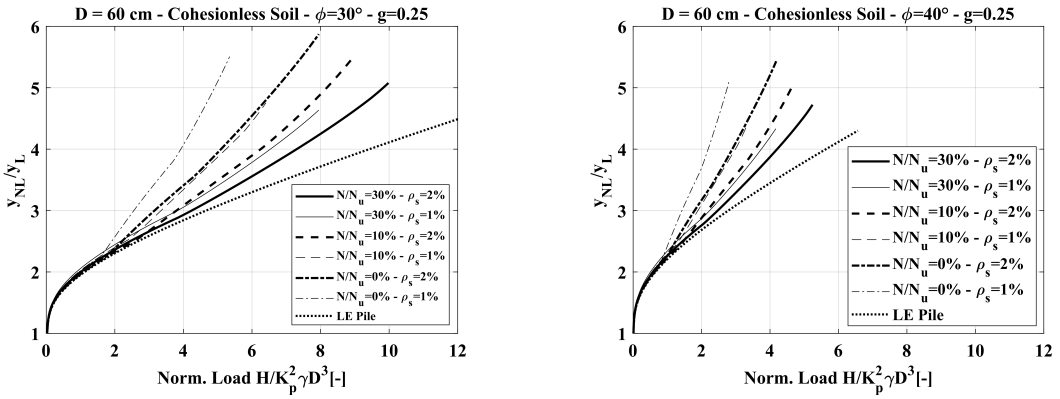

Figure 7.28: I_{yY} parameter against normalised horizontal load for a fixed-head pile in cohesionless soils with parameter $g = 0.25$; D=60 cm

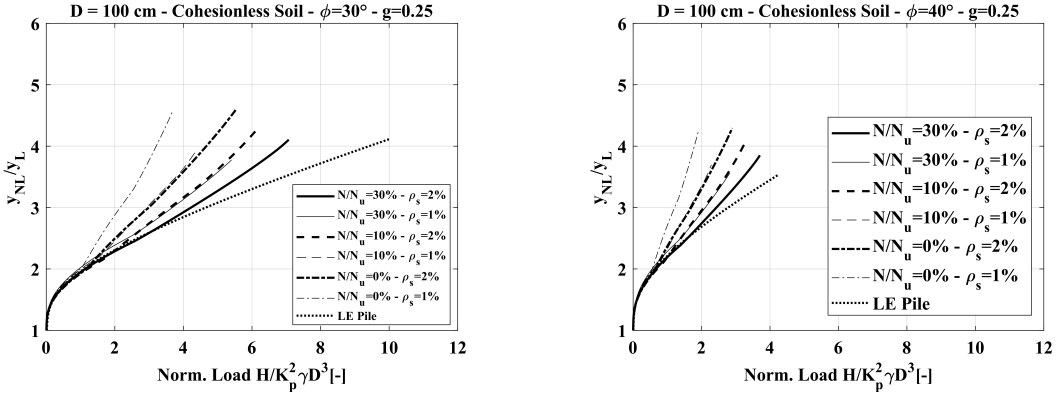

Figure 7.29: I_{yY} parameter against normalised horizontal load for a fixed-head pile in cohesionless soils with parameter $g = 0.25$; D=100 cm

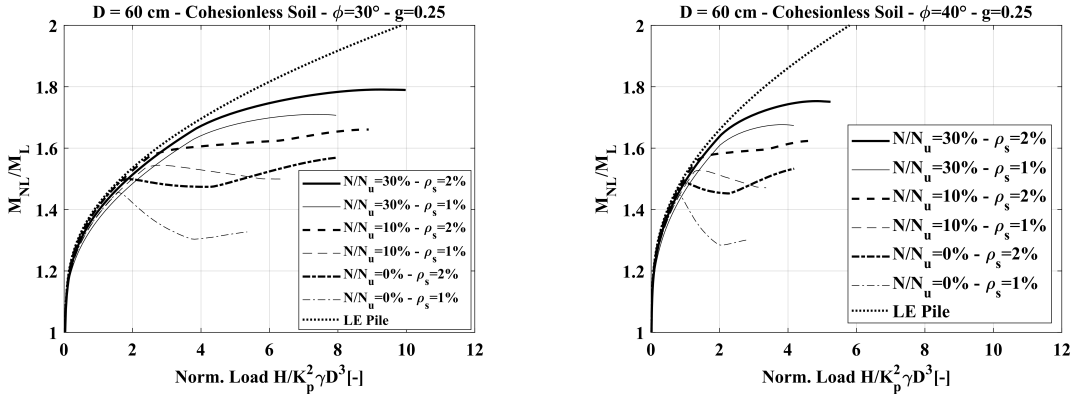

Figure 7.30: I_{MY} parameter against normalised horizontal load for a fixed-head in cohesionless soils, with parameter $g = 0.25$; D=60 cm

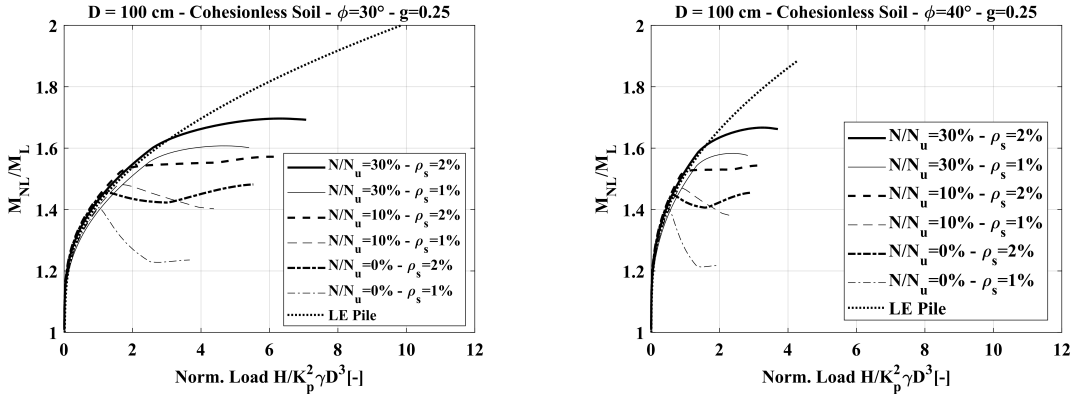

Figure 7.31: I_{MY} parameter against normalised horizontal load for a fixed-head in cohesionless soils, with parameter $g = 0.25$; D=100 cm

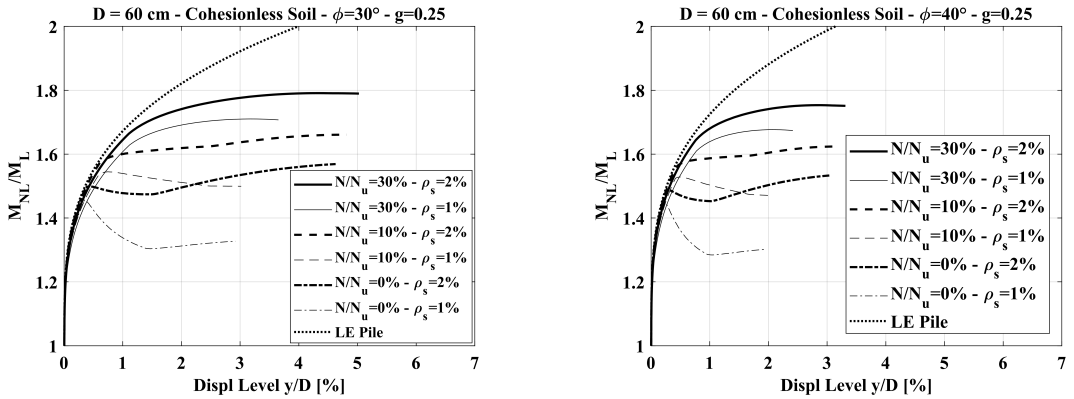

Figure 7.32: I_{MY} parameter against displacement level for a fixed-head in cohesionless soils, with parameter $g = 0.25$; D=60 cm

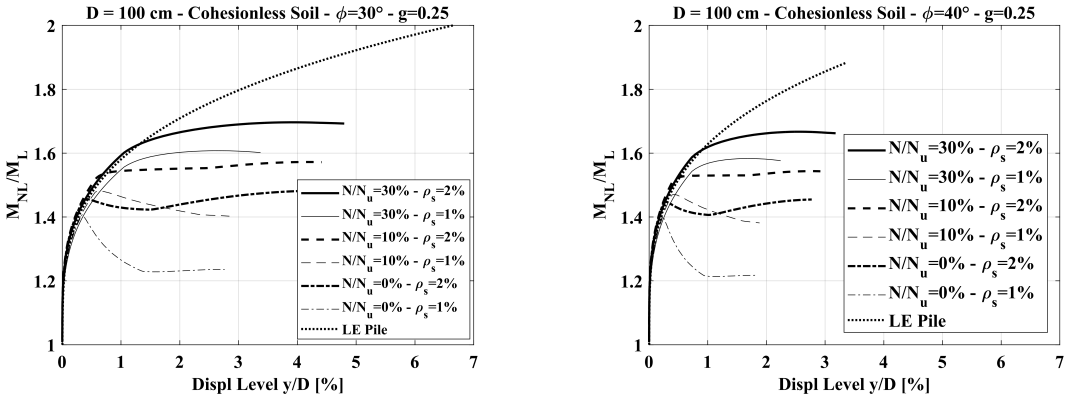

Figure 7.33: I_{MY} parameter against displacement level for a fixed-head in cohesionless soils, with parameter $g = 0.25$; D=100 cm

Looking at the results, the following remarks can be drawn:

- the progressive variation of the initial pile-soil relative stiffness, K_0, during the increase of the load level, and caused by the reduction of both the pile and soil stiffness, increases the values of displacements that were obtained by an analysis in which the pile was considered linear-elastic with a constant flexural-rigidity;
- the increase of the displacement is dependent on the steel reinforcement ratio and on the compressive axial load acting on the pile section. The displacements grow with the decrease of the compressive axial load and of the reinforcement ratio; this is due to the fact that increasing the axial load level the linear-elastic behaviour of the pile is kept up to bigger load levels, as a result of the increase of the cracking moment value;
- the maximum bending moment is dependent on the variation of the pile-soil relative stiffness with respect to the initial value K_0, considering as independent variable the horizontal load level; when the displacement level is considered as independent variable, in more flexible piles are observed smaller bending moments;
- a variation of the ultimate soil resistance profile causes a variation in the response. For lower values of c_u or ϕ the response is more affected by the variation of the pile-soil relative stiffness;
- for bigger values of the initial relative stiffness ratio, K_0, the response is more affected by the relative stiffness variation: the displacements increase more for higher K_0 values.

7.2 Pair of piles: parametric study

7.2.1 Elastic analysis: literature overview

Studying the horizontal response of a pair of identical piles, equally loaded, it was observed as they are subjected (due to the presence of the adjacent pile), to an increase of both the head displacement and rotation, compared to a single isolated pile subjected to the same load. This consideration leads to define the so-called 'interaction factors' for a laterally loaded pair of piles (Poulos, 1971):

- $\alpha_y = \frac{\text{additional pile head displ. due to adjacent pile}}{\text{pile head displ. due to the load acting on itself}}$;
- $\alpha_\theta = \frac{\text{additional pile head rot. due to adjacent pile}}{\text{pile head rot. due to the load acting on itself}}$;

Once known these interaction factors, it was considered that the analysis could be extended to the generic group composed by a number m of piles applying the superposition principle. The reference studies are those realized by Poulos (1971), Randolph (1981), El Sharnouby and Novak (1985; 1986) and Chow (1987).

The parametric analyses performed on pair of piles considered the following schemes:

- Loads acting at the pile-head: horizontal load or bending moment;
- Constraint conditions at the pile-head: free-to-rotate of fixed-head;
- Soil homogeneity: Young modulus constant or variable (linearly increasing) with depth;

Table 7.1 summarizes the analysis types carried out by each authors; all these analyses were carried out in the linear-elastic field.

Table 7.1: Parametric analyses performed on pair of piles

	Linear analysis				Non linear analysis
Authors	Homog. soil	Non-Homog. soil	Free-Head	Fixed-Head	
Poulos (1971)	X	-	X	X	-
Randolph (1981)	X	X	X	X	-
El Sharnouby et al. (1986)	X	X	X	X	-
Chow (1987)	X	X	X	X	-

The trends of the interaction factors depend on both the pile-head constraint condition and the load-type. For this reason, different coefficients were introduced, each of them related to the specific scheme studied (Poulos, 1971):

- α_{yH} = interaction factor related to the head displacement for a free-to-rotate pile loaded by a horizontal force;
- $\alpha_{\theta H}$ = interaction factor related to the head rotation, reported to for a free-to-rotate pile loaded by a horizontal force;
- α_{yM} = interaction factor related to the pile head displacement, for a free-to-rotate pile loaded by a moment;
- $\alpha_{\theta M}$ = interaction factor related to the head rotation, for a free-to-rotate pile loaded by a moment;
- α_{yF} = interaction factor related to the pile-head displacement, for a fixed-head pile loaded by a horizontal force;

By the theorem of reciprocity $\alpha_{yM} = \alpha_{\theta H}$. The previous considerations about the critical length can be extended to the pair of piles. For this reason, is more rational the use of a relative stiffness, K, simply defined as the ratio between the pile and soil stiffness.

The parameters that most affect the interaction factors are:

- the relative spacing s/D between the piles;
- the angle β (see Figure 7.34);
- the pile-soil relative stiffness, K.

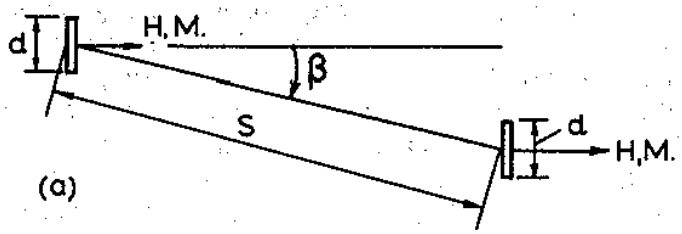

Figure 7.34: Departure angle β between a pair of piles (Poulos and Davis, 1980)

The parametric analyses in the available literature, permit to draw the following considerations:

- the factors α decrease as the relative spacing s/D increases;
- the factors α decrease when the angle β increases from $0°$ to $90°$;
- the factors α increase as the relative stiffness K increases;
- the factor α_{yF}, relative to the displacement of a fixed-head pile, is bigger that the factor α_{yH}, relative to displacement of a free-to-rotate piles;
- for free-to-rotate piles, the values of α relative to a moment are smaller than those related to a horizontal load;
- for free-to-rotate piles, the factors α relative to the displacements are bigger than those related to the rotation;
- the factors α in a homogeneous elastic medium are greater than those in a medium with an elastic modulus variable with depth (approximately the double, according to Randolph, 1981).

7.2.2 Elastic analysis using the developed BEM-method

In this section are presented the results of a parametric study carried out on pair of piles in a homogeneous soil using the proposed BEM method. The pile-soil stiffness ratio was taken to be $E_p/E_s = 1000$, the pile slenderness ratio $L/D = 25$ and the departure angles studied were $\beta = 0°$ and $\beta = 90°$. The pile-pile interaction factors are defined as:

- $\alpha_y = \frac{\text{additional pile head displ. due to adjacent pile}}{\text{pile head displ. due to the load acting on itself}}$;
- $\alpha_\theta = \frac{\text{additional pile head rot. due to adjacent pile}}{\text{pile head rot. due to the load acting on itself}}$;

The interaction factors (α) are computed varying the pile spacing s/D. The results (Figure 7.35, Figure 7.36 and Figure 7.37) are compared with the analytical expressions proposed by El Sharnouby and Novak (1986).

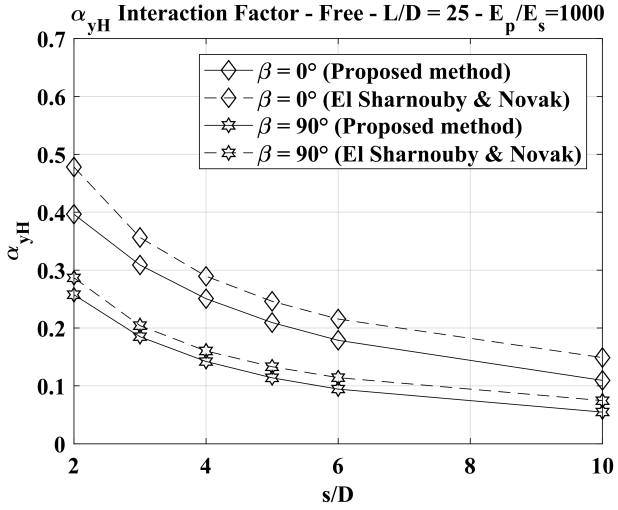

Figure 7.35: Horizontal displacement pile-pile interaction factor of piles in homogeneous soil (free-head)

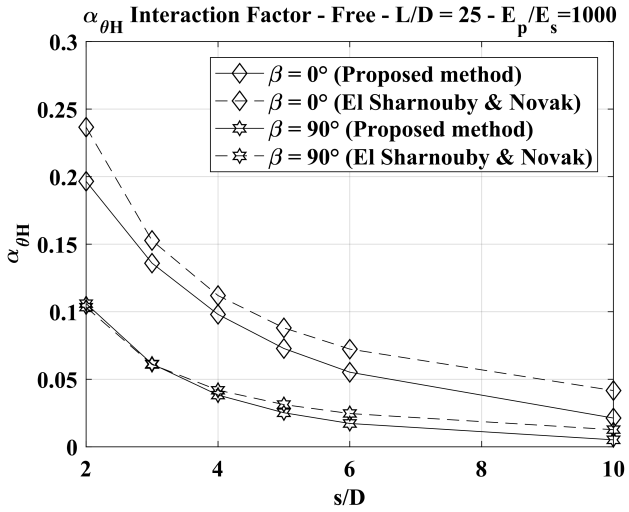

Figure 7.36: Rotation pile-pile interaction factor of piles in homogeneous soil

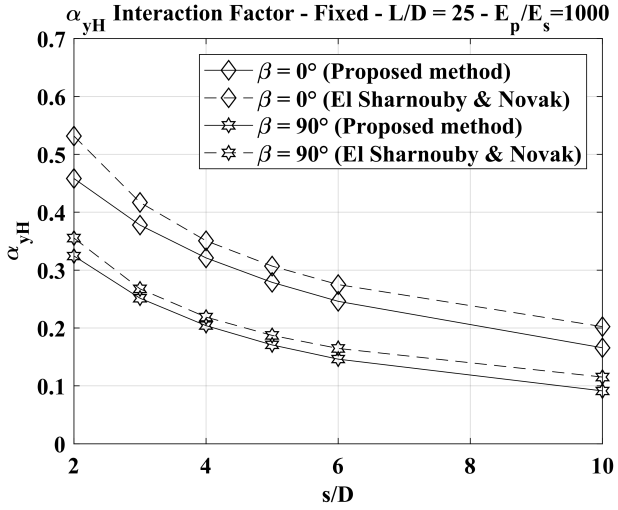

Figure 7.37: Horizontal displacement pile-pile interaction factor of piles in homogeneous soil (fixed-head)

In order to evaluate the effect of the elastic modulus profile on the interaction factors (considering only a departure angle $\beta = 0°$), the same analyses performed before were carried out in a non-homogeneous soil (Gibson's profile, with a soil modulus linearly increasing with depth and having $E_p/(E_s(z = 25D) = 1000)$). The results are shown in Figure 7.38, Figure 7.39 and Figure 7.40.

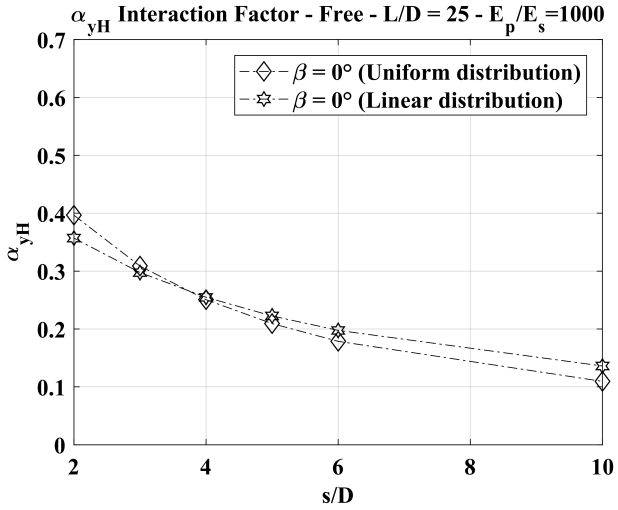

Figure 7.38: Effect of the elastic modulus profile on the horizontal displacement pile-pile interaction factor of piles (free-head)

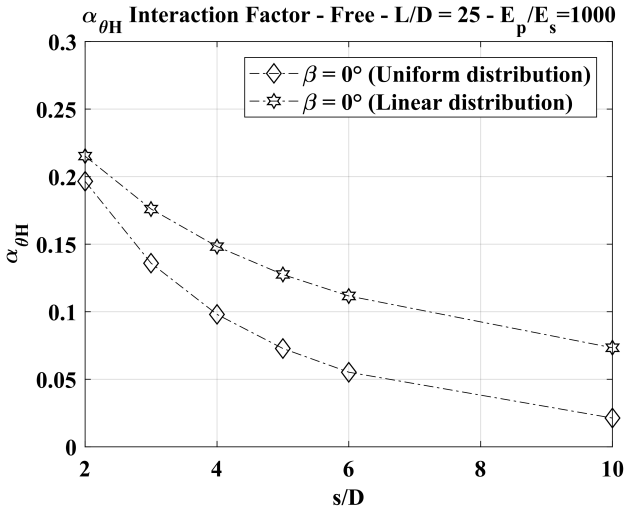

Figure 7.39: Effect of the elastic modulus profile on the rotation pile-pile interaction factor of piles (free-head)

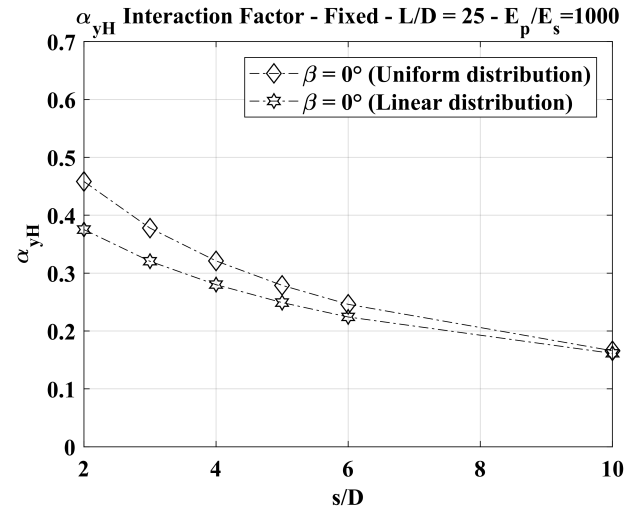

Figure 7.40: Effect of the elastic modulus profile on the horizontal displacement pile-pile interaction factor of piles (fixed-head)

7.3 Pile group: parametric study

7.3.1 Elastic analysis using the developed BEM-method

In this section are shown the results of three parametric studies on pile group in linear elastic condition using the proposed BEM method.

The first study is about a fixed-head pile group with 16 piles. The ratio of pile length to diameter is 25 and the pile flexibility factor K_R is equal to 10^{-5} (defined as $K_R = (E_p I_p)/(E_s L^4)$, I_p is the second moment of area of the pile). Here the Poisson's ratio for the soil was taken as 0.499. E_p/E_s was chosen to be 79.6 and the rigid cap is just clear of the ground. The load distributions against pile spacing are plotted in Figure 7.41. The results are here compared with those obtained by El Sharnouby and Novak (1985) and Zhang and Small (2000) for the same problem. It may be seen that

these results are in fairly good agreement with the results obtained using the proposed method.

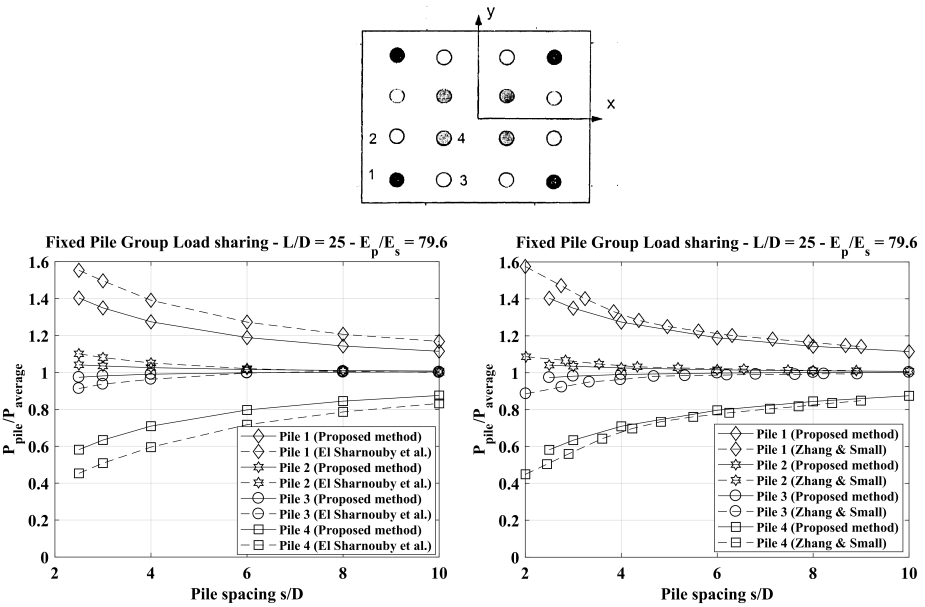

Figure 7.41: Typical horizontal load distributions in fixed head pile group

The second parametric study has been performed in order to demonstrate the use of the proposed method for the analysis of laterally loaded pile groups. The most critical parameters were examined to show their effects on the maximum displacement of a 4x3 pile group (12 piles). The ratios of the embedded pile length to pile diameter (L_{em}/D) were chosen to be 10, 20, 40. The Poisson's ratios of the soil was assumed to be 0.35. The ratio of the exposed pile length H_0 to the pile diameter was 2.5 and the pile spacing ratio (s/D) was taken as 5.

Varying the pile-soil stiffness ratio E_p/E_s from 10^1 (flexible pile) to 10^6 (rigid pile) the proposed calculation program was used to calculate the displacements of the pile group. The normalised displacements are plotted in Figure 7.42 against the pile-soil stiffness ratio, and are compared with the results obtained by Zhang and Small (2000). It may be seen from Figure 7.42 that the horizontal displacements of the pile group decrease rapidly with the pile-soil stiffness ratio.

The results corresponding to three different pile lengths show that there is almost no influence of the pile lengths on the displacement of the pile group for a pile-soil stiffness ratio less than 10^3 and for pile slenderness ratios in excess of 10. However, when the piles become substantially rigid (E_p/E_s up to 10^6), the shorter piles will obviously produce higher displacement than the longer piles.

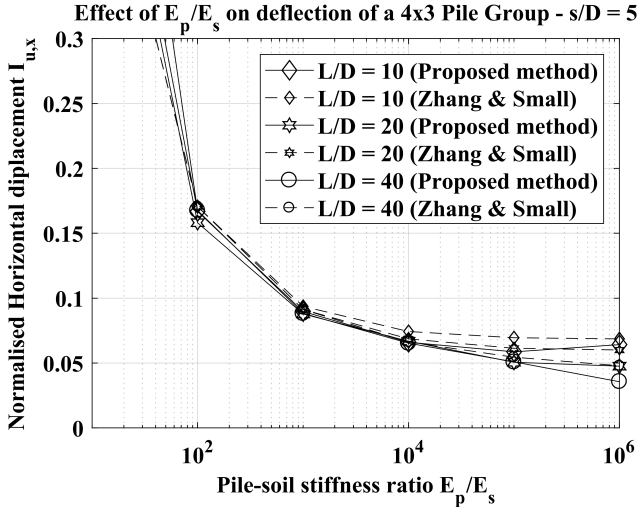

Figure 7.42: The effect of pile-soil stiffness ratio on deflection of pile groups under horizontal loads

The third parametric study was performed using three different types of elastic soils, where the modulus increases with depth. The soil models are shown in Figure 7.43.

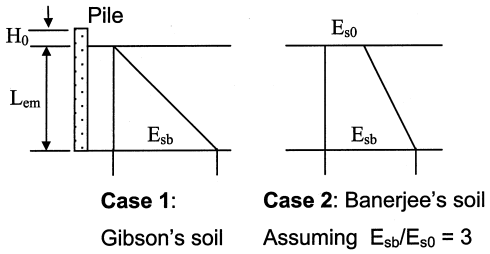

Figure 7.43: Soil types used in the parametric study

It is assumed that the pile group with 12 piles (4x3 pile group) is embedded in the different soil types. The stiffness of the different soils can be expressed as:

$$E_s(z) = E_{s0} + m(\frac{z}{L_{em}})^n \tag{7.29}$$

If $m = 0$, the above equation represents a homogeneous soil with a constant elastic modulus, i.e. $E_{s0} = E_{sb}$; if $E_{s0} = 0$ and $n = 1$, it represents Gibson's soil; if $E_{s0} > 0$ and $n = 1$, it is a Banerjee's soil. The soil modulus E_{sb} was taken as 7 MPa at the pile tip and the ratio L_{em}/D was taken as 20. The pile-soil stiffness ratio E_p/E_{sb} was 4000. Other parameters were the same as used in the previous parametric study. Figure 7.44 shows that the pile spacing has a significant effect on displacements of the group when the pile spacing is less than about 6 times the pile diameter.

Furthermore, these results show that the homogeneous soil is one of the best soils with respect to resistance of deflection of a pile group. On the contrary, the Gibson's soil is the poorest one as may be expected. Moreover, beyond a value of pile spacing of $s/D = 6$, the effect of a change in spacing on the displacement of the group examined will become much less.

For the pile group, moments in pile 1 corresponding to two pile spacing ($2D$ and $6D$) are plotted in Figure 7.45 and Figure 7.46. With a pile spacing ratio of $2D$ as shown in Figure 7.45, the largest value of both positive and negative moment in pile 1 is higher than that in pile 1 with a pile spacing ratio of 6 as plotted in Figure 7.46. This demonstrates that a relatively small pile spacing ratio (i.e. less than 6) may lead to a large moment in the pile and is therefore a less economical use of the piles. All the results of this third parametric study are compared with those obtained by Zhang and Small (2000) using the software APRAF.

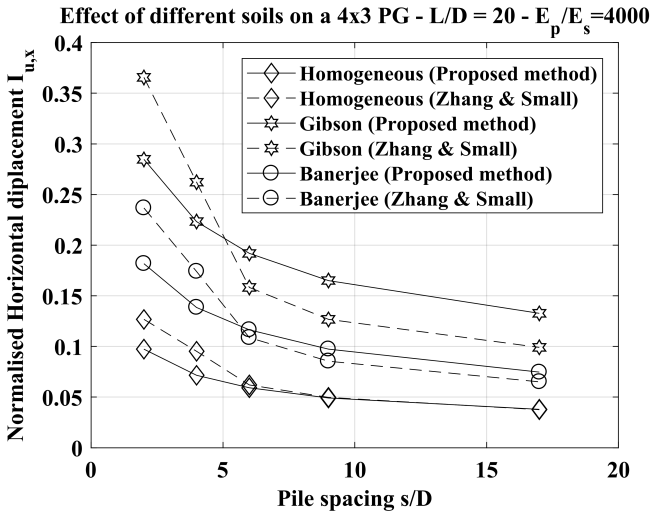

Figure 7.44: The effect of different soils on the displacement of pile groups under horizontal loading

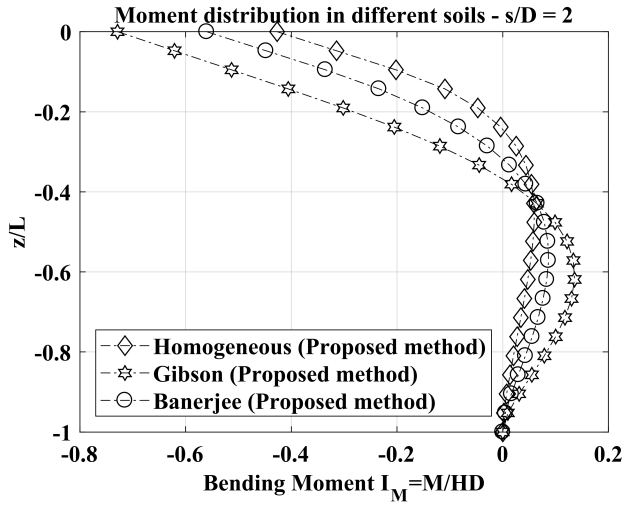

Figure 7.45: Moment distribution in a pile embedded in different soils with close pile spacing

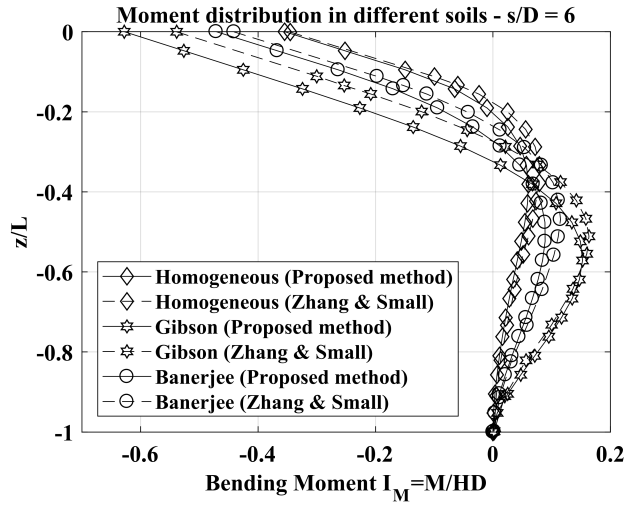

Figure 7.46: Moment distribution in a pile embedded in different soils with large pile spacing

7.4 Piled Raft: parametric study

7.4.1 Elastic analysis using the developed BEM-method

In this section are shown the results of some parametric studies (linear elastic condition) conducted on piled-raft foundation subjected to lateral load using the proposed BEM method.

The first parametric study was carried out on a square piled-raft foundation with 16 (4x4) piles embedded in a deep uniform soil. Poisson's ratio of the soil was taken to be 0.35, the elastic modulus of the soil, E_s, was taken equal to 10 MPa, the pile diameter was 0.5 m and the pile slenderness ratio, L/D = 30 (pile length L = 15 m).

In order to evaluate the effect of the pile-soil stiffness ratio on the load distribution (between the 4x4 pile-group and the raft) and on the displacement the analyses were carried out using a spacing ratio, s/D, equal to $5D$, while the pile-soil stiffness ratio was taken equal to: 10, 100, 1000, 10000. The normalised horizontal displacement can be expressed as:

$$I_{u,xx} = \frac{E_s D y}{H} \tag{7.30}$$

The results (Figure 7.47 and Figure 7.48) are compared with those obtained by Small and Zhang (2006). The analyses, with the proposed method, were carried out considering the pile-heads both fixed and free to rotate. As expected, an increase of the pile-soil stiffness ratio leads to a reduction in the horizontal normalised displacement of the piled-raft and to an increase of the load carried by the 4x4 pile-group.

Moreover, the effect of the pile-spacing on the load distribution (between the 4x4 pile-group and the raft) and on the displacement was examined. The analyses were carried out using a pile-soil stiffness ratio equal to 2000, while the pile-spacing value investigated were: $2D$, $3D$, $4D$, $6D$ and $10D$. The results (Figure 7.49 and Figure 7.50) are compared with those obtained by Small and Zhang (2006).

The analyses, with the proposed method, were carried out considering the pile-heads fixed. The increase of the pile-spacing ratio has a pronounced effect on the

horizontal normalised displacement (significant reduction) of the piled-raft and leads to an important reduction of the horizontal load carried by the pile-group.

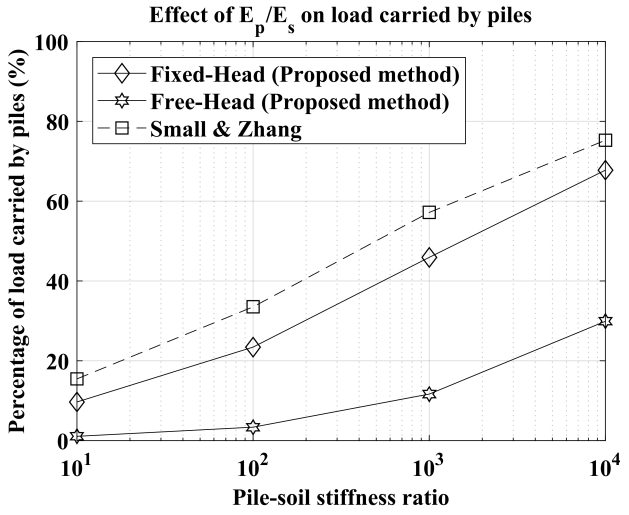

Figure 7.47: Effect of pile-soil stiffness ratio on the percentage of load carried by the piles

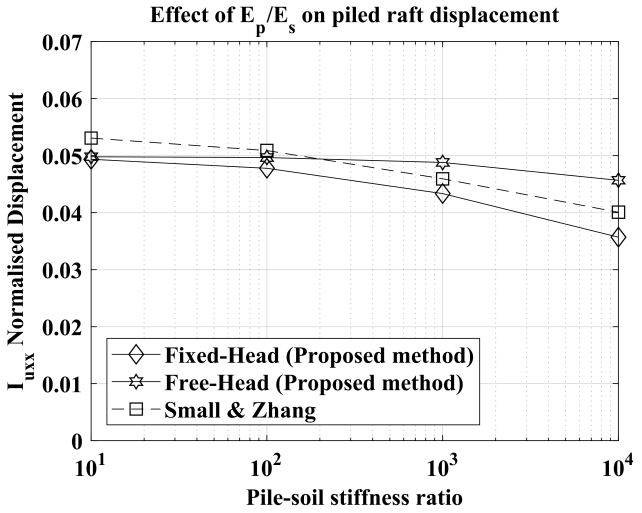

Figure 7.48: Effect of pile-soil stiffness ratio on piled raft displacement

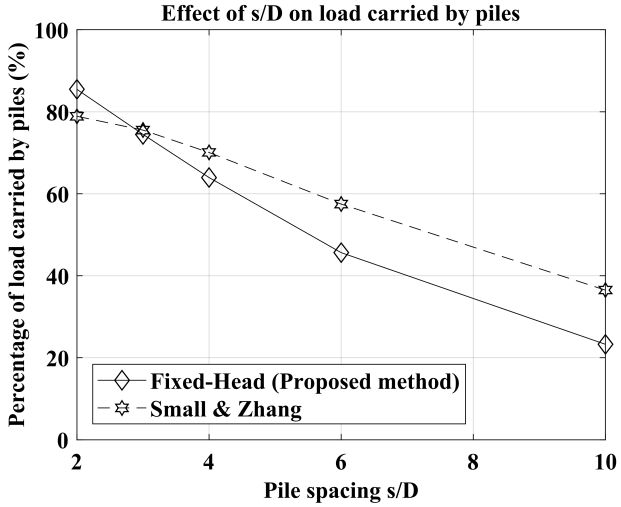

Figure 7.49: Effect of pile spacing ratio on the percentage of load carried by the piles

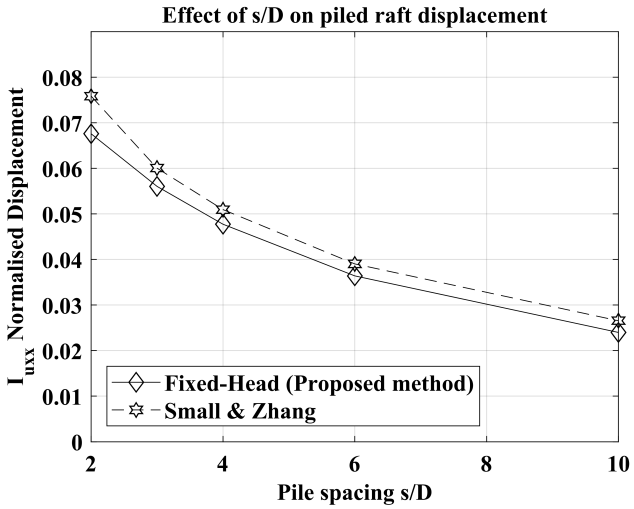

Figure 7.50: Effect of pile spacing ratio on piled raft displacement

The second parametric study was carried out on a square piled-raft foundation with 9 (3x3) piles embedded in a deep uniform soil. The cap or raft connecting the pile heads is assumed to be constructed in contact with the ground or just clear of the ground. Poisson's ratio of the soil was taken to be 0.49, the elastic modulus of the soil, E_s, was taken equal to 30 MPa, the pile diameter was 1.0 m and the pile slenderness ratio, L/D = 25 (pile length L = 25 m). In order to evaluate the effect of the pile-soil stiffness ratio on the load distribution (between the 3x3 pile-group and the raft) and on the displacement the analyses were carried out using a spacing ratio, s/D, equal to $5D$, while the pile-soil stiffness ratio was taken equal to: 100, 1000, 10000, 100000.

The results (Figure 7.51 and Figure 7.52) are compared with those obtained by Small and Zhang (2002). As expected, an increase of the pile-soil stiffness ratio leads to a reduction in the horizontal normalised displacement of the piled-raft and to an increase of the load carried by the 3x3 pile-group.

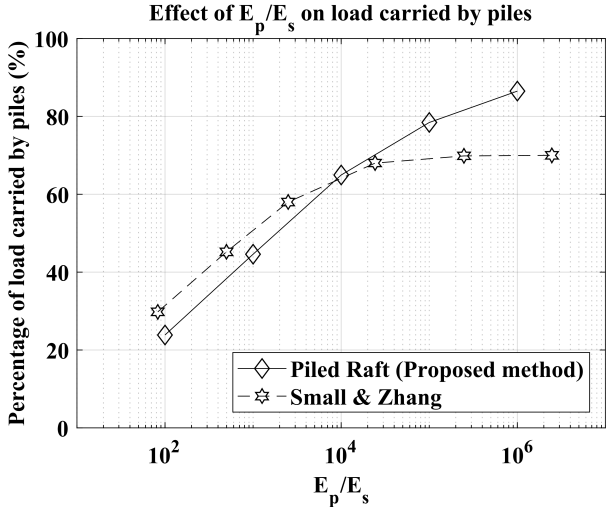

Figure 7.51: Effect of pile-soil stiffness on the percentage of load carried by the piles

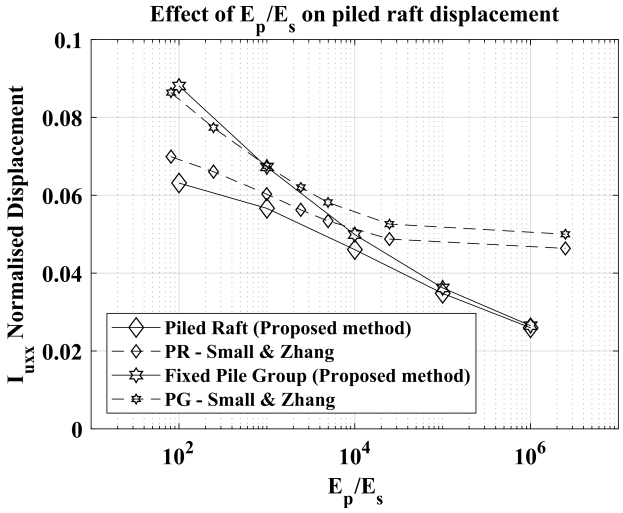

Figure 7.52: Effect of pile-soil stiffness ratio on piled raft displacement

The third parametric study was carried out on a square piled-raft foundation with 16 (4x4) piles. Poisson's ratio of the soil was taken to be 0.35, the elastic modulus of the soil, E_s, was taken equal to 30 MPa, the pile diameter was 1.0 m and the pile slenderness ratio, L/D = 18.75 (pile length L = 18.75 m).

In order to evaluate the effect of the pile-soil stiffness ratio on the displacement the analyses were carried out using a spacing ratio, s/D, equal to $6D$, while the pile-soil stiffness ratio was taken equal to: 100, 1000, 10000, 100000. The laterally loaded piled raft is embedded in three different kind of soil as shown in Figure 7.53 (Gibson's soil $E_{s1}/E_s = 0$, Banerjee's soil $E_{s1}/E_s = 0.5$ and a homogeneous soil $E_{s1}/E_s = 1.0$; E_{s1} is the soil modulus at the soil surface and E_s is the soil modulus at the pile tip).

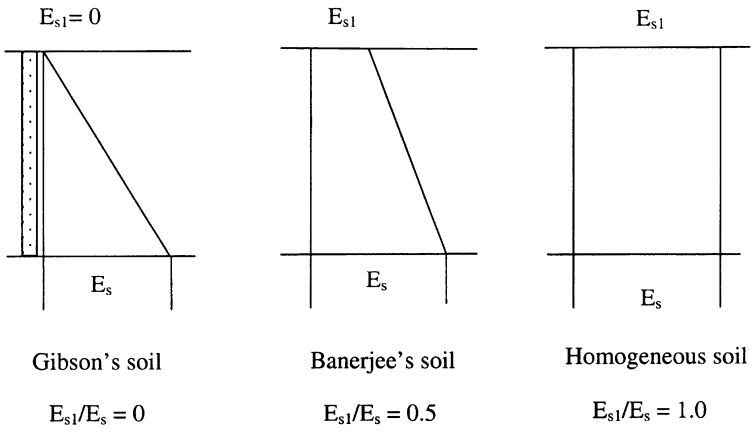

Figure 7.53: Soil types used in the parametric study

In the evaluation of the normalised horizontal displacement the modulus at the pile tip is considered. The results for normalised displacement are plotted in Figure 7.54 against the pile soil stiffness ratio E_p/E_s (where again E_s is the soil modulus at the pile tip). It may be seen that the displacement of the piled raft is greatest in the Gibson's soil and smallest in the homogeneous soil. With increase of pile stiffness, the displacement of the piled raft in the Gibson's soil will be reduced significantly.

This example and the results obtained (compared with those of Small and Zhang, 2002) show that the proposed method may deal with soils where the soil stiffness can vary with depth or from layer to layer and can provide, for the most common values of pile-soil stiffness ratio (ranging between 100 and 10000), results in agreement with the method proposed by Zhang and Small and based on the finite layer theory.

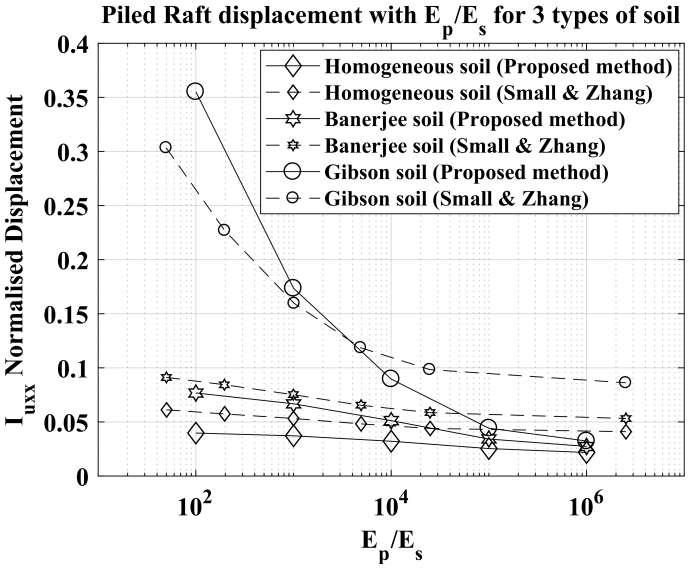

Figure 7.54: Variation of displacement with pile-soil ratio for three types of soil

The fourth parametric study was carried out realizing similar analyses as performed by Kitiyodom and Matsumoto (2002). In this work the authors presented an approximate method which employs a flexibility matrix method to combine the

individual stiffnesses of a pile group and a raft. This approximate method allows estimation of the piled raft response from the results of the analysis of the raft and the pile group studied alone. The method is written in the matrix form as:

$$\begin{bmatrix} 1/k_p & \alpha_{pr}/k_r \\ \alpha_{rp}/k_p & 1/k_r \end{bmatrix} (\frac{P_p}{P_r}) = (\frac{w_p}{w_r}) \tag{7.31}$$

Where w_p is the average displacement of the pile group in the piled raft, w_r the average displacement of the raft in the piled raft, P_p the total load carried by the pile group in the piled raft, P_r the total load carried by the raft in the piled raft, k_p the overall stiffness of the pile group alone, k_r the overall stiffness of the raft alone, α_{rp} the interaction factor of the pile group on the raft and α_{pr} the interaction factor of the raft on the pile group.

Randolph (1983) assumed that the average displacement of the pile group, w_p, is equal to the average displacement of the raft, w_r (i.e. the average displacement of the piled raft $w_{pr} = w_p = w_r$), and the off-diagonal terms of the flexibility matrix are equalled ($\alpha_{pr}/k_r = \alpha_{rp}/k_p$). He also suggested that the influence of the pile group on the raft is more likely than the influence of the raft on the pile group to result in an average displacement of the raft similar to the above work compatible value. Thus, α_{rp}/k_p is a more reliable parameter for determining piled raft behaviour than α_{pr}/k_r. The load carried by the pile group, P_p, and the raft, P_r, and the overall stiffness of the piled raft, k_{pr} can be found in terms of α_{rp} as shown in the following expressions:

$$P_p = \frac{[1 - k_r(\alpha_{rp}/k_p)]w_{pr}}{(1/k_p) - k_r(\alpha_{rp}/k_p)^2} \tag{7.32}$$

$$P_r = \frac{[(k_r/k_p)(\alpha_{rp}/k_p)]w_{pr}}{(1/k_p) - k_r(\alpha_{rp}/k_p)^2} \tag{7.33}$$

$$k_{pr} = \frac{P_p + P_r}{w_{pr}} = \frac{[k_p + k_r(1 - 2\alpha_{rp})]}{[1 - (k_r/k_p)\alpha_{rp}^2]} \tag{7.34}$$

Randolph (1983) also assumed that the value of α_{rp} for a single pile pile-raft unit is directly applicable to a piled raft foundation having more than one pile. This means that for a known value of α_{rp}, approximate values for the average displacement of the piled raft and the load distribution between the pile group and the raft can be calculated. The values of α_{rp} and α_{pr} can be calculated from the value of P_p, P_r, k_p, k_r and w_{pr} by means of the equations:

$$\alpha_{rp} = \frac{k_p}{P_p}(w_{pr} - \frac{P_r}{k_r}) \tag{7.35}$$

$$\alpha_{pr} = \frac{k_r}{P_r}(w_{pr} - \frac{P_p}{k_p}) \tag{7.36}$$

In order to obtain all the values of P_p, P_r, k_p, k_r and w_{pr}, it is necessary to perform three separate analyses. The values of k_p and k_r are obtained from analyses of the pile group and the raft in isolation. Then, a full analysis of the piled raft is performed to obtain P_p, P_r and w_{pr}.

A parametric study for laterally loaded square piled rafts was performed and is presented here. The analyses were conducted on square piled rafts varying the number of piles between 4 (2x2) and 25 (5x5). The ranges of the dimensionless parameters

were set as 3-9 for the pile spacing ratio s/D, as 10^2-10^5 for the pile soil stiffness ratio E_p/E_s, while the pile slenderness ratio was set equal to $L/D = 25$. Figures from Figure 7.55 to Figure 7.64 show the calculated values of α_{rp} and α_{pr}.

These values are compared (when available) with those obtained by Kitiyodom and Matsumoto (2002). Both the values of α_{rp} and α_{pr} increase with the number of piles. It can be seen that the effect of E_p/E_s on α_{rp} is small and that the value of α_{pr} increases as the pile spacing increases (or as the pile stiffness decreases), while the opposite happens for the value of α_{rp}.

These figures may be used as design charts to estimate the stiffness of piled rafts subjected to lateral loading, k_{pr}, using the value of α_{rp}, and to estimate the load distribution, P_p and P_r using the expressions above.

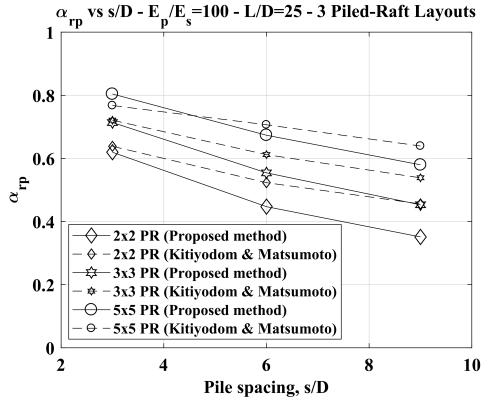

Figure 7.55: Calculated α_{rp} values for different piled raft layouts ($E_p/E_s = 100$)

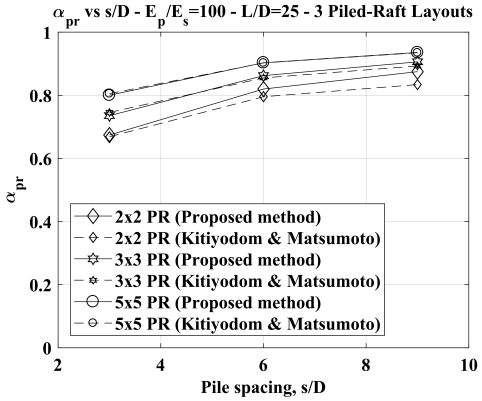

Figure 7.56: Calculated α_{pr} values for different piled raft layouts ($E_p/E_s = 100$)

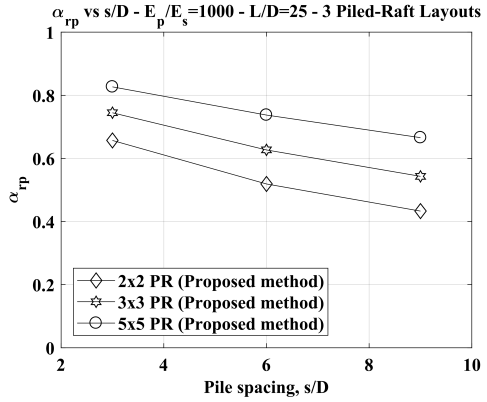

Figure 7.57: Calculated α_{rp} values for different piled raft layouts ($E_p/E_s = 1000$)

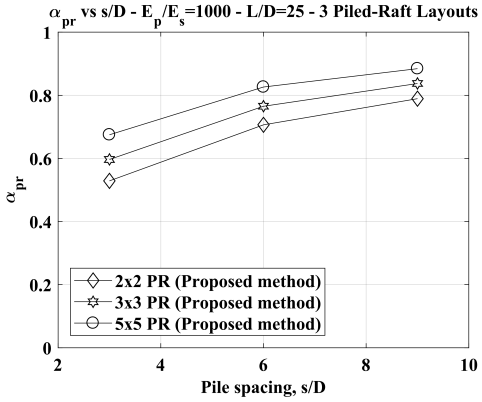

Figure 7.58: Calculated α_{pr} values for different piled raft layouts ($E_p/E_s = 1000$)

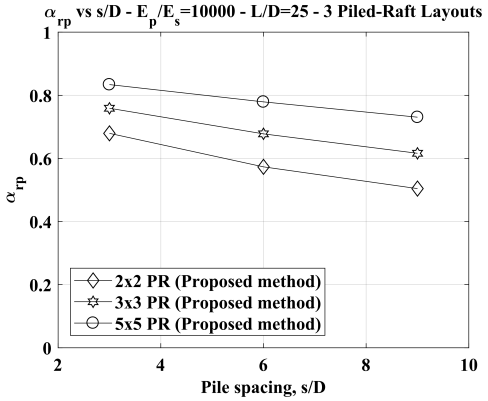

Figure 7.59: Calculated α_{rp} values for different piled raft layouts ($E_p/E_s = 10000$)

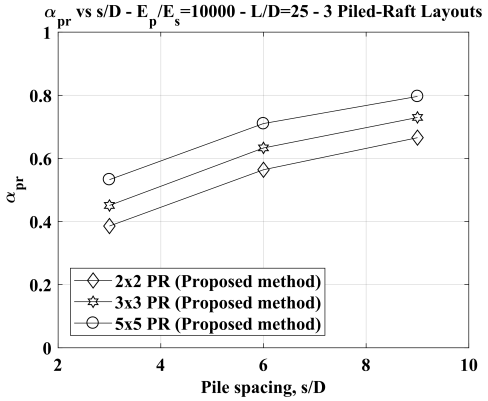

Figure 7.60: Calculated α_{pr} values for different piled raft layouts ($E_p/E_s = 10000$)

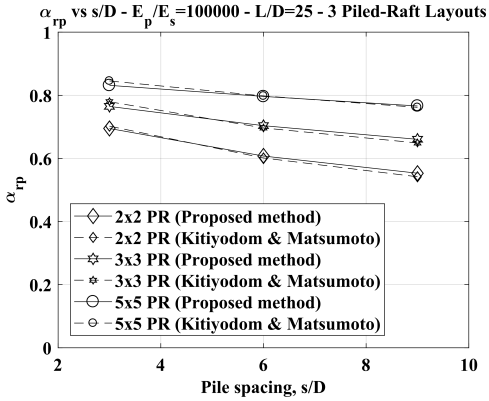

Figure 7.61: Calculated α_{rp} values for different piled raft layouts ($E_p/E_s = 100000$)

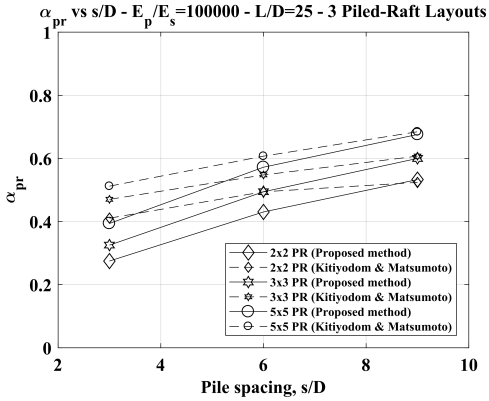

Figure 7.62: Calculated α_{pr} values for different piled raft layouts ($E_p/E_s = 100000$)

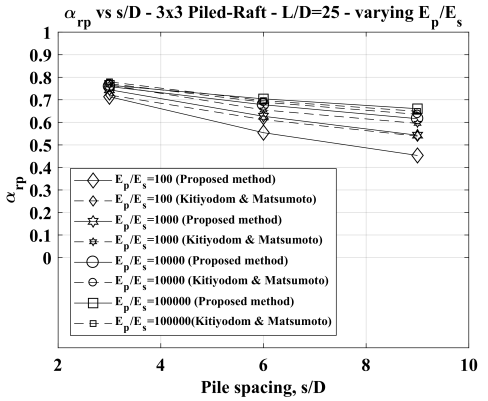

Figure 7.63: Calculated α_{rp} values for different E_p/E_s ratios in a 3x3 piled raft

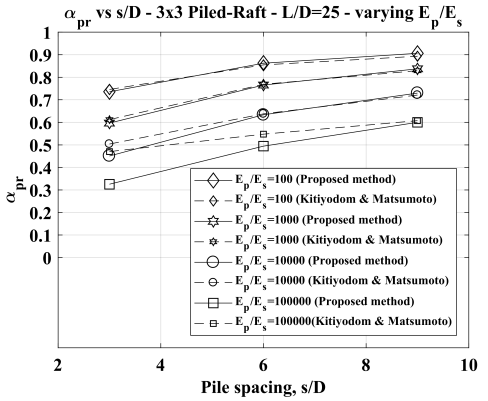

Figure 7.64: Calculated α_{pr} values for different E_p/E_s ratios in a 3x3 piled raft

Chapter 8

Conclusions

The main aim of this PhD thesis was the development and the validation of a 'Hybrid BEM - p-y curves' method for the analysis of single piles and of a BEM-based method for the analysis of pile-groups and piled-rafts under static horizontal loads.

In Chapter 1 a short introduction to the topic of the research project was presented, in which has been mainly focused the attention on the scanty number of experimental tests and FEM or BEM numerical results about piled-raft foundations subjected to pure lateral loads.

In Chapter 2 the main parameters and factors that affect the response of a single pile, a pile group and a piled raft under this loading condition were described, on the basis of the most important research works found in literature. Basically, it has been shown that:

- the response of a single pile is mostly affected by: a) the restraint conditions at the pile-head, b) the pile-soil relative stiffness and c) the way in which the load is applied (statically, cyclically or dynamically), while the actual pile length is not a significant parameter to be considered (with the only exception for short/rigid piles);

- the response of a pile group is mostly affected by: a) the pile-soil relative stiffness, b) the relative spacing between the piles, c) the stiffness properties of the connecting structure and d) the presence of group effects like the shadowing and the edge effect, that are responsible for the load distribution between the piles in the group and for the common decrease of the stiffness of the overall foundation system. In general, for an equal average load at each pile, the displacement of the pile group is greater than the displacement of a single isolated pile; in the same way, for a given displacement at the pile-head, the load supported by an isolated pile is higher than the average load supported by a pile within the group.

- single piles and pile groups subjected to cyclic or dynamic lateral loads show a worse performance compared to the same piles under static loading. However, this PhD thesis has as its main purpose the intent to develop a calculation code that can deal with the analysis of piled-rafts systems, that represents a really more complex soil-structure interaction problem compared to the single pile case. For this reason, the attention has been focused on static loads. It's important to underline that, even nowadays, it's really hard to properly model and study not only a piled-raft but even a single pile with FEM codes considering cyclic or dynamic loading, due to the high computational cost required.

In a piled-raft foundation the horizontal loads are resisted by: 1) the piles; 2) the passive resistance of the soil on the front of the embedded structure; 3) the frictional

resistance along the embedded sides and 4) the frictional resistance along the base of the raft. However, in the context of this work only the piles and the resistance offered by the base of the raft are considered. Only few publications were found that described tests performed to investigate the lateral-load resistance of pile caps considering only the resistance offered by the soil along the base of the raft.

In this chapter the main findings obtained with centrifuge tests (Horikoshi and Matsumoto, 2003), small scale laboratory tests (Katzenbach and Turek, 2005; Matsumoto et al., 2010; Unsever et al., 2015; Hamada et al. ,2015) and full-scale field tests (Kim et al. 1974) were reported. The main findings of the authors were:

- the initial stiffness of a piled raft is not always higher than that of a raft alone (because the piles reduce a lot the contact pressure between raft and soil);
- the horizontal stiffness of the piled rafts is larger than that of a pile group with the same configuration as the piled raft, because the raft acts as a 'horizontal displacement reducers';
- the bending moments of the piles in the piled raft are reduced, compared with those in the pile group;
- rotation of the raft decreases as the pile-head connection rigidity becomes lower, although the horizontal stiffness also becomes lower;
- higher horizontal load is transferred to the piles in the piled raft with rigid pile head connection, which leads to higher initial horizontal stiffness compared with that in the piled raft with hinged pile head connection;
- the total horizontal resistance in a rigid connection piled raft is higher than in a hinged connection model;
- the proportion of the raft load rapidly decreased as the piled raft displacement increased. The reduction in the proportion of the raft load was more significant in the rigid connection model, which was related to a higher horizontal stiffness of the piles;
- for small horizontal displacements and high vertical load levels the major part of the horizontal load was carried by the raft.

Moreover, until now, the available literature about the influence of the vertical loads on single piles, pile groups and piled-rafts response to horizontal loads provides scanty and contradictory results.

In Chapter 3 some of the available analysis methods for single piles, pile groups and piled raft were presented. In detail were described:

- Winkler-based approaches (i.e., '$p - y$ curves');
- BEM-based methods;
- the Strain-Wedge-Model (Ashour and Norris (1998, 2004));
- the 'plate-beam-spring' model proposed by Kitiyodom and Matsumoto (2002, 2005);
- the method proposed by Small and Zhang (2006).

The last two simplified methods are able to study also piled-raft with the raft in contact with the soil.

The first one was implemented by Kitiyodom and Matsumoto (2002, 2005) on the computer program PRAB (Piled Raft Analysis with Batter piles). The authors model the flexible raft as a thin plate element and piles as elastic beam elements, while the soil is treated as springs. To model all the 'structural element-soil-structural element' interactions this model uses the Mindlin's solutions both for vertical and lateral forces. However, all the springs can have a linear elastic or a linear elastic-perfectly plastic behaviour (because of a limiting soil resistance profile), thus it is strictly necessary, to choose properly the soil elastic modulus. Usually for laterally loaded piles application, typical values for the elastic modulus range between the 10 and 30% of the elastic modulus at small strain level.

The last one, proposed by Small and Zhang (2006), is able to analyse piled-raft foundations under general loadings also in the case in which the pile-cap or raft is in contact with the ground. The soil is divided into multiple horizontal layers, the raft is modelled as a thin plate and the piles as elastic beams. The approach used by Small and Zhang is based on the finite layer theory, a theory developed by Small and Booker (1986) that permits the analysis of horizontally layered materials. Also in this case the soil can have or a linear elastic or a linear elastic-perfectly plastic behaviour. In both the last two methods is not considered the non-linear behaviour for reinforced concrete pile sections. Moreover, even if the authors underlined the ability of their computer program to study piled-raft under general loading conditions, no significant results were presented about the influence of the vertical loads on the response of the foundation under horizontal forces.

In Chapter 4 some FEM analysis results were presented. The main aim of these FEM-analyses was to try to better understand the responses, under horizontal loads, of single piles, pair of piles (having different spacing), pile groups and finally piled-rafts (with a vertical load acting over the raft). The analyses were realized using Plaxis3D AE.

When it was decided to use this finite element program, to study piled raft systems, the idea was to use the results obtained as benchmarks to validate the proposed BEM-method, however, on the basis of the results published by Unsever et al. (2015), is not so clear if Plaxis can simulate and capture well the actual behaviour of a piled-raft system. In fact, this FEM analysis overestimated the horizontal load carried by the piled raft (and thus even the bending moments in the piles). For this reason, in this thesis, it was preferred to compare the results obtained with the proposed BEM method with those of full-scale, 1-g and centrifuge tests. The FEM analyses were performed:

- on fixed-head single piles to study the developing of the active and the passive wedges of soil, respectively behind and in front of the pile shaft and responsible for the interactions between the piles in a group;
- on fixed-head pair of piles to investigate the load distributions and maximum pile bending moments, varying the pile spacing ratio s/D and considering two departure angles: $\beta = 0°$ (the pair of piles are parallel to the load direction) and $\beta = 90°$ (the pair of piles are orthogonal to the load direction);
- on fixed-head pile groups to better understand group effects and so the interaction mechanisms, considering 4 different group layouts (2x2 ($s/D = 6$), 3x3 ($s/D = 3$), 3x3 ($s/D = 6$) and 5x5 ($s/D = 3$));

- on piled-rafts (subjected to the same vertical load, chosen to be 1/3 of the bearing capacity of the raft alone) varying the layout of the pile-group beneath the raft (the same 4 layouts used for the simple pile-groups analyses were used), and considering two different values for the pile length (L=20 m and L=10 m), in order to study the performances of different piled-raft systems supporting the same vertical load but having different contact pressures at the interface between the soil and the raft, because of the different number and position of the piles.

The main findings of the FEM analyses on piled-rafts were:

- not always the efficiency of the piled raft (defined as the ratio between the horizontal load carried by the piled raft and the load carried by the raft alone at a same displacement level and subjected to the same vertical load (= 15 MN)) is bigger than that of the raft alone. It was noted that the piled raft efficiency is higher when the piles in the pile-group have a length of 10 m compared to the same piled-raft systems with a pile length equal to 20 m. This is due to the fact that, when the piles are shorter a bigger vertical load rate is transferred by the raft directly to the soil beneath the raft. In this case the raft can contribute in a better way to the overall lateral response. However, it is obvious that if the raft carries a bigger rate of the vertical load also the vertical settlement of the foundation increases. In order to define the best design solution, in terms of performance and costs, it is necessary to find the solution that can reduce properly the settlement (in order to guarantee the requirements of the superstructure) and that at the same way can improve the performance, as much as possible, under lateral loads;

- the efficiency factor of a pile group in a piled-raft and the efficiency factor of a simple pile group (no raft in contact with the ground and no vertical load applied) are practically the same for the soil condition and piled-raft layouts studied in this work;

- the percentage of the horizontal load carried by the raft decreases with the increase of the lateral displacement, while the vertical load distribution between the raft and the piles remains practically unchanged during the lateral load phases. With the horizontal load increase the front rows of piles are subjected to an increase of the axial load and the rear rows to a decrease, because the raft starts to rotate;

- when the contact pressure between the raft and the soil is small (= the raft carries a low rate of the total vertical load applied) the pile group response in the piled-raft and the load distribution between the different pile rows is practically the same as observed in the case of a simple pile group (raft not in contact with the ground). The well-known shadowing effect affects the behaviour of the pile group;

- when the contact pressure between the raft and the soil is high (= the raft carries a significant rate of the total vertical load applied) the pile group response in the piled-raft and the load distribution between the different pile rows is completely different compared to that observed in the case of a simple pile group. The pile rows located at the rear of the foundation carry a bigger horizontal load rate compared to the front row of piles. This result can be justified by the raft-piles interactions, and, as observed by Katzenbach and Turek (2005), by the increase of stresses and stiffness in the soil beneath the raft. Moreover, in this case, for a

given horizontal load applied at the pile-head the maximum bending moment is less than that observed in the single pile case and in the same pile in a simple pile group;

- in general, practically always the piled raft systems responses have a slightly lower initial lateral stiffness and lateral resistance (at the same displacement level) compared to the sum of the raft alone and the simple pile group responses (note: for the raft alone analyses were used vertical loads able to reproduce the average contact pressures between the raft and the soil like in the piled-raft systems; the simple pile groups analyses were performed without the application of the vertical load).

In the first part of Chapter 5 the developed 'Hybrid BEM-p-y curves' method for the analysis of a single pile subjected to horizontal loads was presented. The analysis is performed using a non-linear incremental tangent method. The pile is modelled as a vertical strip, geometrically defined by the outer diameter D and length L of the actual pile, discretized in 60 blocks having variable length with depth. The proposed method allows to analyse both steel-pipes and reinforced concrete piles.

For reinforced concrete piles the 'moment-curvature-axial load' relationship is obtained by imposing the equilibrium equations to the translation and rotation at the geometric center of gravity of the section varying the curvature and the deformation at the most compressed fiber in the section. This model has as an additional feature the possibility to take into account of the influence of tension stiffening.

A parametric study with this model suggests that for r.c. elements characterized by circular section with diameter higher than 1 m and with a reinforcement ratio higher than 1%, such as usual bridge piers, the influence of the tension stiffening can be neglected. The influence of tension stiffening can become sensible for low diameter (around 60 cm, such as some foundation piles) and low values of the reinforcement ratio.

The 'far-field' soil (far from the pile shaft) is modelled as an elastic half-space. The Mindlin's solution is used to evaluate the pile-soil interactions. The 'near-field' soil and its non-linear response is introduced by placing non-linear springs in series to each pile-half-space node, having a shape dependent on the soil-type. In the present study the 'p-y' curves proposed by Matlock (1970), Reese L. C. et al. (1974), Welch and Reese (1972) and Reese et al. (1975) are used. Currently, it's possible to analyse only free-to-rotate or fixed-head single-piles.

In the second part of Chapter 5 the developed BEM method for the analysis of pile groups and piled-rafts subjected to horizontal loads was presented. The originality of the proposed approach lies in its ability to provide a complete BEM analysis of the soil continuum (in which all the main interactions are modelled). The approach has been extended to include the raft analysis (including its reciprocal interaction with the piles) by discretizing the raft-soil interface into a number of rectangular elements, whose behaviour is evaluated using the traditional Mindlin's and Cerutti's solutions.

The proposed method is characterized by the following features:

- horizontally layered elastic soil;
- non-linear behaviour for reinforced concrete pile sections;
- non-linear soil behaviour (incremental analysis);
- pile-soil, pile-pile, raft-pile interactions modelled using the Mindlin's solution;

- pile-raft and soil-raft interactions modelled using the Cerutti's solution;
- pile groups and piled-rafts under horizontal loading and bending moments can be analysed considering two restraint conditions at the pile heads (hinged or fixed);
- influence of vertical loads, using an improved version of the Poulos-Davis-Randolph (PDR) method. With this method is possible to estimate the load distribution between the pile-group and the raft and thus, the induced vertical stresses, caused by a vertical load acting over the raft, at each pile-soil and raft-soil interface block (specifically, at the center point of each block in which the entire foundation-system has been discretized);
- the influence of suction can be considered for partially saturated soil condition, close to the ground surface, by means of the Modified-Kovacs model.

In the analysis of pile groups and piled-rafts, the program adopts the following further assumptions:

- non-symmetrical extinction distance for the interaction between couple of blocks belonging to different piles in the group; this distance is defined according to the suggestion by Reese and Van Impe (2001);
- group effects (shadowing - overlapping of passive soil wedges) for small spacings. The so-called shadowing effect has been implemented using an approach similar to that described in Ashour and Norris (2004) for the definition of group interactions effect caused by the overlapping of passive wedges of soil.

At the raft-soil interface the sliding mechanism will initiate when the shear stress at the interface exceeds a value defined by a simple frictional law. Once reached the ultimate shear stress at a raft-soil interface block, sliding starts, and thus for this block the compatibility equation is removed.

The analysis is currently restricted to the assumption of a perfectly rigid raft (under horizontal loading). Each pile-head and each point of the raft move the same quantity at each step. While in the analysis under vertical loads, the raft flexibility is taken into account in an approximate way (using the approach suggested by Mayne and Poulos (1999)).

The non-linear soil response is modelled, in an approximate manner, by adopting a quasi-hyperbolic elastic modulus reduction curve. The quasi-hyperbolic relation is characterized by the presence of an exponent, g, to adjust the shape of the reduction curve. The appropriate value for g to perform the analysis can be easily estimated trying to obtain the best-fit with the load-deflection curve of a horizontal test on a single pile or with the load-deflection curve obtained with other available codes, like the 'Hybrid BEM - p-y curve' approach presented before.

The first main feature of the proposed methods relies on the input data required for the soil properties, because both the strength parameters and the elastic modulus of the soil can be found in a standard site investigation. The soil elastic modulus required here is the shear modulus at small strain level.

The second main feature relies on the proper modelling of the actual flexural behaviour of r.c. piles compared to more advanced FEM codes and the possibility to take into account also of the tension stiffening effect. Both the proposed methods were developed using Matlab (MATLAB, 2016).

In Chapter 6 the prediction results obtained using the developed methods were presented. The analysis solutions were compared with the experimental results that refer to a total of 22, 15 and 6 well-documented load tests found in literature, respectively for the single pile, the pile group and the piled raft case.

The analyses had the purpose to validate the computational model for predicting the behaviour of these foundation systems. These were conducted not as back-analyses but as direct predictions using directly the actual pile mechanical and geometrical properties and the soil strength and stiffness parameters according to the interpretation of the in-situ and laboratory tests data provided by the authors.

The results obtained have shown the possibility of providing a good forecasting of the most representative aspects (pile-head displacement and rotation and maximum bending moment) of the response of all these foundation systems. Specifically, the error committed in the prediction of load at each displacement level reached during the tests are practically always included in a range of $\pm$ 20% and $\pm$ 30%, respectively for the single pile and the pile group case.

Complete details about the case histories studied and specific comparisons between measured and computed results are presented in Chapter 6 for the piled-rafts. It should be highlighted, in particular, the capability of the proposed method to capture the load distribution between the piles in the group and the raft.

In Chapter 7 an overview of the main parametric studies results found in literature on single piles, pair of piles, pile groups and piled-rafts (carried out with some of the analysis methods described in Chapter 3) was presented, in order to highlight the influence of the parameters that mostly affect the response of these foundation systems (such as the pile-soil relative stiffness, the pile slenderness ratio and the relative spacing between the piles).

Within this chapter the results of a parametric study on single pile, performed using the developed BEM-based method, were shown. The analyses were realized considering three different conditions: 1) with both the pile and the soil having a linear elastic behaviour; 2) with the pile having a linear elastic behaviour and the soil a non-linear behaviour; 3) with both the pile and the soil having a non-linear behaviour.

In the second and third type of the analyses, the non-linearity of the soil was introduced using the elastic modulus reduction curve, considering two values for the exponent g (= 0.25 and 1.0), while for the definition of the ultimate soil resistance profile, the relationships proposed by Matlock (1970) (for cohesive soils) and by Reese et al. (1974) (for cohesionless soils) were used.

The non-linear behaviour of the pile was considered by means of the definition of the 'bending moment-curvature' relationship for the reinforced concrete pile cross section. In this parametric study two values of the pile diameter were investigated (D=0.60 and D=1.0 m), and the effect of the steel reinforcement ratio and of the compressive axial force acting over the pile section were evaluated. In this case, both the pile and the soil stiffness decrease during the analysis, so in this condition the pile-soil relative stiffness ratio is dependent on the load level. Finally other parametric studies were realized on pair of piles, pile groups and piled-rafts, and the results were compared with those obtained by other authors.

Future prospects

In the light of what explained above, a possible development of this thesis work could be oriented on the following aims:

- extend the data-base of single piles, pile groups and piled rafts load tests;

- improve the developed BEM-method in the raft modelling in order to take into account of the raft flexibility. This feature is necessary in case of 'large piled-raft' (piled raft systems in which the ratio between the pile length and the raft width is less than 1.0), in which the raft flexibility needs to be considered. This work, instead, was mainly oriented on 'small piled-raft' (piled raft systems in which the ratio between the pile length and the raft width is more than 1.0), because practically all the lateral load tests (centrifuge tests, 1-g tests and full-scale tests) were performed on this type of foundation. In 'small piled-raft' the raft can be assumed reasonably as rigid;

- improve the developed BEM-method to consider the possibility that the vertical load can act simultaneously with the horizontal one. Now, it's possible to realize a preliminary analysis under vertical load (using an improved version of the PDR method). This is useful to define the vertical load distribution between the raft and the pile group and thus to evaluate in an approximate way the contact pressure at the raft-soil interface and the induced vertical stresses in the soil beneath the raft.

Appendix A

Appendix

A.1 Elastic equations used for laterally loaded pile analysis

The horizontal displacement w_{ij} induced at a point i belonging to the half space by a horizontal force Q applied in the point j can be obtained by the Mindlin's (1936) solution:

$$w_{ij} = b_{ij} Q_j \tag{A.1}$$

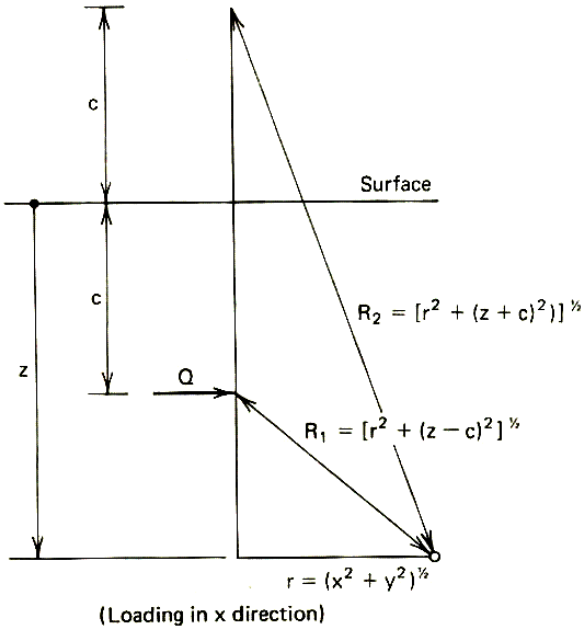

Figure A.1: Definition of point-load problem (Poulos and Davis, 1980)

where: b_{ij} = is given by Mindlin's solution in this form:

$$b_{ij} = \frac{1}{16\pi G(1-\nu)}\left[\frac{3-4\nu}{R_{1ij}} + \frac{1}{R_{2ij}} + \frac{x_{ij}^2}{R_{1ij}^3} + \frac{(3-4\nu)x_{ij}^2}{R_{2ij}^3} + \frac{2c_j z_i}{R_{2ij}^3}\left(1 - \frac{3x_{ij}^2}{R_{2ij}^2}\right) + \frac{4(1-\nu)(1-2\nu)}{R_{2ij} + z_i + c_j}\left(1 - \frac{x_{ij}^2}{R_{2ij}(R_{2ij} + z_i + c_j)}\right)\right] \tag{A.2}$$

where:

- $z_{1ij} = z_i - c_j$;

- $z_{2ij} = z_i + c_j$;
- $R_{1ij}^2 = r_{ij}^2 + z_{1ij}^2$;
- $R_{2ij}^2 = r_{ij}^2 + z_{2ij}^2$;
- $r_{ij} = \sqrt{x_{ij}^2 + y_{ij}^2}$.

Douglas and Davies (1964) integrated this equation over a rectangular area, and obtained the following solution. At the upper corners A and B (see Figure 8.107), for a uniform horizontal pressure p,

$$\rho_x = \frac{pb}{32\pi G(1-\nu)}[(3-4\nu)F_1 + F_4 + 4(1-2\nu)(1-\nu)F_5] \tag{A.3}$$

At the lower corners D and C,

$$\rho_x = \frac{pb}{32\pi G(1-\nu)}[(3-4\nu)F_1 + F_2 + 4(1-2\nu)(1-\nu)F_3] \tag{A.4}$$

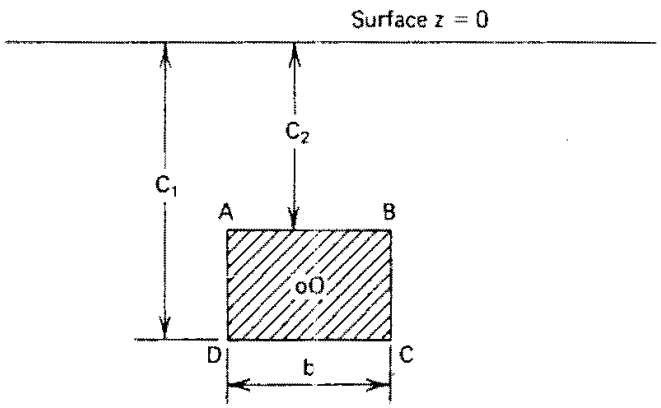

Figure A.2: Definition of rectangular area (Poulos and Davis, 1980)

where:

$$K_1 = \frac{2c_1}{b} \tag{A.5}$$

$$K_2 = \frac{2c_2}{b} \tag{A.6}$$

$$F_1 = -(K_1 - K_2)ln[\frac{(K_1 - K_2)}{2 + \sqrt{4 + (K_1 - K_2)^2}}] - 2ln[\frac{2}{(K_1 - K_2) + \sqrt{4 + (K_1 - K_2)^2}}] \tag{A.7}$$

$$F_2 = 2ln[\frac{2(K_1+\sqrt{1+K_1^2})}{(K_1+K_2)+\sqrt{4+(K_1+K_2)^2}}] + (K_1+K_2)ln[2+\frac{\sqrt{4+(K_1+K_2)^2}}{(K_1+K_2)}] - K_1^2[\frac{\sqrt{4+(K_1+K_2)^2}}{(K_1+K_2)} - \frac{\sqrt{1+K_1^2}}{K_1}] \tag{A.8}$$

$$F_3 = -2K_1ln(\frac{K_1}{1+\sqrt{1+K_1^2}}) + (K_1+K_2)ln[\frac{(K_1+K_2)}{2+\sqrt{4+(K_1+K_2)^2}}] - ln[\frac{(K_1+K_2)+\sqrt{4+(K_1+K_2)^2}}{2(K_1+\sqrt{1+K_1^2})}] + \frac{(K_1+K_2)}{4}[\sqrt{4+(K_1+K_2)^2} - (K_1+K_2)] - K_1(\sqrt{1+K_1^2}-K_1) \tag{A.9}$$

$$F_4 = -2ln[\frac{2(K_2+\sqrt{1+K_2^2})}{(K_1+K_2)}] + (K_1-K_2)ln[\frac{2+\sqrt{4+(K_1+K_2)^2}}{(K_1+K_2)}] + K_2^2[\frac{\sqrt{4+(K_1+K_2)^2}}{(K_1+K_2)} - \frac{\sqrt{1+K_2^2}}{K_2}] \tag{A.10}$$

$$F_5 = 2K_2ln(\frac{K_2}{1+\sqrt{1+K_2^2}}) - (K_1+K_2)ln[\frac{K_1+K_2}{2+\sqrt{4+(K_1+K_2)^2}}] + ln[\frac{(K_1+K_2)+\sqrt{4+(K_1+K_2)^2}}{2(K_2+\sqrt{1+K_2^2})}] - (\frac{K_1+K_2}{4})[\sqrt{4+(K_1+K_2)^2} - (K_1+K_2)] - K_2(K_2-\sqrt{1+K_2^2}) \tag{A.11}$$

For the displacement at other points in the same plane, the principle of superposition may be employed.

Bibliography

Abagnara, V (2009). "Modellazione e analisi di pali sotto carichi orizzontali". PhD thesis. University of Naples: Federico II.

Abbasa, J, Z Chik, and M Taha (2015). "Influence of axial load on the lateral pile groups response in cohesionless and cohesive soil". In: *Frontiers of Structural and Civil Engineering* 9.2, pp. 176–193. ISSN: 2095-2430. DOI: 10.1007/s11709-015-0289-7.

Anagnostopoulos, C and M Georgiadis (1993). "Interaction of Axial and Lateral Pile Responses". In: *Journal of Geotechnical Engineering* 119.4, pp. 793–798. ISSN: 0733-9410. DOI: 10.1061/(ASCE)0733-9410(1993)119:4(793).

API (2007). *Recommended Practice for Planning , Designing and Constructing Fixed Offshore Platforms — Working Stress Design*. Vol. 24-WSD. December 2000, p. 242. ISBN: 5957529001.

Ashour, M, G Norris, and P Pilling (1998). "Lateral Loading of a Pile in Layered Soil Using the Strain Wedge Model". In: *Journal of Geotechnical and Geoenvironmental Engineering* 124.April, pp. 303–315. ISSN: 1090-0241. DOI: 10.1061/(ASCE)1090-0241(1998)124:4(303).

Ashour, M, P Pilling, and G Norris (2004). "Lateral Behavior of Pile Groups in Layered Soils". In: *Journal of Geotechnical and Geoenvironmental Engineering* 130.June, pp. 580–592. ISSN: 1090-0241.

Aubertin, M, M Mbonimpa, B Bussière, and RP Chapuis (2003). "A model to predict the water retention curve from basic geotechnical properties". In: *Canadian Geotechnical Journal* 40.6, pp. 1104–1122.

Banerjee, PK and TG Davies (1978). "The behaviour of axially and laterally loaded single piles embedded in nonhomogeneous soils". In: *Géotechnique* 28.3, pp. 309–326. URL: http://www.icevirtuallibrary.com/content/article/10.1680/geot.1978.28.3.309.

Barton, Y (1985). "Response of Pile Groups to Lateral Loading in the Centrifuge". In: *Publication of: Balkema (AA)*. URL: http://trid.trb.org/view.aspx?id=278772.

Basile, F (1999). "Non-linear analysis of pile groups under general loading conditions". PhD Thesis. University of Glasgow. URL: http://theses.gla.ac.uk/id/eprint/4315.

Beatty, CI (1970). "Lateral test on pile groups". In: *Foundation Facts* 6(1), pp. 18–21.

Broms, BB (1964). "Lateral Resistance of Piles in Cohesionless Soils". In: *Journal of the Soil Mechanics and Foundation Division* 90.SM3, pp. 123–158. ISSN: 0044-7994.

Brown, DA, C Morrison, and LC Reese (1988). "Lateral Load Behavior of Pile Group in Sand". In: *Journal of Geotechnical Engineering* 114.11, pp. 1261–1276. ISSN: 0733-9410.

Brown, DA, LC Reese, and MW O'Neill (1987). "Cyclic lateral loading of a large-scale pile group". In: *Journal of Geotechnical Engineering* 113.11, pp. 1326–1343.

Budhu, M and TG Davies (1987). "Nonlinear analysis of laterality loaded piles in cohesionless soils". In: *Canadian Geotechnical Journal* 24.2, pp. 289–296.

— (1988). "Analysis of Laterally Loaded Piles in Soft Clays". In: *Journal of Geotechnical Engineering* 114.1, pp. 21–39.

Butterfield, R and PK Banerjee (1971). "The elastic analysis of compressible piles and pile groups". In: *Géotechnique* 21.1, pp. 43–60.

Calderone, AJ, DE Lehman, and JP Moehle (2000). "Behavior of reinforced concrete bridge piers having varying aspect ratios and varying lengths of confinement". In: *Report PEER*.

Caputo, V and C Viggiani (1984). "Pile foundations analysis: a simple approach to nonlinearity effects". In: *Rivista Italiana di Geotecnica* 18.1, pp. 32–51.

Carbonell-Marquez, JF, LM Gil-Martin, M Alejandro Fernandez-Ruiz, and E Hernandez-Montes (2014). "Effective area in tension stiffening of reinforced concrete piles subjected to flexure according to Eurocode 2". In: *Engineering Structures* 76, pp. 62–74. ISSN: 01410296. DOI: 10.1016/j.engstruct.2014.06.041.

Castel, A, T Vidal, and R François (2007). "Effective Tension Active Cross-Section of Reinforced Concrete Beams After Cracking". In: *Materials and Structures* 39.1, pp. 115–126.

Ceb-Fip (1993). *CEB-FIP model code 1990*. DOI: 10.1680/ceb-fipmc1990.35430.

Chow, YK (1987). "Axial and lateral response of pile groups embedded in nonhomogeneous soils". In: *International Journal for Numerical and Analytical Methods in Geomechanics* 11.6, pp. 621–638.

Cox, WR, DA Dixon, and BS Murphy (1984). "Lateral-load tests on 25.4-mm (1-in.) diameter piles in very soft clay in side-by-side and in-line groups". In: *Laterally Loaded Deep Foundations: Analysis and Performance, ASTM STP 835*, pp. 122–139.

Cox, WR, LC Reese, and BR Grubbs (1974). "Field testing of laterally loaded piles in sand." In: *6th Annual Offshore Technology Conference, Houston, Texas, 1*, pp. 459–472.

Cunha, RP and HH Zhang (2006). "Behavior of piled raft foundation systems under a combined set of loadings". In: *10 th." Int. Conf. on Piling and Deep Foundations"*, pp. 242–251.

Davies, TG and M Budhu (1986). "Non-linear analysis of laterally loaded piles in heavily overconsolidated clays". In: *Géotechnique* 36.4, pp. 527–538.

Dente, G and G Gullà (1983). "Risposta alle azioni orizzontali di un palo immerso in un semispazio alla Gibson". In: *Rivista Italiana di Geotecnica*. URL: http://http://www.associazionegeotecnica.it/sites/default/files/rig/RIG_1983_4_194.pdf.

Douglas, DJ and EH Davis (1964). "The Movement of Buried Footings due to Moment and Horizontal Load and the Movement of Anchor Plates". In: *Géotechnique* 14.2, pp. 115–132.

Duncan, JM and CY Chang (1970). "Nonlinear Analysis of Stress and Strain in Soil". In: *ASCE Journal of the Soil Mechanics and Foundations Division* 96.5, pp. 1629–1653.

Dunnavant, TW and MW O'Neill (1989). "Experimental Model for Submerged, Stiff Clay". In: *Journal of Geotechnical Engineering* 115.1, pp. 95–114. DOI: 10.1061/(ASCE)0733-9410(1989)115:1(95).

EC2-1 (2005). *Eurocode 2: Design Of Concrete Structures, Part 1–1: General rules and rules for buildings*.

El Sharnouby, B and M Novak (1985). "Static and low-frequency response of pile groups". In: *Canadian Geotechnical Journal* 22.1, pp. 79–94. ISSN: 0008-3674. DOI: 10.1139/t85-008. URL: http://www.nrcresearchpress.com/doi/abs/10.1139/t85-008.

— (1986). "Flexibility coefficients and interaction factors for pile group analysis". In: *Canadian Geotechnical Journal* 23.4, pp. 441–450. ISSN: 0008-3674. DOI: 10.1139/t86-074.

Evangelista, A (1976). "Pali inclinati isolati ed in gruppo immersi in un mezzo elastico". In: *Rivista Italiana di Geotecnica* 3, p. 206.

Fahey, M and JP Carter (1993). "A finite element study of the pressuremeter test in sand using a nonlinear elastic plastic model". In: *Canadian Geotechnical Journal* 30.2, pp. 348–362. URL: http://www.nrcresearchpress.com/doi/abs/10.1139/t93-029.

Fleming, K, A Weltman, M Randolph, and K Elson (2008). *Piling engineering*. CRC Press. ISBN: 9780415266468.

Focht, JA and KJ Koch (1973). "Rational analysis of the lateral performance of offshore pile groups". In: *5th Offshore Technology Conference, Dallas*, pp. 701–708.

Gazetas, G and G Mylonakis (1998). "Seismic soil-structure interaction: new evidence and emerging issues". In: *Geotechnical Earthquake Engineering and Soil Dynamics*, pp. 872–886.

Gibbs, HJ and WG Holtz (1957). "Research on determining the density of sands by spoon penetration testing." In: *4th International Conference on Soil Mechanics and Foundation Engineering, London, 1*, pp. 35–39.

Hamada, J, T Tsuchiya, T Tanikawa, and K Yamashita (2015). "Lateral loading tests on piled rafts and simplified method to evaluate sectional forces of piles". In: *Geotechnical Engineering* 46.2, pp. 29–42. ISSN: 00465828.

Hardin, BO and VP Drnevich (1972). "Shear Modulus and Damping in Soils: Dsesign Equations and Curves". In: *Soil Mechanics and Foundations Division* SM7, pp. 667–692.

Hartmann, F and P Jahn (2001). "Boundary element analysis of raft foundations on piles". In: *Meccanica* 1, pp. 351–366. URL: http://link.springer.com/article/10.1023/A:1015097016148.

Hetenyi, M (1946). *Beams on elastic foundation*. Ann Arbor: The University of Michigan Press, p. 255.

Hoit, MI, M McVay, C Hays, and PW Andrade (1996). "Nonlinear Pile Foundation Analysis Using Florida-Pier". In: *Journal of Bridge Engineering* 1.4, pp. 135–142. ISSN: 1084-0702. DOI: 10.1061/(ASCE)1084-0702(1996)1:4(135). URL: http://ascelibrary.org/doi/abs/10.1061/(ASCE)1084-0702(1996)1:4(135).

Horikoshi, K, T Matsumoto, Y Hashizume, T Watanabe, and H Fukuyama (2003). "Performance of piled raft foundations subjected to static horizontal loads". In: *International Journal of Physical Modelling in Geotechnics* 3.2, pp. 37–50. ISSN: 1346-213X. DOI: 10.1680/ijpmg.2003.030204. URL: http://www.icevirtuallibrary.com/content/article/10.1680/ijpmg.2003.3.2.37.

Huang, AB and CK Hsueh (2001). "Effects of construction on laterally loaded pile groups". In: *Journal of Geotechnical and Geoenvironmental Engineering* May, pp. 385–397.

Hussien, MN, T Tobita, S Iai, and M Karray (2014). "On the influence of vertical loads on the lateral response of pile foundation". In: *Computers and Geotechnics* 55, pp. 392–403. ISSN: 0266352X. DOI: 10.1016/j.compgeo.2013.09.022. URL: http://linkinghub.elsevier.com/retrieve/pii/S0266352X13001584.

Ilyas, T, CF Leung, YK Chow, and SS Budi (2004). "Centrifuge Model Study of Laterally Loaded Pile Groups in Clay". In: *Journal of Geotechnical and Geoenvironmental Engineering* 130.3, pp. 274–283. ISSN: 1090-0241. DOI: 10.1061/(ASCE)1090-0241(2004)130:3(274). URL: http://ascelibrary.org/doi/abs/10.1061/(ASCE)1090-0241(2004)130:3(274).

Jain, NK, G Ranjan, and G Ramasamy (1987). "Effect of vertical load on flexural behaviout of piles". In: *Geotechnical Engineering* 18.2, pp. 185–204.

Jamiolkowski, M (1985). "New development in field and laboratory testing of soils". In: *Proc. 11th ICSMFE* 1, pp. 57–153.

Kaklauskas, G, V Gribniak, and D Bacinskas (2009). "Shrinkage influence on tension stiffening in concrete members". In: *Engineering Structures* 31.6, pp. 1305–1312. DOI: 10.1016/j.engstruct.2008.10.007.

Karasev, OV, GP Talanov, and SF Benda (1977). "Investigation of the work of single situ-cast piles under different load combinations". In: *Soil Mechanics and Foundation Engineering* 14.3, pp. 173–177. ISSN: 0038-0741. DOI: 10.1007/BF02092686. URL: http://link.springer.com/10.1007/BF02092686.

Karthigeyan, S, VVGST Ramakrishna, and K Rajagopal (2006). "Influence of vertical load on the lateral response of piles in sand". In: *Computers and Geotechnics* 33.2, pp. 121–131. ISSN: 0266352X. DOI: 10.1016/j.compgeo.2005.12.002.

— (2007). "Numerical Investigation of the Effect of Vertical Load on the Lateral Response of Piles". In: *Journal of Geotechnical and Geoenvironmental Engineering* 133.5, pp. 512–521. ISSN: 1090-0241. DOI: 10.1061/(ASCE)1090-0241(2007)133:5(512).

Katzenbach, R and J Turek (2005). "Combined pile-raft foundation subjected to lateral loads". In: *Proc. 16th Int. Conf. On Soil Mechanics and Geotechnical Engineering*, pp. 2001–2004.

Khalili-Tehrani, P et al. (2014). "Nonlinear Load-Deflection Behavior of Reinforced Concrete Drilled Piles in Stiff Clay". In: *Journal of Geotechnical and Geoenvironmental Engineering* 140.3, pp. 1–14.

Kim, JB, RJ Brungraber, and LP Singh (1979). "Pile Cap Soil Interaction from Full-Scale Lateral Load Tests". In: *Journal of the Geotechnical Engineering Division* 105.5, pp. 643–653. ISSN: 0093-6405.

Kimura, M and F Zhang (2000). "Seismic evaluations of pile foundations with three different methods based on three-dimensional elasto-plastic finite element analysis." In: *Soils and Foundations* 40.5, pp. 113–132. ISSN: 1341-7452. DOI: 10.3208/sandf.40.5_113.

Kitiyodom, P and T Matsumoto (2002). "A simplified analysis method for piled raft and pile group foundations with batter piles". In: *International Journal for Numerical and Analytical Methods in Geomechanics* 26.13, pp. 1349–1369. ISSN: 0363-9061. DOI: 10.1002/nag.248. URL: http://doi.wiley.com/10.1002/nag.248.

Kitiyodom, P, T Matsumoto, and K Horikoshi (2005). "Analyses of vertical and horizontal load tests on piled raft models in dry sand". In: *Proceedings of the International Conference on Soil Mechanics and Geotechnical Engineering* 16.4, pp. 2005–2008.

Kondner, RL (1963). "Hyperbolic Stress-Strain Response: Cohesive Soils". In: *Journal of the Soil Mechanics and Foundations Division* 89.1, pp. 115–144.

Krishnan, R, G Gazetas, and A Velez (1983). "Static and dynamic lateral deflexion of piles in non – homogeneous soil stratum." In: *Géotechnique* 33.3, pp. 307–325.

Kuhlemeyer, RL (1979). "Static and Dynamic Laterally Loaded Floating Piles". In: *Journal of the Geotechnical Engineering Division* 105.2, pp. 289–304.

Kulhawy, FH and PW Mayne (1990). *Manual on estimating soil properties for foundation design*. Palo Alto, California: Research Project 1493-6, Electric Power Research Institute.

Kwak, HG and JY Song (2002). "Cracking analysis of RC members using polynomial strain distribution function". In: *Engineering Structures* 24.4, pp. 455–468. ISSN: 01410296. DOI: 10.1016/S0141-0296(01)00112-2.

Landi, G (2006). "Pali soggetti a carichi orizzontali: indagini sperimentali ed analisi". PhD thesis. University of Naples: Federico II.

Lee, SC, JY Cho, and FJ Vecchio (2011). "Model for post-yield tension stiffening and rebar rupture in concrete members". In: *Engineering Structures* 33.5, pp. 1723–1733. ISSN: 01410296. DOI: 10.1016/j.engstruct.2011.02.009.

Lehman, DE and JP Moehle (2000). "Seismic performance of well-confined concrete bridge columns". In: *Pacific Earthquake Engineering Research Center*, p. 295.

Leung, CF and YK Chow (1987). "Response of pile groups subjected to lateral loads". In: *International Journal for Numerical and Analytical Methods in Geomechanics*. URL: http://onlinelibrary.wiley.com/doi/10.1002/nag.1610110307/abstract.

Maffei, B, W Salvatore, and R Valentini (2007). "Dual-phase steel rebars for high-ductile r.c. structures, Part 1: Microstructural and mechanical characterization of steel rebars". In: *Engineering Structures* 29.12, pp. 3325–3332. ISSN: 01410296. DOI: 10.1016/j.engstruct.2007.09.002.

Mander, JB, MJN Priestley, and R Park (1988). "Theoretical Stress-Strain Model for Confined Concrete". In: 114.8, pp. 1804–1826. DOI: 10.1061/(ASCE)0733-9445(1988)114:8(1804).

Mandolini, A, G Russo, and C Viggiani (2005). "Pile foundations: experimental investigations, analysis and design". In: *Proc. XVI ICSMFE, vol. 1*. Osaka, Japan, pp. 177–213.

Mandolini, A and C Viggiani (1992). "Terreni ed opere di fondazione di un viadotto sul fiume Garigliano." In: *Rivista Italiana di Geotecnica* 26.2, pp. 95–113.

Manfredi, G and M Pecce (1998). "A refined R.C. beam element including bond–slip relationship for the analysis of continuous beams". In: *Computers & Structures* 69.1, pp. 53–62. ISSN: 00457949. DOI: 10.1016/S0045-7949(98)00078-9.

MATLAB (2016). *version 9.0.0.341360 (R2016a)*. Natick, Massachusetts: The MathWorks Inc.

Matlock, H (1970). "Correlations for design of laterally loaded piles in soft clay". In: *Proc 2nd Annual Offshore Technol Conf* 1, pp. 577–594. DOI: 10.4043/1204-MS.

Matsumoto, T et al. (2010). "Load Tests of Piled Raft Models With Different Pile Head Connection Conditions and Their Analyses". In: *Soils and Foundations* 50.1, pp. 63–81. ISSN: 0038-0806. DOI: 10.3208/sandf.50.63.

Mayne, PW (2006). "In-Situ Test Calibrations for Evaluating Soil Parameters, Characterization & Engineering Properties of Natural Soils". In: *Proc. Singapore*. Vol. 3. Taylor & Francis Group, London, pp. 1602–1652.

Mayne, PW and JB Kemper (1988). "Profiling OCR in Stiff Clays by CPT and SPT". In: *Geotechnical Testing Journal* 11.2, p. 139. DOI: 10.1520/GTJ10960J. URL: http://www.astm.org/doiLink.cgi?GTJ10960J.

Mayne, PW and GJ Rix (1995). "Correlations between cone tip resistance and shear wave velocity in natural clay". In: *Soils and Foundations* 35.2, pp. 107–110.

McVay, M, R Casper, and TI Shang (1995). "Lateral response of three-row groups in loose to dense sands at 3D and 5D pile spacing". In: *Journal of Geotechnical Engineering* 50, pp. 436–441.

McVay, M, L Zhang, T Molnit, and P Lai (1998). "Centrifuge testing of large laterally loaded pile groups in sands". In: *Journal of Geotechnical and Geoenvironmental Engineering* October, pp. 1016–1026. URL: http://ascelibrary.org/doi/abs/10.1061/(ASCE)1090-0241(1998)124:10(1016).

Meyerhof, GG (1957). "Discussion on research on determing the density of sands by spoon penetration test". In: *Proc. 4th ICSMFE, 1*, p. 110.

Mindlin, RD (1936). "Force at a point in the interior of a semi-infinite solid". In: *Journal of Applied Physics* 7.5, pp. 195–202.

Mokwa, RL (1999). "Investigation of the Resistance of Pile Caps to Lateral Loading". PhD thesis. PhD thesis, Virginia Polytechnic Institute and State University, Blacksburg, VA.

Mokwa, RL and JM Duncan (2001). "Experimental evaluation of lateral-load resistance of pile caps". In: *Journal of Geotechnical and Geoenvironmental Engineering* February, pp. 185–192. URL: http://ascelibrary.org/doi/abs/10.1061/(ASCE)1090-0241(2001)127:2(185).

— (2003). "Rotational restraint of pile caps during lateral loading". In: *Journal of Geotechnical and Geoenvironmental Engineering* September, pp. 829–837. URL: http://ascelibrary.org/doi/abs/10.1061/(ASCE)1090-0241(2003)129:9(829).

Mondal, TG and SS Prakash (2015). "Effect of Tension Stiffening on Torsional Behaviour of Square RC Columns". In: *Advances in Structural Engineering*. New Delhi: Springer India, pp. 2131–2144. DOI: 10.1007/978-81-322-2187-6_163.

Morelli, F, C Amico, W Salvatore, N Squeglia, and S Stacul (2017). "Influence of Tension Stiffening on the Flexural Stiffness of Reinforced Concrete Circular Sections". In: *Materials* 10.6, p. 669. DOI: dx.doi.org/10.3390/ma10060669.

Ng, CWW, L Zhang, and DCN Nip (2001). "Response of Laterally Loaded Large-Diameter Bored Pile Groups". In: *Journal of Geotechnical and Geoenvironmental Engineering* 127.August, pp. 658–669. ISSN: 1090-0241. DOI: 10.1061/(ASCE)1090-0241(2001)127:8(658).

Ochoa, M and MW O'Neill (1989). "Lateral Pile Interaction Factors in Submerged Sand". In: *Journal of Geotechnical Engineering* 115.3, pp. 359–378. ISSN: 0733-9410. DOI: 10.1061/(ASCE)0733-9410(1989)115:3(359). URL: http://ascelibrary.org/doi/abs/10.1061/(ASCE)0733-9410(1989)115:3(359).

O'Neill, M (1984). *A study of the effects of scale, velocity, and cyclic degradability on laterally loaded single piles in overconsolidated clay*. Houston Tex.: University of Houston Dept. of Civil Engineering.

O'Neill, MW, OI Ghazzaly, and HB Ha (1977). "Analysis Of Three-Dimensional Pile Groups With Nonlinear Soil Response And Pile-Soil-Pile Interaction". In: *Offshore Technology Conference*. Offshore Technology Conference, pp. 245–256. DOI: 10.4043/2838-MS. URL: https://www.onepetro.org/conference-paper/OTC-2838-MS.

Ottaviani, M (1975). "Three-dimensional finite element analysis of vertically loaded pile groups". In: *Géotechnique* 25.2, pp. 159–174. ISSN: 0016-8505. DOI: 10.1680/geot.1975.25.2.159. URL: http://www.icevirtuallibrary.com/content/article/10.1680/geot.1975.25.2.159.

Papadopoulou, MC and EM Comodromos (2010). "On the response prediction of horizontally loaded fixed-head pile groups in sands". In: *Computers and Geotechnics* 37.7-8, pp. 930–941. ISSN: 0266352X. DOI: 10.1016/j.compgeo.2010.07.011. URL: http://linkinghub.elsevier.com/retrieve/pii/S0266352X10000960.

Plaxis BV (2015). *User manual, Plaxis 3D Anniversary Edititon*.

Popovics, S (1973). "A numerical approach to the complete stress-strain curve of concrete". In: *Cement and Concrete Research* 3.5, pp. 583–599. ISSN: 00088846. DOI: 10.1016/0008-8846(73)90096-3.

Portugal, JC and PS Sêco e Pinto (1993). "Analysis and design of piles under lateral loads." In: *2nd International Geotechnical Seminar on Deep Foundations on Bored and Auger Piles, Ghent, Belgium*, pp. 309–312.

Poulos, HG (1968). "Analysis of the Settlement of Pile Groups". In: *Géotechnique* 18, pp. 449–471. ISSN: 0016-8505.

— (1971a). "Behavior of laterally loaded piles: I-single piles". In: *Journal of the Soil Mechanics and Foundations Division*.

— (1971b). "Behavior of laterally loaded piles II. Pile groups". In: *Journal of the Soil Mechanics and Foundations Division*.
— (1972). "Behavior of Laterally Loaded Piles: III—Socketed Piles". In: *Journal of the Soil Mechanics and Foundations Division*.
— (1973a). "Analysis of piles in soil undergoing lateral movement". In: *Journal of the Soil Mechanics and Foundations Division*.
— (1973b). "Load-deflection prediction for laterally loaded piles". In: *Australian Geomechanics Journal*.
— (1979). "Group factors for pile-deflection estimation". In: *Journal of the Geotechnical Engineering Division*.
— (1990). *User's guide to program DEFPIG 3/4 Deformation analysis of pile groups, Revision 6, School of Civil Engineering, University of Sidney*.
— (2000). "Practical design procedures for piled raft foundations". In: *Design applications of raft foundations*. Hemsley J.A. ed., Thomas Telford, pp. 425–467.
Poulos, HG and EH Davis (1974). *Elastic Solutions for Soils and Rock Mechanics*. New York, N.Y.: John Wiley and Sons, Inc.
— (1980). *Pile foundation analysis and design*. John Wiley & Sons.
Price, G and IF Wardle (1981). "Horizontal load tests on steel piles in London clay." In: *10th International Conference on Soil Mechanics and Foundation Engineering, Stockholm, 2*, pp. 803–808.
— (1987). "Lateral load tests on large diameter bored piles." In: *Contractor Report 46, Transport and Road Research Laboratory, Department of Transport, Crowthorne, England*.
Randolph, MF (1981). "The response of flexible piles to lateral loading". In: *Géotechnique* 31.2, pp. 247–259. ISSN: 0016-8505. DOI: 10.1680/geot.1981.31.2.247. URL: http://www.icevirtuallibrary.com/content/article/10.1680/geot.1981.31.2.247.
— (1994). "Design methods for pile groups and piled rafts". In: *Proc. of 13th ICSMFE, 1994*. URL: http://ci.nii.ac.jp/naid/80007736524/.
Reese, LC, RW Cox, and FD Koop (1974). "Analysis of Laterally Loaded Piles in Sand". In: *Proceedings of the Sixth Annual Offshore Technology Conference - (2) - paper no. OTC 2080*. Houston, Texas.
Reese, LC, WR Cox, and FD Koop (1975). "Field testing and analysis of laterally loaded piles in stiff clay". In: *Offshore Technology Conference*, pp. 671–690.
Reese, LC and WF Van Impe (2001). *Single piles and pile groups under lateral loading*. AA Balkema, Rotterdam.
Reese, LC and ST Wang (1993). *LPILE 4.0, Ensoft Inc, Austin, Texas*.
Reese, LC and RC Welch (1975). "Lateral Loading of Deep Foundations in Stiff Clay". In: *Journal of the Geotechnical Engineering Division* 101, pp. 633–649.
Reese, LC, ST Wang, J Arrellaga, and J Hendrix (2000). *Computer program GROUP for Windows user's manual, version 5.0, Ensoft, Austin, Texas*.
Remaud, D, J Garnier, and R Frank (1998). "Laterally loaded piles in dense sand : Group effects". In: *Int. Conf. Centrifuge 98, Sep 1998, Tokyo, Japan*, pp. 533–538.
Rix, GJ and KH Stokoe (1992). "Correlation of initial tangent modulus and cone resistance". In: *International Symposium on Calibration Chamber Testing*. Potsdam, New York, pp. 351–362.
Robertson, PK and RG Campanella (1983). "Interpretation of cone penetration tests. Part I: sand". In: *Canadian Geotechnical Journal* 20.4, pp. 718–733.
Rollins, KM, JD Lane, and TM Gerber (2005). "Measured and Computed Lateral Response of a Pile Group in Sand". In: *Journal of Geotechnical and Geoenvironmental Engineering* 131.January, pp. 103–114.

Rollins, KM, KT Peterson, and TJ Weaver (1998). "Lateral load behavior of full-scale pile group in clay". In: *Journal of Geotechnical and Geoenvironmental Engineering* June, pp. 468–478. URL: http://ascelibrary.org/doi/abs/10.1061/(ASCE)1090-0241(1998)124:6(468).

Rollins, KM and A Sparks (2002). "Lateral resistance of full-scale pile cap with gravel backfill". In: *Journal of Geotechnical and Geoenvironmental Engineering* September, pp. 711–723. URL: http://ascelibrary.org/doi/abs/10.1061/(ASCE)1090-0241(2002)128:9(711).

Rollins, KM et al. (2006). "Pile Spacing Effects on Lateral Pile Group Behavior: Analysis". In: *Journal of Geotechnical and Geoenvironmental Engineering* 132, pp. 1272–1283.

Rowe, PW (1956). "The single pile subject to horizontal force". In: *Géotechnique* 6.2, pp. 70–85.

Ruesta, PF and FC Townsend (1997). "Evaluation of Laterally Loaded Pile Group at Roosevelt Bridge". In: *Journal of Geotechnical and Geoenvironmental Engineering* 123.December, pp. 1153–1161.

Salvatore, W, G Buratti, B Maffei, and R Valentini (2007). "Dual-phase steel re-bars for high-ductile r.c. structures, Part 2: Rotational capacity of beams". In: *Engineering Structures* 29.12, pp. 3333–3341. ISSN: 01410296. DOI: 10.1016/j.engstruct.2007.09.003.

Schanz, T, PA Vermeer, and PG Bonnier (1999). "The hardening soil model: formulation and verification". In: *Beyond 2000 in computational geotechnics 10 years of PLAXIS. International proceedings of the International Symposium beyond 2000 in Computational Geotechnics Amsterdam The Netherlands 1820 March 1999*.

Sigrist, V (1995). *Zum Verformungsvermögen von Stahlbetonträgern (On the deformation capacity of reinforced concrete girders, in German), Report n. 210*. Tech. rep. Zurich, Switzerland: Institute of Structural Engineering, Swiss Federal Institute of Technology.

Skempton, AW (1986). "Standard penetration test procedures and the effects in sands of overburden pressure, relative density, particle size, ageing and overconsolidation". In: *Géotechnique* 36.3, pp. 425–447. ISSN: 0016-8505. DOI: 10.1680/geot.1986.36.3.425. URL: http://www.icevirtuallibrary.com/doi/10.1680/geot.1986.36.3.425.

Small, JC and JR Booker (1986). "Finite layer analysis of layered elastic materials using a flexibility approach. Part 2—circular and rectangular loadings". In: *International Journal for Numerical Methods in Engineering* 23.April 1983, pp. 959–978. URL: http://onlinelibrary.wiley.com/doi/10.1002/nme.1620230515/abstract.

Small, JC and HH Zhang (2002). "Behavior of Piled Raft Foundations Under Lateral and Vertical Loading". In: *International Journal of Geomechanics* 2.1, pp. 29–45. ISSN: 1532-3641. DOI: 10.1061/(ASCE)1532-3641(2002)2:1(29).

— (2006). "Piled raft foundations subjected to general loadings". In: *Developments in Theoretical Geomechanics*, pp. 57–72.

Sorochan, EA and VI Bykov (1976). "Performance of groups of cast-in place piles subject to horizontal loading". In: *Soil Mechanics and Foundation Engineering* 13.3, pp. 157–161. ISSN: 0038-0741. DOI: 10.1007/BF01705310. URL: http://link.springer.com/10.1007/BF01705310.

Spillers, WR and RD Stoll (1964). "Lateral response of piles". In: *Journal of the Soil Mechanics and Foundations Division*.

Stramandinoli, RSB and HL La Rovere (2008). "An efficient tension-stiffening model for nonlinear analysis of reinforced concrete members". In: *Engineering Structures*

30.7, pp. 2069–2080. ISSN: 01410296. DOI: 10.1016/j.engstruct.2007.12.022.

Stroud, MA (1974). "The standard penetration test in insensitive clays and soft rock." In: *Proceedings of the 1st European Symposium on Penetration Testing, Stockholm, Sweden, vol. 2(2)*, pp. 367–375.

Terzaghi, K (1955). "Evaluation of Coefficients of Subgrade Reaction". In: *Géotechnique* 5, pp. 297–326.

Unsever, YS, T Matsumoto, and MY Ozkan (2015). "Numerical analyses of load tests on model foundations in dry sand". In: *Computers and Geotechnics* 63.January, pp. 255–266. ISSN: 18737633. DOI: 10.1016/j.compgeo.2014.10.005.

Viggiani, C, A Mandolini, and G Russo (2011). *Piles and pile foundations*. Taylor and Francis.

Welch, RC and LC Reese (1972). "Lateral Load Behavior of Drilled Shafts". In: *Research Report Number 89-10 - The Texas Highway Department* 89.

Wolff, TH (1989). "Pile capacity prediction using parameter functions, Results of a pile prediction Symposium". In: *ASCE Geo. Special Publication No. 23*.

Wu, G (2006). *VERSAT-P3D: A computer program for dynamic 3-dimensional finite element analysis of single piles and groups. Wutec Geotechnical Interational, Vancouver, Canada*.

Wu, G, W Liam Finn, and J Dowling (2015). "Quasi-3D analysis: Validation by full 3D analysis and field tests on single piles and pile groups". In: *Soil Dynamics and Earthquake Engineering* 78, pp. 61–70.

Zafir, Z and WE Vanderpool (1998). "Lateral response of large diameter drilled shafts: 1-15/ US 95 load test program". In: *Proceedings of the Thirty-Third Engineering Geology and Geotechnical Engineering Symposium, University of Nevada, Reno*, pp. 161–176.

Zhang, H and JC Small (1999). "Analysis of Axially and Laterally Loaded Pile Groups Embedded in Layered Soils". In: *Proceedings 8th Australia New Zealand Conference on Geomechanics: Consolidating Knowledge. Australian Geomechanics Society*, p. 475.

Zhang, HH and JC Small (2000). "Analysis of capped pile groups subjected to horizontal and vertical loads". In: *Computers and Geotechnics* 26.1, pp. 1–21. ISSN: 0266352X. DOI: 10.1016/S0266-352X(99)00029-4.

Zhukov, NV and IL Balov (1978). "Investigation of the effect of a vertical surcharge on horizontal displacements and resistance of pile columns to horizontal loads". In: *Soil Mechanics and Foundation Engineering* 15.1, pp. 16–22. ISSN: 0038-0741. DOI: 10.1007/BF02145324. URL: http://link.springer.com/10.1007/BF02145324.